Phase relations in the system Cu-Fe-Ni-S and their application to the slow cooling of PGE Matte

By

Willemien Viljoen

Submitted in partial fulfillment of the requirements for

the degree PhD Science in

the Faculty of Natural and Agricultural Science

University of Pretoria

October 2001

TABLE OF CONTENTS

LIST OF FIGURES

LIST OF TABLES

LIST OF PHOTOGRAPHS

LIST OF APPENDICES

ACKNOWLEDGEMENTS

I would like to thank the following people and institutions:

Jeff Taylor from Johnson Matthey for valuable discussions related to the project.
Anglo American Platinum Ltd for providing the financial means for this project.
Juliana Bruwer for practical advice during the progress of the project.
Roland Merkle from the University of Pretoria for constant supervision.
Peter Gräser from the University of Pretoria for aiding in the EMP analysis.
Sabine Verryn from the University of Pretoria for providing XRD analyses.
Isaiah Mahlanga, Peter Seibya, and Marko Claasen from the Sectioning Lab at the University of Pretoria for preparing the polished sections.
My Husband for his moral support.
The Creator of the Universe for the beautiful things He has made with which we keep ourselves busy.

ABBREVIATIONS

°C	degrees Celsius
ci	confidence interval
EMP	Electron Microprobe
E1,2,3	Eutectic point 1,2,3
Fig.	Figure
Glass	quartz glass
Heaz. / Hz	Heazlewoodite
kV	kilo Volts
µm	micro meter
nm	nano meter
nA	nano Ampere
No. Anal.	Number of analyses
PGE	Platinum Group Element
PGM	Platinum Group Mineral
s	standard deviation
Std. Dev.	Standard deviation
UG2	Upper Group (layer) 2
wt%	weight percentage
at%	atomic percentage

ABBREVIATIONS FROM BRUWER (1996) FOR ISOTHERMAL SECTIONS IN THE Cu-Ni-S SYSTEM

L_1	Sulphur liquid containing approximately 1 wt% Cu and Ni
L_2	Immiscible Cu-rich sulphide liquid
L_3	Immiscible metal-rich liquid
$L_{(2,3)}$	Homogeneous liquid field forming an eutectic at approximately 575°C
L_4	Liquid field that separates from the $L_{(2,3)}$ field and exists around 800°C
µ	High temperature Digenite ($Cu_{2-x}S$)
θ	High temperature Heazlewoodite ($Ni_{3\pm x}S_2$
λ	High temperature Millerite ($Ni_{1-x}S$)
η	Vaesite (NiS_2)
α	Cu-Ni alloy
+	Phase assemblages are noted with a "+" between co-existing phases, refers to the field where these phases co-exist

ABSTRACT

The aim of this investigation is to determine the influence of a small amount of Fe on the Cu-Ni-S system within the framework of the beneficiation processes of Platinum Group Metals from the Merensky Reef of the Bushveld Complex, South Africa. Aspects under evaluation are: the phase relations within the Cu-Ni-Fe-S system at less than 10 wt% Fe, the difference in cooling paths as the Fe content and temperature vary, and the variation in composition of the phases that form between 1200° and 700°C.

The investigation was performed in 100°C intervals from 1200°C to 700°C at four different Fe contents (i.e. 1, 3, 5 and 10 wt%). High purity metal and sulphur powders were reduced and dried respectively and experiments were carried out in evacuated quartz glass tubes. Modified high-temperature furnaces with an accuracy of 1°C were used for equilibration reactions, which lasted between a few hours (at 1200°C and 1100°C) up to a couple of months (at 800°C and 700°C). Experiments were quenched in tap water to preserve the phase relations at the required temperature. Electron microprobe analyses were collected to determine the chemical composition of solid and quenched melt phases. Spot analyses were performed on the solid phases and area analyses, using the defocused beam technique, to determine the average composition of the quenched melt phases. Results were plotted on a quaternary diagram and projections onto the Cu-Ni-S ternary diagram were used to compare between diagrams with different starting Fe contents. Diagrams at similar starting Fe contents and different temperatures were combined to produce diagrams depicting the cooling path from 1200°C to 700°C (the paths to complete solidification were extrapolated).

Alloy is the first phase to crystallize in an average converter matte (provided the composition is favorable) and also the primary collector of PGE's in the matte. In this investigation it was confirmed that at a fixed bulk Fe content, a decrease in temperature causes a decrease in the Cu/Ni of the cotectic alloy. Additionally, it has also been established that at a fixed temperature, an increase in the Fe content of the bulk will cause a decrease in the Cu/Ni of the cotectic alloy. Therefore, if all other parameters are kept stable, it can reasonably be accepted that an increase in the bulk Fe content will produce an increasingly Ni-rich alloy.

The composition of the cotectic melt is essential in determining the cooling path towards the eutectic point where alloy, digenite and heazlewoodite coexist. The cotectic melt in the assemblage (alloy+digenite+melt) shows an increase in Ni, Fe and sulphur content, with an increasing Fe content in the bulk. This causes the cotectic to shift towards higher sulphur contents, which results in a larger stability field for alloy. The implications are twofold: Firstly higher Fe contents increase the amount of alloy that will crystallize from the melt, and secondly it would require a larger variation in starting composition (particular the Cu/Ni) to alter the path of crystallization of a matte.

The stable phases are strongly influenced by the amount of Fe present in the bulk composition: The more Fe available, the more Fe will be incorporated in the crystal structures of phases. The relationship is, however, not linear and generally the more Fe available in the bulk the wider the range of Fe contents in the phase. In assemblages containing alloy, the alloy phase has consistently the highest partitioning coefficient for Fe. In other assemblages, Fe does not show any preference for a particular phase, regardless of the sequence of crystallization or temperature of equilibration.

PREAMBLE

The definition given by Collins (1990) for a mineral is: "a naturally occurring element or compound of non-biological origin, having an ordered atomic structure and characteristic chemical composition, physical properties, and crystal form". Although the phases (e.g. "digenite", "millerite", "vaesite" and "covellite") in the Cu-Ni-Fe-S system from this investigation might show the same structure and characteristics as the natural occurring minerals, they can not, in the strict sense of the word, be classified as minerals. The sulphide phases in the various sub-systems (Chapter 2) and those from this investigation are all synthetic sulphides. However, because there is no referral to the natural minerals themselves, the sulphides in this investigation will be named by their natural equivalents with the understanding that they are all synthetic.

1. INTRODUCTION

1.1 Background

The largest resources of Platinum Group Elements (PGE's) are found in the Bushveld Complex situated in the central portion of the Transvaal in South Africa. Three reefs varying in mineralogy and ore grade are currently mined for PGE's. These are the Merensky Reef, UG2 and Plat Reef (Viljoen & Schurmann, 1998; Cawthorn, 1999).

Figure 1.1 is a simplified flow diagram is given of a typical route to recover PGE's from these ores. After milling and flotation, the concentrate (which still contains a large fraction of oxides and silicates) is molten in a furnace to produce two immiscible melts. The lighter silicate melt (furnace slag) is tapped continuously and discarded while the heavier sulphide melt (matte) is tapped at regular intervals and further treated (Hiemstra, 1988). This is followed by conversion of the matte (by air or air-oxygen mixes) that involves oxidation of most of the Fe, which then reacts with added SiO_2 to form fayalite (Fe_2SiO_4) slag (Mostert & Roberts, 1973). The simultaneous oxidation of sulphur leads to the formation of SO_2 (Cooper, 1984). The converted matte contains Cu, Ni, S and small amounts of Fe and Co as well as trace amounts of PGE's, gold and silver. The conversion process enriches the PGE content in the matte by approximately 3-fold, compared to furnace matte. This matte is poured into large ingots (lined with a refractory material) where it is slow cooled over a period of approximately 5 days. Depending on the bulk composition and temperature, the matte crystallizes slowly according to a specific path of crystallization. Ideally, a magnetic alloy fraction will crystallize first from the matte and act as collectors of most of the PGE's.

Platinum Group Elements have a preferred partitioning into an alloy phase compared to sulphide or oxide phases (Distler et al., 1977; Fleet & Stone, 1991; Peach & Mathez, 1996, Crocket et al., 1997; Fleet et al., 1999). In this case the PGE's will be captured by a crystallizing Cu-Ni-alloy. The fully crystallized matte is then milled and magnetically separated to remove the now PGE-concentrated alloy fraction from the sulphide fraction (Mostert & Roberts, 1973; Schouwstra et al., 1998). This PGE-concentrate is further treated chemically to separate and concentrate the different Platinum Group Elements.

For this study the key step in the process is the slow cooling of the matte that will both save time and money by reducing the amount of material that must be chemically treated to unlock the PGE's. To ensure an optimum recovery of the PGE's, the starting composition and temperature of the matte must be within calculated limits to regulate the path of crystallization (Mostert & Roberts, 1973; Bruwer & Merkle, 1998 and Jones, 1999).

1.2 Aim of Study

The setting for this study is the pyrometallurgical processes in the beneficiation of platinum group elements from a Cu-Ni-Fe-sulphide ore. To understand the relevancy of the Cu-Ni-Fe-S system in the beneficiation of PGE's, a short summary of the processes involved in treatment of the ore are given in Figure 1.1.

The aim of the study is to investigate the influence of low concentrations of Fe on the Cu-Ni-S system. Of particular interest are: (1) the compositions of the alloy and digenite co-existing with melt (generally referred to as the cotectic alloy, cotectic digenite and cotectic melt) in the different isothermal sections; (2) the Fe content of sulphide and alloy phases as a function of the Fe to the starting composition, and (3) the partitioning of Fe between co-existing solid phases. The focus is not to present complete phase diagrams, and some phase diagrams will appear incomplete in areas of less relevancy to this project.

After conversion, the relevant Cu-Ni-matte (at the plant) contains approximately 3 wt% Fe. However, to determine the influence of Fe on the Cu-Ni-S system it was decided to perform experiments at lower (1 wt%), higher (5 wt%) and much higher (10 wt%) concentrations of Fe, than in the average matte. The percentage Ni is approximately 50%, Cu approximately 28% and sulphur approximately 21% (Hiemstra, 1988, Mostert & Roberts, 1973 and Jones, 1999). Bruwer and Merkle (1998) demonstrated that at low Fe contents the crystallization paths of converter mattes are very sensitive to the amount of sulphur present.

A prerequisite for understanding the crystallization paths of a slow-cooled matte is the phase diagrams for the system Cu-Ni-Fe-S as an approximation of converter matte composition. Available information includes phase diagrams of the sub-systems and their applications to natural occurring systems (see Chapter 2). To predict and optimize the conditions necessary for a converter matte to collect PGM's in an extractable fraction, the characteristics of the Cu-Ni-Fe-S system needed to be investigated experimentally.

To assure the direct relevancy of this project to the beneficiation of Cu, Ni and PGE's from a Merensky Reef and UG2-type Cu-Ni-PGE ore, some constraints were put on the parameters for the investigation. The temperature range was confined to 700° - 1200°C at 100°C intervals and the Fe content was set at 1, 3, 5, and 10wt% Fe. The starting temperature of a converter matte is normally in the vicinity of 1200°C, where only alloy phases are stable. At lower temperatures sulphide phases would become stable, competing with the alloy phases for incorporating the PGE's. Higher experimental temperatures than 1200°C were not needed because there would not be any additional phases in the pure Cu-Ni-Fe-S system. Decreasing the experimental temperatures in 100°C intervals were small enough steps to detect any important change of phase relations in the system. Experiments were not performed below 700°C for two reasons: Firstly, equilibration times at these low temperatures

become very long (possibly 6 to 12 months) and would carry on beyond the time restrictions of this study. Secondly, at 700°C most of the PGE's in the matte would have been collected by the alloy and sulphide phases.

Figure 1.1: Simplified flow diagram showing the route of slow cooling for PGM beneficiation from a Merensky Reef and UG2-type sulphide ore.

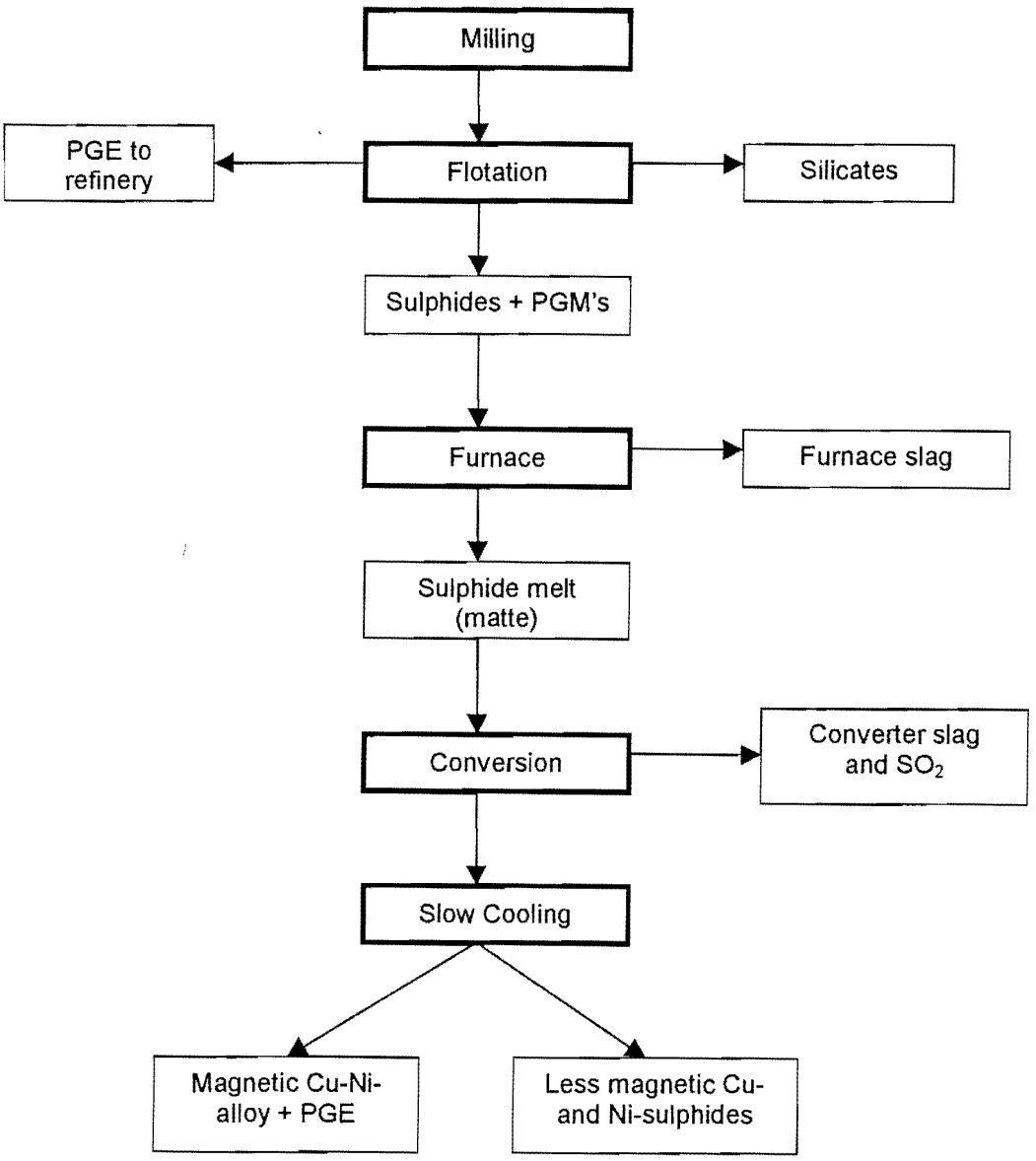

2. UNDERLYING BINARY AND TERNARY SYSTEMS AND THEIR PHASES

Experimental studies on various natural and synthetic systems were performed extensively in the late fifties, sixties and seventies (see below). Although much can be derived from thermodynamic predictions, the actual experiment is still the most reliable method to determine the properties of an investigated system.

Ores and natural mineral assemblages have rather been described by the sub-systems than the complete Cu-Ni-Fe-S system. Summarized below are the relevant binary and ternary systems as been discussed by researchers over the years.

2.1 The Ni-S system

Minerals occurring in the Ni-S system were experimentally investigated and described by Arnold and Kullerud (1956) and Kullerud and Yund (1962). Arnold and Kullerud (1956) described the NiS-NiS_2 join to be a solid solution of the omission type and suggested a formula of $Ni_{1-x}S$. A follow-up study (Kullerud and Yund, 1962) with the use of quenched experiments in evacuated quartz glass tubes, DTA, and high-temperature X-ray powder diffraction extended on the phases present in the system. Ni-sulphides relevant for this study are:

2.1.1) Heazlewoodite (Ni_3S_2)

Heazlewoodite occurs as two modifications with the inversion temperature at 555° ± 5°C (Rosenqvist, 1954). The low temperature polymorph has a hexagonal (rhombohedral) structure and limited solid solution on either side of the stoichiometric Ni_3S_2. The high-temperature form shows a compositional variation from 24.0 to 30.0 wt% S between 600° and 700°C, resulting in a general formula of $Ni_{3\pm x}S_2$. Sinyakova et al. (1999) determined through an experimental investigation that heazlewoodite-solid-solution forms between 875°C and 880°C

2.1.2) Millerite (NiS)

Millerite also has a low-temperature hexagonal form (β) that inverts to a high-temperature hexagonal (NiAs atomic structure) polymorph (α) at 379°± 3°C (Alsen, 1923, 1925; Kullerud & Yund, 1962). At a temperature of 600°C, the high-temperature form can contain a maximum of 37.8 wt% S (Arnold & Kullerud, 1956). According to the investigation of Arnold and Kullerud (1956), the β-millerite often occurs in long needle-shaped crystals whereas the α-millerite seldomly occurs as single crystals. In the temperature range 700° - 800°C, the α-NiS inverts

to α-$Ni_{1-x}S$. The melting point, as determined by Eugster and Kullerud (1956), is 800.5°± 1.0°C.

2.1.3) Polydymite (Ni_3S_4)

A diagnostic characteristic of polydymite is polysynthetic twinning and the replacement of Ni by Fe to form $(Ni, Fe)_3S_4$ in natural systems (Tarr, 1935). Polydymite forms part of the linnaeite (Co_3S_4) series together with violarite (Ni_2FeS_4) (Palache et al., 1944). Kullerud and Yund (1962) found that the synthesis of polydymite was hampered by slow reaction rates. Other compounds (like Ni_7S_6, $Ni_{1-x}S$, and NiS_2) that grow at the same time will grow faster and persist longer metastably. According to Rosenqvist (1954), polydymite was not observed in experiments at 400°C. Therefore, the chances of encountering this phase are very remote.

2.1.4) Vaesite (NiS_2)

Vaesite has the pyrite structure and was synthesized from 170° to 680°C (De Jong & Willems, 1927; Lundqvist, 1947). To synthesize vaesite requires the formation of NiS first and long reaction times. Vaesite is stoichiometric within the limits of $NiS_{2.000\pm.0.0004}$ according to Kullerud and Yund (1962).

2.2 The Cu-S system

The Cu-S system was investigated by Roseboom (1966) at temperatures between 25° and 700°C. The thermochemical properties were investigated by Kellogg (1967) between 526.75° and 1326.75°C and thermodynamic data are summarized by Chakrabarti and Laughlin (1983). The relevant minerals in this system are:

2.2.1) Digenite (Cu_2S)

At temperatures between 76° and 83°C low-digenite is inverted to high-digenite. The inversion temperature of high-digenite to high-chalcocite is not well defined, but these two minerals are considered equivalent (Roseboom, 1966). At the temperatures relevant for this study high-digenite is considered stable.

2.2.2) Covellite (CuS)

Kullerud (1965) described the stability relations of covellite and determined that it breaks down to high-digenite plus liquid sulphur at 507°C. The mineral named blaubleibender covellite was first described by Moh (1964) and again noted by Barton (1973) but not determined to be a stable phase. Later this "mineral" was described and identified to be yarrowite and spionkopite by Goble (1980).

2.3 The Fe-S system

Kullerud and Yoder (1959) investigated the stability of pyrite in the Fe-S system and the pyrite-pyrrhotite relationship was briefly discussed by Arnold (1956). However, because of the low concentrations of Fe used in this experimental investigation, no distinct Fe-sulphide phases were observed, and a further discussion on mineral phases in this system is not relevant.

2.4 The Ni-Fe-S system

This element combination results in minerals like pentlandite and pyrrhotite that are important ore minerals in natural PGE producing systems. One of the first papers discussing the Ni-Fe-S system was by Hawley et al. in 1943, in which they also describe the solid solution between pyrrhotite and pentlandite.

Describing the subsolidus phase relations in the Ni-Fe-S system, Kullerud (1956) found that the solubility of NiS in FeS at 500°C is about 20 mol% and the solubility of FeS in NiS is about 30 mol%. The solubilities of both sides increase markedly with increasing temperature.

The sulphur-rich portion of the Ni-Fe-S system was investigated between 100° and 1000°C by Clark and Kullerud (1963). Experiments were performed with special emphasis on the pyrite-vaesite join. It was found that the solubility of Fe in NiS_2 (vaesite) and Ni in pyrite is less than 10 % at 550°C, even though vaesite and pyrite are isostructural.

The central portion of the Ni-Fe-S system was discussed between 250° and 600°C by Naldrett, Craig and Kullerud (1967).

A resent investigation in the Fe-Ni-S system by Sinyakova et al. (1999), experimentally determined the surface of the liquidus at low sulphur contents as well as the fields of the monosulphide-solid-solution, heazlewoodite-solid-solution and tenite primary crystallization.

None of the distinct Fe- or Ni-Fe-minerals was observed in this investigation due to the low Fe concentrations used.

2.5 The Cu-Fe-S system

Merwin and Lombard (1937) performed an extensive study on the phase relations in the Cu-Fe-S system between 400° and 950°C, while Yund and Kullerud (1966) evaluated the thermal stabilities of assemblages in this system from 700° to 200°C. Crystal-chemical studies were performed by Morimoto in 1970.

Rooseboom and Kullerud (1958) investigated the solidus in the sulphur rich part of this system between 400° and 800°C, and found that digenite and bornite form a complete solid solution in the presence of liquid and vapor above 550°C. This was confirmed by Barton (1973), who investigated the solid solutions in the Cu-Fe-S system and determined the activities of digenite, chalcocite and $CuFeS_2$. He also present a phase diagram for the Cu-Fe-S join between 400° and 700°C. Cabri (1973) described and attempted to synthesize the phases in this system at lower temperatures (100° and 600°C).

2.6 The Cu-Ni-S system

The bulk of this investigation expands on the experimental study performed by Bruwer (1996) on the Cu-Ni-S system between 700°C and 1200°C (at 100°C intervals). With the low Fe contents researched in this study, the similarities and differences with the Fe-free system are important aspects. The phase diagrams produced by Bruwer (1996) of the Cu-Ni-S system will therefore be briefly discussed at the different isothermal sections, presuming cooling from higher temperature. Stable assemblages are presented in brackets.

2.6.1) At 1200°C

Two immiscible melts coexist at Cu-rich compositions of the system and at Ni-rich compositions a (alloy + melt)-field extends towards higher Cu contents. The position of intersection of the (alloy + melt)-field boundary line with the Cu-Ni join is at approximately 80 wt% Cu and with the Ni-S join at approximately 23 wt% Ni (Figure 2.1).

2.6.2) At 1100°C

Two immiscible melts coexist at Cu-rich compositions of the system and at Ni-rich compositions a (alloy + melt)-field extends towards higher Cu contents but flattens out at about 95 wt% Cu. The position of intersection of the (alloy + melt)-field boundary line with the Cu-Ni join is at approximately 95 wt% Cu and with the Ni-S join at approximately 30 wt% Ni (Figure 2.2).

2.6.3) At 1000°C

At Cu-rich compositions and less than 20 wt% S, digenite and alloy co-exist. At Ni-rich compositions alloy and melt co-exist with the (alloy + melt)-field boundary line intersecting the Ni-S join at approximately 18 wt% S. At more than 50 wt% Cu, low Ni contents, and not more than 20 wt% S, three phases co-exist: alloy, digenite and melt. At higher sulphur contents (about 20 wt%), digenite and melt co-exist (Figure 2.3).

2.6.4) At 900°C

At Cu-rich compositions and less than 20 wt% S, digenite and alloy co-exist. At Ni-rich compositions alloy and melt co-exist with the (alloy + melt)-field boundary line intersecting the Ni-S join at approximately 20 wt% S. At more than 40 wt% Cu, up to 50 wt% Ni, and not more than 20 wt% S, three phases co-exist: alloy, digenite and melt. At higher sulphur contents (between 20 and 25 wt%), digenite and melt co-exist. At high Ni concentrations and less than 50 wt% S, millerite and vaesite both co-exist with a melt. Less melt is present than at higher temperatures (Figure 2.4).

2.6.5) At 800°C

All the solid phases co-exist with melts and some also co-exist only with each other as the quantity of melt decrease. At Cu-rich compositions and less than 20 wt% S, digenite and alloy co-exist. At Ni-rich compositions alloy and melt co-exist with the (alloy + melt)-field boundary line intersecting the Ni-S join at approximately 21 wt% S. At more than 20 wt% Cu, up to 60 wt% Ni and not more than 20 wt% S, three phases co-exist: alloy, digenite and melt. At higher sulphur contents (between 20 and 30 wt%), digenite and melt co-exist. At high Ni concentrations and less than ~50 wt% S, millerite and vaesite co-exist each with a different melt. Heazlewoodite is stable at this temperature (Figure 2.5).

2.6.6) At 700°C

Only digenite, a Ni-rich alloy and heazlewoodite still co-exist with a melt phase. Millerite and vaesite co-exist only with each other and digenite. Only a very small amount of melt is left (Figure 2.6).

2.7 The Cu-Ni-Fe-S system

Kullerud et al. (1969) investigated the phase relations in the three subsystems Cu-Fe-S, Cu-Ni-S and Fe-Ni-S with the silica-tube quenching technique, DTA and high-temperature XRD experiments. They found that extensive liquid immiscibility fields span the sulphur-rich region of all three of the systems while a homogeneous liquid field dominates the central portions of the system. Craig and Kullerud (1969) presented phase diagrams at 1000°C and 850°C of the Cu-Ni-Fe-S system (Figures 2.7 and 2.8), based on experimental work. These phase diagrams were however, drawn without quantitative data and are considered schematic only.

The fractional crystallization of a sulphide liquid in the Fe-Ni-Cu-S system was discussed by Fleet & Pan (1994) at 50 and 52.5 at% S, temperatures between 850 – 1050°C and low pressures. They found that an intermediate solid solution [$(Cu,Fe)S_{1-x}$; iss] is stable up to 900-

950°C in Ni-poor compositions, and a large field of a ternary (Fe,Cu,Ni)S solid solution exists at and below 850°C.

An experimental investigation by Ebel and Naldrett (1996 & 1997) looked at the fractional crystallization of sulphide ores at temperatures between 1050° and 1180°C. Partitioning coefficients for Cu and Ni between monosulphide solid solution and a Fe-Ni-Cu-S liquid are also discussed. Because the study by Ebel and Naldrett looked at high Fe contents the relevancy to this investigation was very limited. A schematic quaternary diagram (Figure 2.9) at 1100°C shows the position of various solid solutions discussed by Ebel and Naldrett (1997). Electron microprobe data is published but their investigation concentrated on the Fe "saturated" part of the quaternary. A similar study by Ballhaus et al. (2001) looked at the role of the metal/S atomic ratio on monosulphide-melt partition coefficients and closed-system fractionation paths in the Fe-Ni-Cu-S system.

Using parameters from the binaries, Kongoli et al. (1998) constructed a modified quasichemical model that predicts the thermodynamic properties of amongst others Fe-Ni-Cu-S mattes over wide range of compositions and temperatures. These model parameters are stored in the databases of the F*A*C*T (1995) thermodynamic computer system, but not utilized (due to costs) in this study.

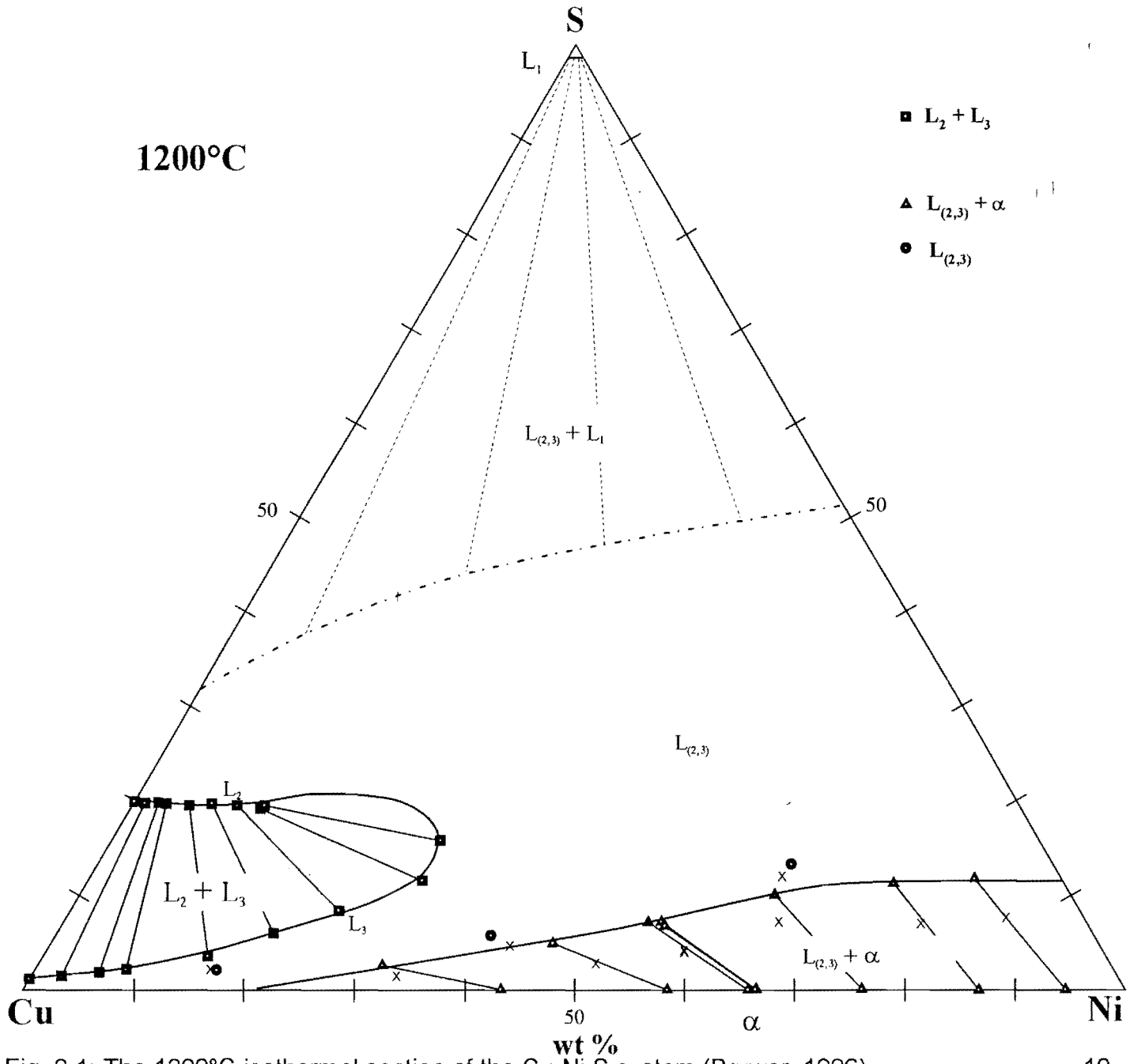

Fig. 2.1: The 1200°C isothermal section of the Cu-Ni-S system (Bruwer, 1996).

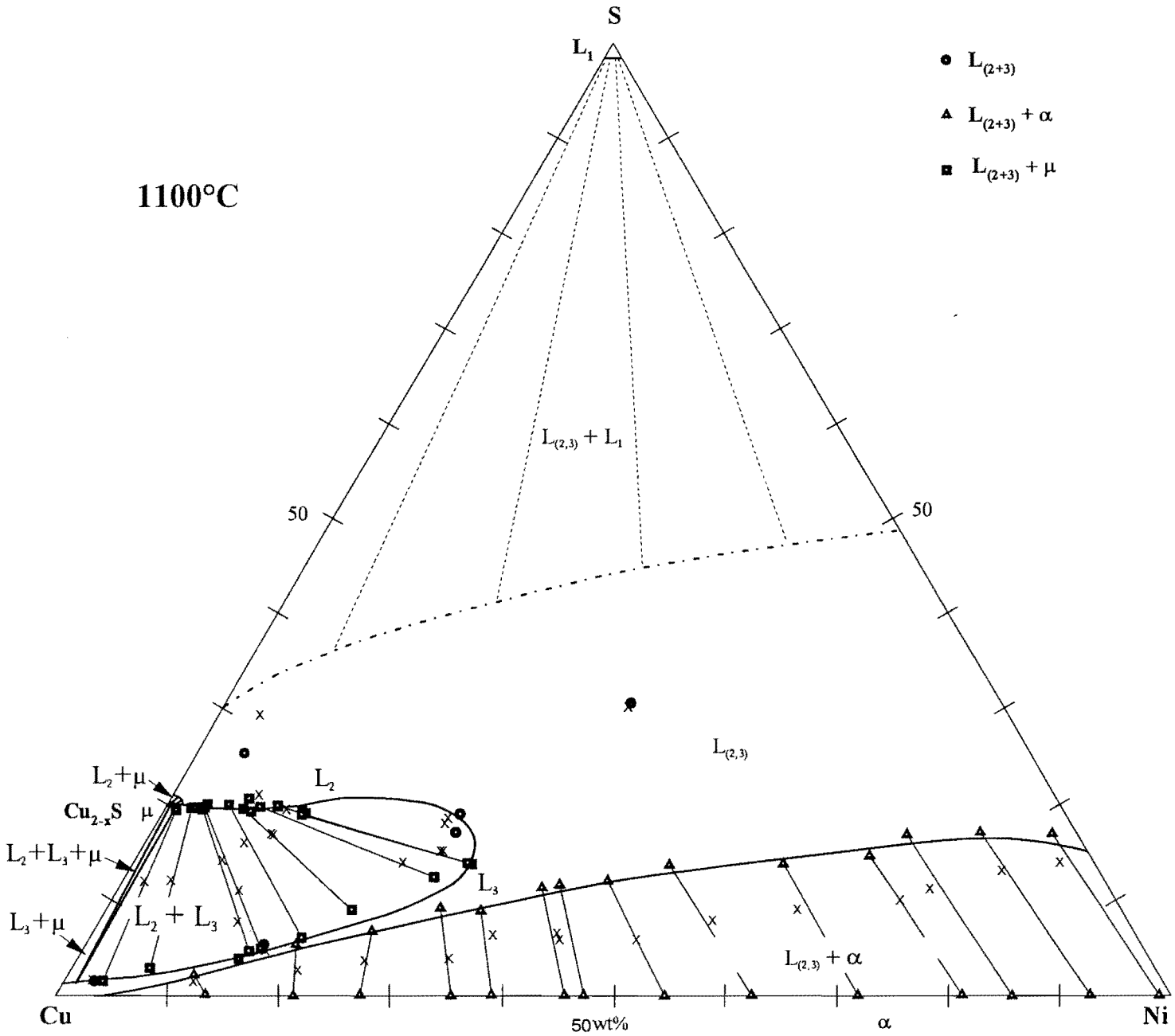

Fig. 2.2: The 1100°C isothermal section of the Cu-Ni-S system (Bruwer, 1996).

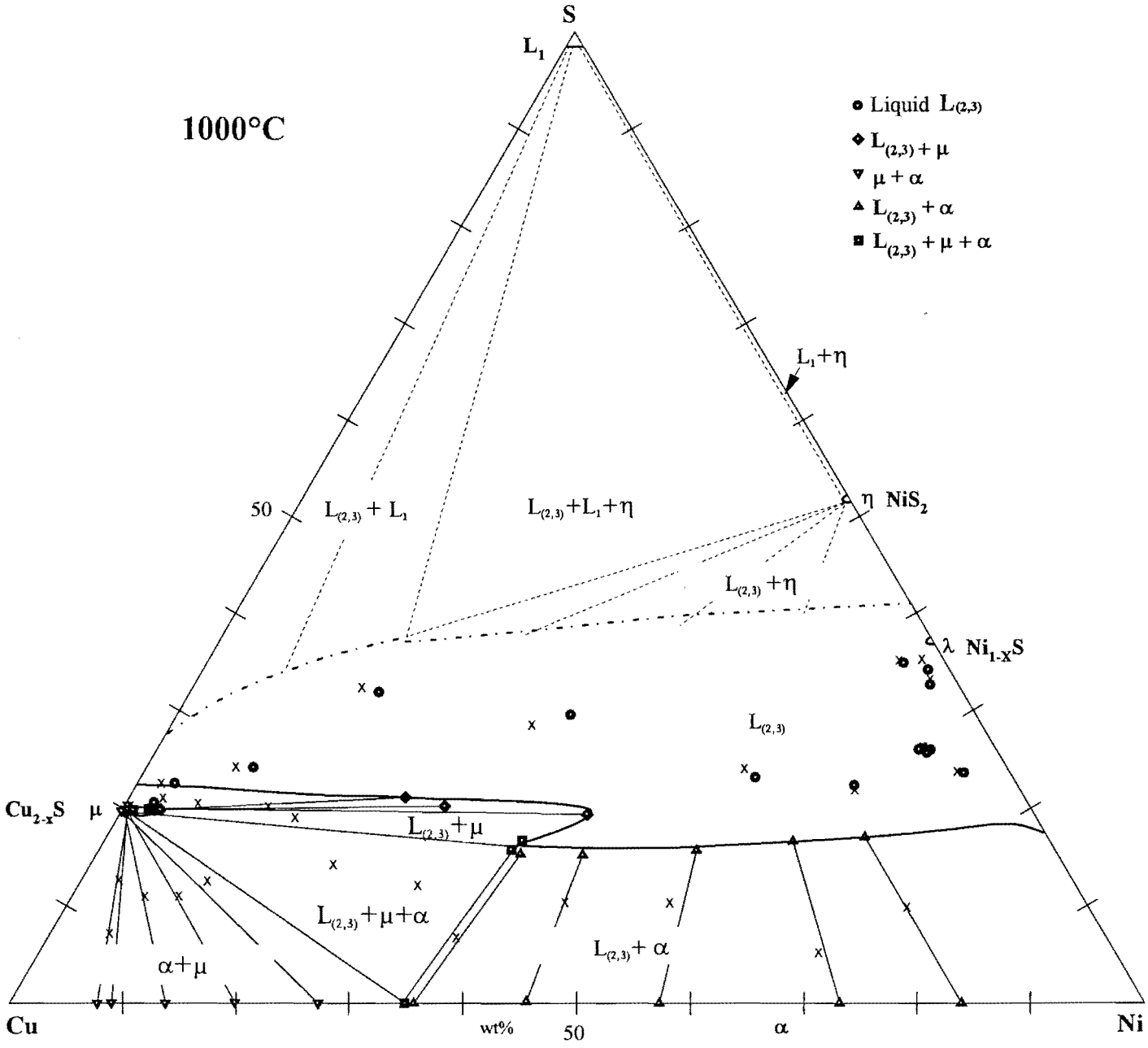

Fig. 2.3: The 1000°C isothermal section of the Cu-Ni-S system (Bruwer, 1996).

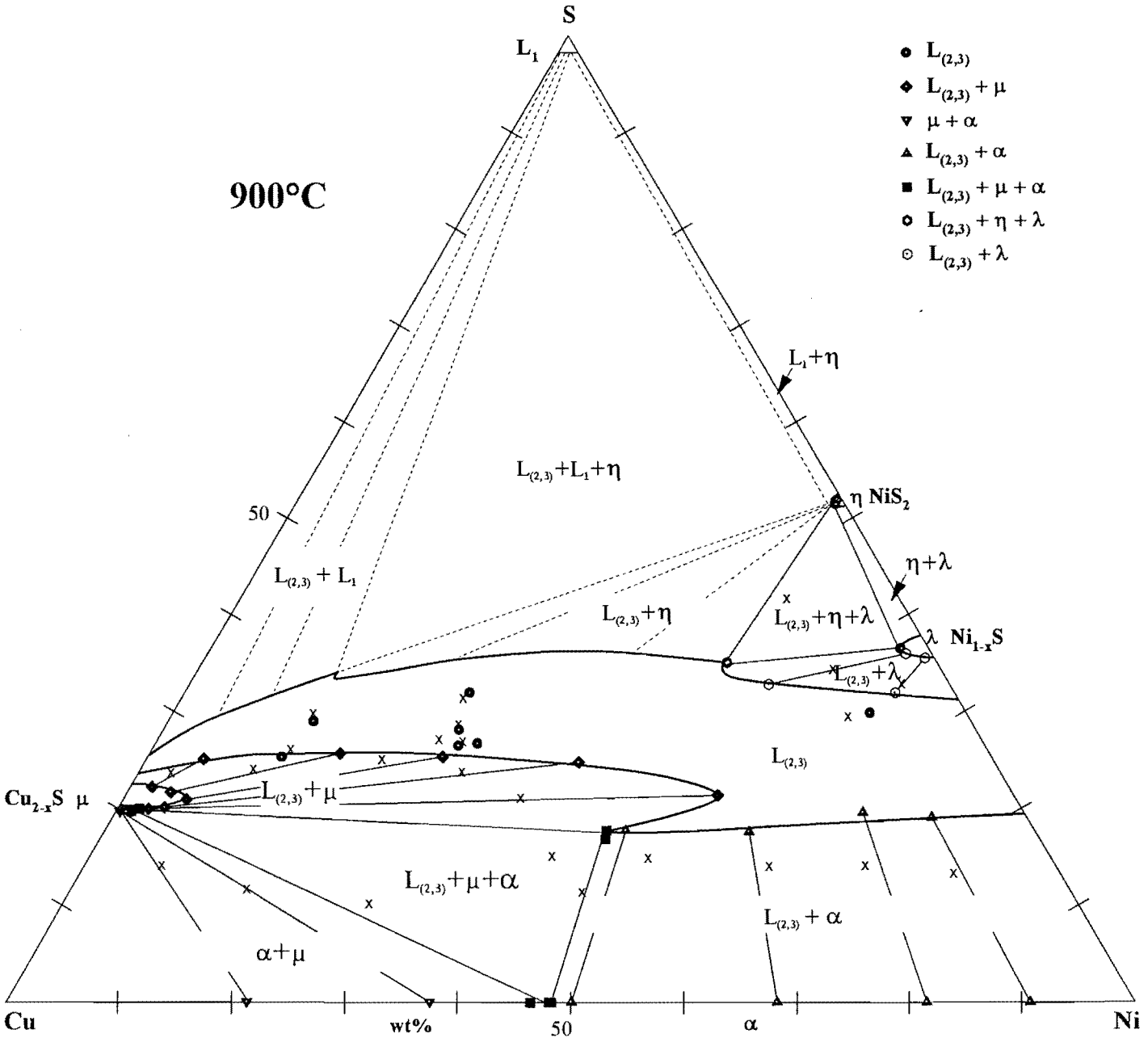

Fig. 2.4: The 900°C isothermal section of the Cu-Ni-S system (Bruwer, 1996).

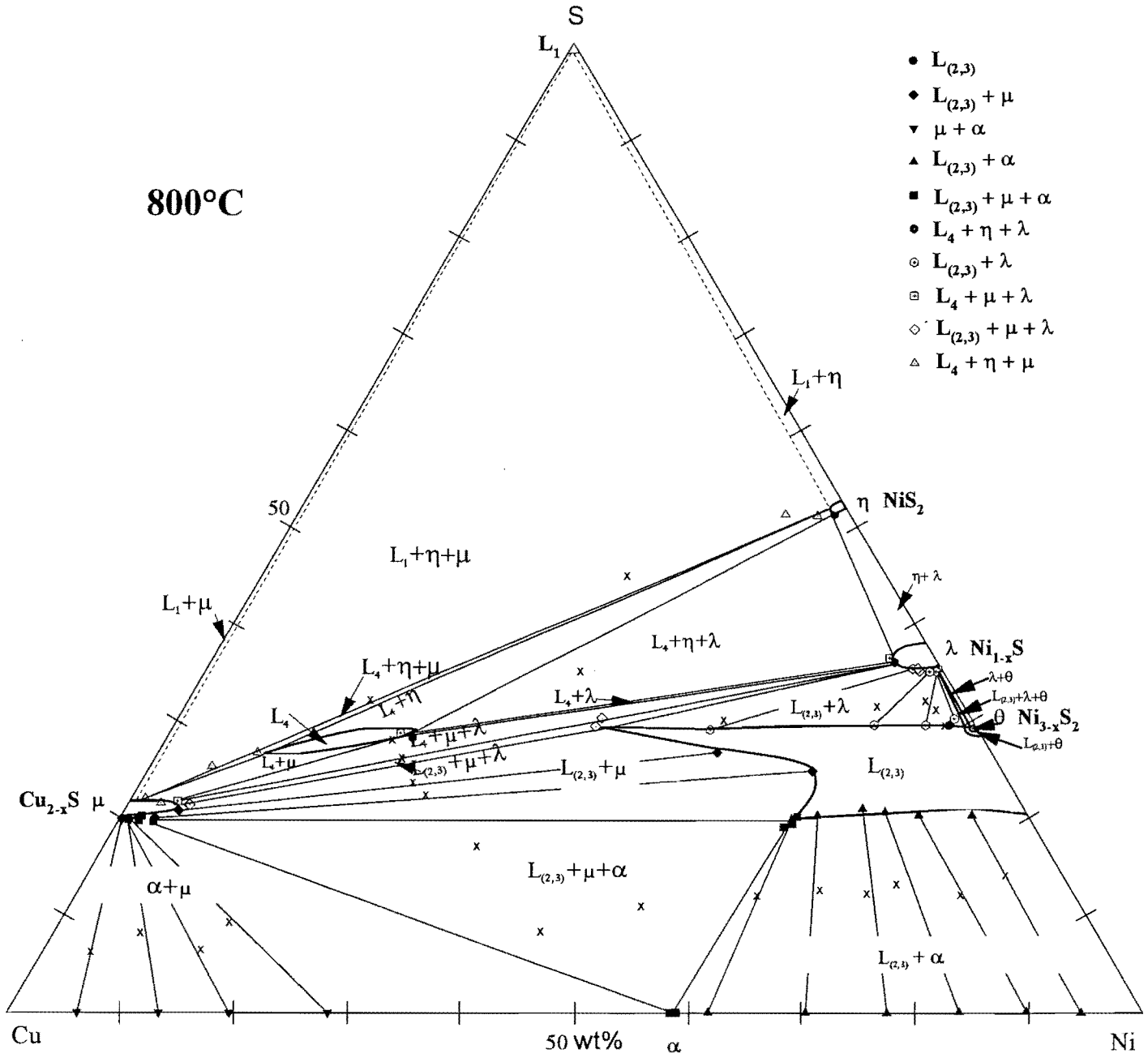

Fig. 2.5: The 800°C isothermal section of the Cu-Ni-S system (Bruwer, 1996).

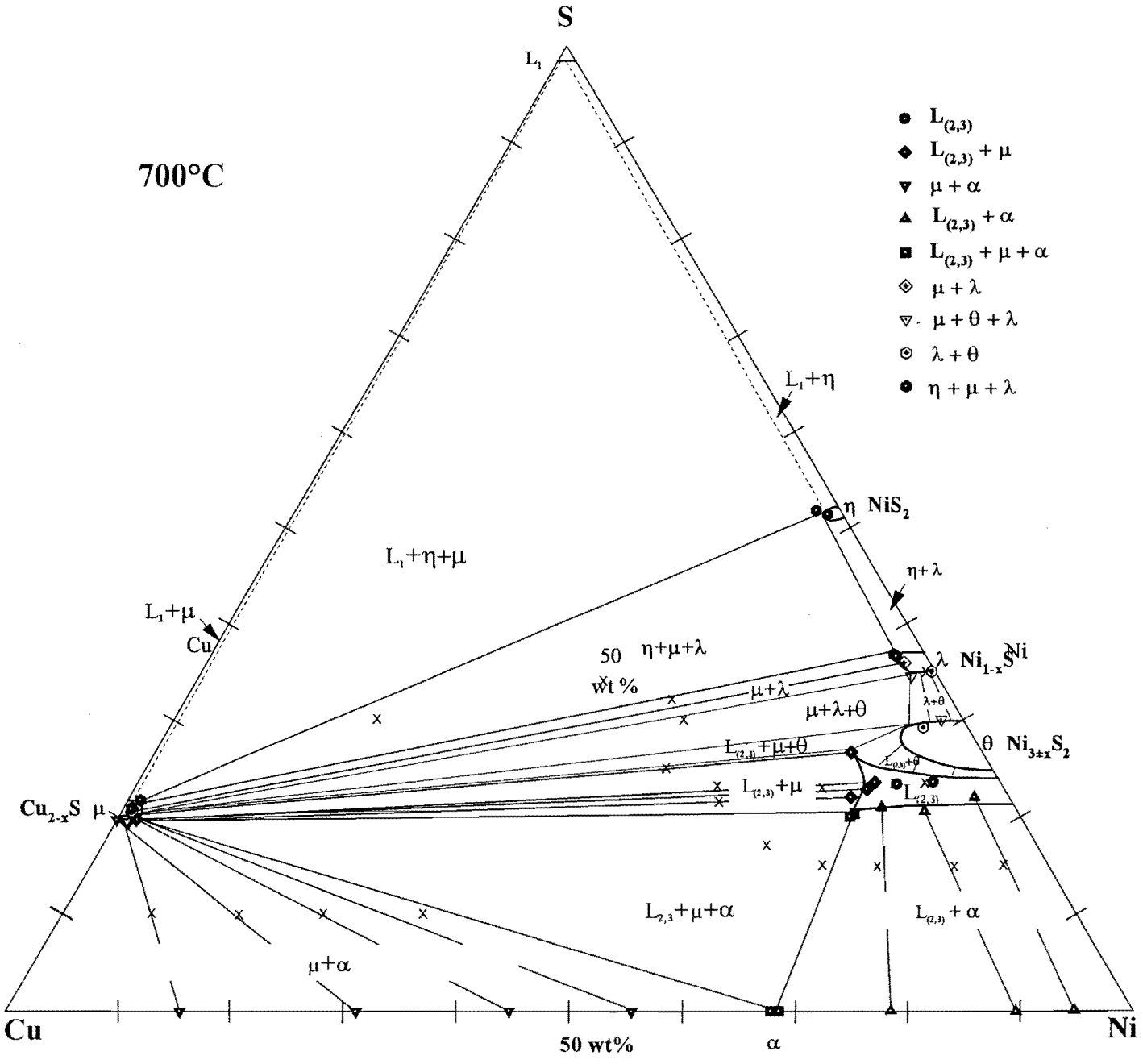

Fig. 2.6: The 700°C isothermal section of the Cu-Ni-S system (Bruwer, 1996).

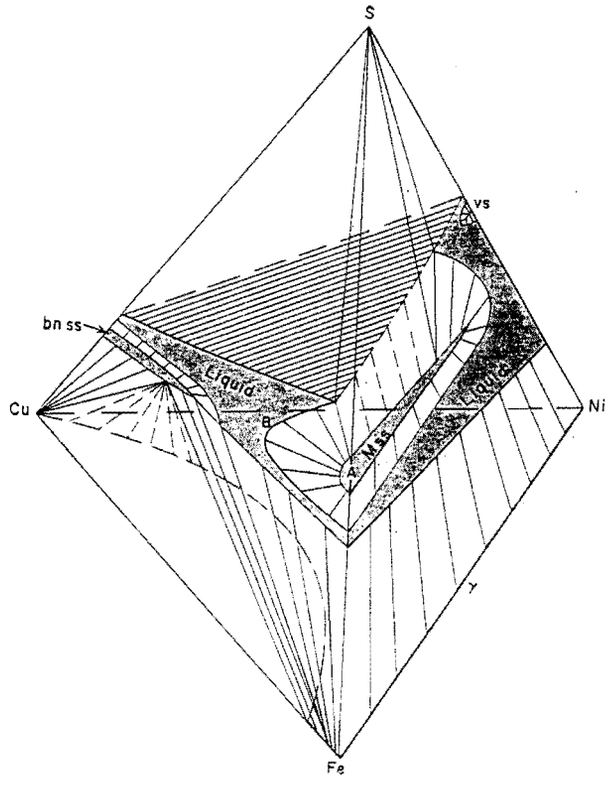

Figure 2.7: Schematic phase relations in the Cu-Ni-Fe-S system at 1000°C (Craig and Kullerud, 1969).

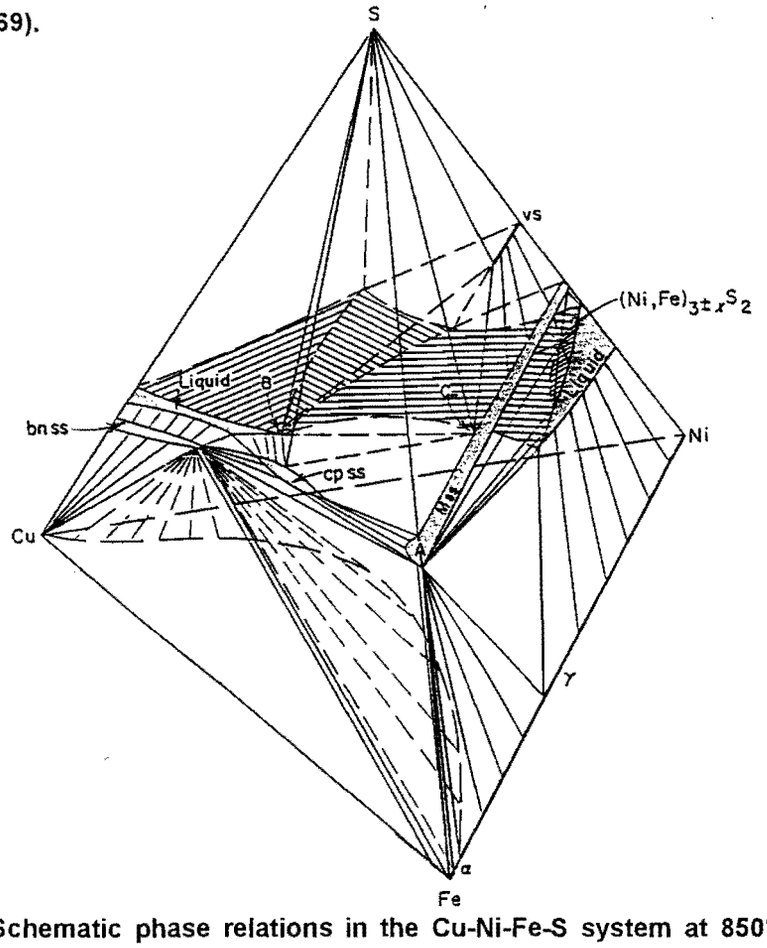

Figure 2.8: Schematic phase relations in the Cu-Ni-Fe-S system at 850°C (Craig and Kullerud, 1969).

3. EXPERIMENTAL PROCEDURES

3.1 Planning of Experiments

The phase diagrams of the Cu-Ni-S system (Bruwer, 1996) were used to plan experiments from 700°C to 1200°C in 100°C intervals. Experiments with the same Cu-Ni-S ratios were repeated with only a variation in the Fe content between 1 wt% Fe, 3wt% Fe, 5 wt% Fe and 10 wt% Fe. The total weight of chemicals per experiment was approximate 0.3g.

The first experiments performed were those for the 1000°C isothermal sections with relative short reaction times (1 month), thereafter those for 700°C, which required longer reaction times (2 to 3 months). The experiments at 900°C and 800°C followed with 1100°C and 1200°C completed last (these high temperature experiments required only a few hours reaction time). In retrospect, the reaction times could have been shortened. However, the feeling was to rather extend the reaction time and to ensure equilibrium than to waste consumables. Experiments that clearly failed after reaction were repeated in the next set of preparations.

3.2 Variation in Starting Fe Content

The content of Fe in the experiments was planned as 1, 3, 5 and 10 wt% of the bulk, respectively. However, due to small variations in weighing the powders into the tubes, the proportions of the final product did not always correspond exactly to the planned starting composition. For example, the planned proportions would be: 10 wt% Cu, 65 wt% Ni, 20 wt% S and 5 wt% Fe. After manual weighing all the powdered elements to an accuracy of 4 decimals, the respective weights are: 0.0284g Cu, 0.202g Ni, 0.0582g S and 0.0146g Fe. Recalculation to weight percentage amounts to: 9.37wt% Cu, 66.62 wt% Ni, 19.20 wt% S and 4.82 wt% Fe. This has the effect that a variation in the starting Fe compositions of experiments existed.

3.3 Reduction Techniques

High purity metal powders and powdered sulphur (Table 3.1) were weighed into quartz glass tubes (with an inner diameter of 4mm and an outer diameter of 6mm), evacuated and melt shut at one end. Metal powders had to be reduced first to remove any surface oxidation on the grains. Initially, the metal powders were reduced before the weighing stage in an H_2 - Ar atmosphere, at 600° to 700°C. The system was first flushed with Ar at a temperature of ~ 200° and then the Ar and H_2 gasses were added at an approximate rate of two bubbles per second. After ~ 6 hours the furnace was turned off and the gas shut at the gas bottles – remaining gas in the tubes maintained the closed atmosphere. This method, however, has

some drawbacks: very fine powders have the tendency to fuse together (sinter), making crushing of the powders (which was by hand in an agate crucible) very tedious and long. The concern was that during this long process of crushing and milling, the grain surfaces might undergo oxidation again (especially metallic Fe).

To avoid this problem, a special container was devised to hold the tubes in a horizontal position in a large borosilicate reduction tube within the muffle furnace (Figure 3.1). With this configuration, the gasses were "blown" directly into the small tubes and reacted with the already weighed metal powders. This method was tested in an experiment with a Cu-oxide powder. The Cu-oxide was weighed into two tubes and then placed in the reduction tube at 400°C for ~ 24 hours. The tubes were weighed before and after and an average loss of ~ 10 wt% was measured. The reduced Cu sample was studied in a polished section to determine the degree of reduction. The result was a complete reduction of all the grains right through to the core of each grain.

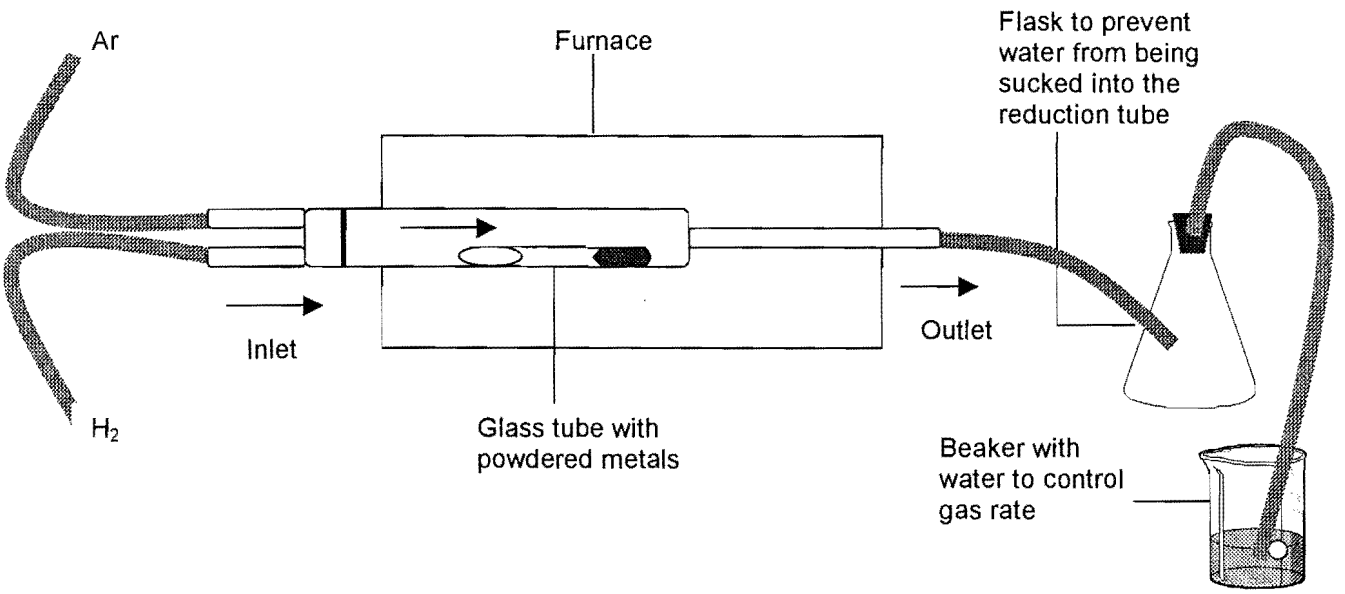

Figure 3.1 Setup for reduction of metals in quartz glass tubes.

The metal powders were reduced in the quartz glass tubes at roughly 400°C (the softening temperature for borosilicate is 820°C) for approximate 12 hours. Immediately after reduction of the metals, dried sulphur powder was added. The powders were covered with a tight fitting quartz glass rod and then the tube was sealed off under vacuum (~2 x 10^{-2} millibar). After each sample was weighed (and sometimes the length recorded to distinguish between samples), the samples were ready to be pre-reacted.

Table 3.1: The percentage purity of chemicals used in experiments of the Cu-Ni-Fe-S system.

Chemical	Purity
Copper (Cu)	99.999 %
Nickel (Ni)	99.99+%
Iron (Fe)	99.99
Sulphur (S)	99.99+

3.4 Heating Techniques

Samples were first placed into a pre-reaction furnace at a temperature between 500° and 700°C. This step was included to ensure that all the free sulphur reacted with the metals. At sudden high temperatures, solid sulphur would turn to gas and result in violent explosions because the sealed glass tube can not withstand such a rapid increase in volume. Limited reaction (of which the extend is difficult to measure without opening the tube) will occur between metals depending on the duration of pre-reaction. After sufficient reaction took place (i.e. not free sulphur visible) samples were quenched in air or immediately transferred to the reaction furnace. To prevent unnecessary strain on the glass, it was found to be better not to quench the samples after pre-reaction, but to proceed immediately to the required reaction temperature.

Samples were then placed into a high-temperature furnace with an accuracy of 1°C (verified with an external thermocouple). The furnaces used for equilibrium reactions were modified to hold 6 corundum tubes with an inner diameter of about 45mm. This modification allows six positions into which samples could be placed. If one sample would brake in one tube the samples in the other tubes were not affected. It was also possible to determine the hot zone in each tube, and to position samples exactly there. However, not all of the six corundum tubes' hot zone were equal in temperature. There was a difference in temperature between tubes of up to 25°C at lower temperatures. This was overcome by measuring the temperature with an external K-type thermocouple and increasing the temperature until the "coolest" tube was at the required temperature in its hot-zone. The thermocouple was again used to determine that position in the other tubes where the desired temperature prevailed.

Initially the samples were melted at a high temperature (between 1000° and 1100°C) to achieve homogenization throughout the entire sample. After a couple of hours the temperature was lowered to the required equilibrium temperature. This melting stage was later abandoned because of early and frequent breakages of the quartz glass tubes. Longer pre-reaction times were found to be sufficient to ensure equilibrium reactions.

The time required to achieve equilibration depends on the temperature and type of reactions investigated. At high temperatures (e.g. >1000°C), reactions take place fast, but at lower

temperatures (e.g. < 800°C), reactions may be hampered by slow reaction kinetics (e.g. the gradual change from a mono-sulphide to a di-sulphide as in the case with Ni-S to NiS_2). Therefore, the time required to achieve equilibrium could take anything from 2 weeks to 2 months or more.

After equilibrium was completed the samples were quenched in water by dropping it in a long cylindrical container. The temperature in the sample dropped within seconds from hundreds of degrees to room temperature. Samples were weighed again to identify each one and then the contents were described. In some experiments, the reactants separated and the extent of equilibrium was uncertain. Physical separation of solids from the melt due to density differences might cause separation, or surface tension between two melts could have cause them to detach from each other. Separation might also be a result of movement during quenching and does not always imply separation during reaction and dis-equilibrium. Experiments that contained two or more separate pieces after quenching were usually discarded and repeated.

3.5 Mounting and Labeling Technique

The glass tubes were carefully broken to release the contents in one piece. The reacted sample was then divided (with a stainless steel knife and a small hammer) into two pieces: one piece was used in a polished section and the other piece was stored as a reference. Because of the size of the samples (<4mm), an average of 5 samples were mounted in one section (with a diameter of 2.5cm) (Figure 3.2) together with a reference Cu-rod. The sections were labeled using the equilibration temperature and an alphabetic symbol. The experiment number carried the section label followed by a number (1 to 5) indicating the position on the section (after polishing) in a clockwise direction.

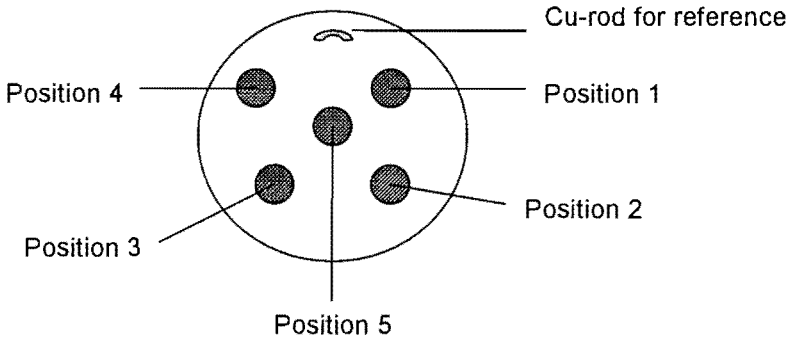

Figure 3.2: Example of a polished section; indicated are the position of the reference Cu-rod and the other positions on the sample.

3.5 Descriptive Techniques

Sections were polished and then described using a reflected light microscope. Sections were carefully studied for the presence of small oxide phases that indicated that the experiment was not conducted in a closed four-element system. The glass tube might have cracked during reaction and allowed air to penetrate the sample. Photographs taken of each experiment at different magnifications assisted in the analytical procedures and served as visual reference.

3.6 Experimental Difficulties

A large number of experiments failed due to cracking of the quartz glass tube during either pre-reaction or reaction. It is believed the particular batch of quartz glass available for these experiments, was not of a suitable quality to withstand reaction at high temperatures (typically higher than 1000°C) or quenching from high temperatures. Eliminating the melting stage and limiting equilibrium reactions at temperatures above 1000°C to a few hours, did help to prevent cracking of the glass. All future experiments were conducted in this fashion to prevent a repetition of such an event with other quartz glass batches.

In some experiments the tapered tip of the glass tube resulting from melting the tube shut at one end caused zoning or uneven mixing of the reactants during reaction. An attempt to limit zoning or separation was made by altering the arrangement of reactants in the tube: A glass rod was placed into the tube first, then the metal- and sulphur powders and then another piece of rod. The tube was then sealed off under vacuum (Figure 3.3). After reaction and quenching of four test samples, the metal-sulphur sample in all of the experiments were in one piece with no external indications of zonation or separation.

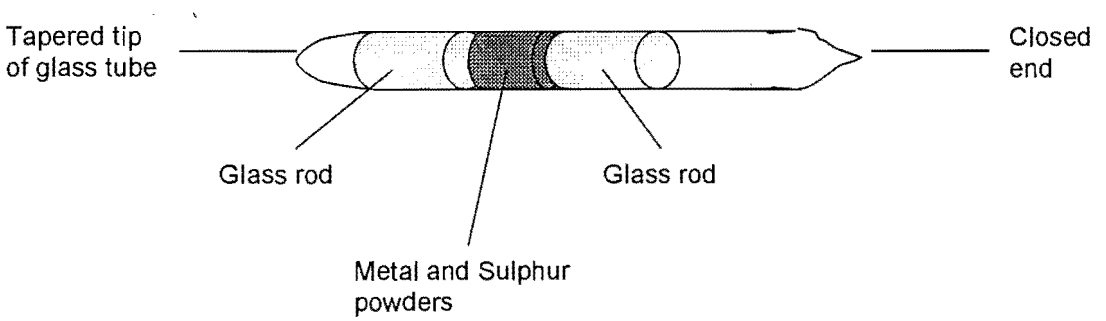

Figure 3.3: The configuration for some of the experimental samples. A quartz glass rod is placed at both ends of the metal and sulphur powders, and then the quartz glass tube is sealed under vacuum.

The second problem of separation of material in the tube during equilibration, is mainly attributed to the fact that a larger volume is left in the tube after reaction of the sulphur with the metals. After quenching it could not be determined whether separation took place during

reaction or during quenching. In the first instance the experiment would be in dis-equilibrium but this is not the case in the second instance. The separated pieces could be re-tubed, but this required grinding and milling of the material to reduce the occupied space in the quartz tube. The process of grinding and milling an already reacted sample was very time consuming and mostly not practical due to the toughness of the alloy in particular. Some of the original starting material was lost in this procedure, and the possibility of oxidation during milling (especially if Fe is present) was an unmeasurable factor to take into account. Normally, a sample of each separated piece was mounted and evaluated optically and analytically to determine dis-equilibrium, based on compositional variation exceeding an analytical uncertainty at the 1 σ level. If dis-equilibrium was suspected the entire experiment was repeated with newly weighed material.

4. ANALYTICAL PROCEDURES

4.1 Analytical Preparation

The polished sections were cleaned and coated with a thin carbon layer (~200 nm) to ensure good conductivity, then placed in a desecrator to keep it dry and free of contamination until it could be analyzed.

4.2 Analytical Techniques

A JEOL Superprobe 733 were used for the wavelength dispersive analyses at a beam current of 20nA and an acceleration potential of 20kv. For large homogeneous phases (i.e. alloys and sulphides) spot analyses were used, and for heterogeneous phases (i.e. sulphides with exsolutions or quenched melts) a defocused beam (with diameter of 40μm) or area analyses (of 1.5μm x 2.0μm) were most effective. Pure Cu, Ni and Fe metals were used as standards for the alloy phases, and millerite, chalcopyrite and troilite were mostly used as standard for the sulphide and melt phases.

A peak seek was performed daily on all the elements to be measured for a specific phase. A general standardization or re-calibration followed, during which the counts for each element (background as well as at peak positions) were detected and compared with the previous day's counts. Counting time on the background was 25 seconds and on the peek 50 seconds. A change in count rates due to some mechanical problem could easily be detected and steps taken to improve conditions for measurement.

Difficulties encountered in collecting electron microprobe (EMP) analyses of quenched sulphide melts are the generally coarse grained texture of these melts and the lack of suitable standards. A sulphide melt cannot be quenched like a silicate melt, but crystallizes in a fine intergrowth of different phases. If spot analyses are used, a large number of single analyses on a closely spaced grid must be collected to obtain a representative composition of the melt in total. The availability of analytical time will influence the number of analyses that can be collected from a single melt phase. In area analyses, the beam is scanning a selected area and only remains on one position for a very short period of time during which data is collected. After the required counting time, the analytical result is representative of the composition of the area. This method requires (apart from a standard with the same phases and textures, see below) that a large enough area (consisting only of melt) is available for analysis. In this investigation, suitable areas for area-analysis could not always be defined. The method of defocused beam analysis involves increasing the diameter of the beam spot to a size larger than most of the grain sizes in the quenched melt. The composition of a small round area is then given, and the mean value of a number of small areas is taken as the average composition. In experiments, where only a small portion of the quenched melt is

intersected in the polished section, this method worked best. However, in situations like these, the possibility of collecting data that fully represent the melt becomes very limited.

In an attempt to improve the results of coarse textured quenched melt phases, melt standards with a known chemical composition were produced in the lab and quenched from 1200°C. These standards differ in composition and texture. Although the standards did not always match exactly the texture and composition of the unknown melt phase, analytical result are in most cases considered "good" (i.e. small standard deviations and matching tie-line angles).

The area and number of analyses were selected based on the texture of the phase to be analyzed. Therefore, an overview on the textural appearance of the different phases is given in the next chapter.

4.3 Reproducibility Tests

To determine the reproducibility of the data, duplicate analyses were collected under identical conditions from alloys and exsolution-free sulphides (Table 4.1). Analyzed twice, the same analytical point should under identical conditions result in identical composition. However, due to variations in the mechanical and electronic conditions as well as normal variations in counting statistics, the values are not identical for each element analyzed. By determining the deviation from duplicate analyses, these variations become quantifiable. The deviation of analytical results given in the EMP analyses could be determined. Any larger variation in the composition will be due to true compositional variations.

The standard deviation was derived, following the recommendations of Kaiser and Specker (1956), with the formula:

$$s = \sqrt{\frac{\sum_{1}^{N/2} (v_i - v_j)^2}{N}}$$

Where: s = standard deviation (1s)
v = duplicate analyses
N = number of analyses

Table 4.1: Reproducibility results for alloy, digenite, millerite and vaesite.

Alloy 1				Alloy 2				Alloy 3			
Elements	Range	Std. Dev.	No. Anal.	Elements	Range	Std. Dev.	No. Anal.	Elements	Range	Std. Dev.	No. Anal.
Cu	44.47 - 42.32	0.42	20	Cu	42.66 -40.22	0.50	20	Cu	45.04 - 40.02	0.37	20
Ni	53.81 - 50.19	0.21	20	Ni	52.87 - 51.35	0.17	20	Ni	50.63 - 48.03	0.19	20
Fe	1.29 - 1.20	0.01	20	Fe	2.64 - 2.54	0.03	20	Fe	5.50 - 4.56	0.02	20

Digenite 1				Digenite 2				Digenite 3			
Elements	Range	Std. Dev.	No. Anal.	Elements	Range	Std. Dev.	No. Anal.	Elements	Range	Std. Dev.	No. Anal.
Cu	74.27 - 69.94	0.48	30	Cu	77.24 - 73.45	0.64	28	Cu	74.66 - 70.22	0.59	28
Ni	0.87 - 0.12	0.03	30	Ni	1.45 - .24	0.01	28	Ni	0.31 - 0.07	0.01	28
Fe	2.05 - 1.81	0.03	30	Fe	0.36 - 0.09	0.03	28	Fe	1.38 - 0.30	0.12	28
S	21.71 - 21.04	0.14	30	S	19.80 - 18.99	0.12	28	S	20.09 - 19.09	0.14	28

Millerite 1				Millerite 2				Millerite 3			
Elements	Range	Std. Dev.	No. Anal.	Elements	Range	Std. Dev.	No. Anal.	Elements	Range	Std. Dev.	No. Anal.
Cu	2.50 - 0.52	0.09	30	Cu	0.12 - 0.06	0.02	30	Cu	3.15 - 0.68	0.05	30
Ni	61.07 - 57.73	0.38	30	Ni	61.41 - 59.27	0.54	30	Ni	59.12 - 56.16	0.35	30
Fe	0.82 - 0.75	0.01	30	Fe	1.26 - 1.18	0.02	30	Fe	1.69 - 1.52	0.02	30
S	39.42 - 36.04	0.15	30	S	37.53 - 36.69	0.20	30	S	37.46 - 36.40	0.22	30

Vaesite 1				Vaesite 2				Vaesite 3			
Elements	Range	Std. Dev.	No. Anal.	Elements	Range	Std. Dev.	No. Anal.	Elements	Range	Std. Dev.	No. Anal.
Cu	1.80 - 1.03	0.06	28	Cu	0.10 - 0.05	0.01	30	Cu	3.52 - 0.51	0.03	56
Ni	46.95 - 45.28	0.40	28	Ni	47.90 - 45.80	0.24	30	Ni	46.84 - 43.02	0.39	56
Fe	0.16 - 0.06	0.01	28	Fe	0.49 - 0.12	0.01	30	Fe	0.23 - 0.04	0.01	56
S	52.21 - 49.73	0.26	28	S	52.33 - 50.72	0.19	30	S	52.20 - 51.36	0.26	56

4.4 Data Evaluation

At the start of the project, a large number of analyses were collected of seemingly homogeneous phases to ensure that there is no change in composition from the rim to the center of the mineral phase. After homogeneity was confirmed of alloys and exsolution-free sulphide phases, the amount of analyses were decreased considerably.

Precision is determined by the reproducibility of analytical results, while accuracy is displayed in the resemblance of analyzed results to expected results. High precision was achieved by frequent standardization and control measurements on standards, as well as monitoring the count rates on these standards. A high kV and mA, and a stable electron beam increased the total counts and decrease the statistical variation that was determined by the number of counts High accuracy was obtained by testing the standardization on a specimen with known composition and correcting any deviations larger than ± 3s that is not due to the heterogeneity of the specimen.

Data were carefully evaluated and the reliability of analyses were tested statistically. Because most of the quenched melts are heterogeneous with two or three components, the standard deviations of the melt analyses are relatively high in comparison with the alloy and sulphide phases. It was therefore felt necessary to follow an independent approach to determine the average composition of the melt and the reliability of this average value. This was conducted by applying Resampling Statistics (Simon, 1997; Westfall & Young, 1992) which involves the random selection of analyses from a data set. The selection is repeated for e.g. 15000 times, each time using the original data set as a "pool" to construct a new data set. The original data set is thus randomly duplicated to create a new data set with much more data. Statistical calculations of this new data set will be a closer representation of the smaller data set. An example of such a recalculation is given in Appendix A.

After resampling was performed on the analyses from selected melt phases, the mean values did not change (which underlines the reliability of the analytical approach) but the confidence intervals (ci) for the average composition of these melts were much better defined. EMP results treated in this manner are indicated on the tables for the different equilibrium temperatures (Appendix C). The total number of successful experiments carried out and electron microprobe analyses collected are summarized in Table 4.2.

Table 4.2: Total amount of experiments and analyses.

Temperature	Total Experiments	Total Analyses
1200	22	1348
1100	31	2947
1000	41	3141
900	60	5589
800	61	4632
700	36	2905
Total	**251**	**20562**

The means of the recalculated values were plotted on quaternary and ternary diagrams with the aid of a statistics package (Statistica). Due to limitations in displaying a four composnent system in two

dimensions it was necessary to evaluate the shape of the liquidus in the third dimension, and whether a projection onto the Cu-Ni-S ternary is an acceptable estimation.

In a system with three components at a fixed temperature and pressure, an univariant point (i.e. a position in a two phase field like Alloy+Melt) will have one degree of freedom according to the phase rule.

$$P + F = C + 2$$

(where P = number of phases, F = degrees of freedom, C = number of components)

$$2 + F = 3 + 0$$

$$F = 1$$

However, in a four component system, the degrees of freedom is two:

$$P + F = C + 2$$

$$2 + F = 4$$

$$F = 2$$

This implies that to uniquely define a tie-line in this two-phase field, two variables must be fixed. If the Cu/Ni ratio in the starting composition and the temperature of equilibration is fixed, a plot of the Fe: S content in the melt will give an indication of the shape of the liquidus in the dimension not observed in the projection onto the Cu-Ni-S ternary. This was evaluated for 4 experiments at 1200°C and 4 experiments at 1100°C temperature intervals (Table 4.3 and Fig. 4.1). These experiments have the same Cu/Ni ratio i.e. ~ 0.12 at 1200°C and ~ 0.50 at 1100°C. Incorporating the 95% confidence intervals, the sulphur content in the melt could not be safely distinguished (the lower sulphur content of experiment 12m4 is attributed to a small proportion of a very coarse grained melt which contains large dentritic alloy). This plot shows that although the shape of the liquidus in the third dimension for small quantities of Fe is not smooth, the slope is still very steep and that a projection from a prism onto the Cu-Ni-S ternary will be valid for descriptive purposes. Projections from a prism appear similar to plots in a Fe-free system as shown in Figures 4.2 and 4.3. A numerical example of the conversion of a bulk composition to the plotted values in the Cu-Ni-S ternary, is given in Table 4.4.

Table 4.3: The EMP results for the melt phase in the assemblage (Alloy+Melt) from experiments at 1200°C and 1100°C and a Cu/Ni ratio in the starting composition of ~ 0.12 and ~ 0.50 respectively (ci = 95% confidence interval).

1200°C	Exp. No.	Fe	S	*ci for S*	*S - ci*	*S + ci*
	12l4	0.52	19.21	*1.41*	*17.80*	*20.62*
	12m4	1.09	16.16	*1.41*	*14.75*	*17.57*
	12n4	1.42	20.37	*1.33*	*19.04*	*21.70*
	12o4	4.03	20.04	*0.93*	*19.11*	*20.97*
1100°C	**Exp. No.**	**Fe**	**S**	***ci for S***	***S - ci***	***S + ci***
	11b3	0.52	15.95	*1.21*	*14.74*	*17.16*
	11d3	2.20	13.82	*1.34*	*12.48*	*15.16*
	11f2	3.00	14.47	*1.20*	*13.27*	*15.67*
	11h3	6.19	15.21	*0.97*	*14.24*	*16.18*

Table 4.4: A numerical example of the conversion of a bulk composition to the plotted Cu, Ni, S values. For a projection onto the ternary Cu-Ni-S plane, the value of Fe is taken to be 0.

Bulk composition					Normalized values				
Cu	**Ni**	**Fe**	**S**	**Total**	**Cu**	**Ni**	**Fe**	**S**	**Total**
27.33	54.55	8.94	9.18	100	27.33/ 91.06	54.55/ 91.06	0	9.18/ 91.06	1
27.33	54.55	0	9.18	91.06	X100	X100		X100	X100
					30.01	59.91	0	10.08	100

If the starting composition indicates that the experiment did fall into a multi-phase stability field but not all of the phases in the assemblage occur in the section, it was assumed that other phases could exist. It was decided not to grind the polished section down any further for fear of loosing other experiments in the same section (that have a different three-dimensional size). For example, in the 3 component stability field containing the cotectic alloy, digenite and melt (Fig. 4.4), some of these phases may not be intersected in the polished section. If the starting composition and/or the composition of the observed phases indicate that the experiment does fall into this field then the observed phase(s) were treated as being part of a 3-phase assemblage. In cases where more than one experiment (in the same isothermal section) forms part of the same 3-phase assemblage the mean values of the phases from the different experiments were calculated.

Starting compositions are not indicated on the phase diagrams to simplify the diagrams, but are given in Appendix B. Dotted tie-lines are extrapolation to a composition based on the direction of adjacent tie-lines and/or available field boundary lines. Dotted field boundary lines are indications of where the stability fields could be, but are not well defined due to insufficient data points.

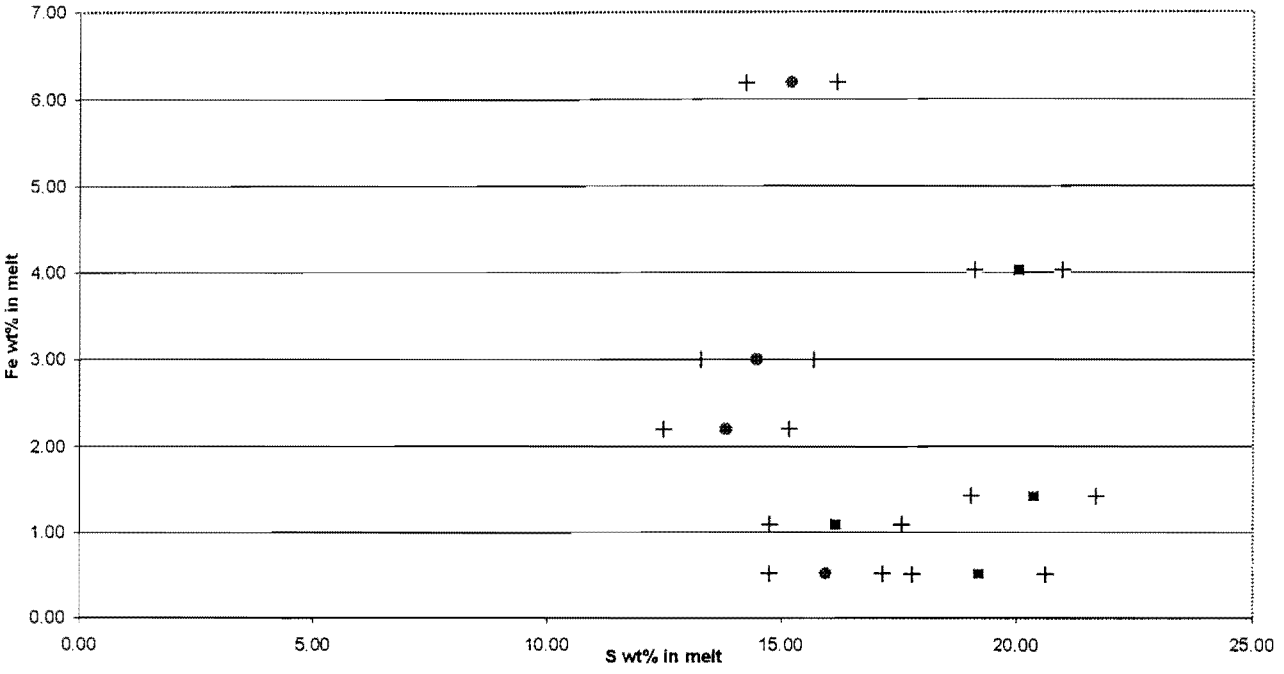

Figure 4.1 :Composition of melt in equilibrium with alloy. At 1200°C (squares) with a Cu/Ni of ~0.12 and at 1100°C (circles) with a Cu/Ni ratio of ~0.50. Also indicated are the 95% confidence intervals (crosses).

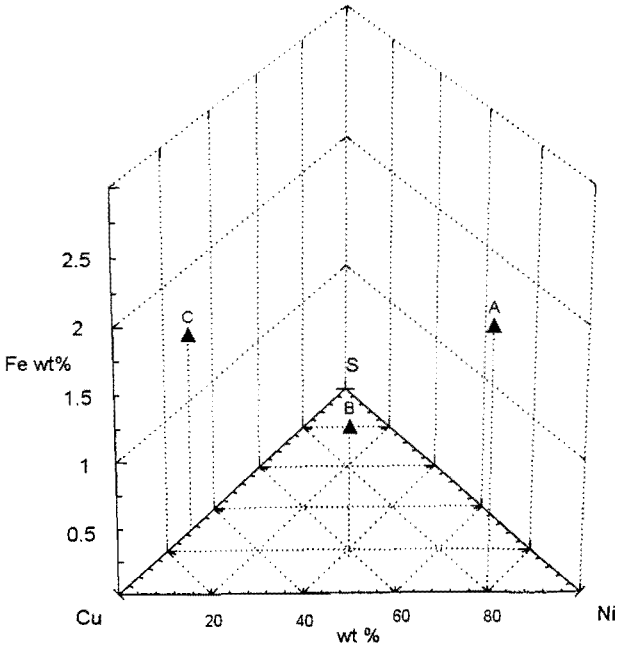

Figure 4.2: A graphic presentation of three data points (A, B and C) in a quaternary diagram. The axis for Fe extends perpendicular to the triangle into the third dimension

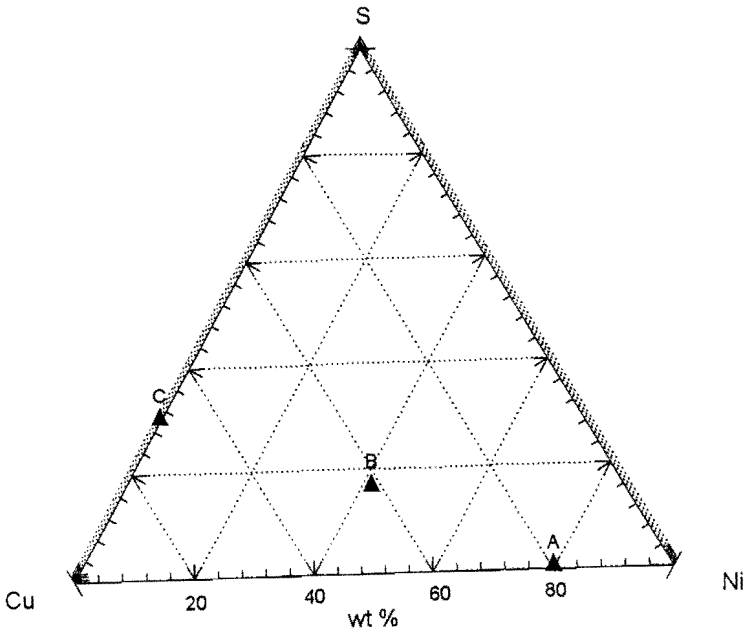

Figure 4.3: A projection of the three data points (A, B and C) onto the floor of the quaternary diagram.This plot is similar to a plot in the Fe-free ternary system Cu-Ni-S, and the Fe value of the points can not be derived from this plot.

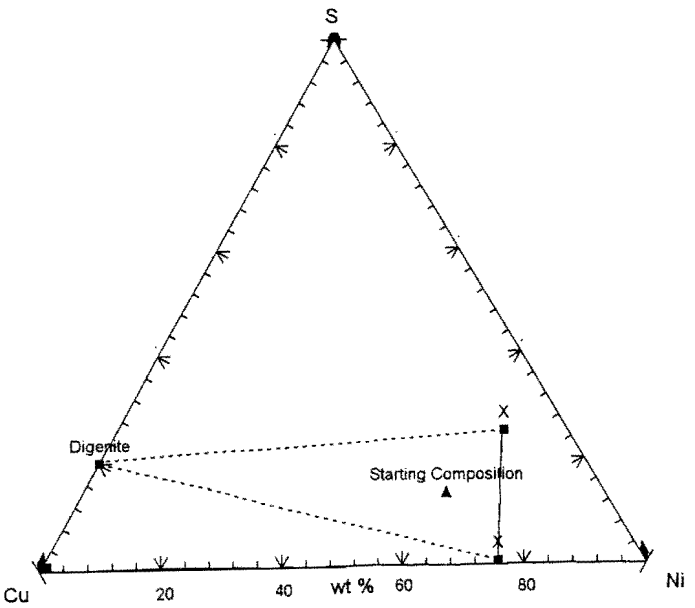

Figure 4.4: The starting composition indicates that the experiment x falls into the three component stability field, even though only two of the three phases (marked x) are observed.

5. PHASES AND TEXTURAL CHARCTERISTICS

Obtaining a representative section is also influence by the phases present. If a large amount of alloy is present, brittle sulphides and quenched melts are likely to break in small pieces and detach from the harder alloys during cutting. Experiments containing only alloy and digenite often formed a spongy texture. During grinding and polishing of such a sample, the brittle digenite might be ripped out from between the alloy in the sample.

The solid phases are texturally and compositionally homogeneous, with the exception of exsolution textures in digenite and some millerite. Sulphide melts can not be quenched successfully and therefore represent mixtures of crystallized sulphide and/or alloys, giving it a heterogeneous texture.

5.1 Alloys

Alloy phases occur mostly as well defined homogenous grains. There are no compositional or textural differences between the core and the rims of the alloy grains. The rims of the grains are mostly smooth but sometimes appear uneven with evaginations when in contact with a melt in which alloy is one of the components (Photograph 5.1). It appears that small alloy grains, which formed on quenching from the melt, overgrow onto the larger (older) alloy grain. The small alloy grains in a quenched melt phase often appear as perfectly euhedral crystals (Photograph 5.2) which may arrange themselves in skeletal patterns (Photograph 5.3).

5.2 Digenite

Digenite has a light blue colour in plane polarized light and occurs as irregular or rounded grains. In quenched melt, digenite often displays skeletal growth patterns (Photograph 5.4). Digenite may, or may not, contain exsolutions, depending on the equilibrium temperature.

Exsolution-free digenite occurs in association with an alloy phase at temperatures lower than 900°C. Frequently, these exsolution-free digenite contains blobs of metallic Cu at the contacts with the alloy or around gas bubbles in the digenite (Photograph 5.5). The appearance of metallic Cu is not exclusive to exsolution-free digenite but also occurs in assemblages of digenite with exsolutions. A rim of metallic Cu at the contact of exsolution-digenite with melt was occasionally observed.

In digenite with exsolutions, two types of exsolutions occur: skeletal exsolutions (Photograph 5.6) and round exsolutions (Photograph 5.7). The round exsolutions are far more common and vary in size and abundance. Both types of exsolutions can appear together in digenite. In most of the experiments, the exsolutions (both round and skeletal exsolutions) will disappear towards the contact of the digenite grain with other phases. In some experiments, a thin exsolution rim of a Ni-rich sulphide phase was observed at the contact between the digenite and the adjacent phase.

5.3 β-phase

At 800°C and lower, a phase was observed that is optically and chemically different from digenite. In plane polarized reflected light this phase appears brownish and tarnishes easily (it also has a completely different color than digenite when coated with carbon). It is not stoichiometric bornite but contains more sulphur and less Cu than digenite and will be referred to as phase "β".β-phase was only observed in assemblages with vaesite, millerite and melt (i.e. with starting compositions high in sulphur). It always contained round exsolutions of the same type that was observed in digenite (Photograph 5.8). Digenite and β-phase were never observed in the same experiment. This phase will be discussed more comprehensively in chapter 7.

5.4 Covellite

Covellite only occurred in very small quantities adjacent to digenite or β-phase (Photograph 5.9). Kullerud (1965) investigated the stability relations of covellite in the Cu-S system and found that covellite breaks down to digenite and sulphur above 507°C. The presence of covellite in some experiments may indicate a metastable existence due to fast quenching.

5.5 Millerite

Millerite appears yellow and slightly pleochroic in normal polarized light. The millerite grains are anhedral and may contain round (Photograph 5.10) or flame-like exsolutions (Photograph 5.11) of a Cu-rich sulphide. These exsolutions are too small to quantify the exact composition.

5.6 Vaesite

Vaesite has a gray color in plane polarized light, and appears as subhedral or anhedral grains. No exsolutions were observed, but uneven round "inclusions", that appear like gas bubbles, were occasionally detected in the center of grains (Photograph 5.12).

5.7 Melt

The term "melt" refers to the component of the experiment that was still liquid at the time of quenching, but that had cooled down relatively quickly to produce a mixture of phases. The aim when quenching was to produce the finest texture possible, but textures depend on the cooling rate, the starting composition (i.e. proportion and type of solids to melts) and the crystallization temperatures of phases that form on quenching. Diffusion speeds are higher at higher temperatures, so if the composition causes a phase to start crystallizing at higher temperature, it will be coarser. The degree of heterogeneity (i.e. variations in sites of crystallites) differs from experiment to experiment.

Melts in the (alloy+digenite+melt)-assemblage consist of euhedral or skeletal alloy grains, dendritic digenite and a groundmass of a Ni-sulphide (Photograph 5.13). In the melt with a Cu-rich starting composition, the proportion of digenite to Ni-sulphide is high (Photograph 5.14), and likewise the melt

from a Ni-rich starting composition has a higher proportion of Ni-sulphide than digenite (Photograph 5.15). The proportion of alloy in such melts is fairly constant but the composition of the alloy is variable. The melts co-existing only with sulphide(s) have no alloy component (Photograph 5.16).

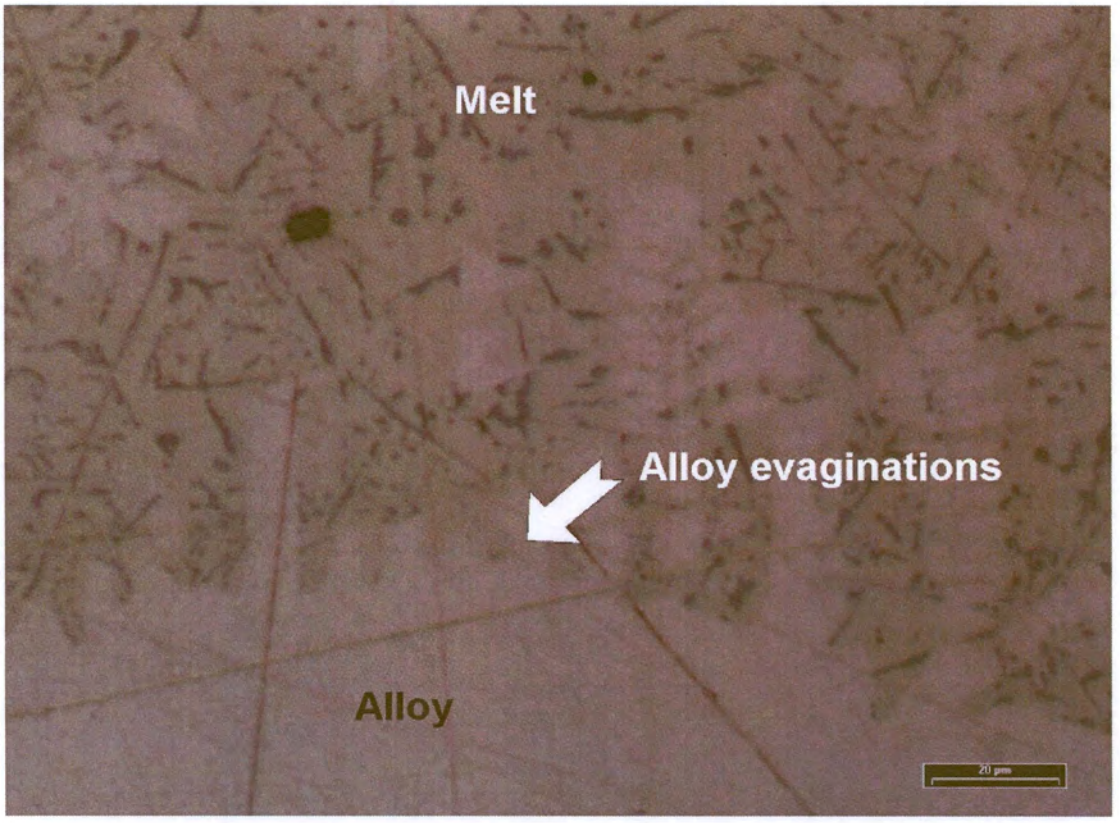

Photograph 5.1: Alloy and associated melt with evaginations of alloy (experiment 7d2).

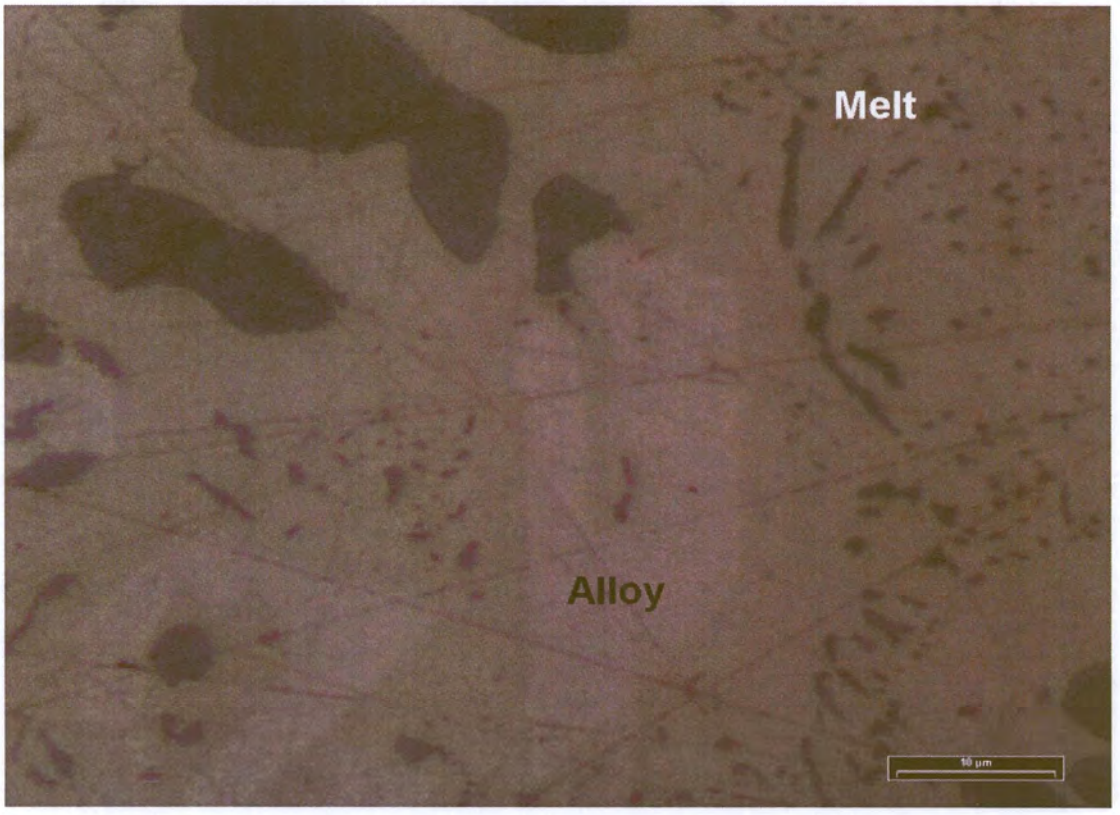

Photograph 5.2: Melt with euhedral alloy crystals (experiment 8a4).

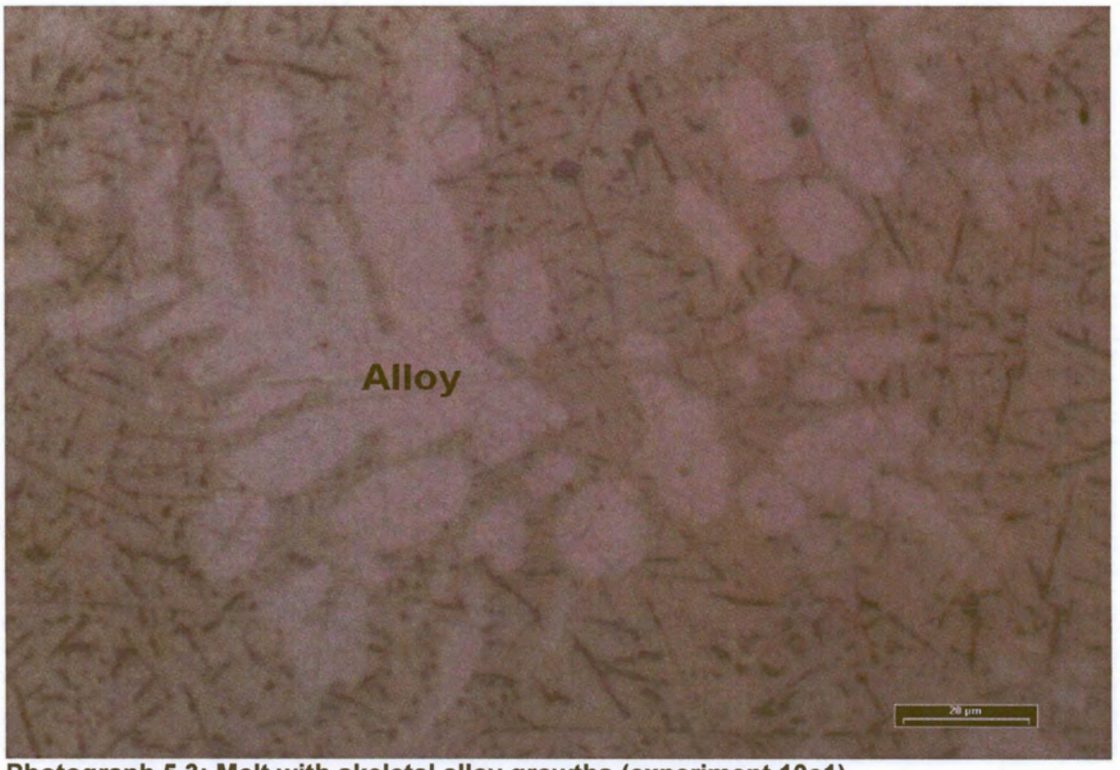

Photograph 5.3: Melt with skeletal alloy growths (experiment 10e1).

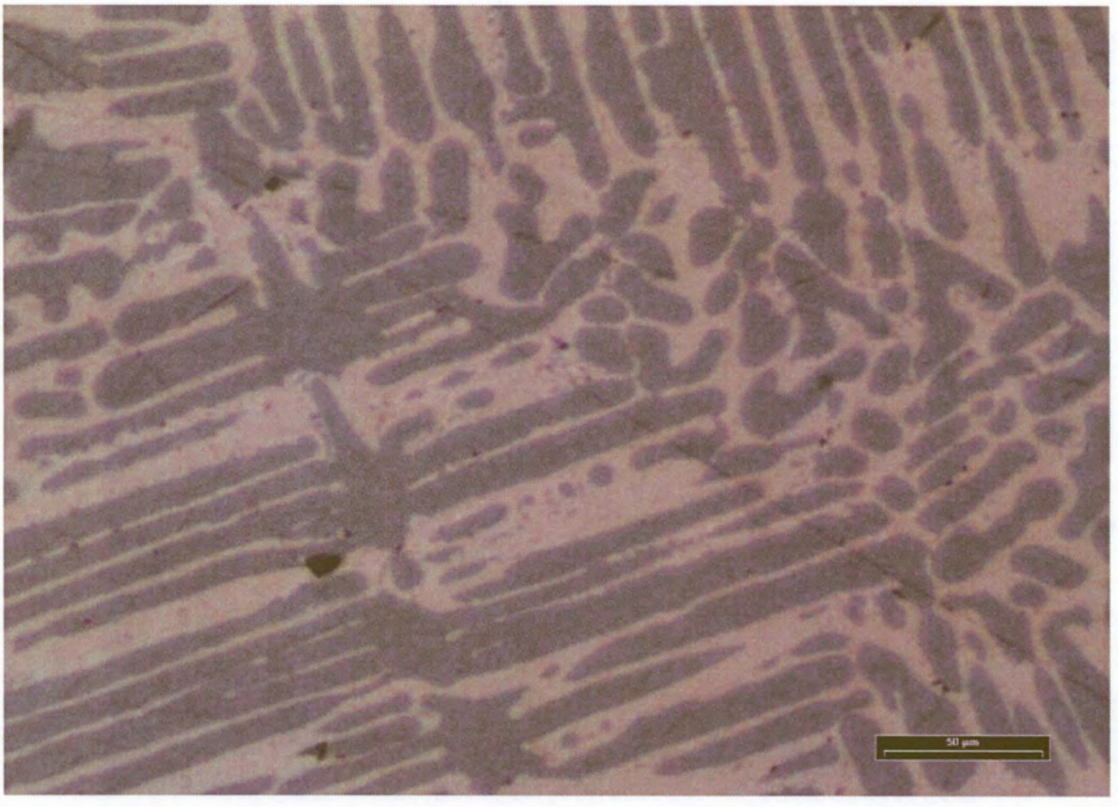

Photograph 5.4: Digenite crystals in melt with dendritic growth (experiment 10i3).

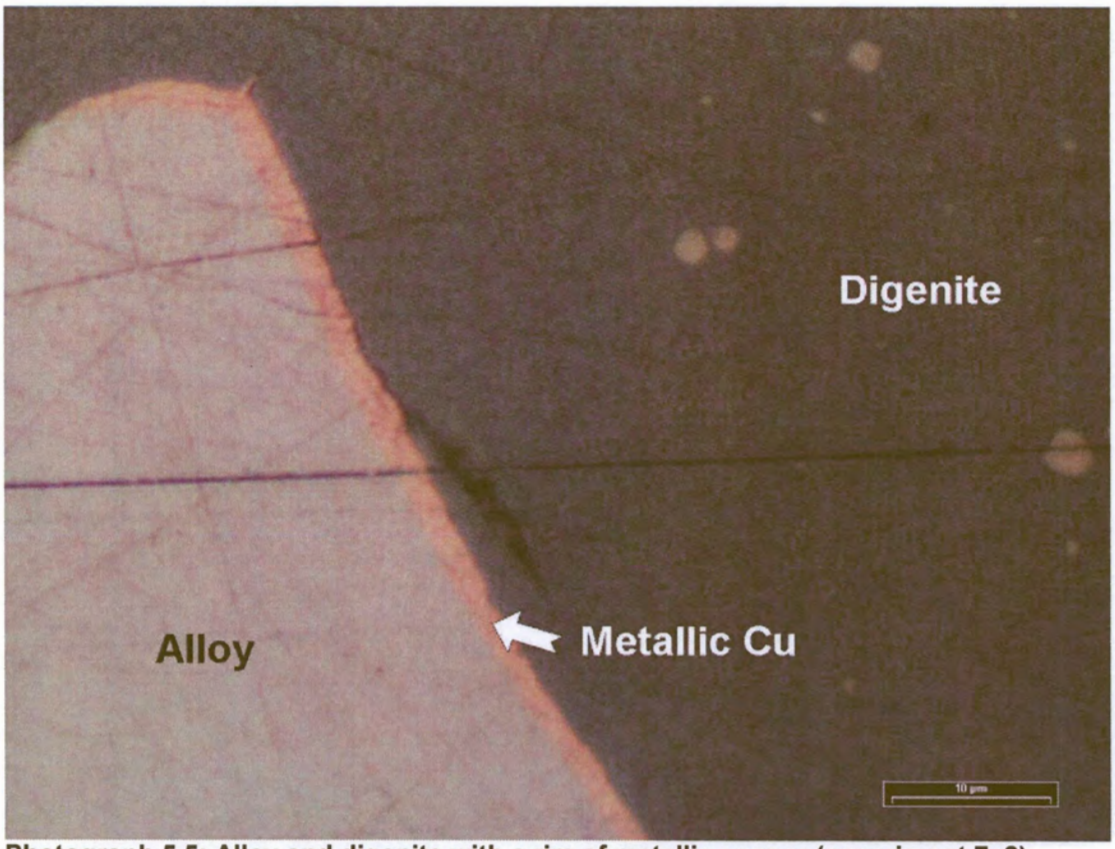

Photograph 5.5: Alloy and digenite with a rim of metallic copper (experiment 7e2).

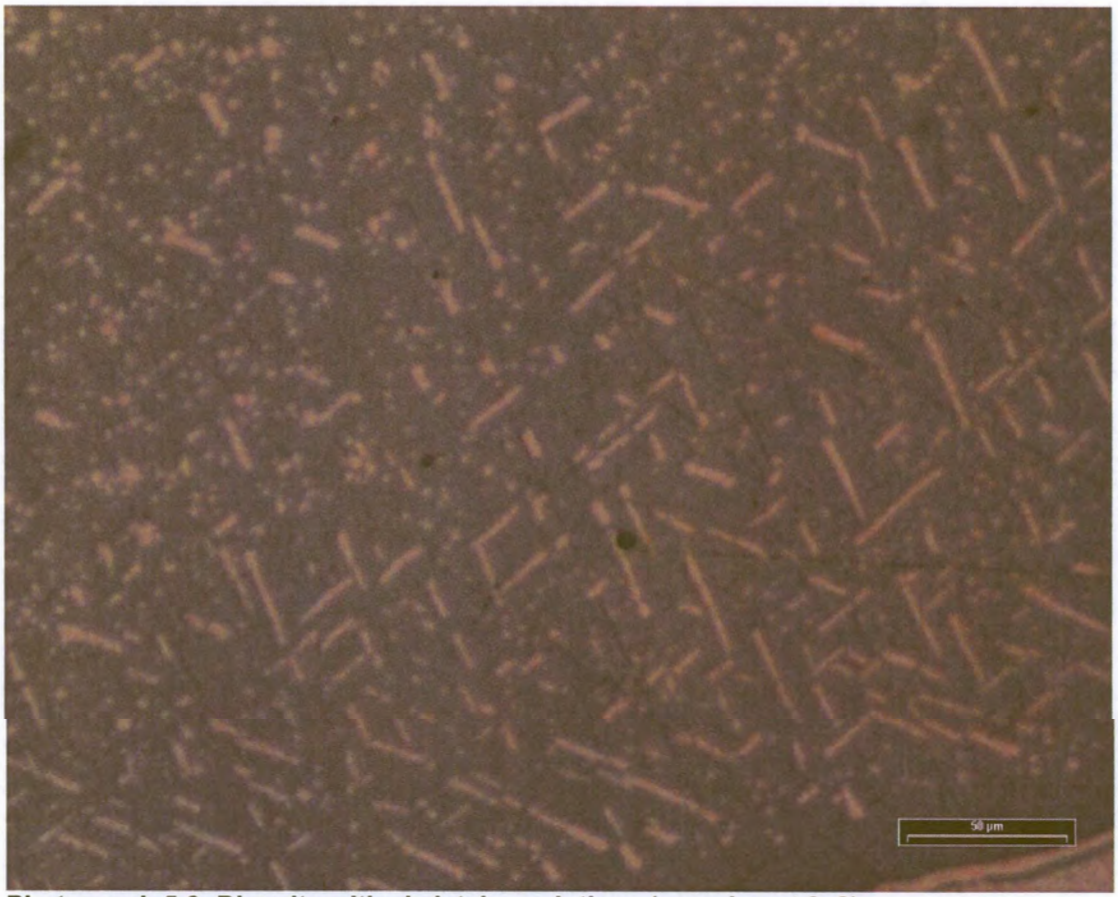

Photograph 5.6: Digenite with skeletal exsolutions (experiment 9e3).

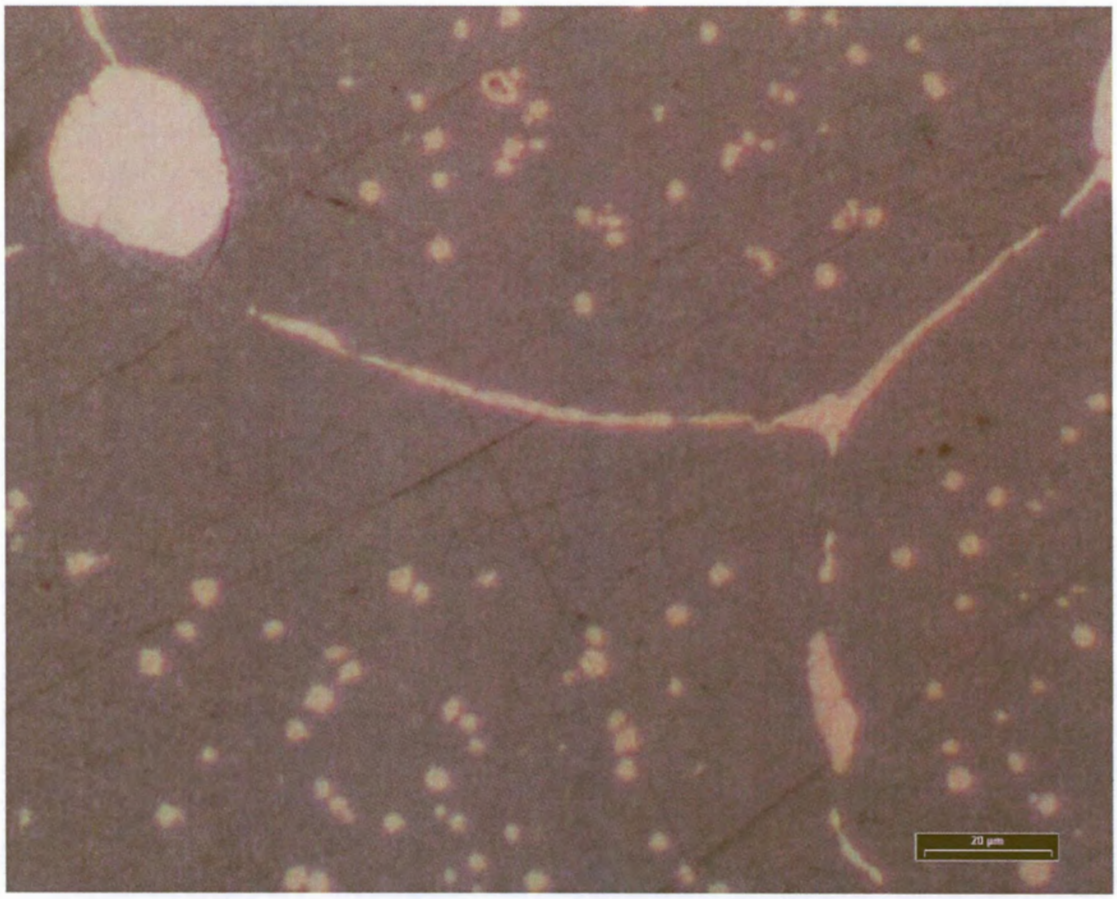

Photograph 5.7: Digenite with round exsolutions (experiment 9d4).

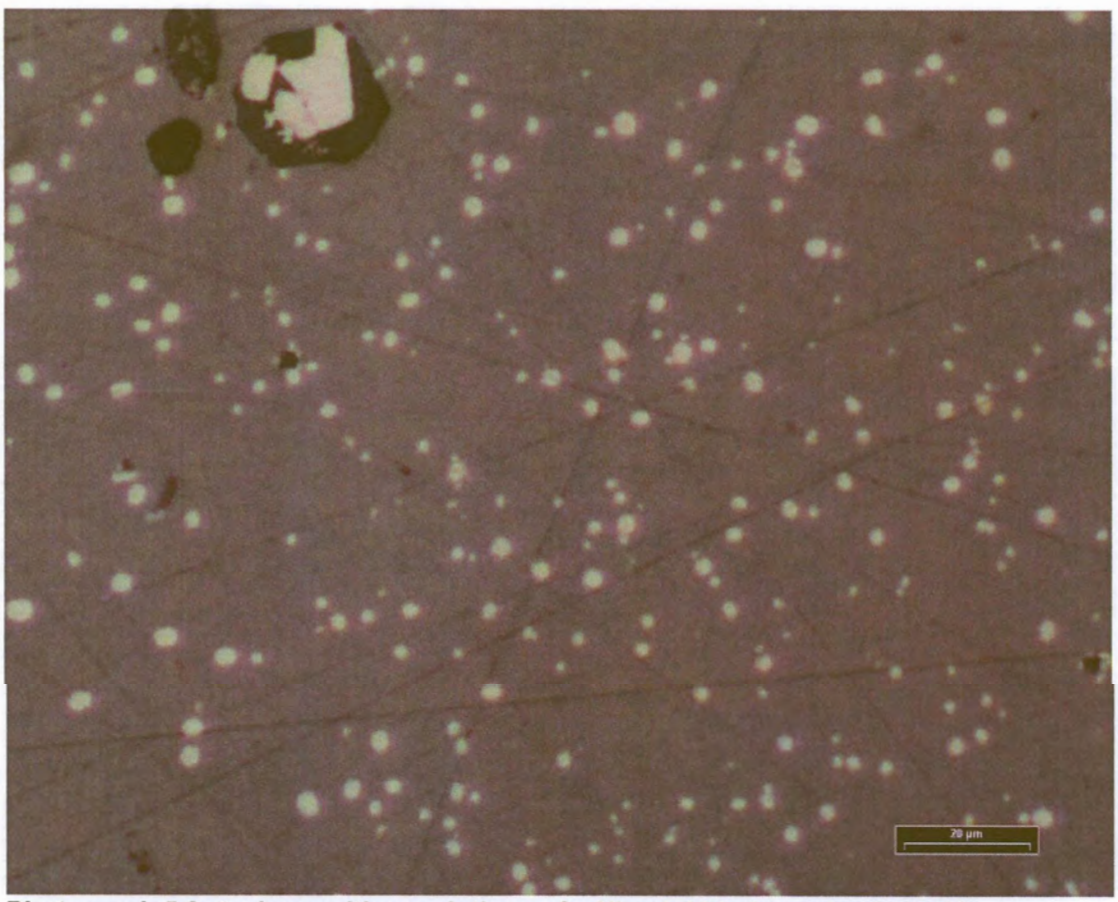

Photograph 5.8: β-phase with exsolutions of a Ni-sulphide (experiment 8m5).

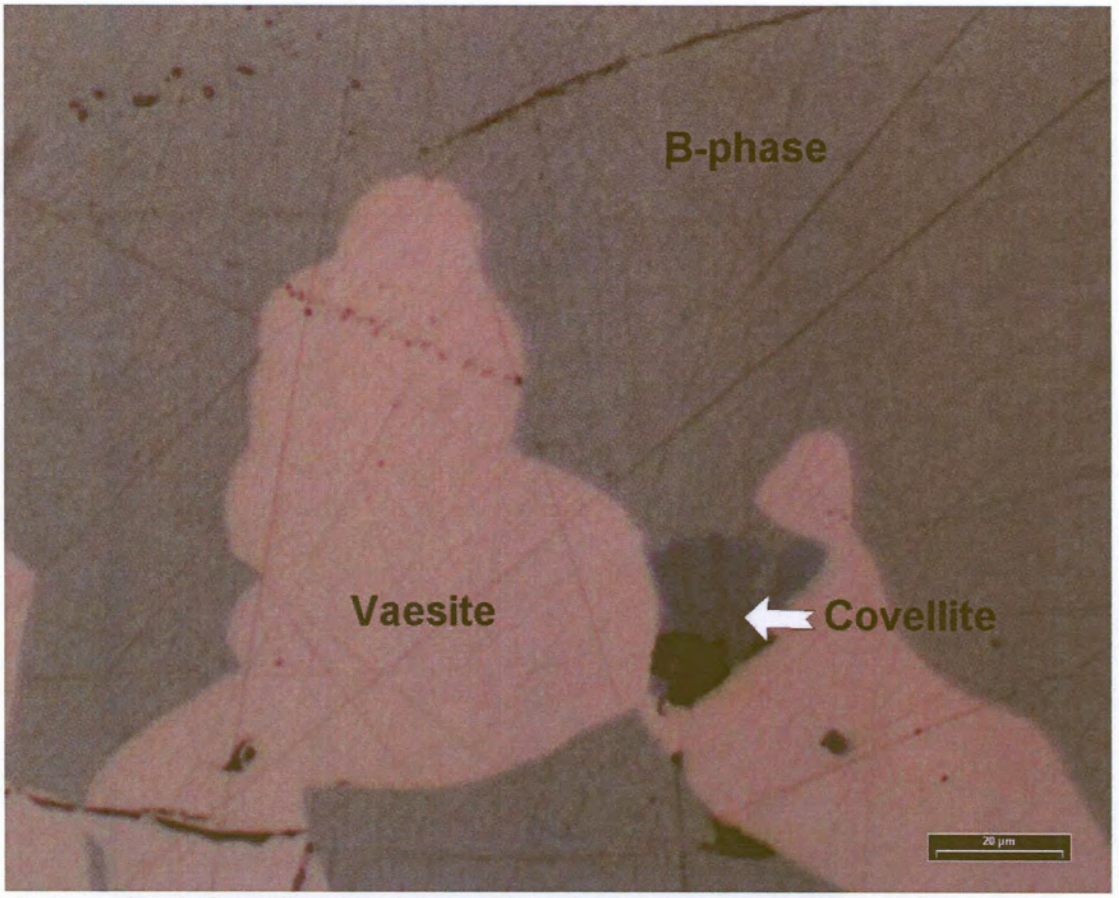

Photograph **5.9: Covellite associated with β-phase (experiment 7h4).**

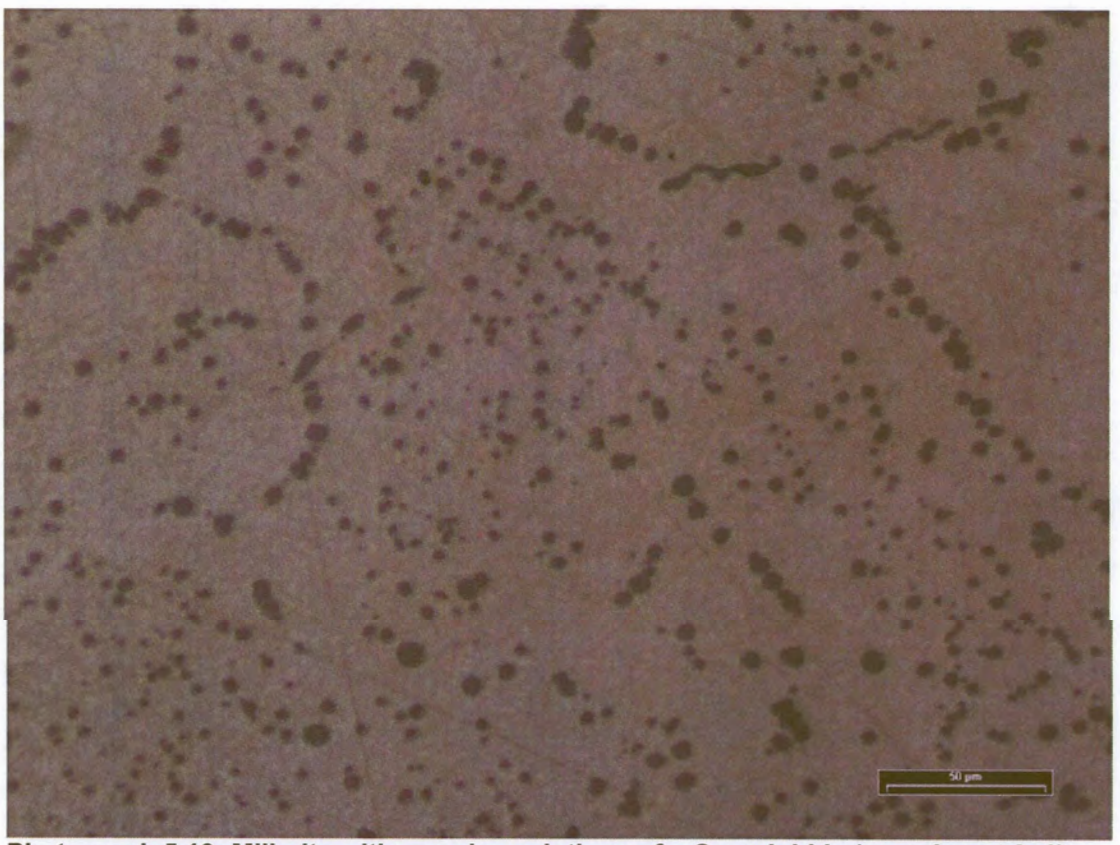

Photograph 5.10: Millerite with round exsolutions of a Cu-sulphide (experiment 8a1).

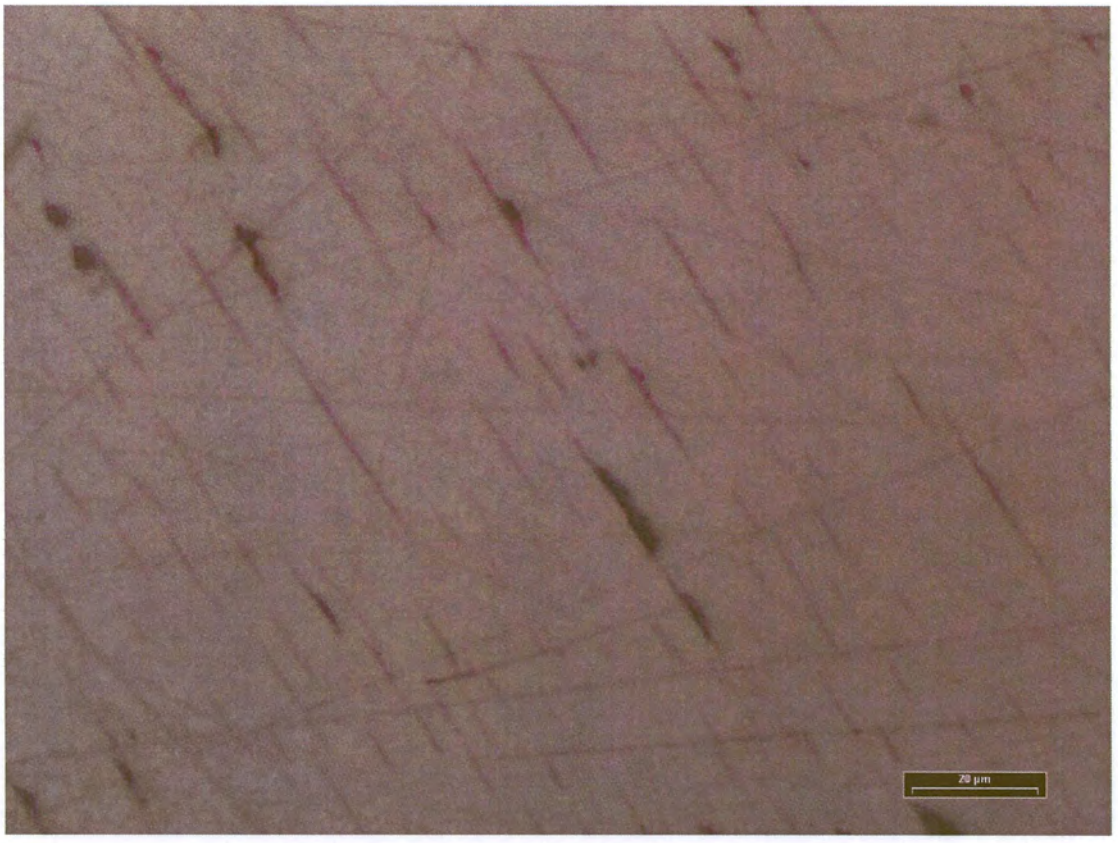

Photograph 5.11: Millerite with skeletal exsolutions (experiment 8m5).

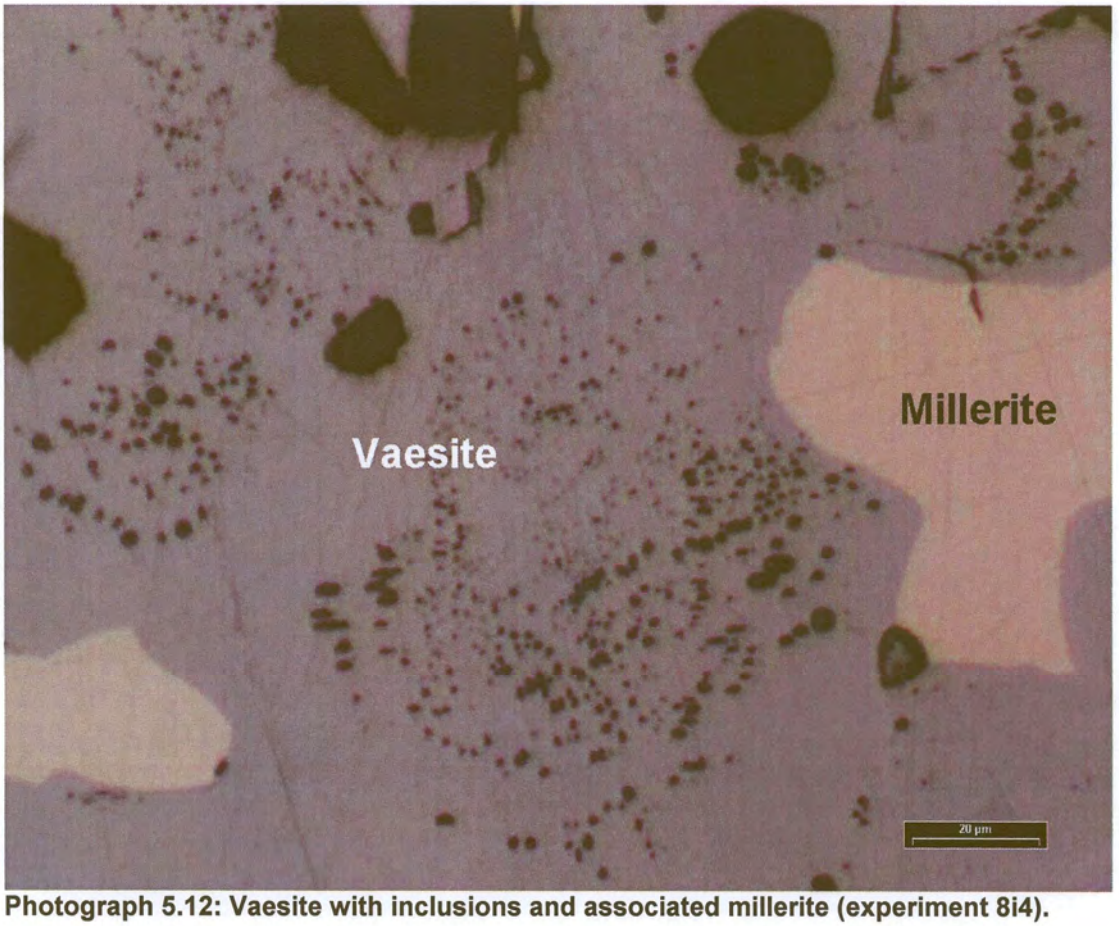

Photograph 5.12: Vaesite with inclusions and associated millerite (experiment 8i4).

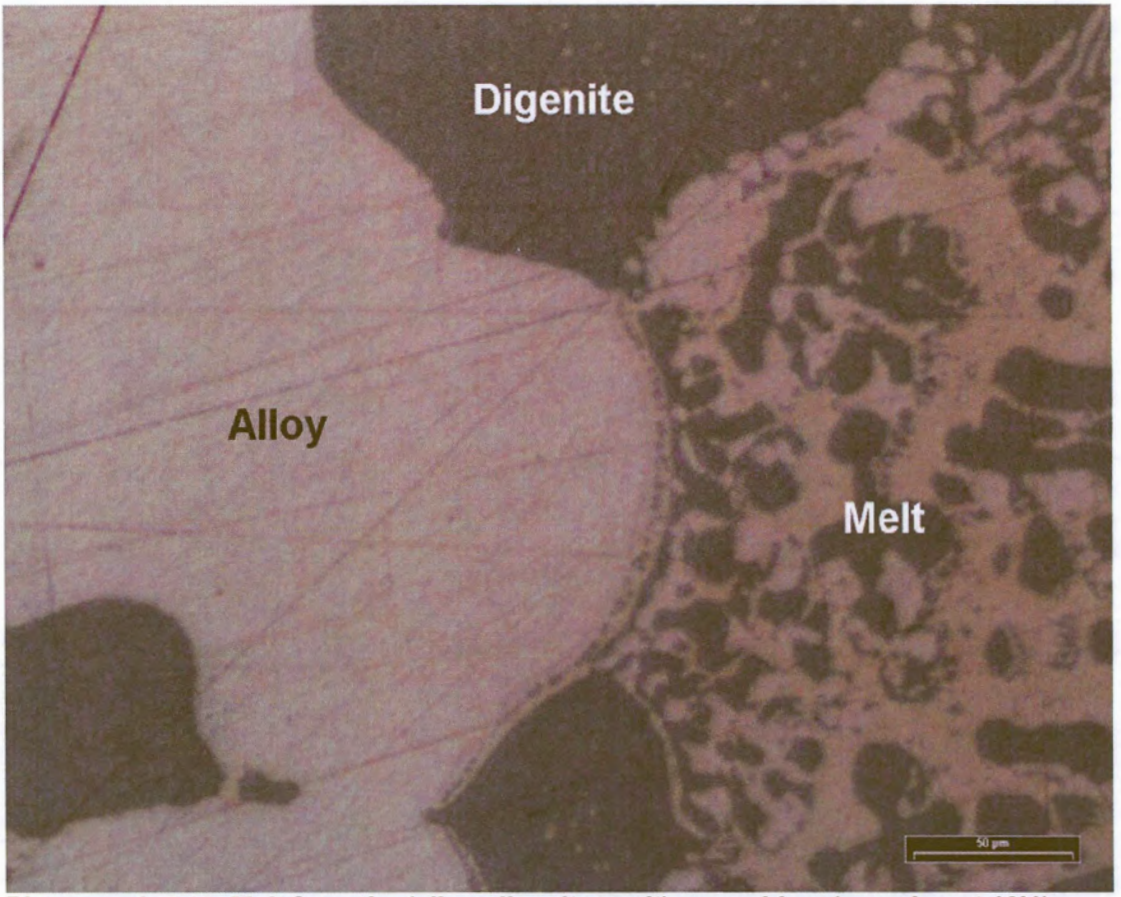

Photograph 5.13: Melt from the (alloy+digenite+melt)-assemblage(experiment 10j1).

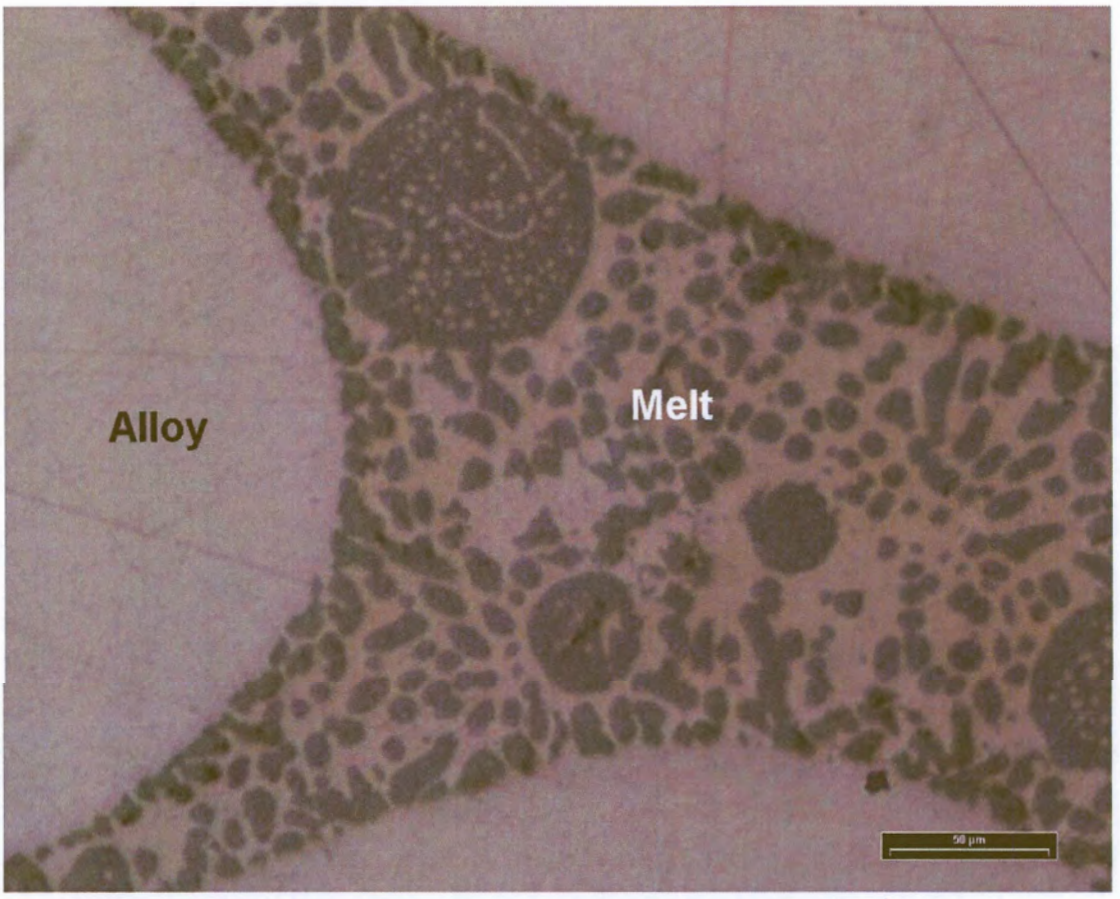

Photograph 5.14: Melt from a Cu-rich starting composition (experiment 10f4).

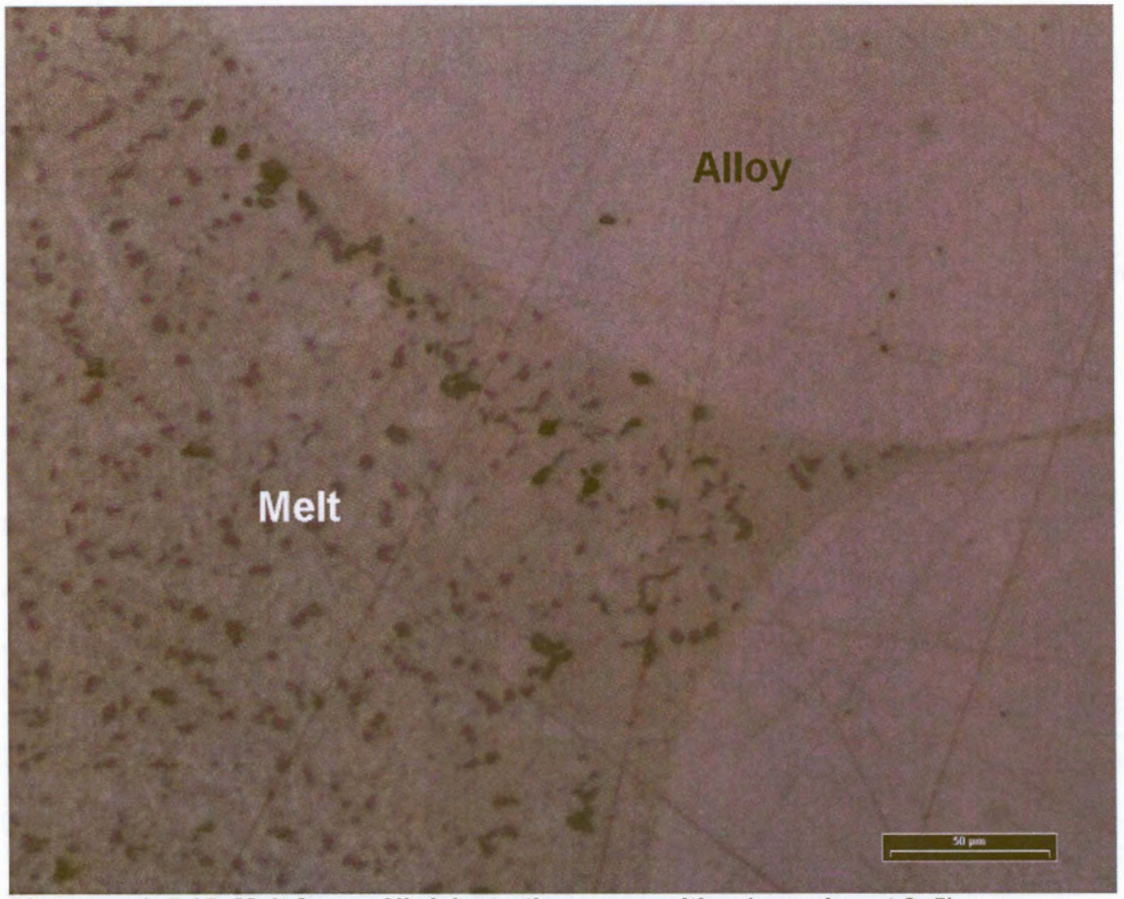

Photograph 5.15: Melt from a Ni-rich starting composition (experiment 8c5).

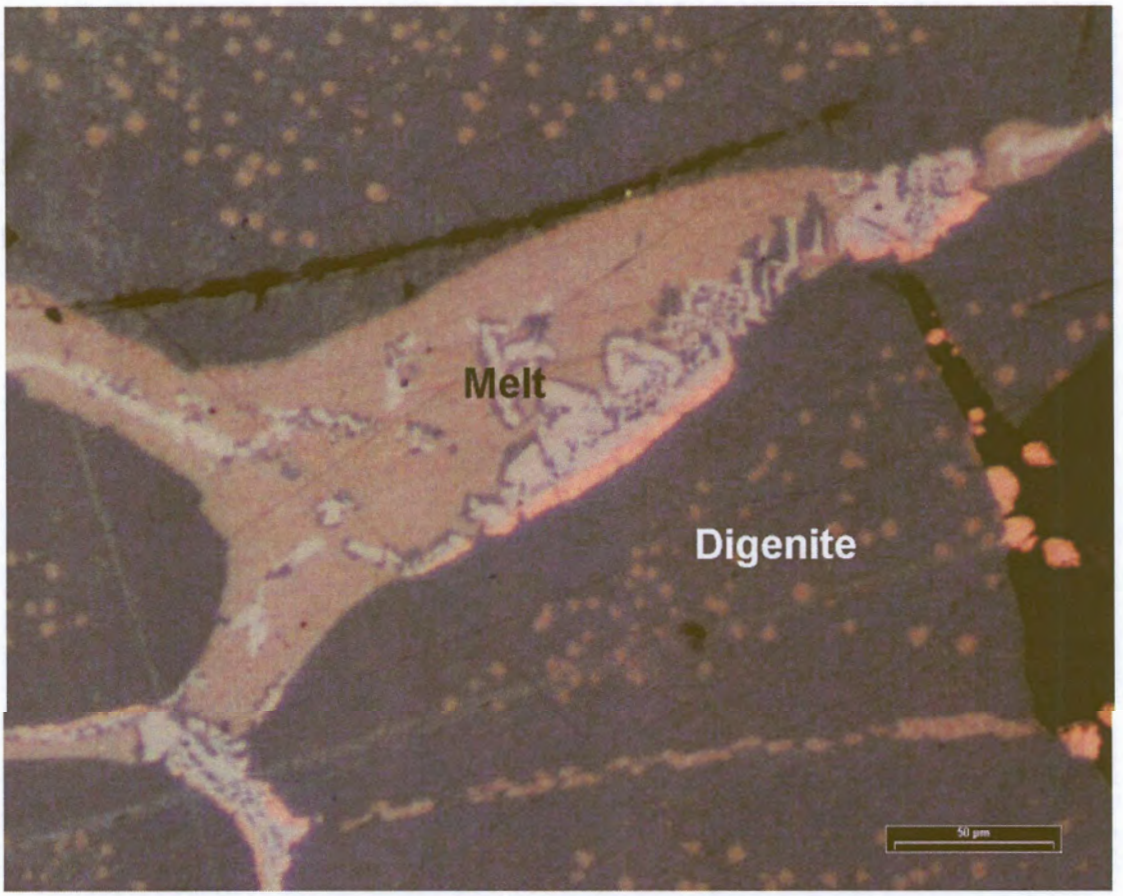

Photograph 5.16: Melt from a (digenite+melt)-assemblage (experiment 8d1).

6. PHASE DIAGRAMS

The starting compositions were based on the phase diagrams of Bruwer (1996). At low Fe concentrations (< 10 wt% Fe), the quaternary phase diagrams is not expected to deviate much from the ternary (Cu-Ni-S) phase diagrams. This means that the major stability fields in the Cu-Ni-S system are anticipated to remain in existence in the Cu-Ni-Fe-S system but will possibly change in size and shape.

Phase diagrams are grouped in temperature classes and sub-grouped according to the starting Fe-content (i.e. 1, 3, 5 and 10 wt% Fe). The average and standard deviations for EMP analyses of phases are listed in Appendix C according to the relevant starting Fe-content. Appendix D groups the experiment labels according to the starting Fe-content in the different stability fields for each isothermal section.

6.1 The 1200°C isothermal sections

The specific isothermal sections are presented in Figures 6.1 to 6.4. At 1200°C (and different Fe contents), the assemblage consists of two phases, a melt and an alloy. At less than ~ 20 wt% sulphur and more than ~ 20 wt% Ni, an alloy phase will be stable in the melt. The compositions of the alloy and coexisting melt depend on the starting composition: with an increase in the starting Fe-content, the composition of the coexisting melt increases in sulphur content. The composition of the melt coexisting with pure Ni-alloy is inferred, using the diagram of Bruwer (1996) as a guideline.

Experiments 12I5 and 12I6 display deviations from the starting composition, and because the precision and accuracy of analysis were high, it can reasonably be argued that the polished surface do not display all the phases present at the specified temperature. In these experiments the sulphur values are notably higher and the metals lower than the starting composition. It can, therefore, be expected that an alloy phase is part of the assemblage, although not detected in the specific section of the experiment.

At starting compositions containing more than 50 wt% Cu and less than ~ 20 wt% sulphur, the melt separates into two immiscible melts with different sulphur contents. The two immiscible melts do not co-exist with an alloy phase. The position of the (2-melt)-field is indicated with a dotted field boundary line after the position and shape of this field in the Fe-free system. The shape and size of the (2 melt)-field were not of interest for the purpose of this study. Therefore, it was not investigated in detail and only a small amount of data points are available.

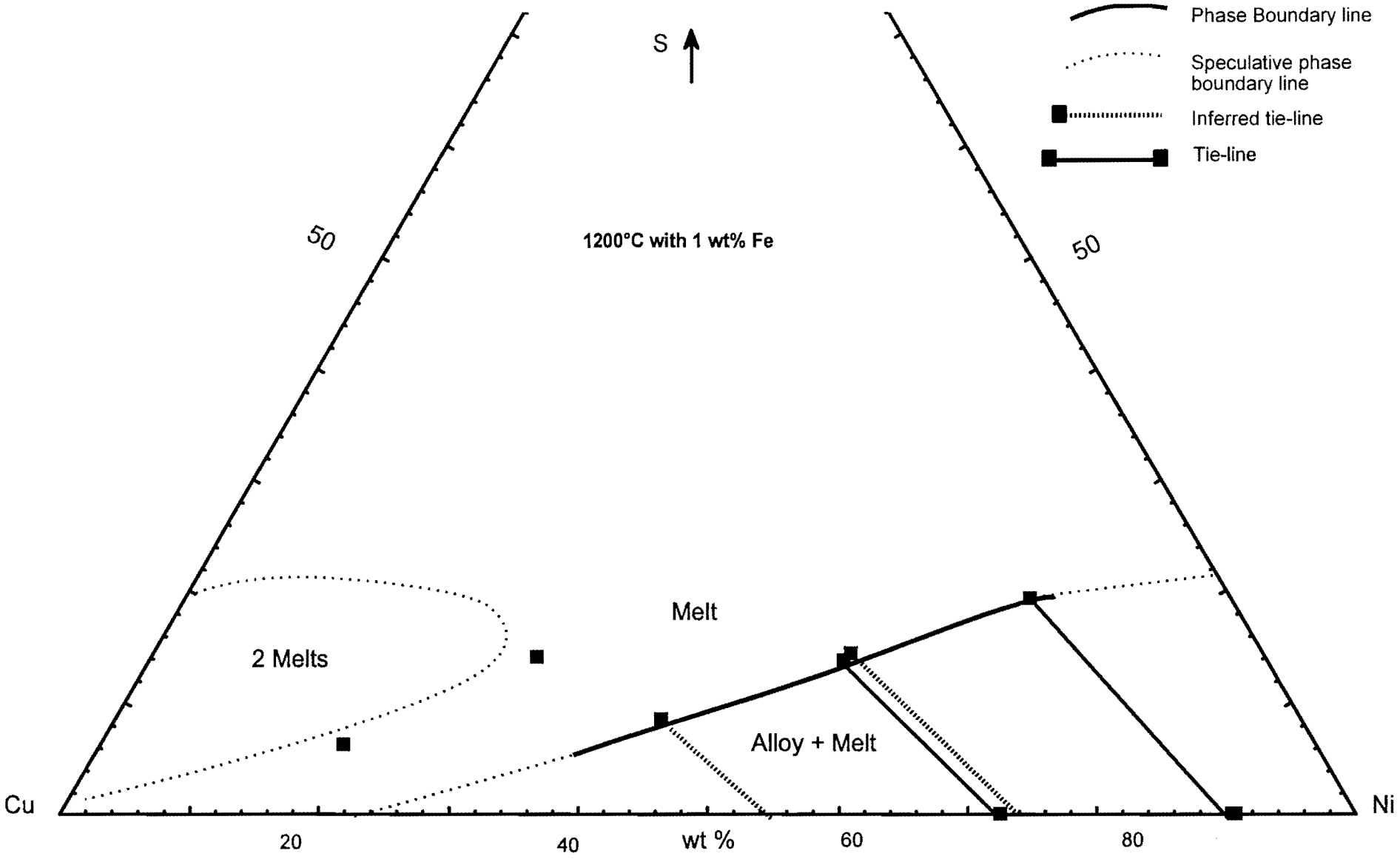

Figure 6.1: Phase relations at 1200°C and 1 wt% Fe in starting compositions.

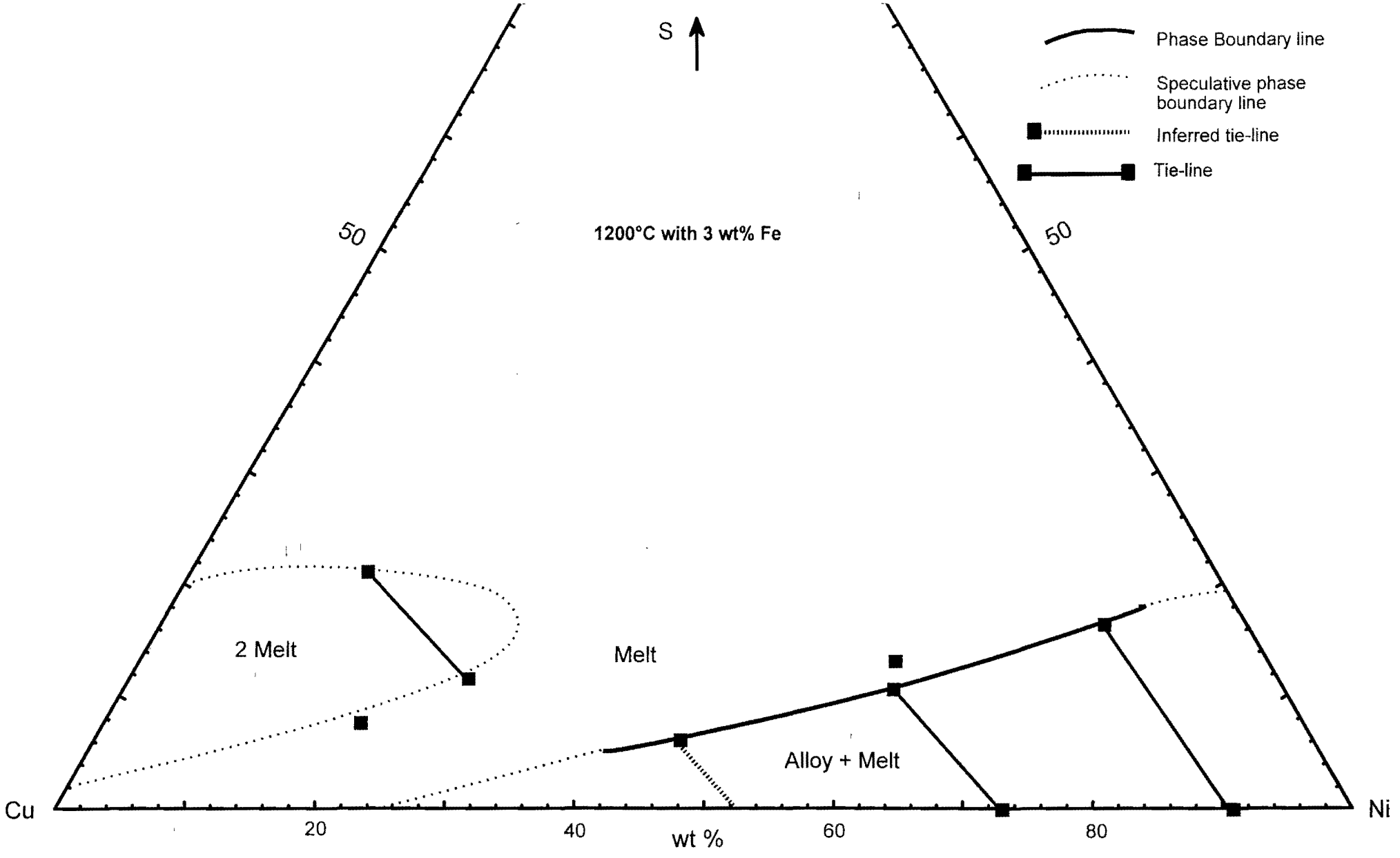

Figure 6.2: Phase relations at 1200°C and 3 wt% Fe in starting compositions.

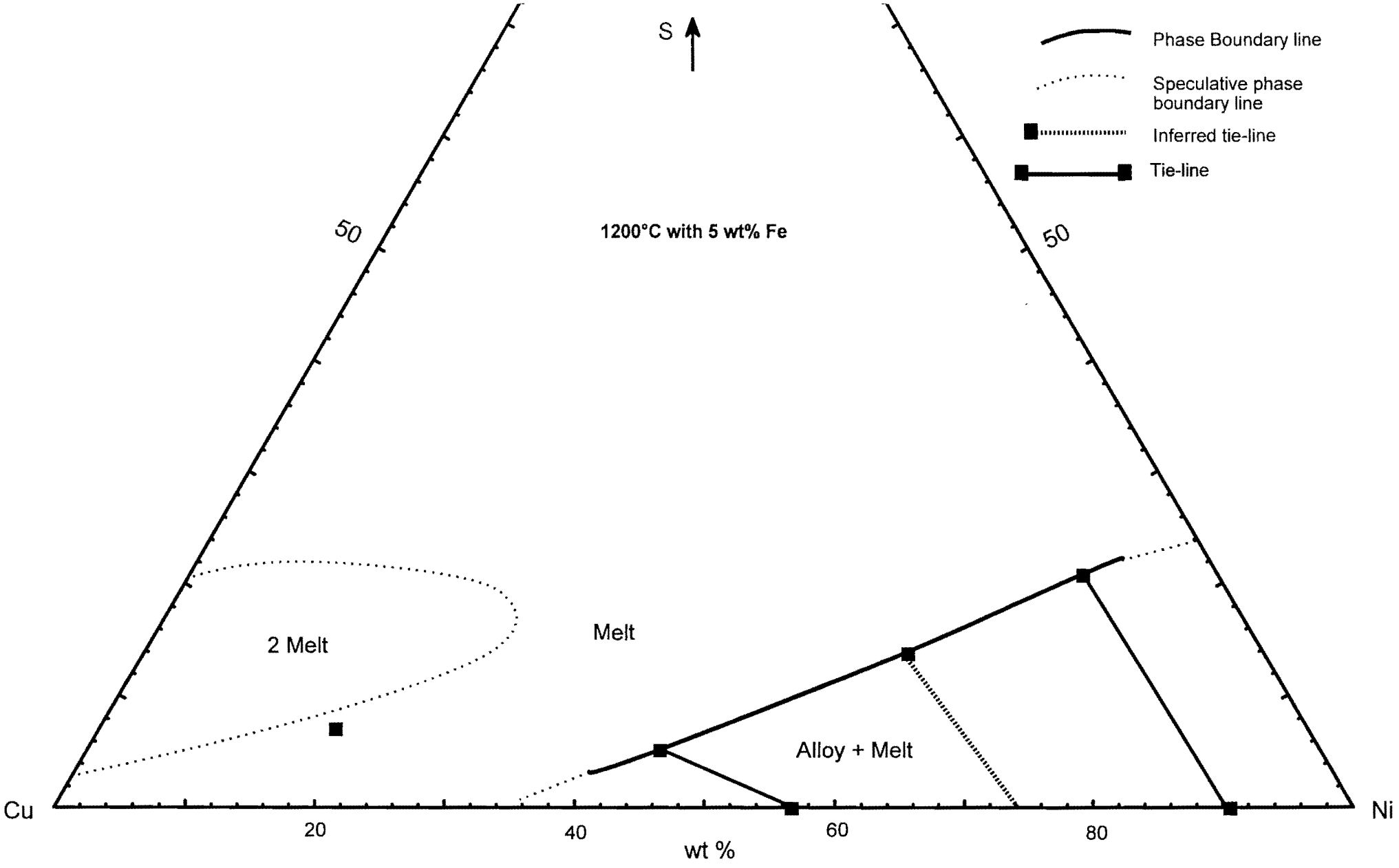

Figure 6.3: Phase relations at 1200°C and 5 wt% Fe in starting compositions.

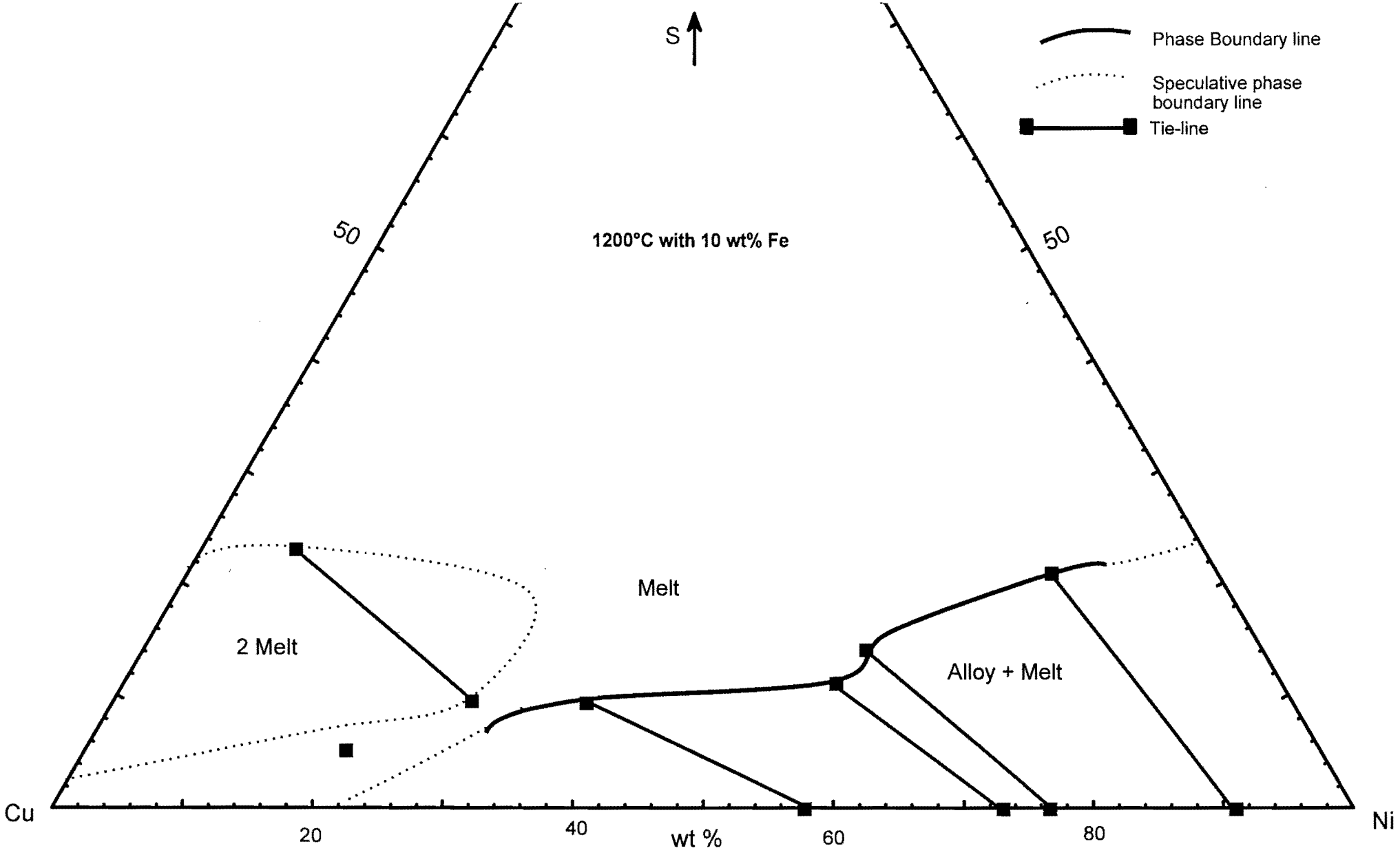

Figure 6.4: Phase relations at 1200°C and 10 wt% Fe in starting compositions.

6.2 The 1100°C isothermal sections

The isothermal sections at 1100°C are presented in Figures 6.5 to 6.8. At 1100°C and compositions containing ≤ 5 wt% Fe, a maximum of two possible phases can exist, a melt and an alloy phase. The melt coexisting with alloy changes composition with a change in the bulk metal content. Alloys with higher Ni-contents coexist with higher sulphur-content melts and higher Fe in the starting composition leads to more sulphur rich compositions of the coexisting melt. Melts with more than ~ 50 wt% Cu and less than ~ 20 wt% sulphur separate into two immiscible melts. Only at less than 10 wt% sulphur in the starting composition would the melt coexist with a Cu-rich alloy.

If the starting composition contains 10 wt% Fe, digenite exists at starting compositions higher than ~ 50 wt% Cu and sulphur contents lower than ~ 20 wt%. Digenite coexists with a Cu-rich alloy at starting compositions containing more than ~ 60 wt% Cu and coexists with a Cu-rich alloy and a melt phase at compositions between ~ 50 and 60 wt% Cu.

When digenite becomes stable it also presents the "problem of apparently crossing tie-lines". In a three-component system, this would indicate that the experiments involved were either in dis-equilibrium or that analyses were unreliable. In this four-component system, however, crossing tie-lines are a result of a three-dimensional projection onto a two-dimensional surface. Digenite from different experiments contains different amounts of Fe that can not be displayed successfully in these diagrams. The effect of projecting data points from a volume representing an imaginable phase field for digenite is shown in Figure 6.9.

6.3 The 1000°C isothermal sections

The isothermal sections at 1000°C are presented in Figures 6.10 to 6.13. Depending on the bulk composition, a Cu-Ni-sulphide assemblage will comprise a maximum of three phases, i.e. alloy, digenite and melt. Ni-rich starting compositions with less than ~ 20 wt% sulphur will result in an alloy coexisting with a melt phase. A bulk composition rich in Cu and between 10 and 20 wt% sulphur will produce digenite coexisting with either alloy, melt, or (alloy+melt). The composition of the melt coexisting with alloy increases in sulphur-content with the increase of Fe in the bulk composition. Similarly, the melt composition coexisting with digenite increases in sulphur-content with the increase in Fe-content.

The change in composition of the melt and alloy coexisting with digenite (referred to as the "cotectic-alloy" and "cotectic-melt") is of interest. Monitoring these two phases with the change in temperature and Fe-content of the bulk gives an indication of the crystallization path of the melt at any given starting composition.

Again, crossing tie-lines are explained by the projection of a three-dimensional phase field onto a two-dimensional diagram.

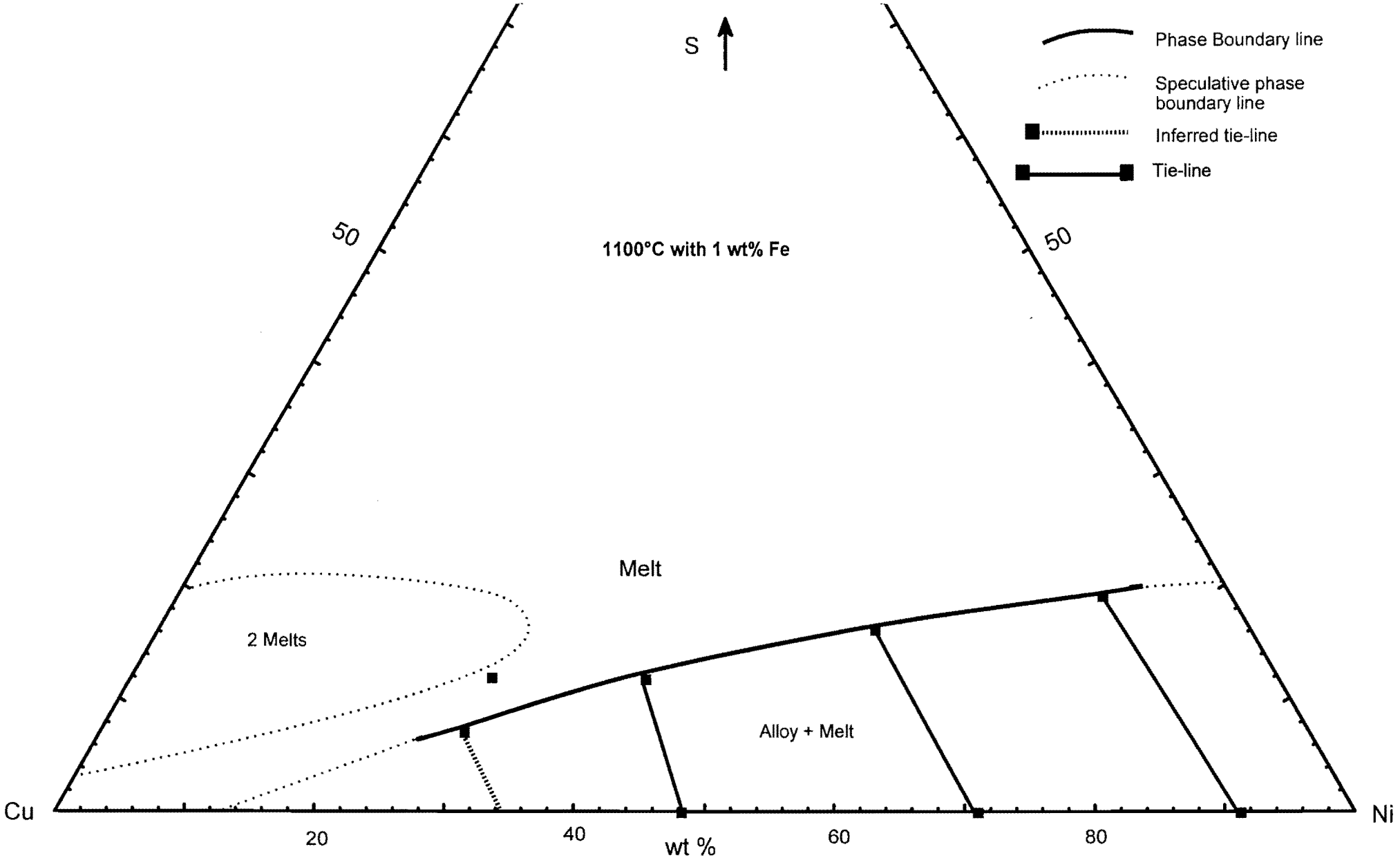

Figure 6.5: Phase relations at 1100°C and 1 wt% Fe in starting compositions.

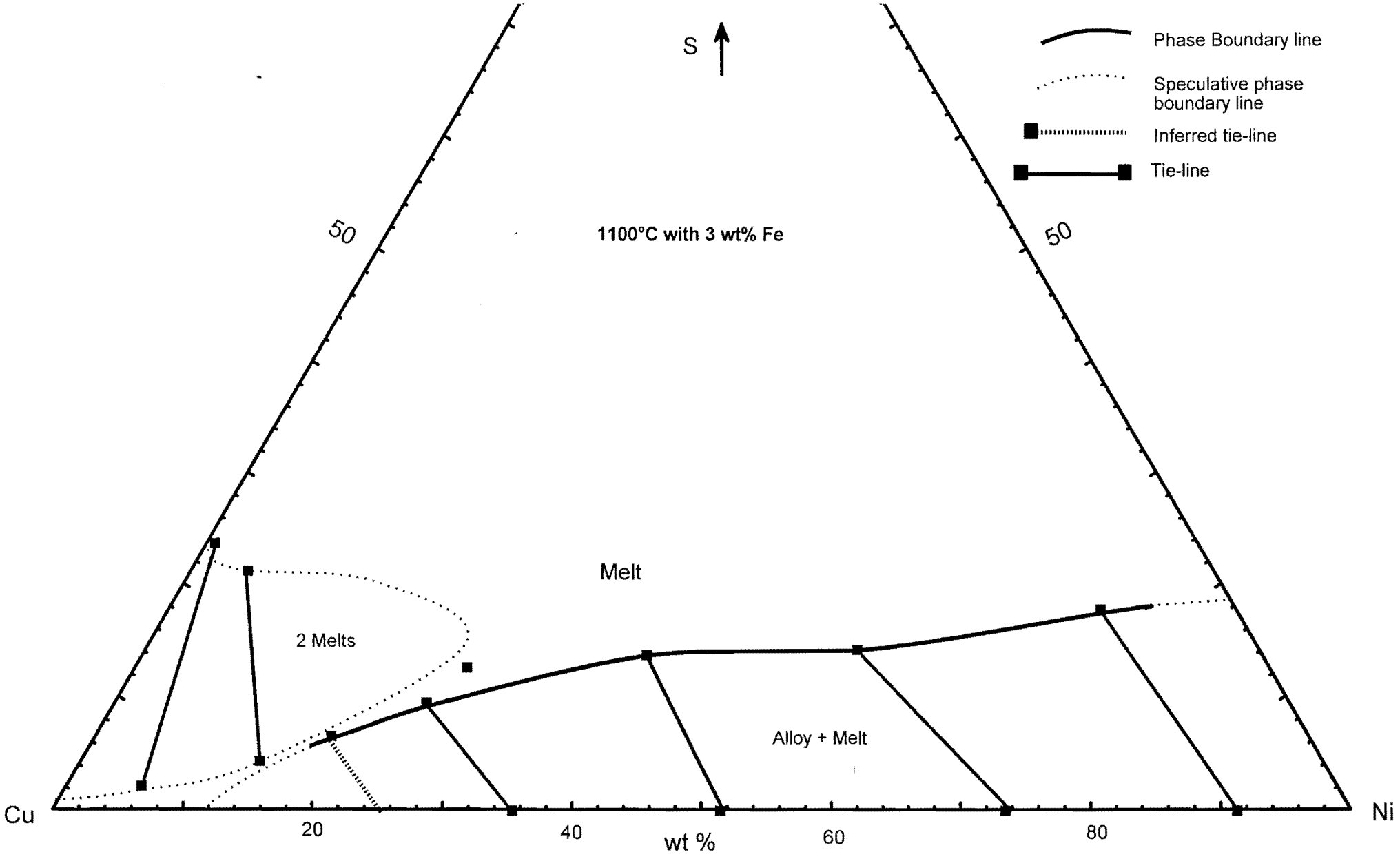

Figure 6.6: Phase relations at 1100°C and 3 wt% Fe in starting compositions.

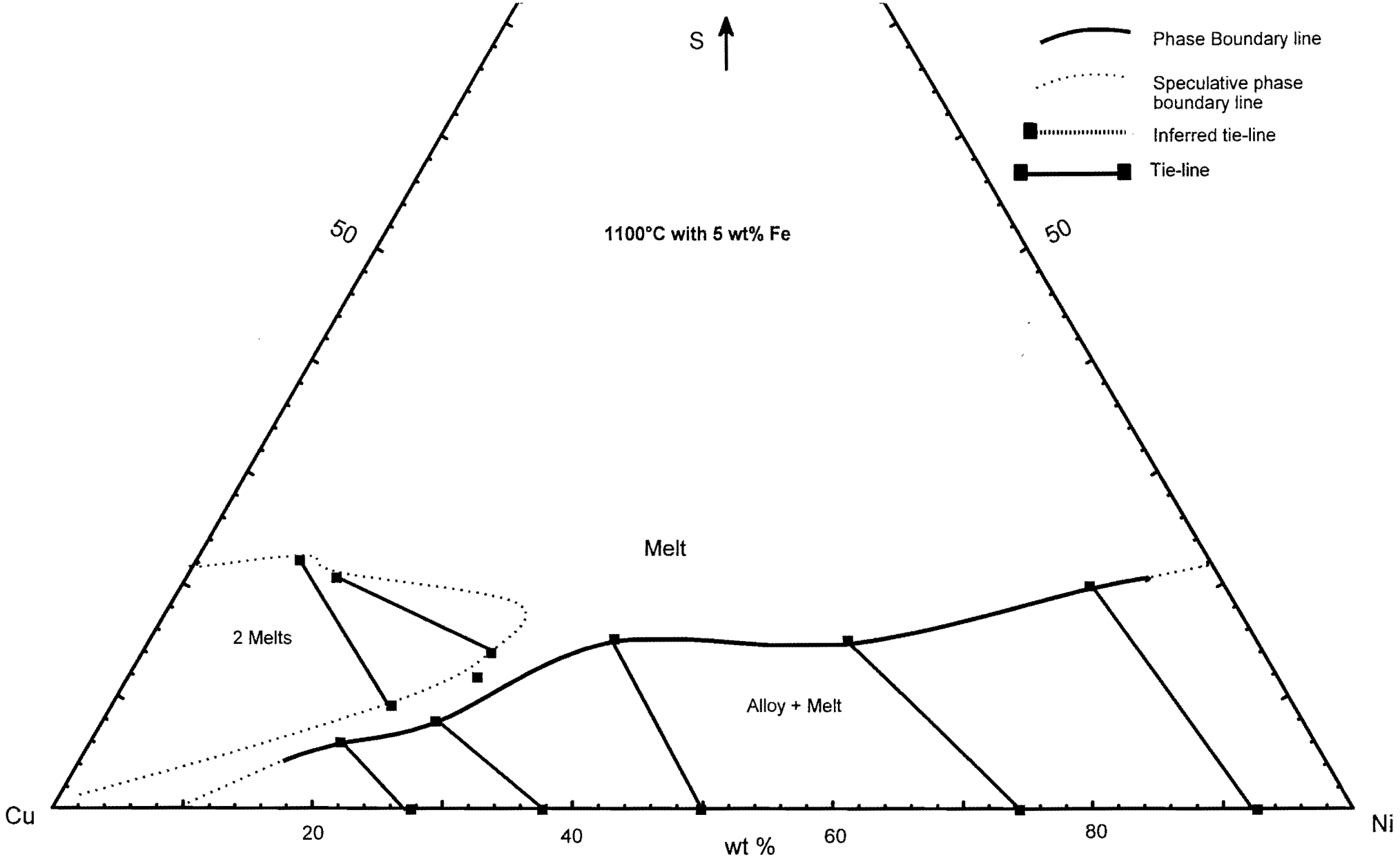

Figure 6.7: Phase relations at 1100°C and 5 wt% Fe in starting compositions.

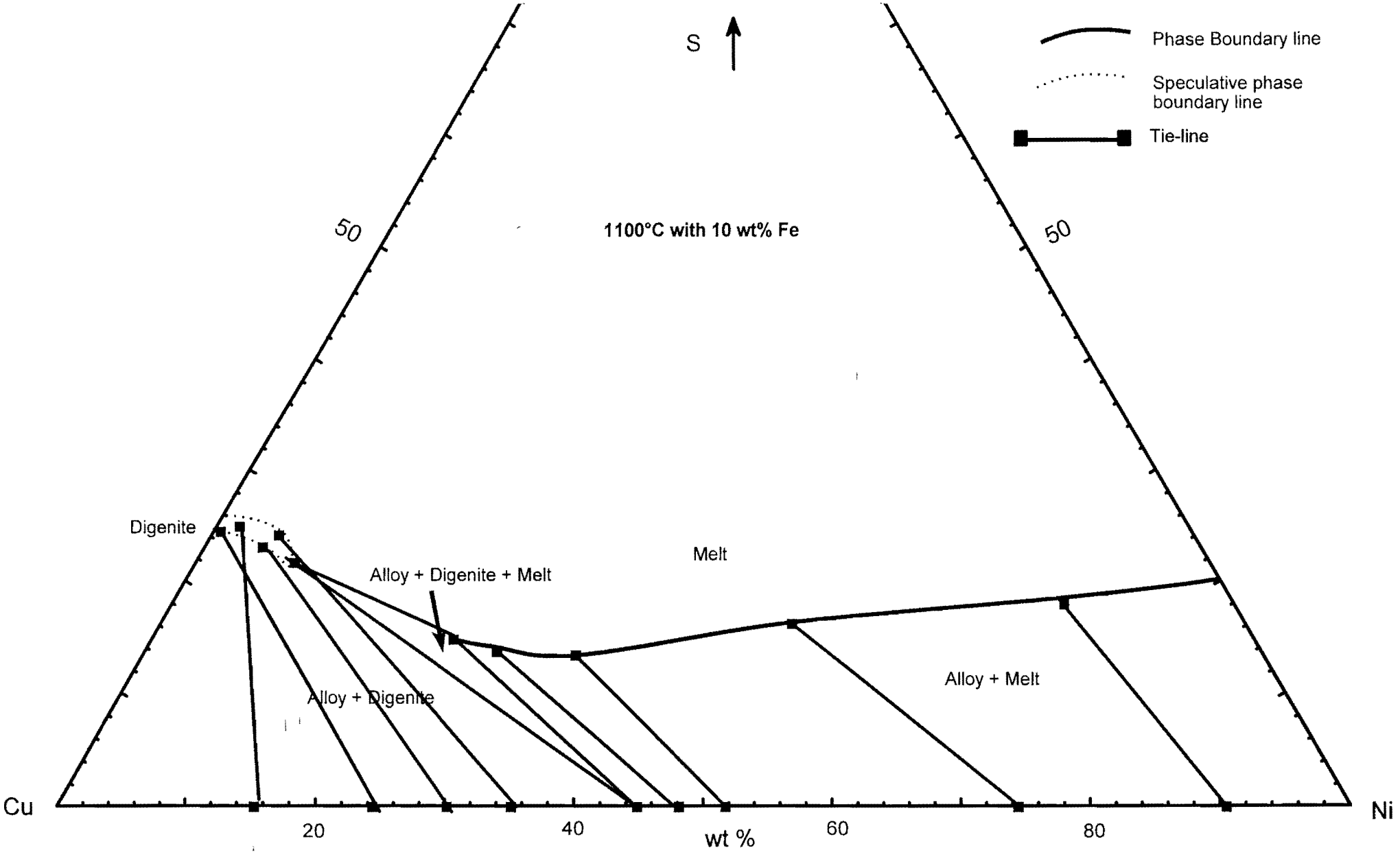

Figure 6.8: Phase relations at 1100°C and 10 wt% Fe in starting compositions.

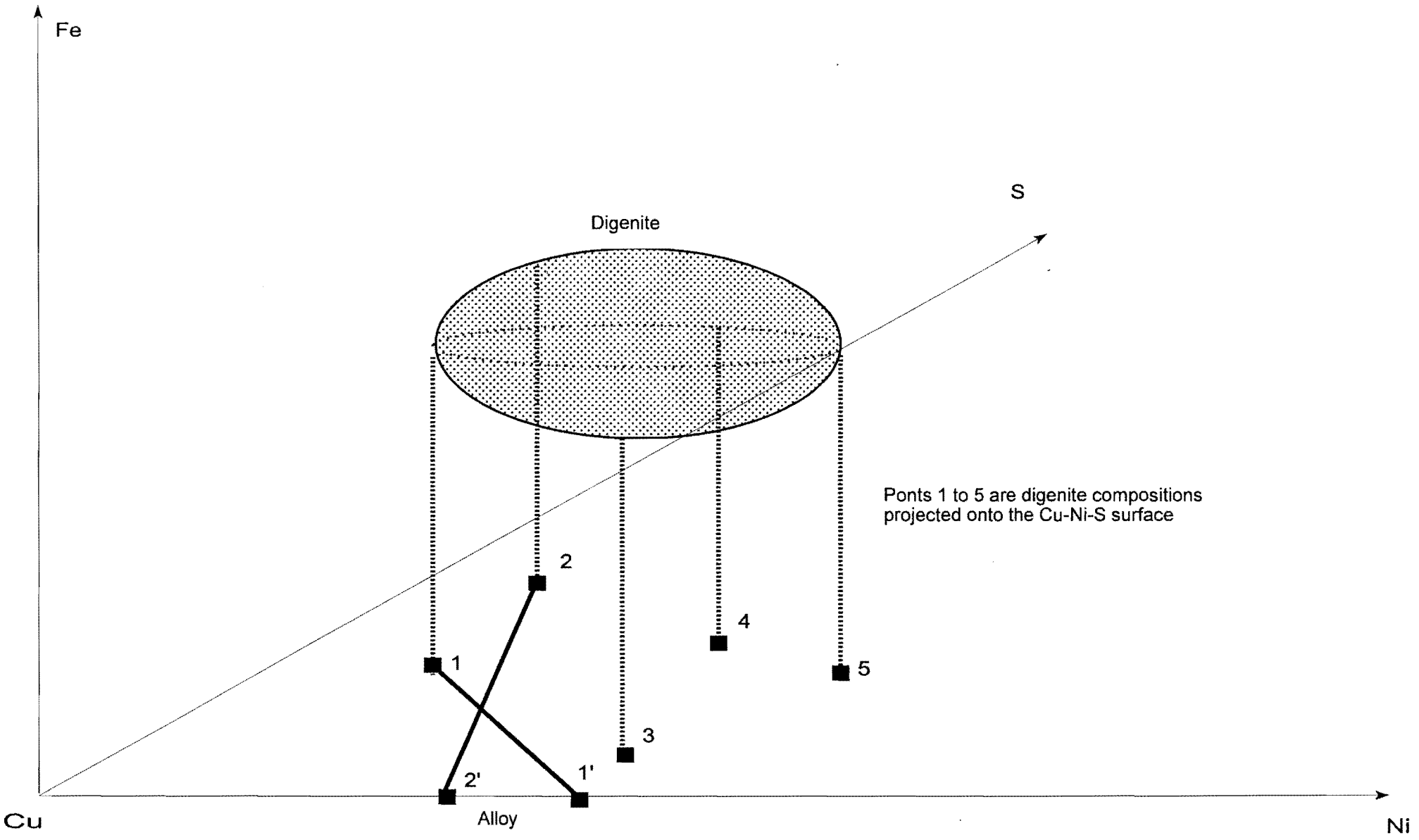

Figure 6.9: Projection of a three-dimensional volume representing an imaginary phase field of digenite, onto a two-dimensional surface. A tie-line from point 2 to 2' (a Cu-rich alloy) would seemingly cross with a tie-line from 1 to 1' (a slightly more Ni-rich alloy). In the third dimension these two tie-lines would not cross.

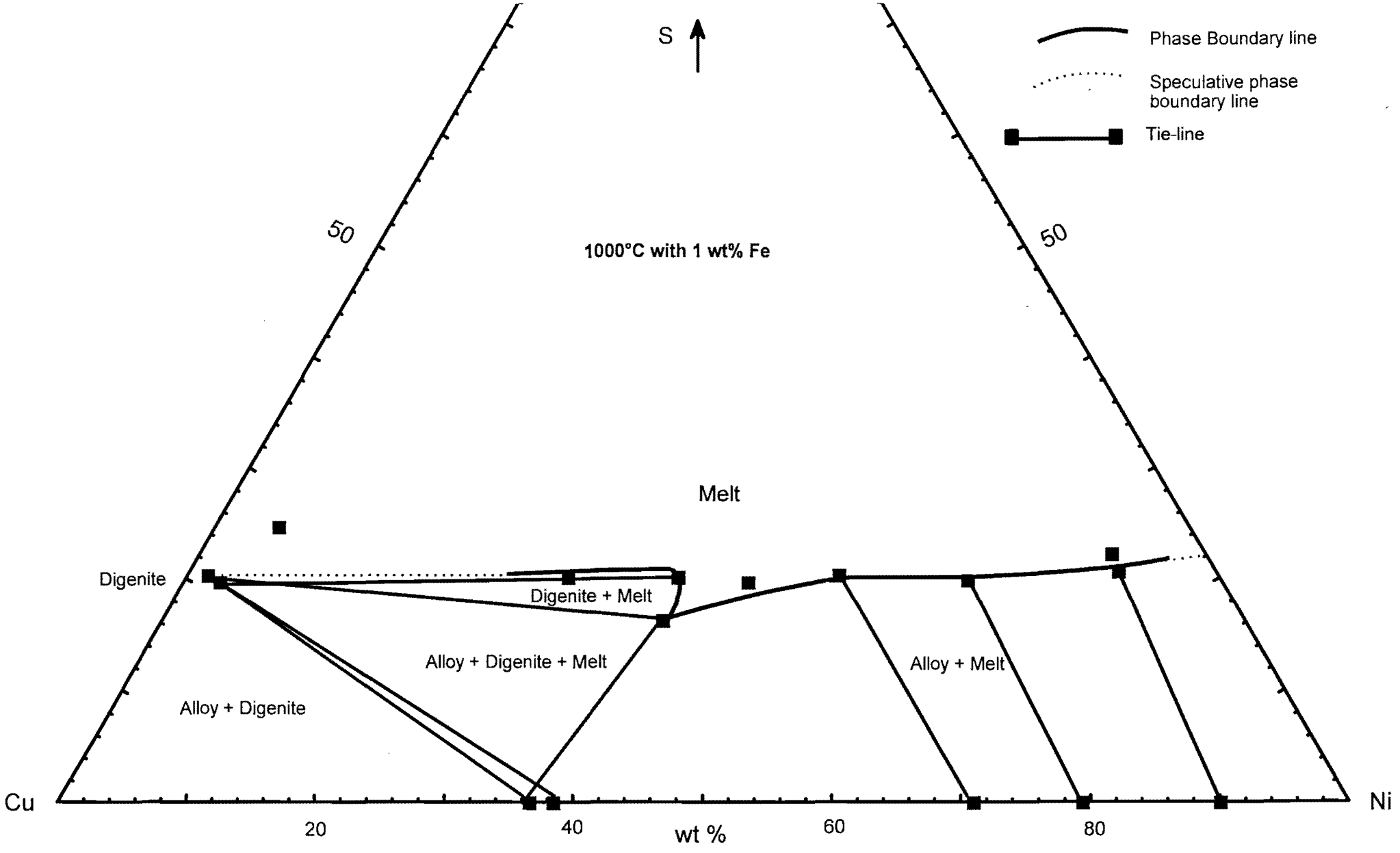

Figure 6.10: Phase relations at 1000°C and 1 wt% Fe in starting compositions.

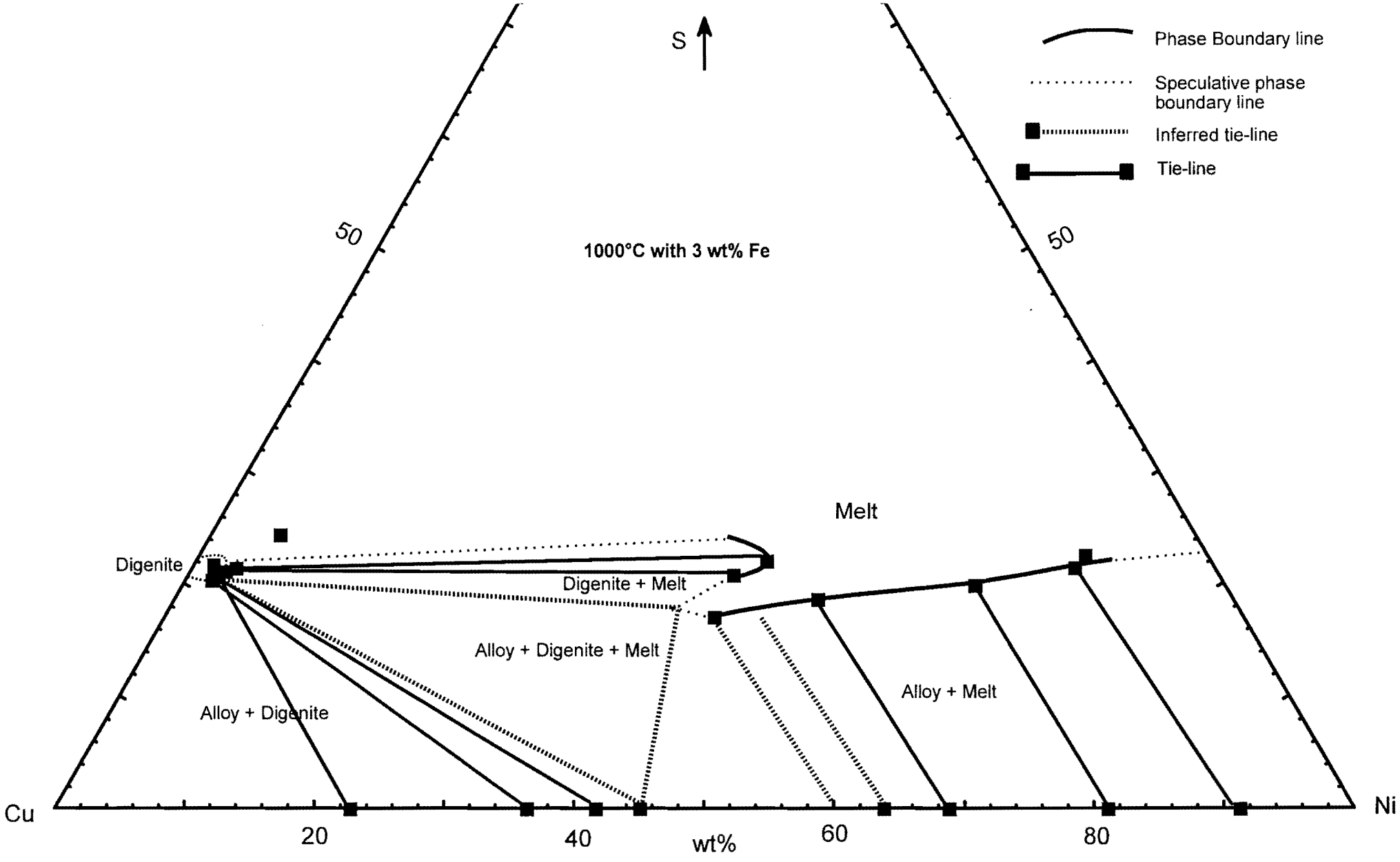

Figure 6.11: Phase relations at 1000°C and 3 wt% Fe in starting compositions.

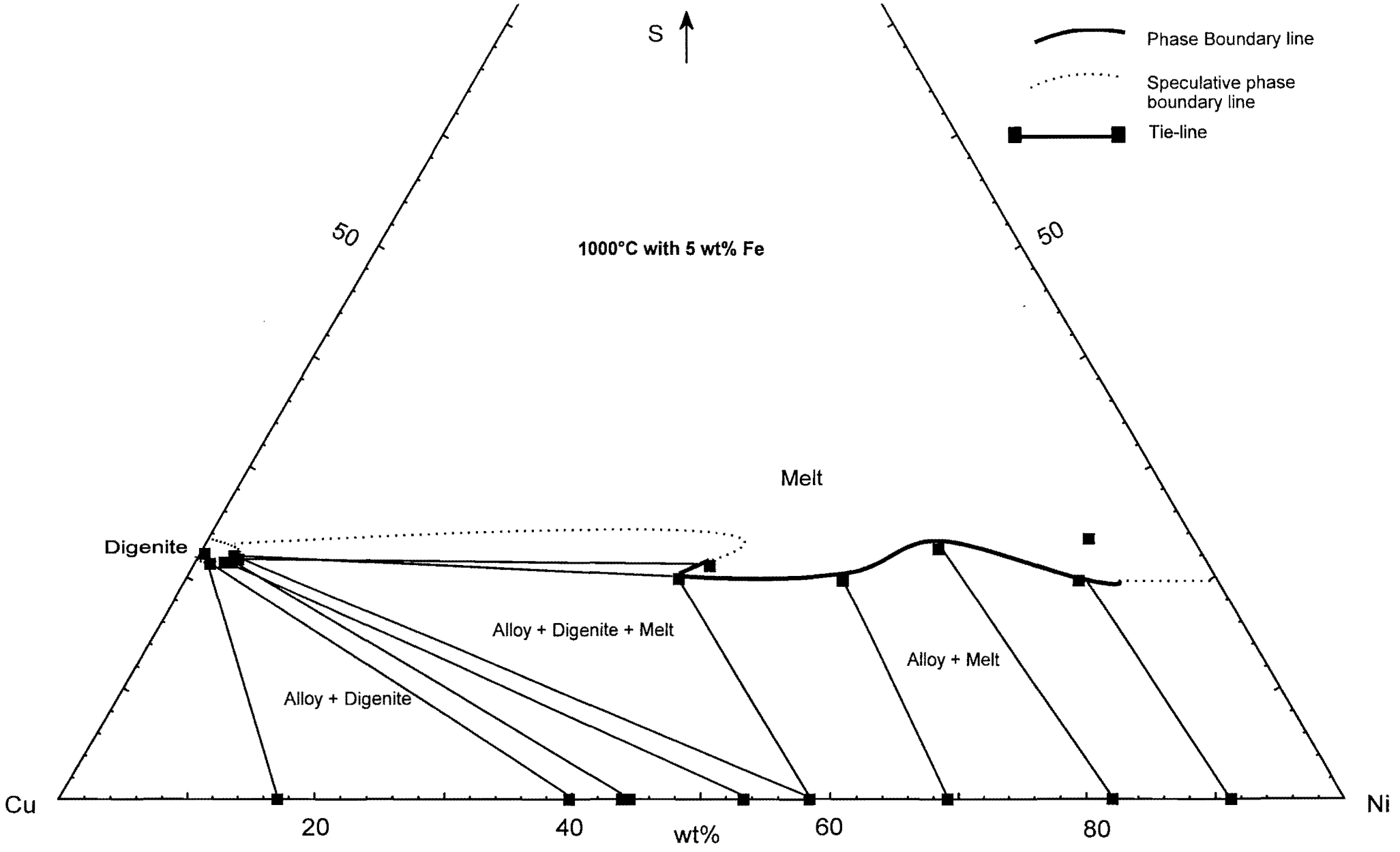

Figure 6.12: Phase relations at 1000°C and 5 wt% Fe in starting compositions.

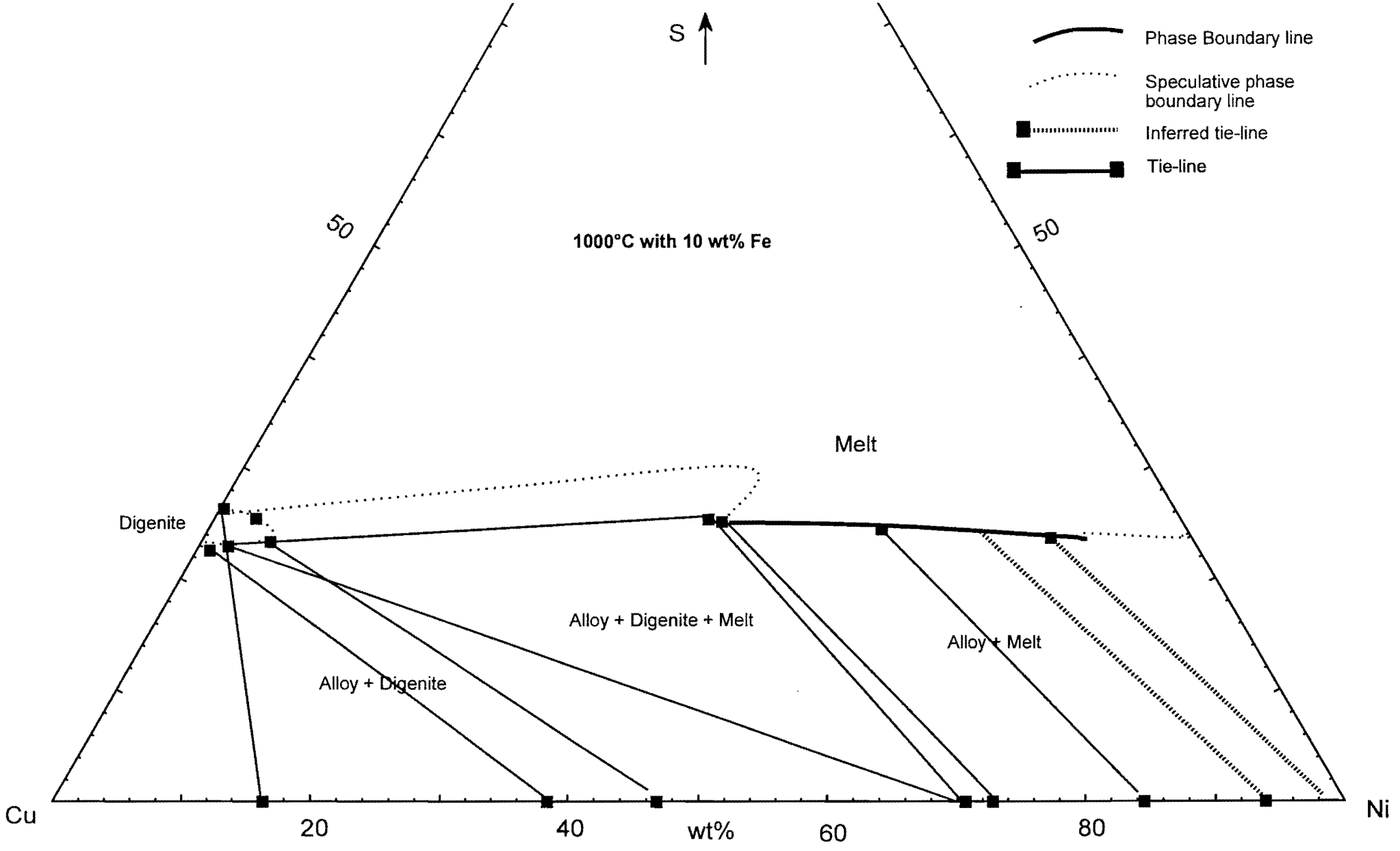

Figure 6.13: Phase relations at 1000°C and 10 wt% Fe in starting compositions.

6.4 The 900°C isothermal sections

The isothermal sections at 900°C are presented in Figures 6.14 to 6.17. An enlargement of the area around digenite appears in the insert. At 900°C, a Cu-Ni-sulphide assemblage will produce four possible phases at low sulphur (< ~ 25 wt%) and three possible phases at high sulphur-contents (> ~ 30 wt%) and low Cu-contents (< ~20 wt%).

At low concentrations of sulphur in the bulk, an alloy phase will coexist with digenite, melt, or (digenite+melt). The composition of the average cotectic alloy and cotectic melt increases in Ni-content with the increase in the concentration of Fe in the starting composition. At sulphur-contents of approximately 25 wt%, and Cu-contents more than ~ 50 wt%, two phases will coexist: a Cu-sulphide and melt. The Cu-sulphide is either digenite or a phase with higher sulphur and Ni-contents defined earlier as "β-phase". Digenite and β-phase were never observed in the same experiment. However, this may just be a result of starting compositions that did not favor these two phases to coexist. Starting compositions that could reflect such an assemblage are very limited and not encountered in this study.

At higher sulphur-contents and low Cu concentrations, crystallization from a Cu-Ni-sulphide melt will result in a three phase assemblage depending on the starting composition; (millerite+vaesite+melt), (millerite+melt) or (millerite+vaesite). With an increase in the Fe-content of the bulk, the melt coexisting with millerite and vaesite becomes enriched in Cu.

6.5 The 800°C isothermal sections

The isothermal sections at 800°C are presented in Figures 6.18 to 6.21. At low sulphur-contents, the phase assemblages at 800°C are very similar with respect to those at 900°C. An alloy phase will coexist with either digenite, (digenite+melt), or only melt, depending on the starting composition. The composition of the cotectic melt does not change much with the addition of Fe to the bulk composition, but the cotectic alloy increases in Ni content with the increase of Fe. The composition of the melt coexisting with an alloy phase does not show a significant increase in sulphur content with an increase in the Fe concentration of the bulk.

In the Fe-free system (Bruwer, 1996), a Cu-rich melt field forms at sulphur contents of ~ 30 wt%. A similar melt exists at low (1 wt%) Fe concentrations but was not encountered in the higher Fe content assemblages. Three possibilities arise: firstly the composition of this melt could change at higher Fe concentrations of the bulk, secondly this melt could disappear completely on addition of Fe to the bulk, or thirdly, the proportion of melt to solids is so small that the likelihood of intersecting this phase in a polished section is very small.

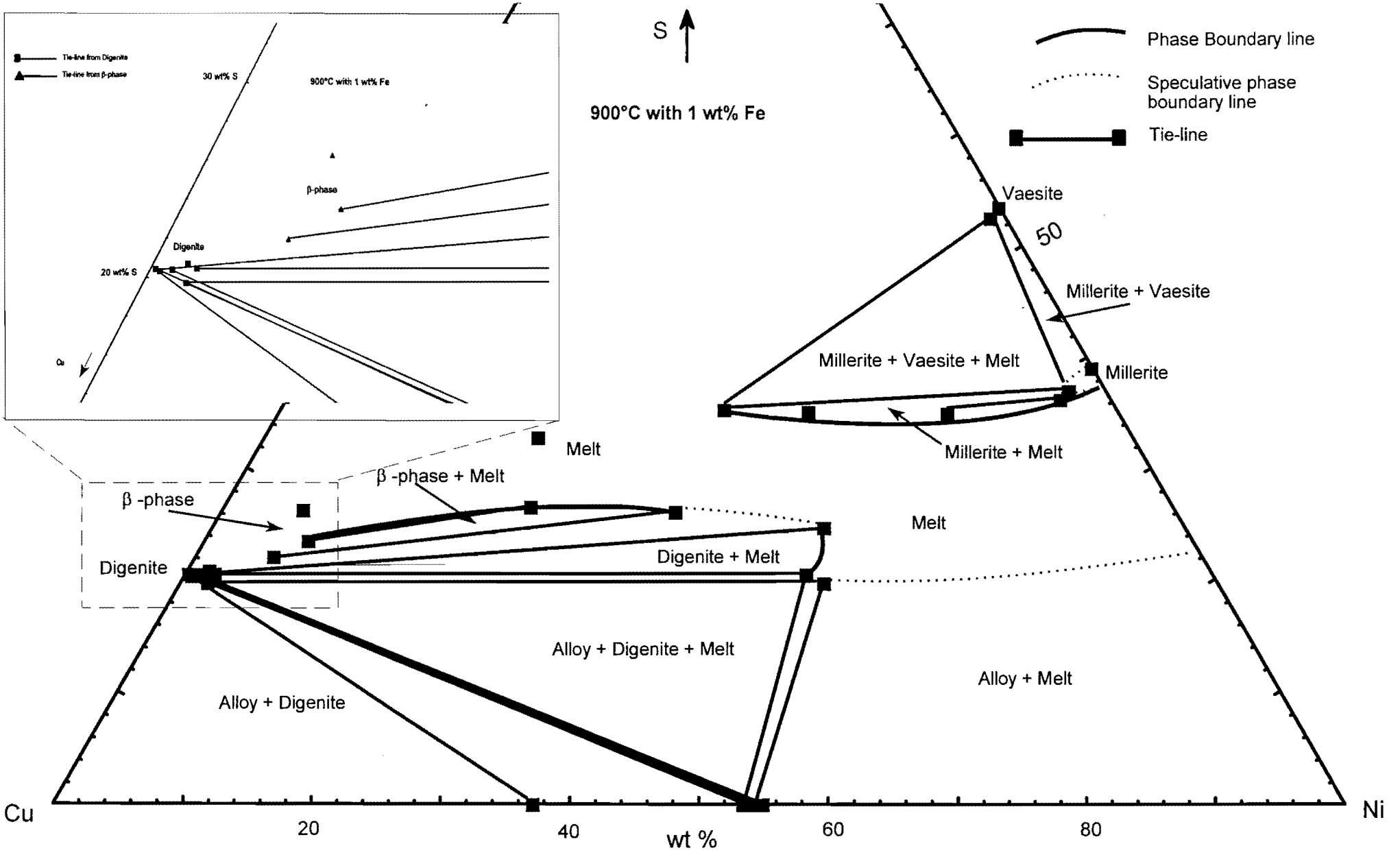

Figure 6.14: Phase relations at 900°C and 1 wt% Fe in starting compositions. The insert shows the area where digenite and the β -phase plot.

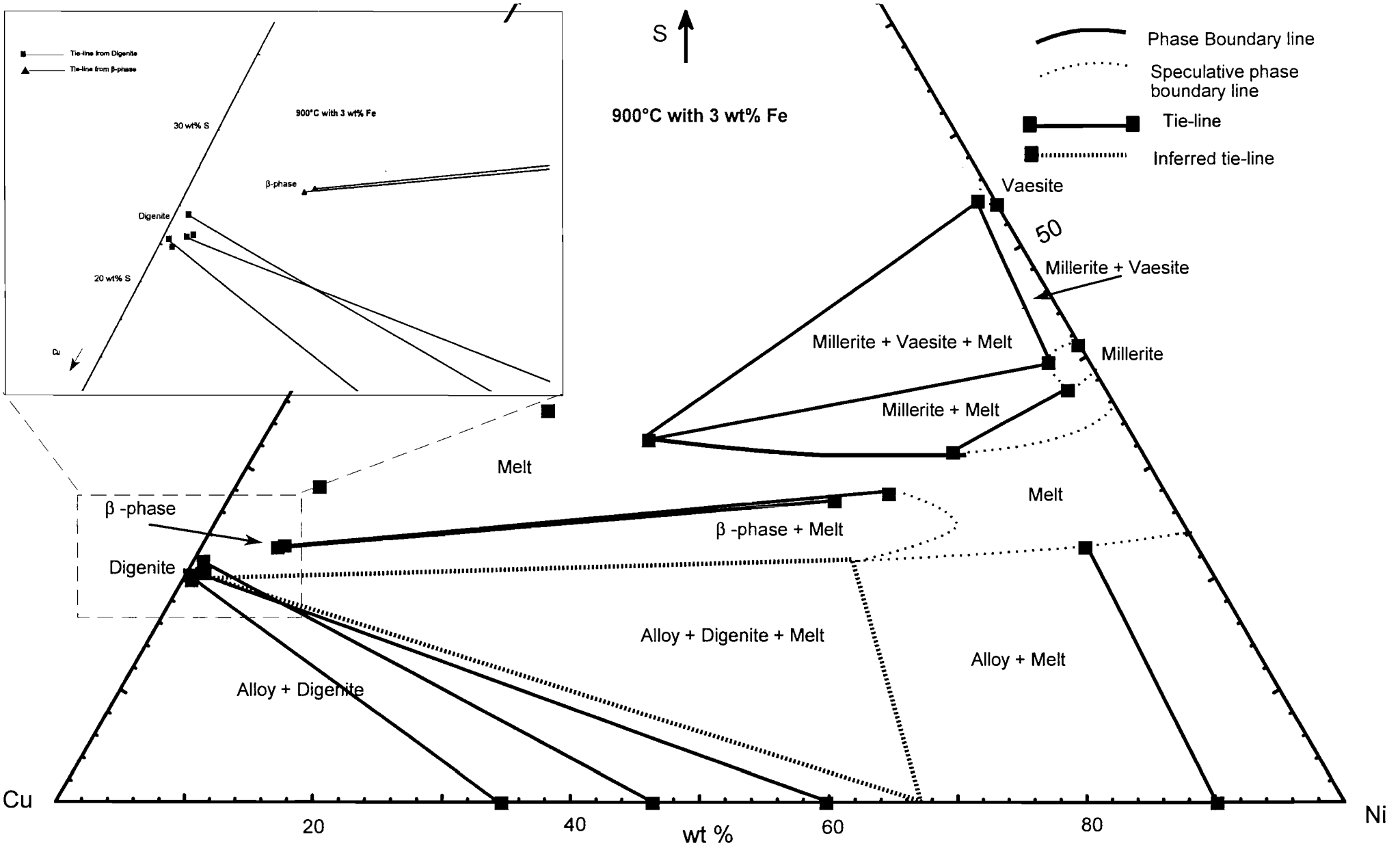

Figure 6.15: Phase relations at 900°C and 3 wt% Fe in starting compositions. The insert shows the area where digenite and the β -phase plot.

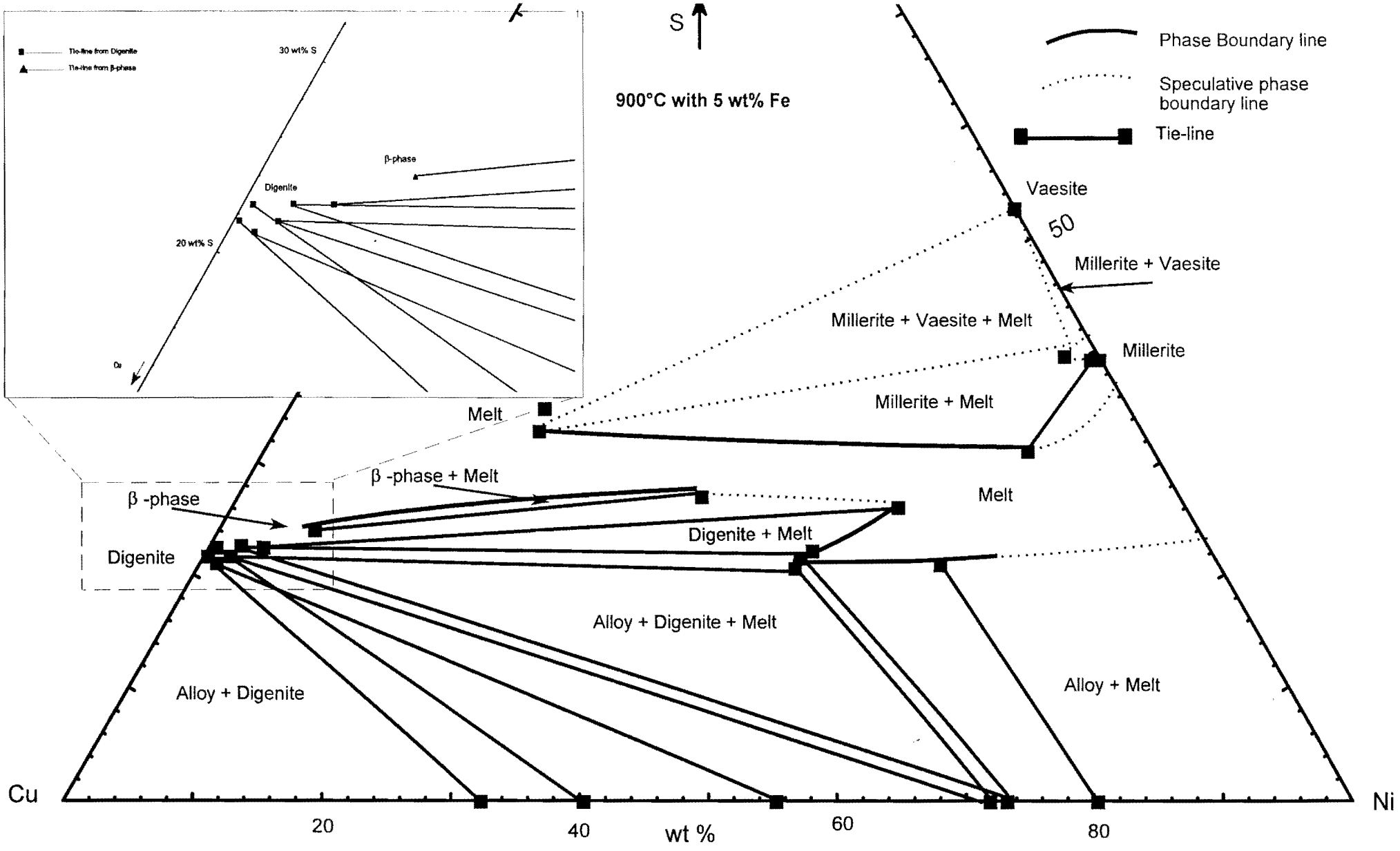

Figure 6.16: Phase relations at 900°C and 5 wt% Fe in starting compositions. The insert shows the area where digenite and the β -phase plot.

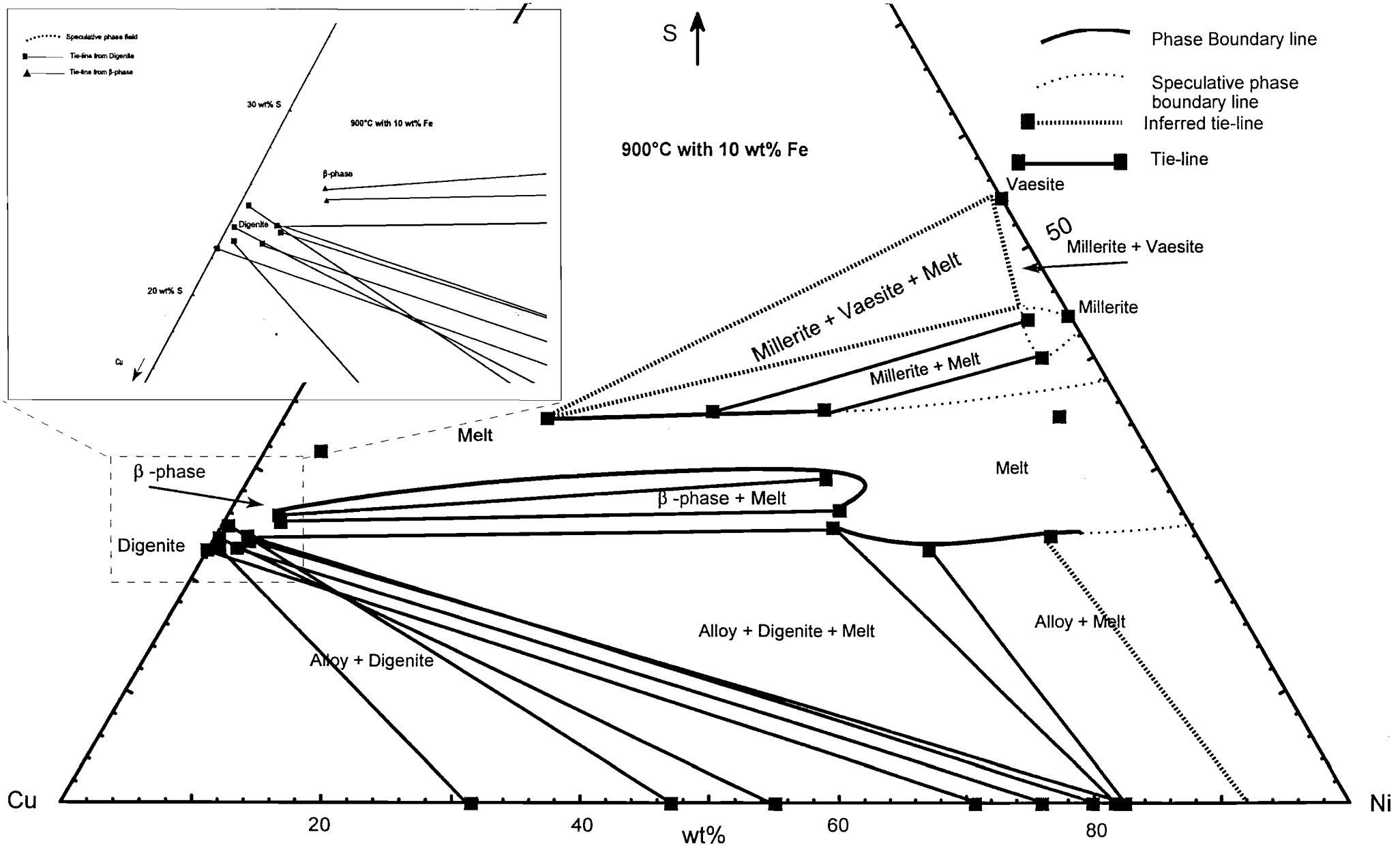

Figure 6.17: Phase relations at 900°C and 10 wt% Fe in starting compositions. The insert shows the area where digenite and the β -phase plot.

If such a Cu-rich melt exists, the assemblages of phases coexisting with the sulphide-melt at sulphur concentrations 30 – 50 wt% become very complex. The aim of this project is not to investigate this part of the system systematically. Therefore, the phase relations are indicated with stippled lines due to a lack of sufficient data. An interesting aspect is the coexistence of millerite, vaesite and a Ni-rich melt with the β-phase, but not with digenite. With an increase in the bulk Fe concentration, the sulphur content of the β-phase and millerite also increases.

Heazlewoodite was described by Bruwer (1996) at temperatures 800°C and lower. This Ni-sulphide was, however, never observed in this study. It is possible that starting compositions were never favourable to encounter heazlewoodite, or, when it did crystallize, that the polished sections did not include it. It is assumed (based on previous studies, section 2.1.1) that this phase would indeed crystallize from 800°C downwards, although the exact composition in the Cu-Ni-Fe-S system is undetermined.

6.6 The 700°C isothermal sections

The isothermal sections at 700°C are presented in Figures 6.22 to 6.25. At low sulphur contents, the phase assemblages remain the same as in the higher temperature isotherms. At high (~ 30 – ~ 50 wt%) sulphur contents three phases are stable: β-phase, millerite and vaesite. The phase relations at ~ 20 to ~ 40 wt% sulphur are superimposed from the high temperature isotherms, and indicated by stippled lines. Again the presence of heazlewoodite is unconfirmed by this investigation.

In all of the experiments, a distinct compositional difference between digenite and β-phase was observed, but the phase relation between these two Cu-sulphides could not be determined. Digenite appears to have a smaller compositional variation than the β-phase (see chapter 7).

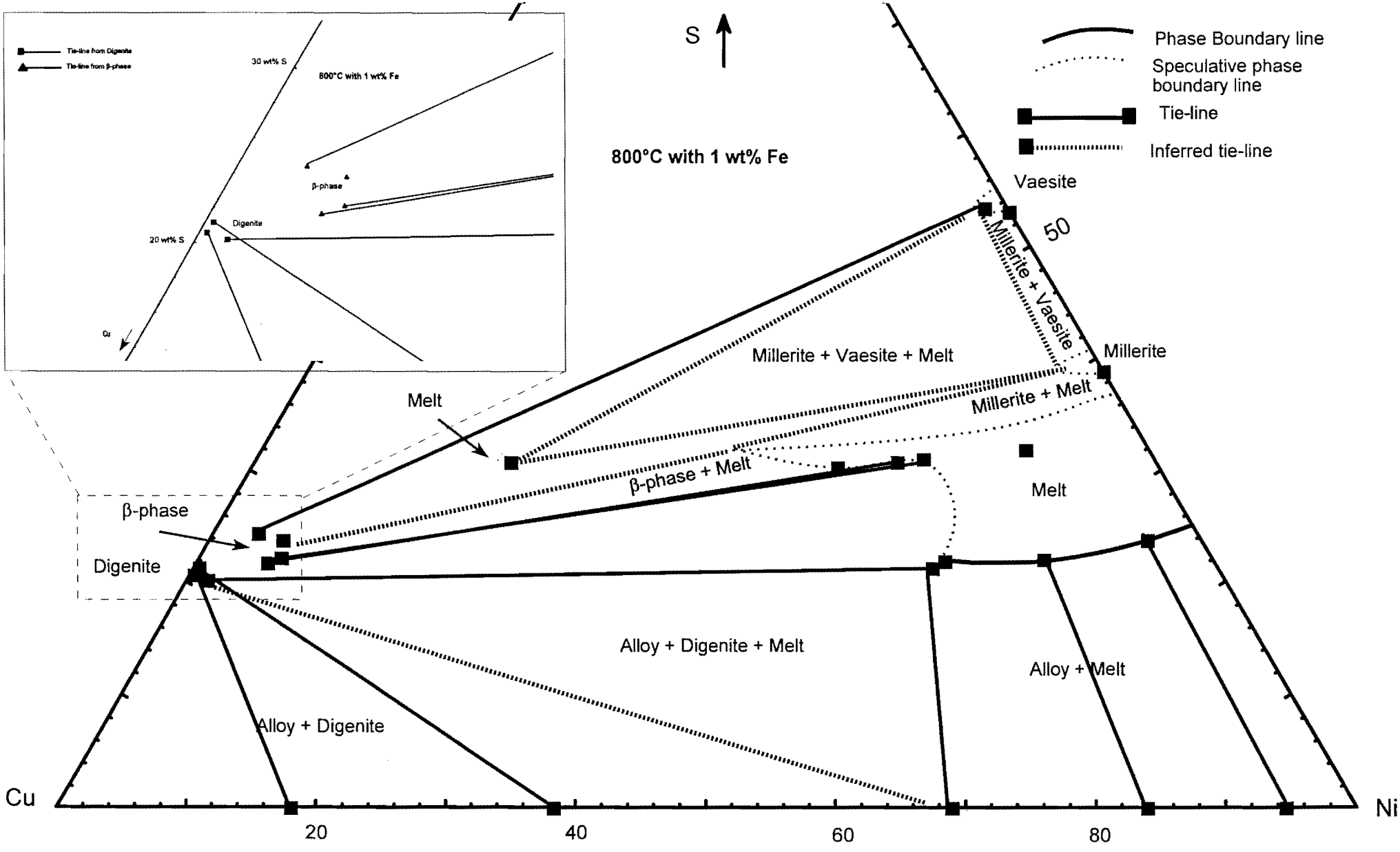

Figure 6.18: Phase relations at 800°C and 1 wt% Fe in starting compositions. The insert shows the area where digenite and β-phase plots.

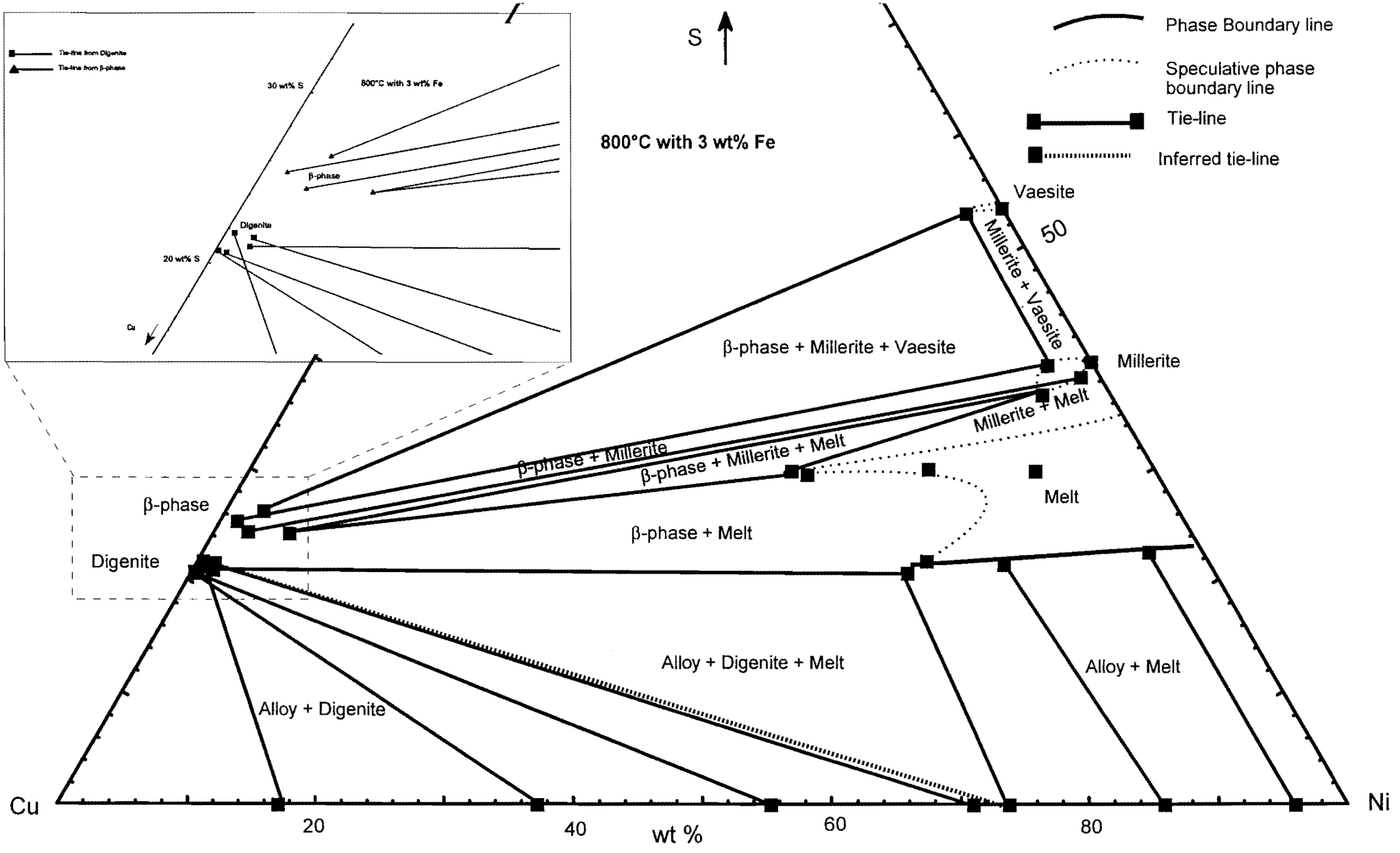

Figure 6.19: Phase relations at 800°C and 3 wt% Fe in starting compositions. The insert shows the area where digenite and β-phase plots.

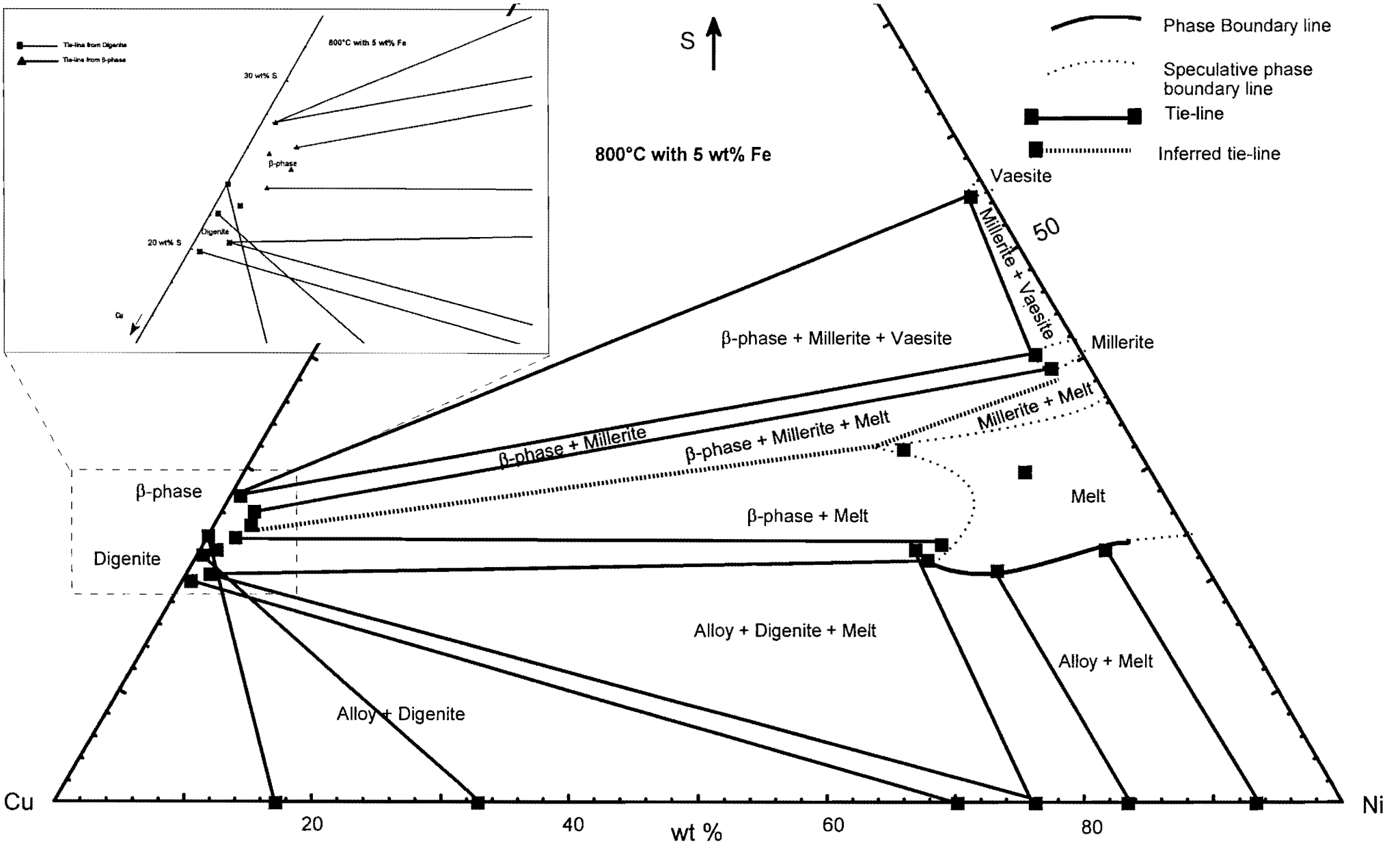

Figure 6.20: Phase relations at 800°C and 5 wt% Fe in starting compositions. The insert shows the area where digenite and β-phase plots.

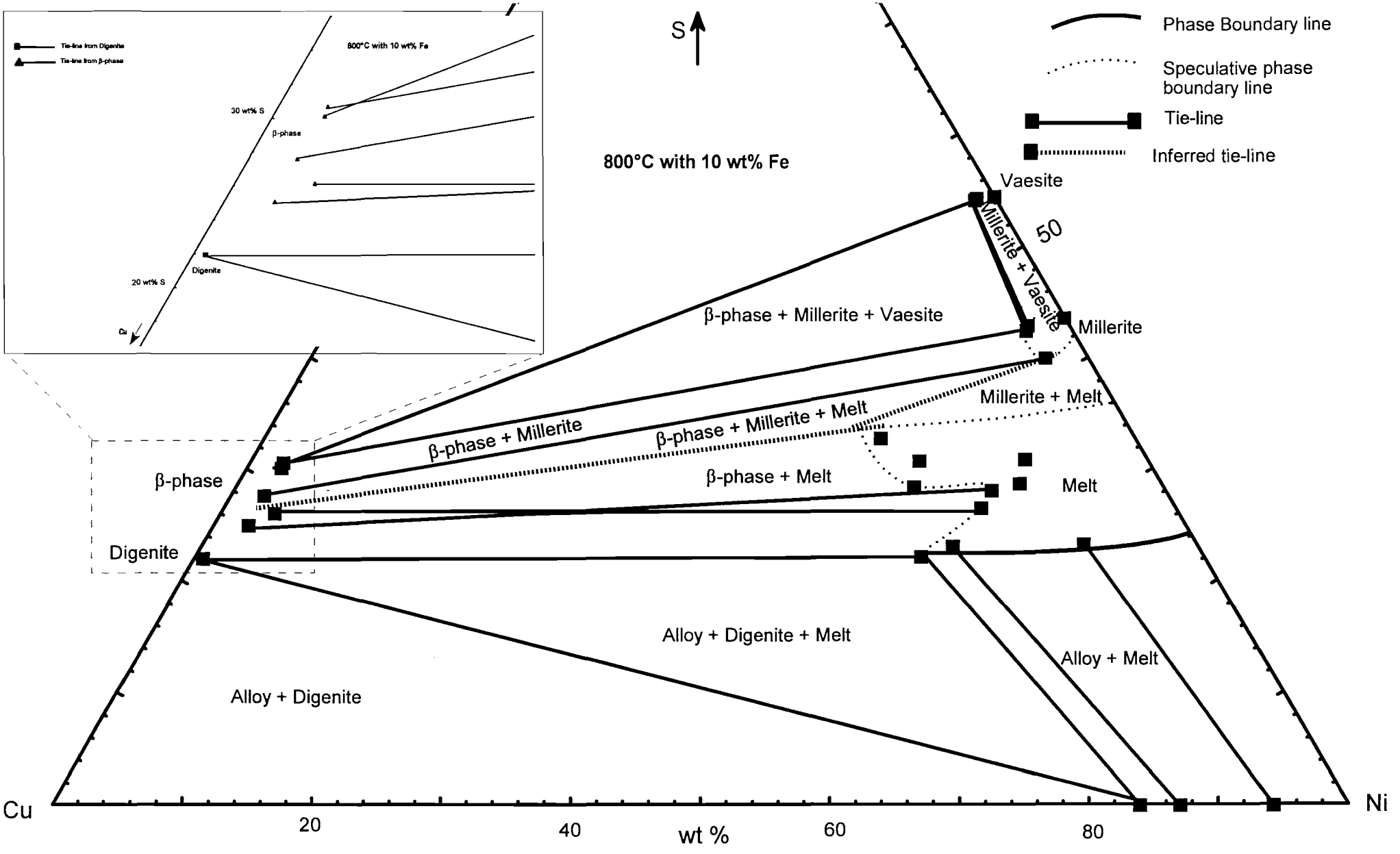

Figure 6.21: Phase relations at 800°C and 10 wt% Fe in starting compositions. The insert shows the area where digenite and -β-phase plots.

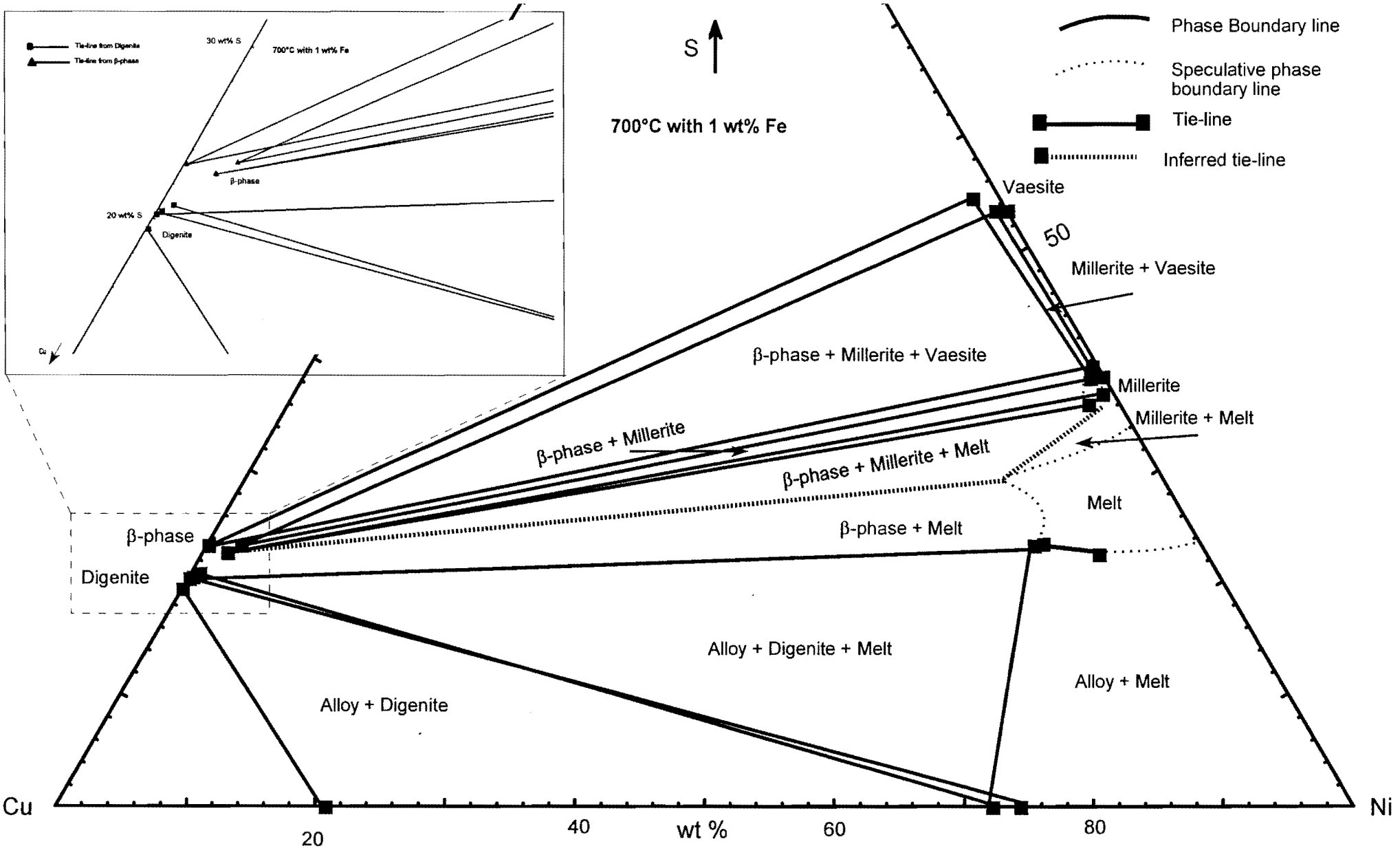

Figure 6.22: Phase relations at 700°C and 1 wt% Fe in starting compositions. The insert shows the area where digenite and β-phase plots.

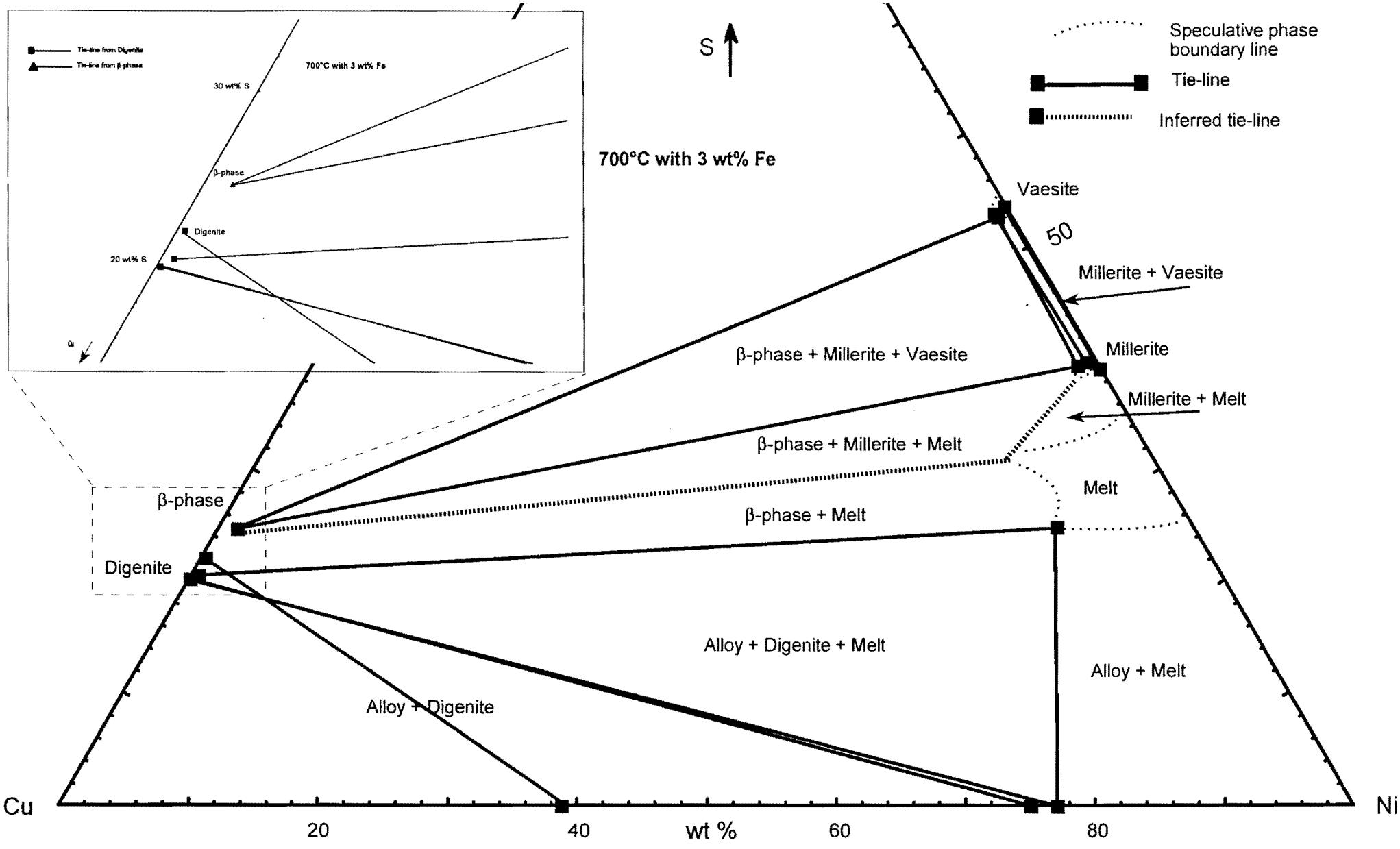

Figure 6.23: Phase relations at 700°C and 3 wt% Fe in starting compositions. The insert shows the area where digenite and β-phase plots.

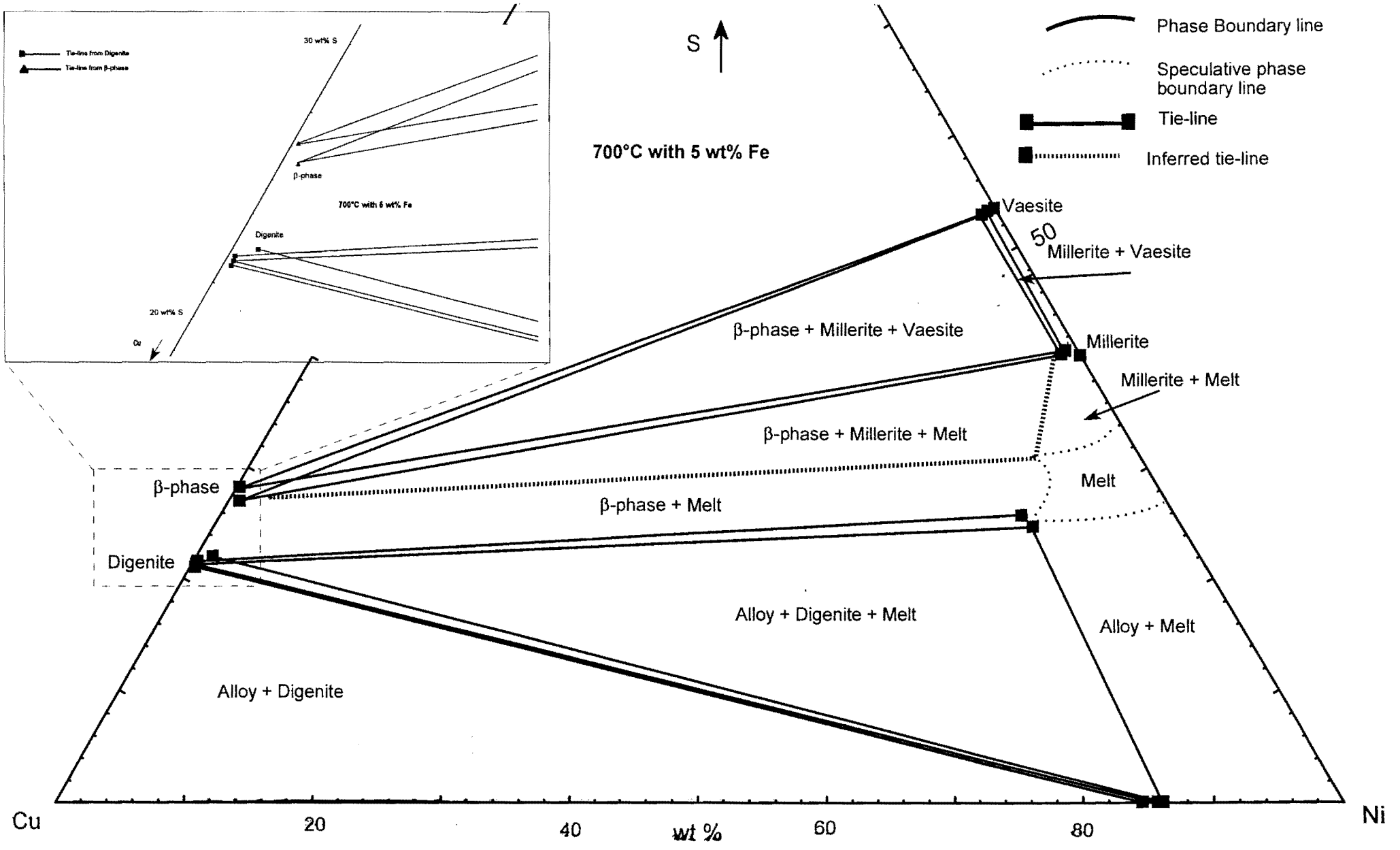

Figure 6.24: Phase relations at 700°C and 5 wt% Fe in starting compositions. The insert shows the area where digenite and β-phase plots.

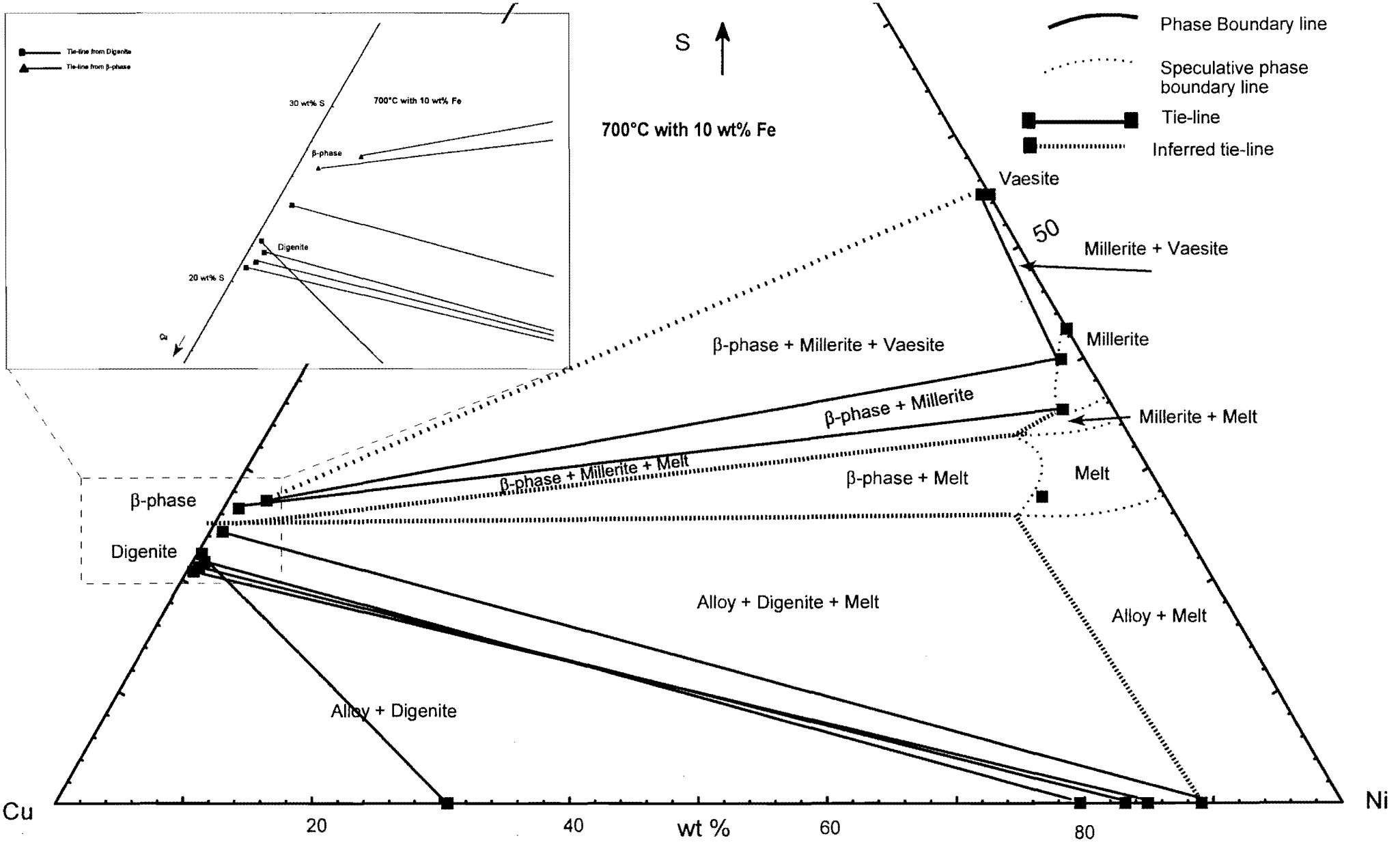

Figure 6.25: Phase relations at 700°C and 10 wt% Fe in starting compositions. The insert shows the area where digenite and β-phase plots.

7. DISCUSSION

The focus of this investigation revolves around the evolution of the projected phase diagrams with increasing Fe content and decreasing temperature, which is in the compositional framework important for slow cooling. The discussion includes the variations caused by different Fe-contents at the same equilibrium temperature, the variations at constant Fe content as a function of temperature, and the influence of the starting composition on the phase relations. The compositional changes of the cotectic alloy and cotectic melt are of special interest since these describe the evolution of the system.

Compositional changes of the various synthetic phases (alloy, digenite, β-phase, millerite and vaesite) were evaluated in relation to changes in the equilibrium temperature, the bulk composition and the mineral assemblage. Significant correlations between these variables are reported.

7.1 The Alloys

Figure 7.1 shows the Cu/Ni ratio against the Fe content of the alloys at different temperatures. No clear relationship is obvious between the Fe content, the Cu/Ni ratio, and the temperature of equilibration.

A plot of the Fe content in the starting composition against the Fe content of the alloys is seen in Figure 7.2. The higher the Fe content in the starting composition, the more Fe is present in the alloy. This is however, not a perfect linear correlation, and the higher Fe available in the bulk, the wider the range of Fe contents in the alloys. There is no correlation between the Cu/Ni ratio and the Fe content of the alloy, neither does the temperature play a role in the amount of Fe included in the alloy (Figure 7.3).

The Cu/Ni ratio against the Fe content of the cotectic alloys (Table 7.1) at the different equilibrium temperatures is presented in Figure 7.4. The Cu/Ni ratio of the cotectic alloys decrease with decreasing temperature at any given Fe content. The Fe content decreases exponentially with increasing Cu/Ni at any temperature.

7.2 The Cotectic melts

Figure 7.5 shows the Cu/Ni ratio against the Fe content of the cotectic melts at the different temperatures (Table 7.2). Three observations can be made: (1) the amount of Fe in the melt increases with the amount of Fe available in the bulk; (2) at a fixed temperature, the Fe content decreases with an increase in the Cu/Ni-ratio of the melt; and (3) similar to the cotectic alloys, the Cu/Ni ratio of the cotectic melts increases with increasing temperature. A plot of the Cu/Ni ratio against the sulphur content in the cotectic melts (Figure 7.6) indicates a slightly higher average sulphur content at lower temperatures (ranging from an average sulphur content of ~19.5 wt% at 1000°C, ~21 wt% at 900°C, ~21 wt% at 800°C and ~24 wt% at 700°C). The Cu/Ni ratios and sulphur

contents for cotectic melts at 800° and 700°C do not vary much from each other and the major compositional difference lies in the Fe content (see Figure 7.6).

Table 7.1: Average EMP data for the cotectic alloys at different temperatures and starting Fe contents.

Fe content category	Temperature (°C)	Cu wt%	Ni wt%	Fe wt%	Cu/Ni
1	1000	61.66	37.03	1.31	1.67
3	1000	52.71	43.04	4.25	1.22
5	1000	38.55	54.24	7.22	0.71
10	1000	24.04	60.83	15.13	0.40
1	900	44.48	53.52	2.00	0.83
3	900	34.26	59.51	6.23	0.58
5	900	24.56	64.91	10.53	0.38
10	900	16.12	67.47	16.41	0.24
1	800	30.39	67.64	1.97	0.45
3	800	25.06	70.28	4.65	0.36
5	800	21.90	70.28	7.82	0.31
10	800	13.85	72.58	13.57	0.19
1	700	28.07	71.53	2.41	0.39
3	700	23.16	73.42	3.43	0.32
5	700	12.70	77.35	9.95	0.16
10	700	9.39	75.76	14.85	0.12

Table 7.2: Average EMP data for the cotectic melts at different temperatures and starting Fe contents.

Fe content category	Temperature (°C)	Cu wt%	Ni wt%	Fe wt%	S wt%	Cu/Ni
1	1000	44.48	38.52	1.04	15.95	1.15
5	1000	40.25	37.06	3.51	19.18	1.09
10	1000	33.58	36.03	6.93	23.48	0.93
1	900	32.17	48.18	0.84	18.81	0.67
5	900	30.87	44.74	3.81	20.58	0.69
10	900	26.45	44.29	6.13	23.12	0.60
1	800	22.30	56.31	0.47	20.92	0.40
3	800	22.52	55.23	1.39	20.87	0.41
5	800	20.97	54.73	2.79	21.52	0.38
10	800	20.90	53.40	4.52	21.18	0.39
1	700	12.87	63.70	0.22	23.21	0.20
3	700	10.40	63.65	1.51	24.45	0.16
5	700	11.39	61.48	2.60	24.55	0.19

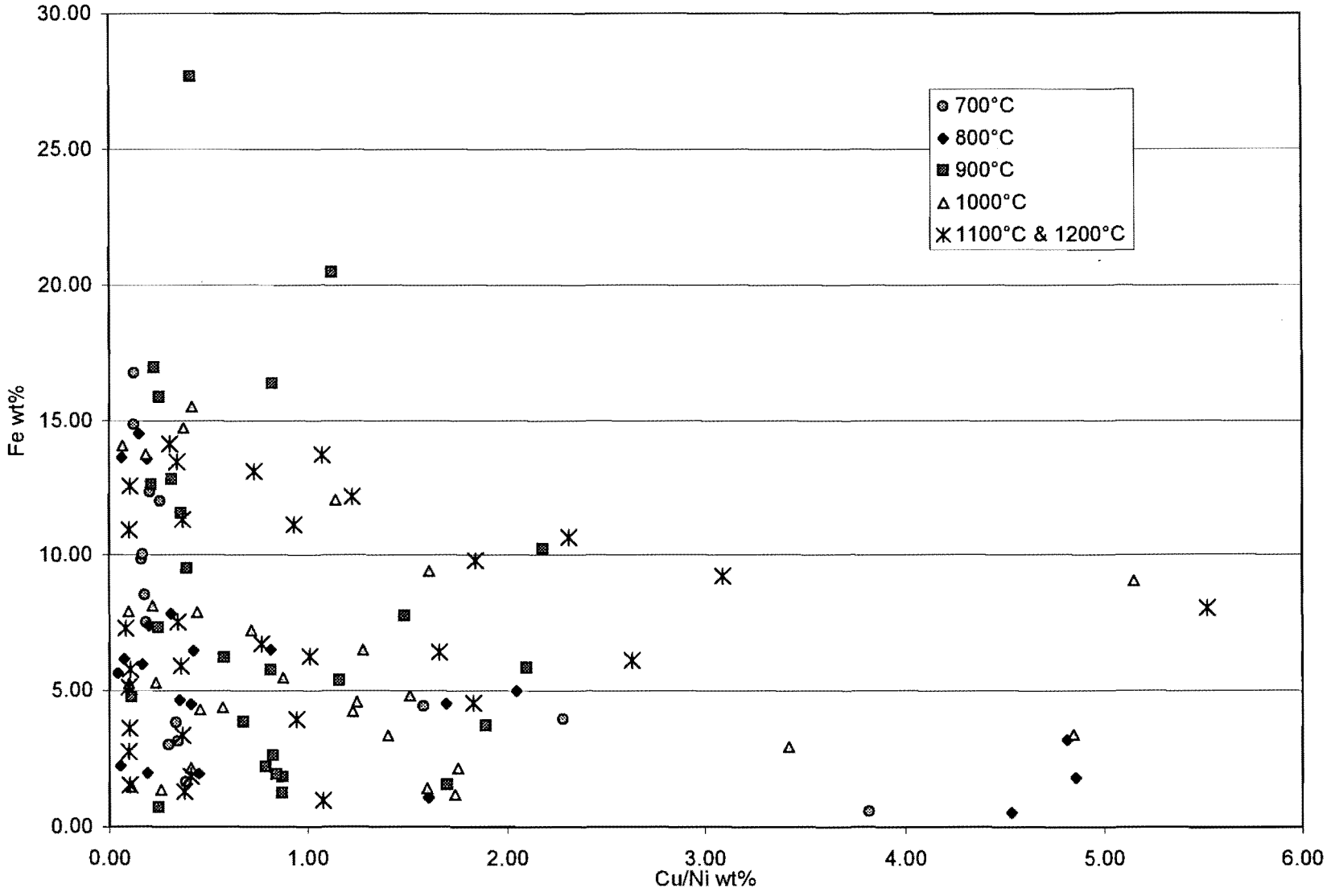

Figure 7.1: The Cu/Ni ratio against the Fe content of the alloys at different temperatures.

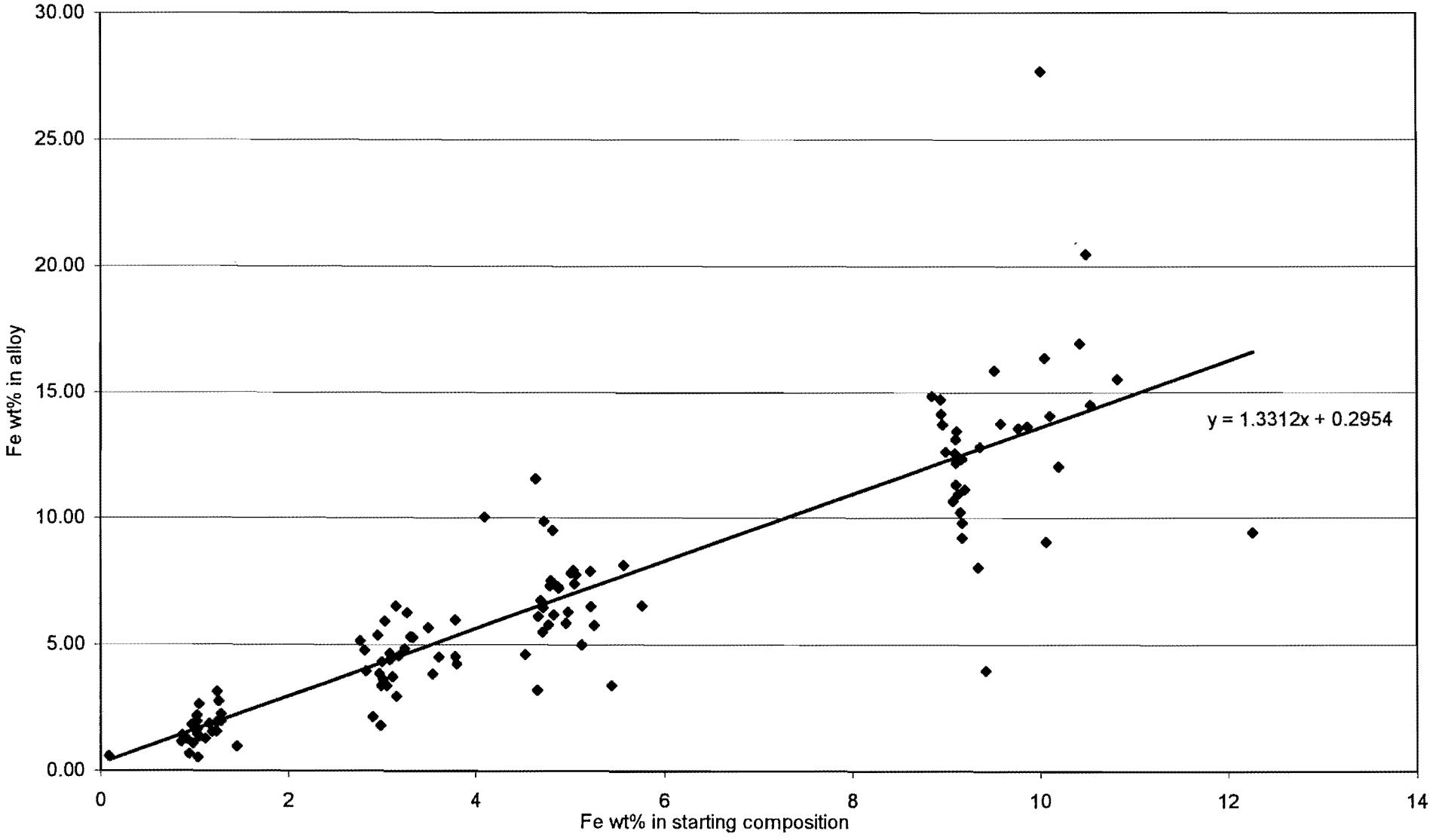

Figure 7.2: The Fe content in the starting composition against the Fe content of the alloys. Shown is a linear regression line through the population .

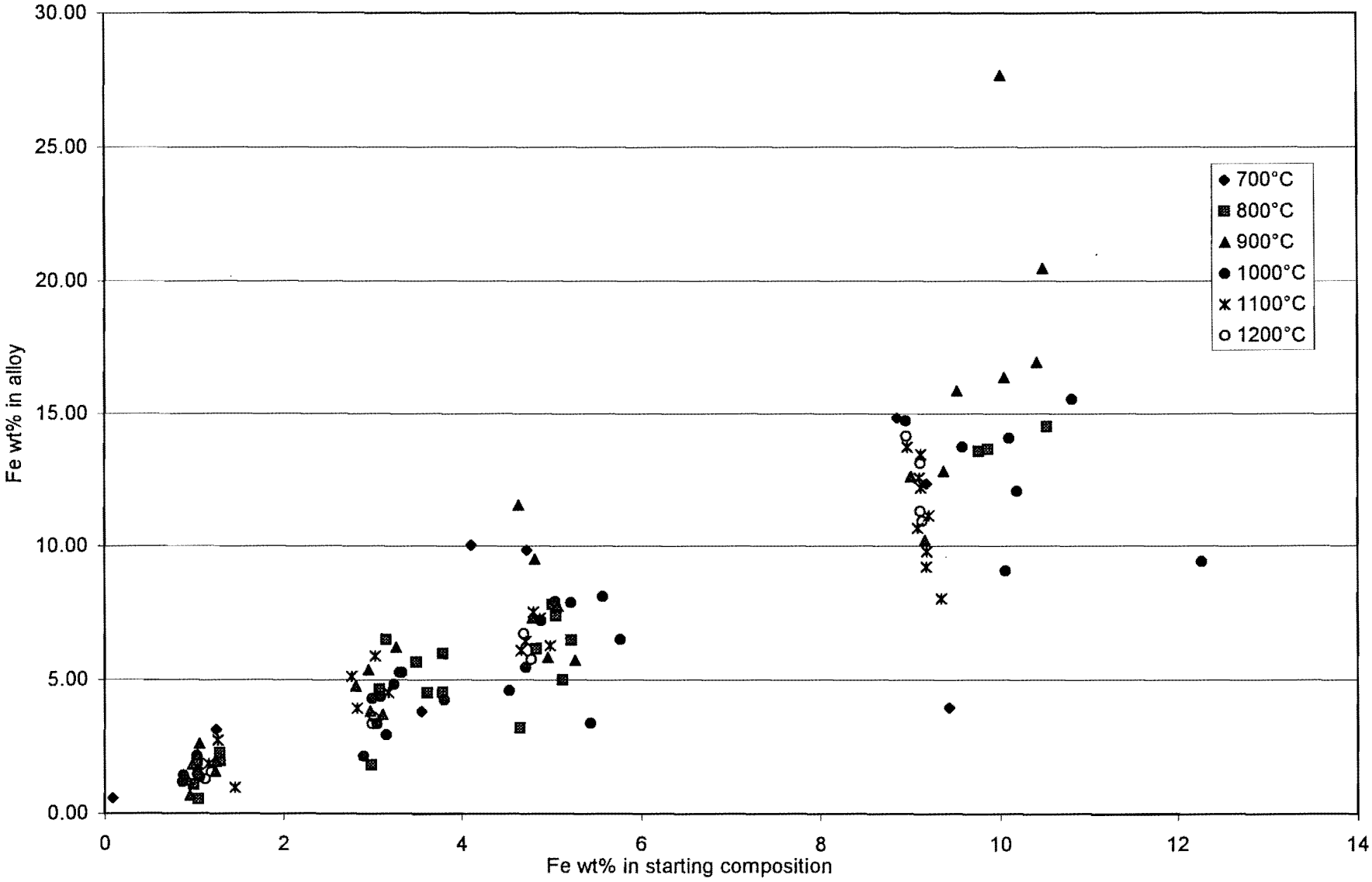

Figure 7.3: Fe in the alloy against Fe in the starting composition as a function of temperature.

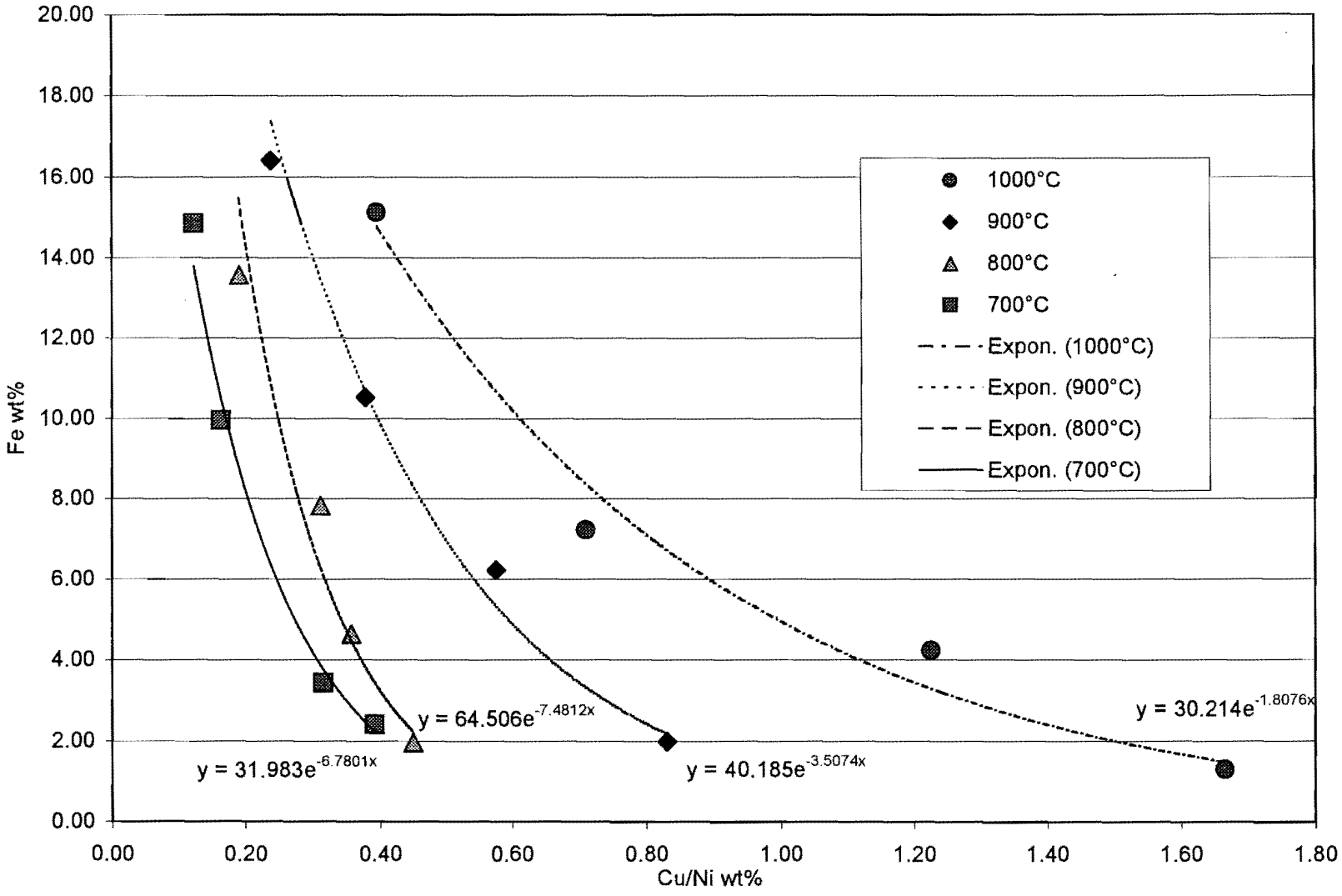

Figure 7.4: The Cu/Ni ratio against the Fe content of the cotectic alloys at the different equilibrium temperatures. Shown are the exponential regression lines for the cotectic alloys at different temperatures.

7.3 Digenite

In Figure 7.7, the Fe content against the sulphur content in digenite at different equilibrium temperatures is shown. The slope of the regression line for digenite at higher temperatures is less steep than those at lower temperatures. Linear regressions for different temperatures show an increase in sulphur content with an increase in Fe in the digenite at any given temperature. The sulphur and Fe content may be an indication that a solid solution exists between digenite and the β-phase. This aspect is discussed in sections 7.4 and 7.5.

Figure 7.8 shows the Fe content of digenite in relation to the amount of Fe in the starting composition. The higher Fe in the starting composition, the more Fe is taken up by the digenite. This is, however, not a perfectly linear relationship. The variation of the Fe content in digenite also becomes larger with the increase of the amount of Fe in the bulk. Also indicated on this diagram is the influence of temperature on the amount of Fe in the digenite. The higher the temperature, the more Fe can enter the digenite structure. The regression line for 800°C does not follow the general trend, because only one composition for digenite in the 10 wt% Fe category is available. Other plots show that the Fe in the digenite is independent of the assemblage (Figure 7.9).

The Ni and Fe content of digenite with and without exsolutions is presented in Figure 7.10. Analyses of digenite with exsolutions always included the exsolutions to represent the composition of the digenite at the temperature of equilibration. Digenite with exsolutions shows a larger variation in Ni content than the digenite without exsolutions, which has Ni contents lower than 1.23 wt%. The Fe content of both populations of digenite shows a wide variation. The presence of exsolutions can not be attributed to the amount of Fe in the digenite.

In Figure 7.11, digenite with different types of exsolutions are indicated on a Fe/Ni plot. The types are: digenite with round exsolutions that disappear towards the contact of digenite with an adjacent phase, digenite with round exsolutions that do not disappear towards the contact and digenite that contain skeletal type of exsolutions. There appears to be no distinct difference between the different types with the limited amount of data available.

Apart from the fact that metallic Cu was only observed in (alloy+digenite)- and (digenite+melt)-assemblages, there are no correlations between the starting composition, equilibrium temperature and mineral assemblage of experiments containing digenite and metallic Cu and those without metallic Cu. These Cu-rims were too small to analyze quantitatively, but the optical color strongly indicates that Cu is the main component. There is no reason to believe that the experiments containing them were in dis-equilibrium. Because they appear very infrequently and in small quantities it is believed that these metallic Cu appearances are in some way related to the process of quenching of the experiments. It is not the scope of this project to investigate this issue any further.

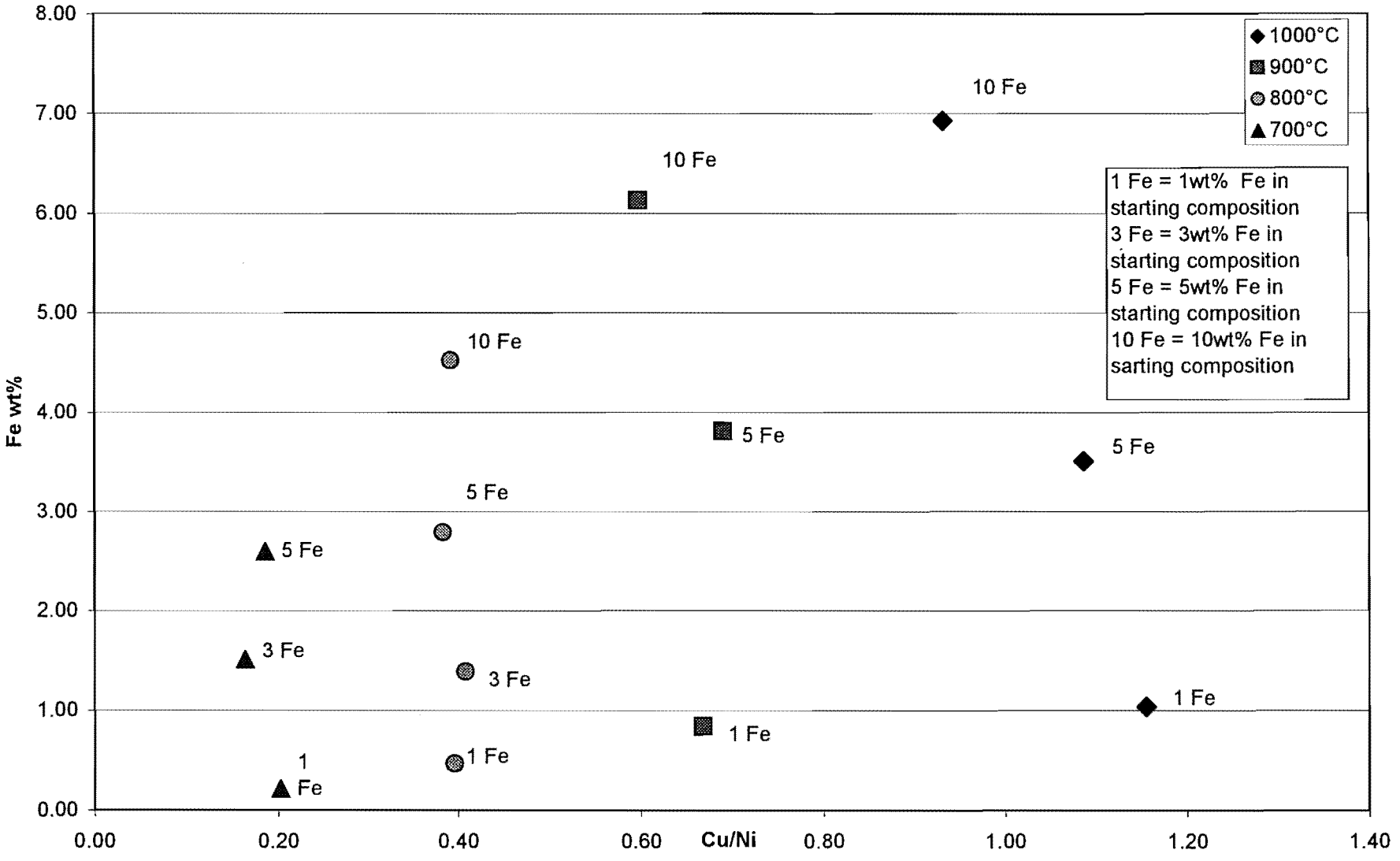

Figure 7.5: The Cu/Ni ratio against the Fe content of the cotectic melts at the different temperatures.

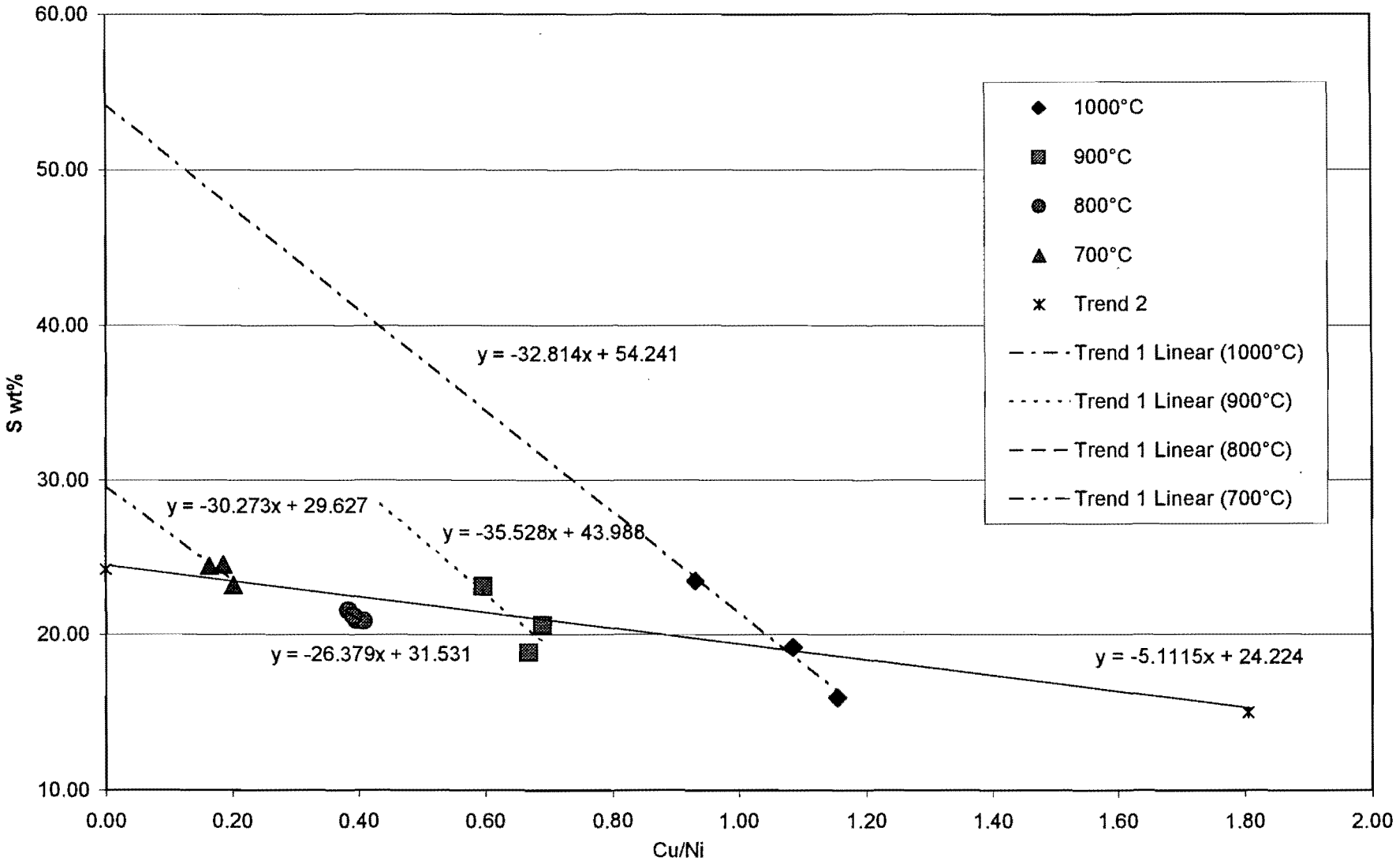

Figure 7.6: The Cu/Ni ratio against the sulphur content for the cotectic melts. Linear trend lines are indicated for each temperature as well as for the whole population.

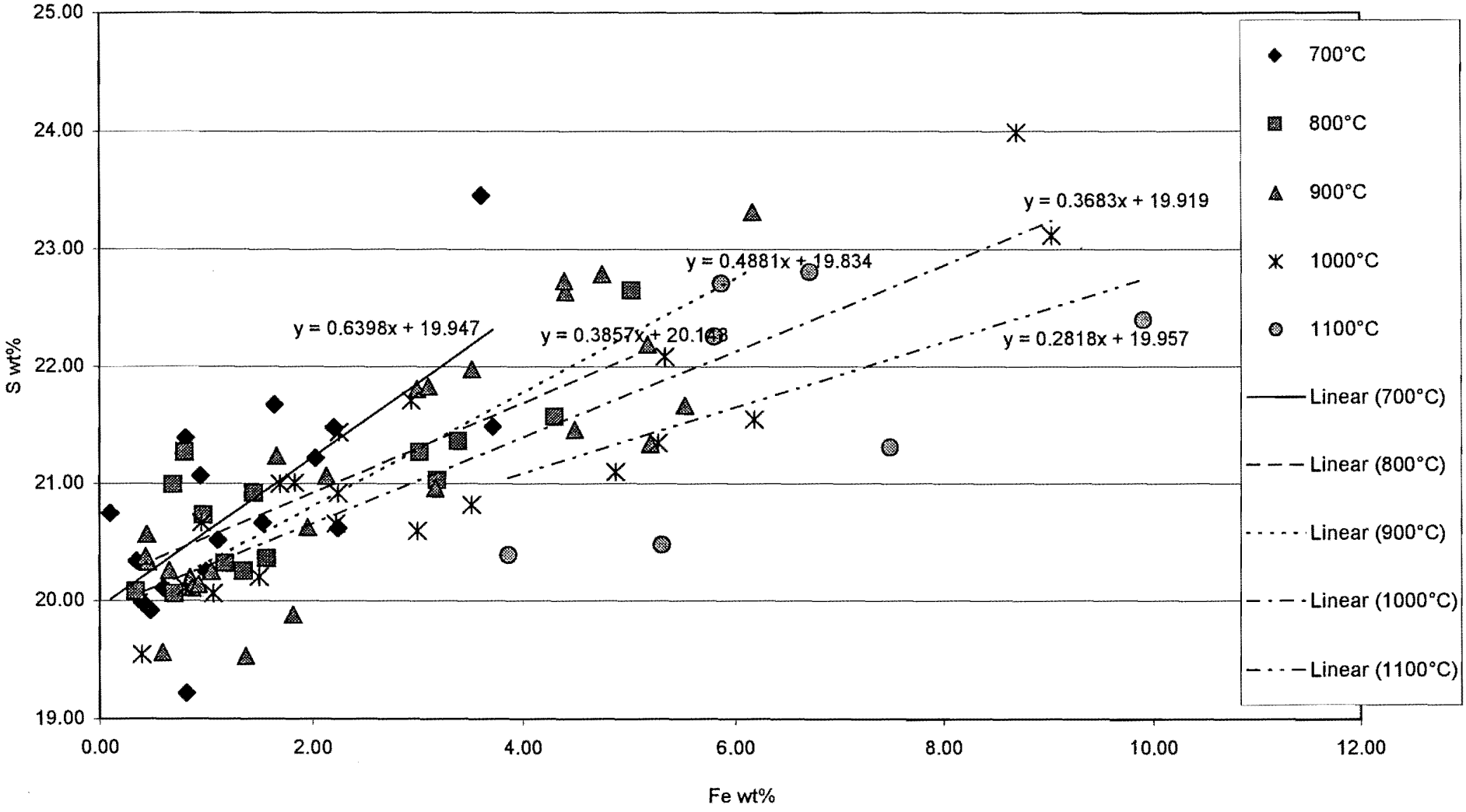

Figure 7.7 The Fe content against the sulphur content in the digenite at different equilibrium temperatures. The linear trend lines are shown at each temperature.

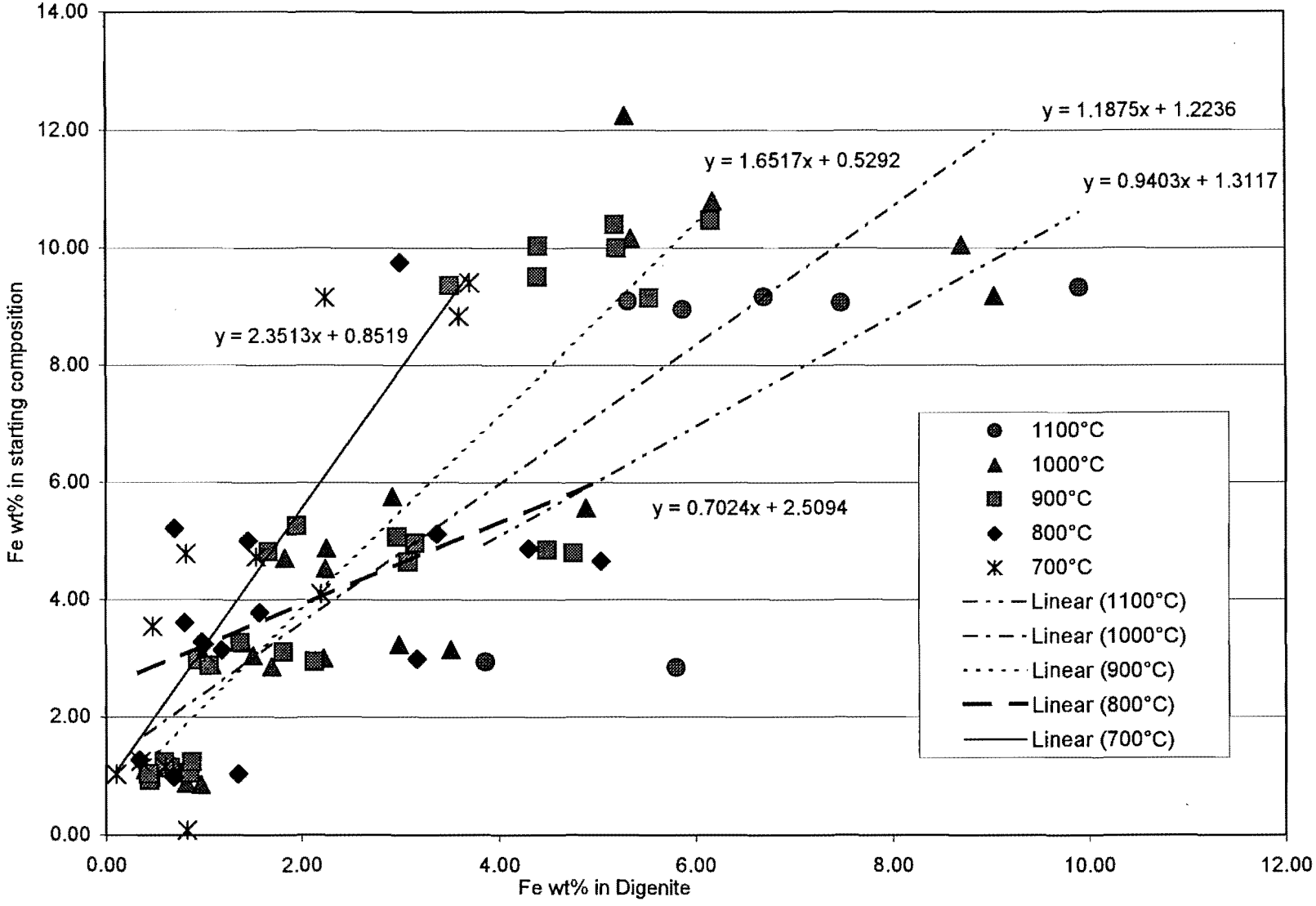

Figure 7.8 The Fe content of digenite in relation with the amount of Fe in the starting composition. Also indicated are the effect of temperature and the regression lines at different temperatures.

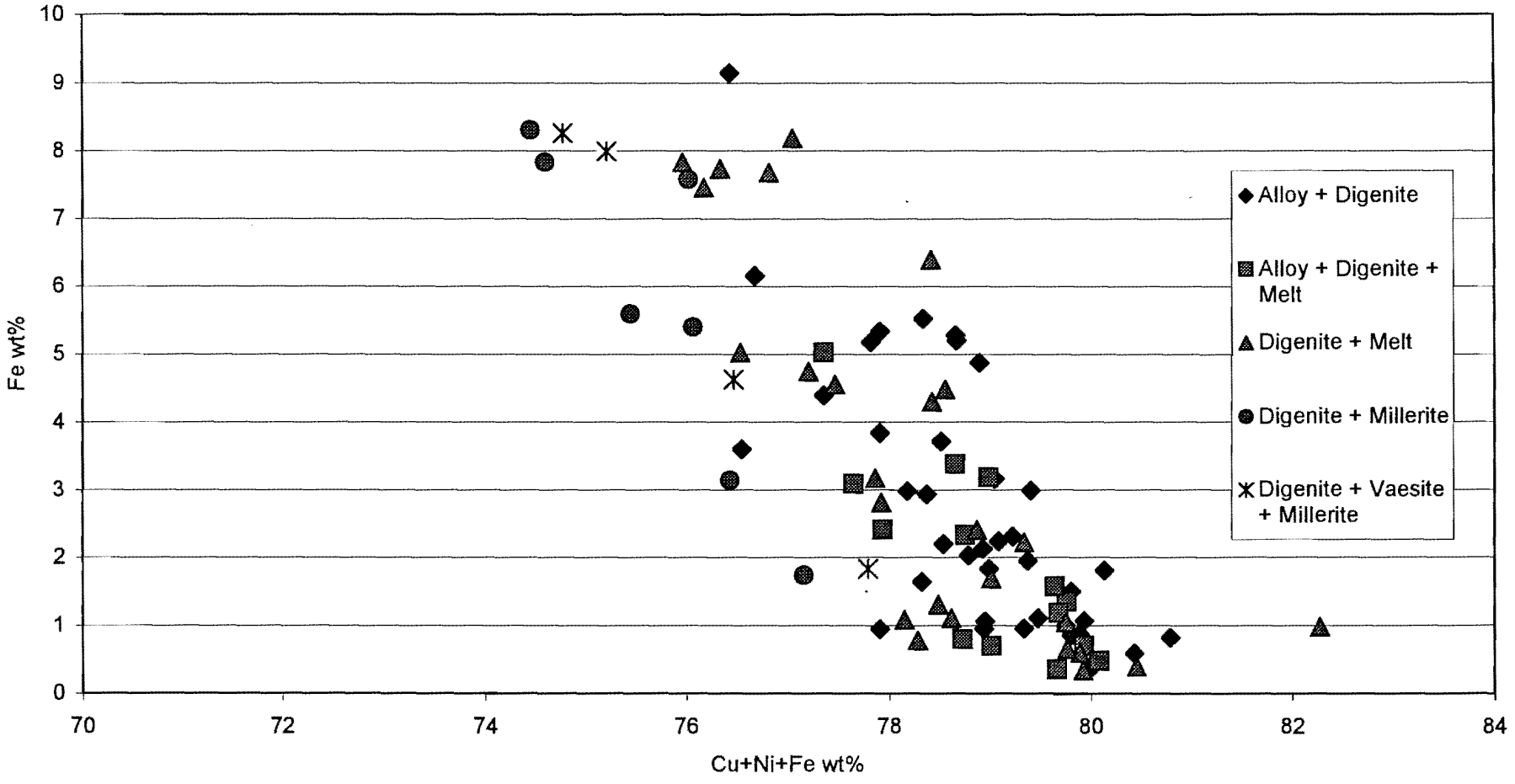

Figure 7.9: Fe content in Digenite is independent of the assemblage

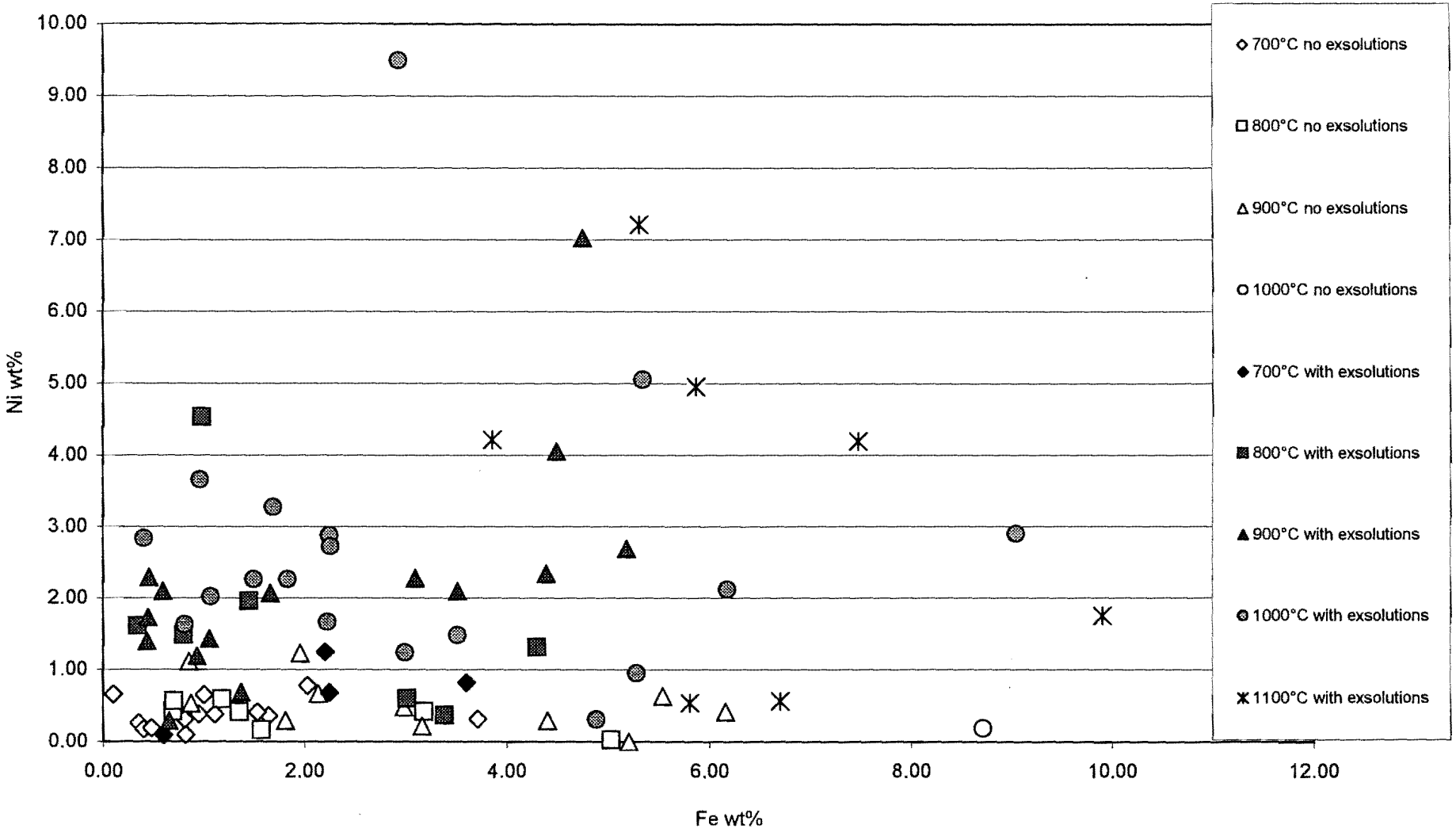

Figure 7.10 The Ni and Fe content of digenites with and without exsolutions.

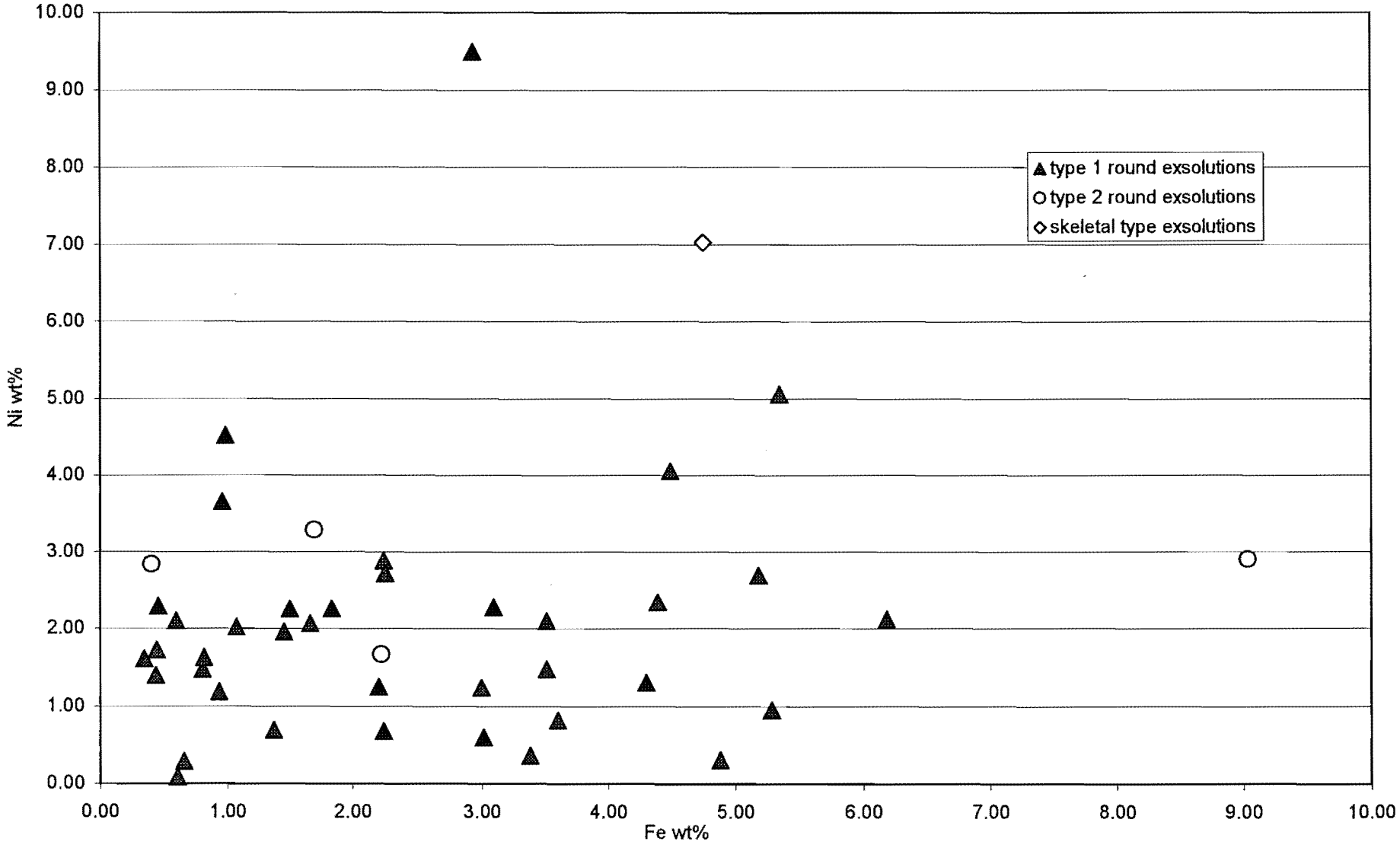

Figure 7.11 The Ni and Fe contents of digenite with different types of exsolutions.

7.4 The β-phase

EMP analyses (Table 7.3) for the β-phase were plotted together with those of digenite to show the compositional differences. Figure 7.12 displays the Cu-S relationship for digenite and the β-phase from all the experiments. The digenite data plots towards higher Cu and lower sulphur contents, while the β-phase has generally lower Cu and higher S contents. There are no other compositional differences between digenite and β-phase. A statistical evaluation between the Cu and sulphur values of digenite and β-phase follows under section 7.5.

The fact that β-phase co-exists only with millerite and vaesite suggests that it needs higher initial sulphur contents to form. With lower sulphur contents in the bulk composition, digenite will be more likely to be stable. The large compositional overlap between these two phases suggests a gradual compositional shift of digenite towards higher sulphur and lower Cu contents at lower temperatures. The empirical formula for the average β-phase is $(Cu_{1.45}Ni_{0.07}Fe_{0.12})_{1.64}S$ and that of the average digenite is $(Cu_{1.78}Ni_{0.04}Fe_{0.07})_{1.90}S$.

The difference in optical appearance may point to structural differences. For this purpose X-ray diffraction patterns were obtained from four experiments containing the β-phase (Appendix E). The aim was to determine weather there is a shift or modification in the XRD-pattern for digenite or whether there is a distinct different phase pattern present.

After careful evaluation of the XRD patterns it was determined that the Cu-sulphide phase present was not digenite, or a compositional variation of digenite. The β-phase resembles best synthetic bornite (Cu_5FeS_4). Digenite is cubic, thus isotropic whereas bornite is tetragonal below 228°C where it displays weak anisotropism, and cubic above 228°C where it is isotropic (Klein & Hurlbut, 1999). The optical appearance of β-phase also mirror that of bornite better than that of digenite. Chemically, stoichiometric bornite contains 63.3 wt% Cu, 11.2 wt% Fe and 25.5 wt% S, but shows extensive solid solution within the Cu-Fe-S system (Klein & Hurlbut, 1999). The β-phase contains on average 68.21 wt% Cu, 7.94 wt% (Fe+Ni) and 23.85 wt% S, which does not make it true synthetic bornite but possibly part of the solid solution of bornite.

Yund and Kullerud (1966) investigated the thermal stability of assemblages in the Cu-Ni-S system from 700°C to approximately 100°C, and found a synthetic phase which they called "x-bornite". This phase is close in optical appearance and composition to bornite, but contains about 0.4 wt% more sulphur. They proposed that "x-bornite" forms when sulphur-rich bornite synthesized at high temperature is annealed between 62° and 140°C. This phase was identified with natural "anomalous bornite" also described by Sillitoe and Clark (1969) that found that "anomalous bornite" in the Copiapo mining district, northern Chile contains 2 wt% less Cu and 2 wt% more sulphur than optically-normal, hypogene bornite. Other natural occurrences of "anomalous bornite" were described by Ixer et al. (1986) and Nylstrom and Wickman (1991) in supergene natural systems (generally temperatures below ~ 150°C). Durazzo and Taylor (1982) also mention "anomalous bornite" in experimental work in the bornite-chalcopyrite system at annealing temperatures between 100° and

350°C. These occurrences of "anomalous bornite" are all described in low temperature systems, and the correlation of "anomalous bornite" to the high temperature β-phase is not concluded.

7.5 Statistical Evaluation of the Composition of Digenite and β-phase

To quantify the compositional difference between digenite and the β-phase, the non-parametric Tukey-test (Tukey, 1959; Neave, 1966; and Neave, 1979) and a Kolmogorov-Smirnov-type (K-S-type) test were performed. For step-by-step overview on how the Tukey-test is performed the summary by Nelson (1975) is recommended, and for the K-S-type test the statistical books by Conover (1980) and Meddis (1975) give a good overview.

With the Tukey-test, the Cu and sulphur data for the digenite and β-phase were compared to determine whether the means for the two populations are statistically different at the 5% and 1% significance levels. This would give an indication. According to the table of critical values given by Nelson (1975), T_N for Cu should be larger than 10 for the 5% significance level and larger than 13 for the 1% significance level. The value T_N for Cu from this study is 16, which is larger than both values. Thus, the difference in the mean of the Cu values for these two populations are statistically significant. The test was not successful distinguishing between the two populations with respect to the sulphur values.

The Kolmogorov Goodness-of-fit Test was applied to first determine the normality of at least one of the populations. Although it can be derived from Figure 7.12 that neither digenite nor β-phase has a normal distribution with regard to their Cu and sulphur values, the Kolmogorov test was applied to verify this. The T value was calculated to be much larger (0.80) than the critical value at both the 95% (0.11) and 99% (0.18) confidence levels for the two-sided test. Therefore, the common t-test used for normal distributions could not be used to test the difference in distribution between the Cu values for digenite and the β-phase, and it was decided to use a non-parametric Kolmogorov-Smirnov-type test.

With the Kolmogorov-Smirnov test a significant difference between the Cu and sulphur values of the digenite and β-phase was investigated. Tests for both the Cu and sulphur distributions of digenite and the β-phase showed that a statistically significant difference between these distribution exists. The critical value for the two-sided test at a 95% confidence level is 0.28, and the T value for Cu was calculated to be 0.68. Similarly, the T value for sulphur (0.77) is also much larger than the critical value of 0.28.

The results from the Tukey- and the K-S-type test proved that there exists a, statistically significant difference between the distribution of the Cu and sulphur values for digenite and the β-phase. Therefore, based on compositional differences and the XRD analyses these two phases are not part of the same solid solution series.

Table 7.3: Average EMP data for the β-phase in weight and atomic percentage.

Experiment no.	Cu wt%	Ni wt%	Fe wt%	S wt%		Cu at%	Ni at%	Fe at%	S at%
7h4	76.51	0.13	0.24	23.11		62.34	0.11	0.22	37.32
7a4	75.19	1.77	0.95	22.09		61.65	1.57	0.89	35.90
7g5	72.80	2.62	1.74	22.84		59.24	2.31	1.61	36.84
7h1	74.11	1.85	1.83	22.20		60.65	1.64	1.70	36.01
7g1	70.46	1.38	4.63	23.53		56.89	1.21	4.25	37.65
7j3	68.21	0.26	4.71	26.82		53.70	0.22	4.22	41.86
7i3	66.42	0.80	7.99	24.78		52.93	0.69	7.24	39.14
7e4	63.69	2.66	8.98	24.67		50.67	2.29	8.13	38.91
7e5	66.54	1.03	8.13	24.30		53.20	0.89	7.40	38.51
8j4	69.83	5.62	1.07	23.48		56.46	4.92	0.98	37.63
8j2	72.04	5.46	1.11	21.39		59.24	4.86	1.04	34.86
8j3	70.72	6.35	1.08	21.84		57.91	5.63	1.01	35.45
8l1	70.45	3.37	2.40	23.79		56.82	2.94	2.20	38.03
8f3	70.77	2.52	3.14	23.58		57.16	2.20	2.89	37.75
8l2	67.20	5.68	3.93	23.19		54.29	4.97	3.61	37.13
8l3	69.51	1.15	5.40	23.94		55.90	1.00	4.94	38.16
8l5	66.94	2.70	5.58	24.78		53.41	2.33	5.07	39.19
8b4	70.79	2.12	4.56	22.53		57.59	1.87	4.22	36.33
8b5	68.74	2.76	5.03	23.47		55.45	2.41	4.62	37.52
8m2	65.86	0.65	8.26	25.23		52.28	0.56	7.46	39.70
8m3	67.39	1.21	7.73	23.68		54.16	1.05	7.07	37.72
8m4	67.44	2.41	5.59	24.56		53.91	2.09	5.08	38.92
8d1	64.32	3.81	7.83	24.04		51.45	3.30	7.13	38.12
8i3	66.44	2.42	8.19	22.95		53.64	2.12	7.52	36.72
8m5	64.46	2.31	7.83	25.40		51.07	1.98	7.06	39.89
8n2	60.16	2.41	10.56	26.88		46.98	2.04	9.38	41.60
8n5	59.33	2.27	11.22	27.18		46.20	1.91	9.94	41.95
9i3	69.31	5.80	2.81	22.07		56.56	5.13	2.61	35.70
9i5	68.50	6.19	3.17	22.14		55.83	5.46	2.94	35.77
9g2	65.08	3.63	7.46	23.83		52.18	3.15	6.81	37.87
9l4	65.16	3.98	7.68	23.18		52.48	3.47	7.04	37.01
9n3	66.79	6.14	1.13	25.94		52.95	5.27	1.02	40.76
9e3	67.61	7.91	1.35	23.13		54.72	6.93	1.24	37.11
9h3	71.39	6.11	0.78	21.73		58.53	5.42	0.73	35.31
Average	**68.21**	**3.08**	**4.86**	**23.85**		**54.90**	**2.69**	**4.42**	**37.99**
Standard Deviation.	**3.71**	**2.09**	**3.14**	**1.54**		**3.62**	**1.84**	**2.82**	**1.92**

7.6 Millerite and Vaesite

In Figure 7.13, the (Ni + Cu + Fe) and sulphur content of the millerite and vaesite from all the experiments are compared. Analyses of millerite show an average metal content of 47.67 ± 1.15 at% (range 49.38 – 54.24 at%) and an average sulphur content of 52.33 ± 1.15 at% (range 45.76 – 50.62 at%). Vaesite has an average metal content of 32.47 ± 0.49 wt% (range 66.56 – 68.55 at% metals) and an average sulphur content of 67.53 ± 0.49 at% (range 31.45 – 33.44 at%). Recalculation to atomic proportions gives a general formula of $(Ni,Cu,Fe)_{0.91}S$ for millerite and $(Ni,Cu,Fe)_{0.96}S_2$ for vaesite.

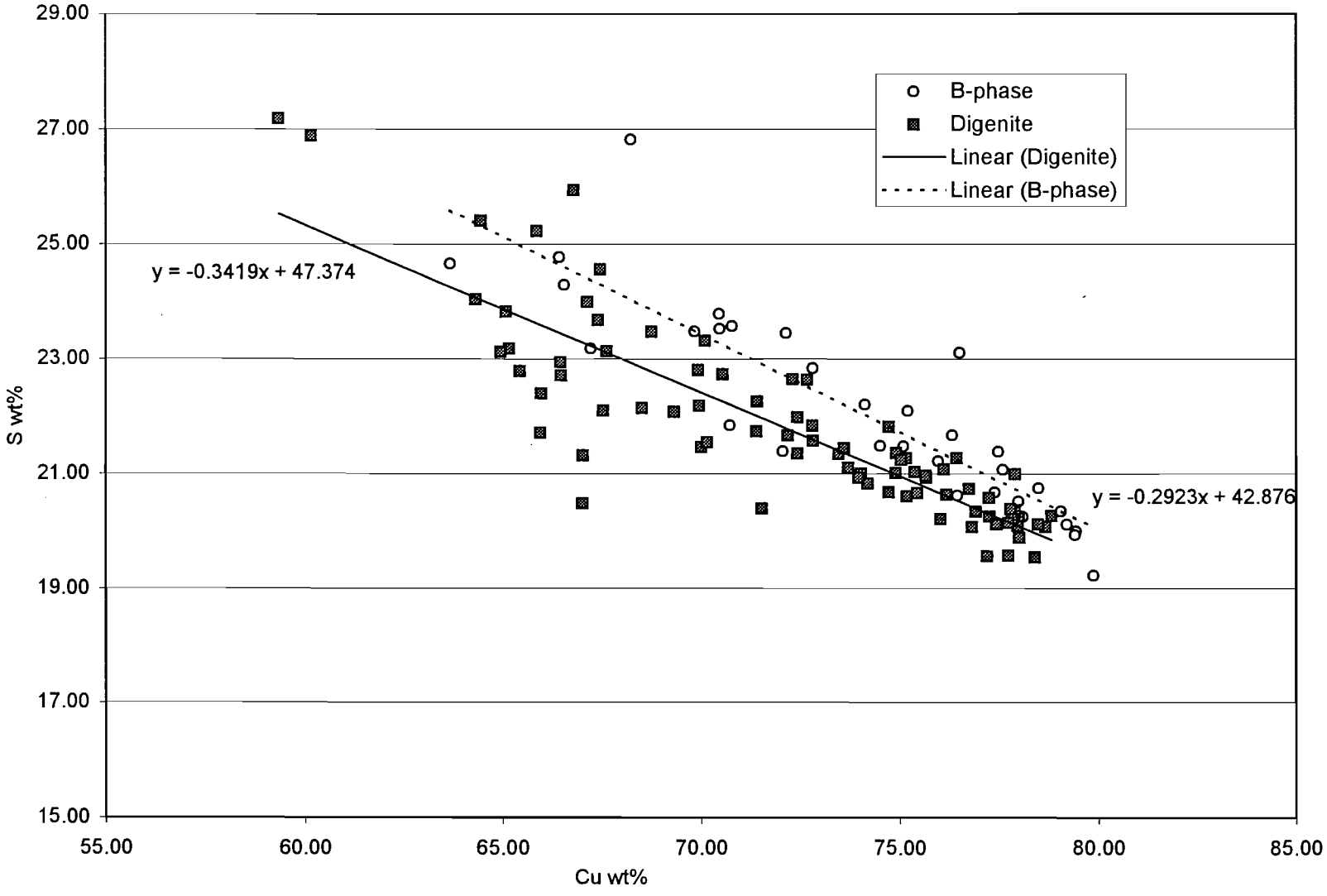

Figure 7.12: A Cu against sulphur plot for digenite and the B – phase. The linear regression lines are indicated with the relevant equations.

The relationship between the Ni and Fe-content in millerite and vaesite from all the [illegible] can be seen in Figure 7.14. Vaesite shows little variation in Ni and Fe contents, and the composition is close to the stoichiometric NiS_2. Analyses of millerite show a negative correlation between Ni and Fe, and a wide variation in Fe contents.

Figure 7.15 is a plot of the Fe content in millerite against the Fe content in the starting composition. The amount of Fe in millerite is strongly dependent on the amount of Fe in the starting composition. For lower starting Fe-contents, the variation in the population is smaller than when larger quantities of Fe are available. The plot for vaesite (Figure 7.16) shows that the starting Fe content will also influence the amount of Fe in the vaesite, although only a small amount of Fe will enter the vaesite structure.

Evaluation of the millerite and vaesite data indicated that there is no significant relationship between the starting composition, equilibration temperature and assemblage.

7.7 Construction of Cooling Paths

For each bulk Fe content (i.e. 1, 3, 5 and 10 wt% Fe), a basic Cu-Ni-S ternary diagram was prepared, containing the average composition of all the sulphides and the average cotectic alloy composition at each temperature. Solidus tie-lines indicate which phases co-exist on complete solidification.

Unto the relevant diagram, the cotectic lines from each temperature isotherm (1200°C to 700°C) were superimposed. The eutectic points on each temperature isotherm were then connected to form a "cooling path isotherm". Where the detailed information lacked sufficient data the lines were inferred using the diagram of Bruwer (1996) as a guideline. The direction of cooling is indicated with arrows on the cotectic lines, each line leading towards an eutectic point. Crossing isotherms and winding cotectic(s) are a result of projection of a three-dimensional surface onto a two-dimensional plane.

7.8 Cooling Paths

The liquidus isotherms and cooling paths of a Cu-Ni-sulphide melt with different starting Fe-contents are shown in Figures 7.17 to 7.20. Indicated on the diagrams are the average compositions of phases in this system based on analyses from this study (the composition of heazlewoodite is schematic). The average compositions of these solid phases change according to the amount of Fe in the starting composition. The cotectic lines indicate the path of crystallization from 1200°C towards complete crystallization of the melt, at the relevant eutectic point. The exact positions of the eutectic points E1, E2 and E3 can not be determined from this study and these points are estimated.

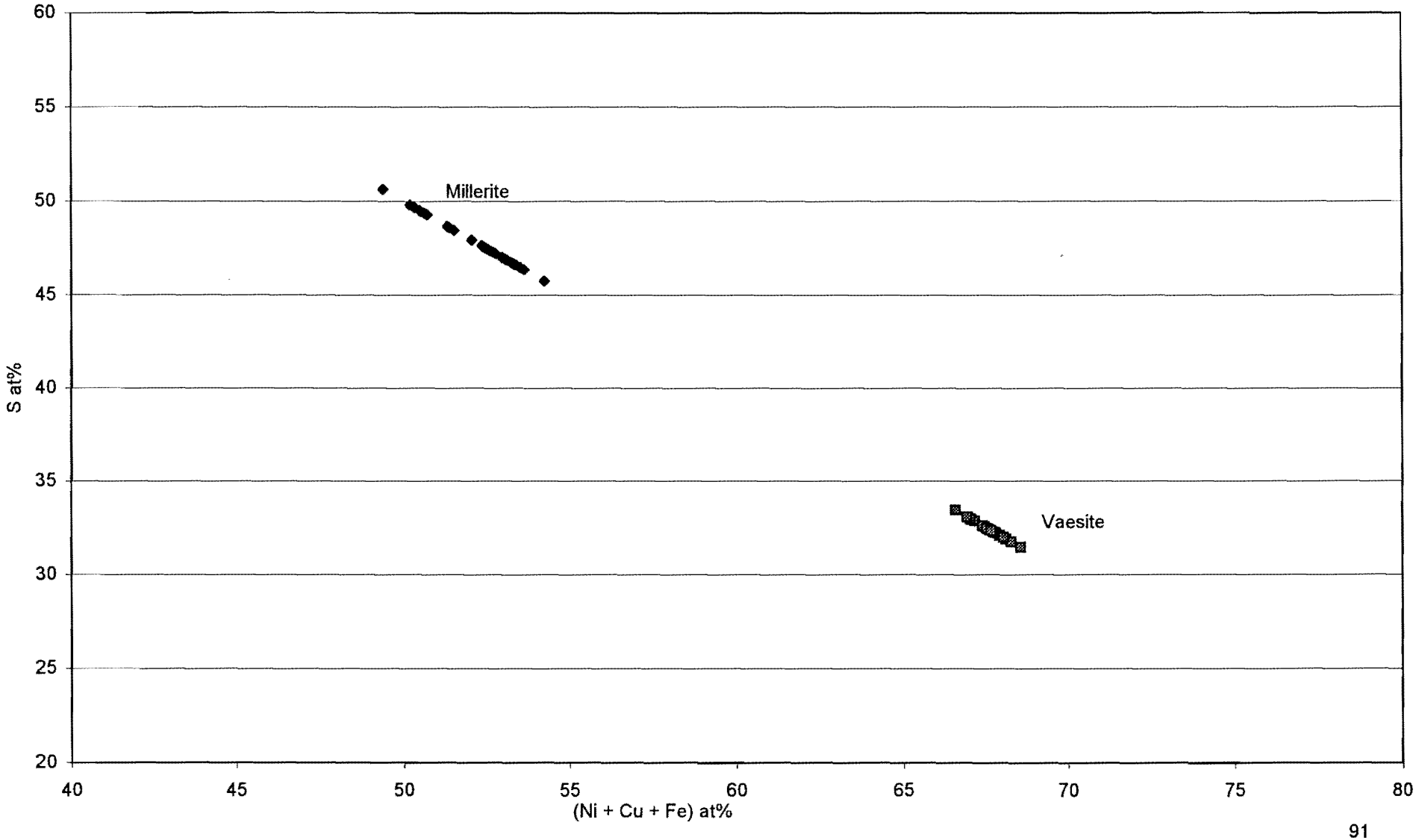

Figure 7.13: The (Ni + Cu + Fe) against the sulphur for millerite and vaesite.

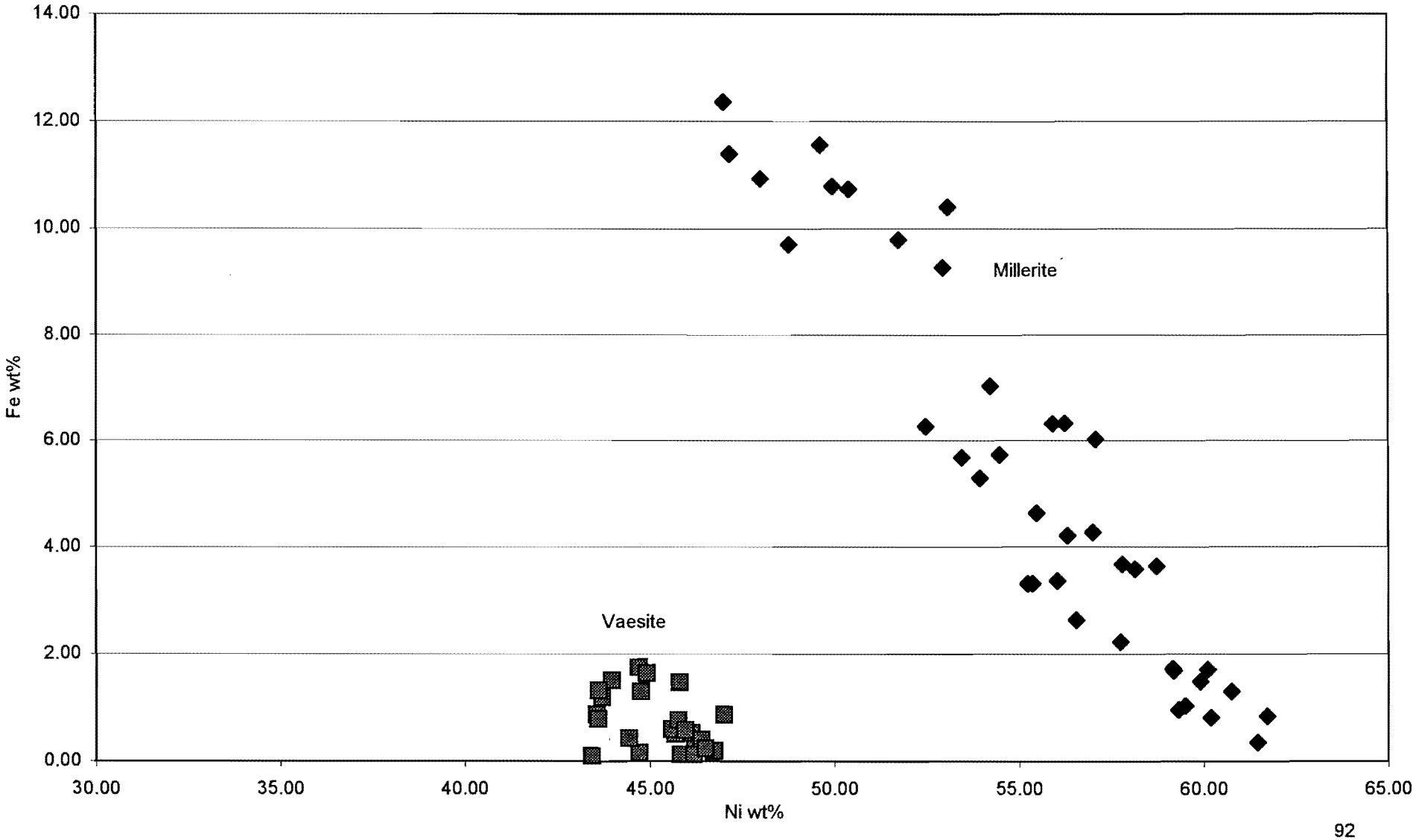

Figure 7.14: The Ni against Fe content in millerite and vaesite.

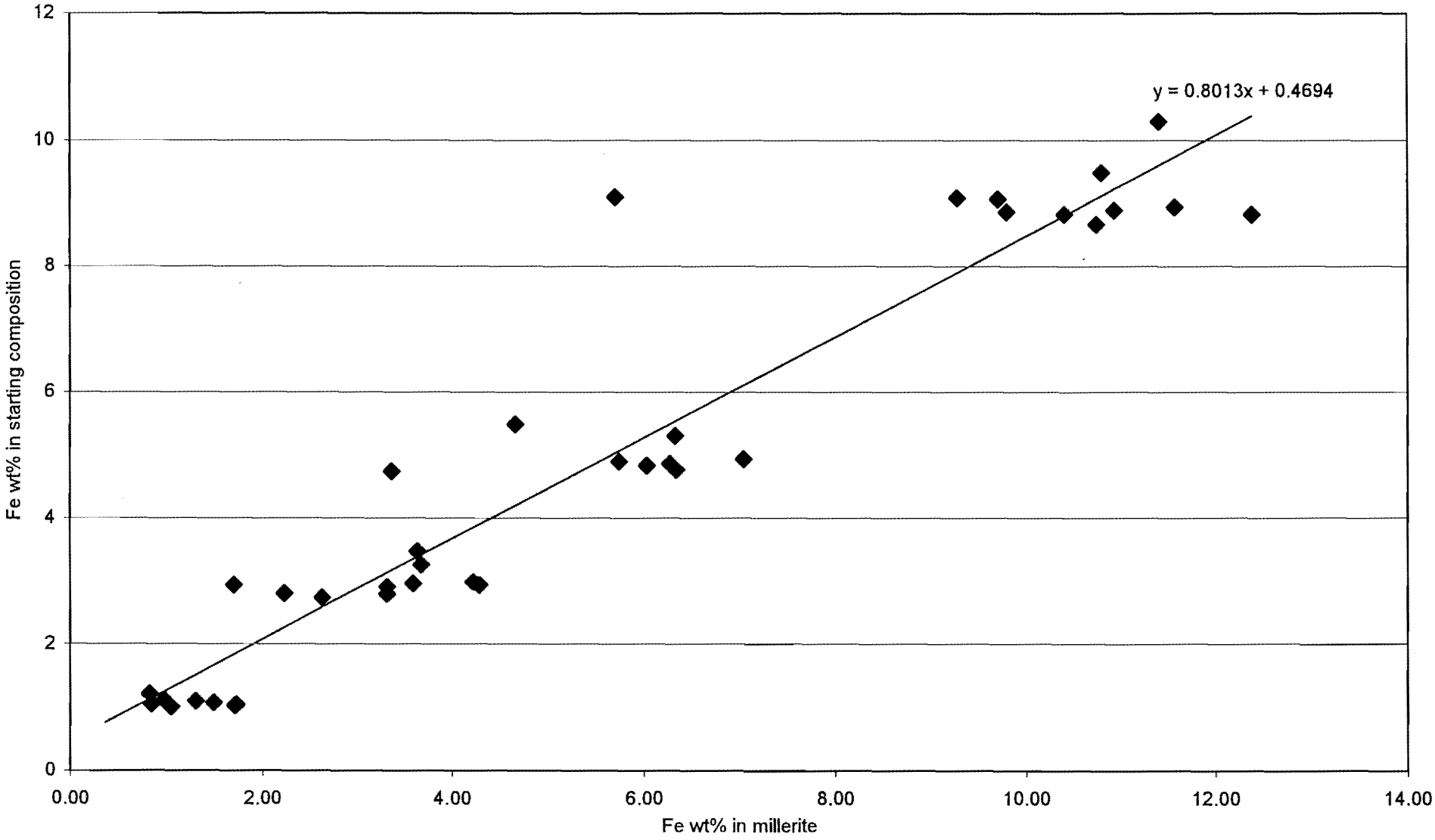

Figure 7.15: The Fe in millerite against the Fe in the starting composition. The linear regression line and equation are indicated on graph.

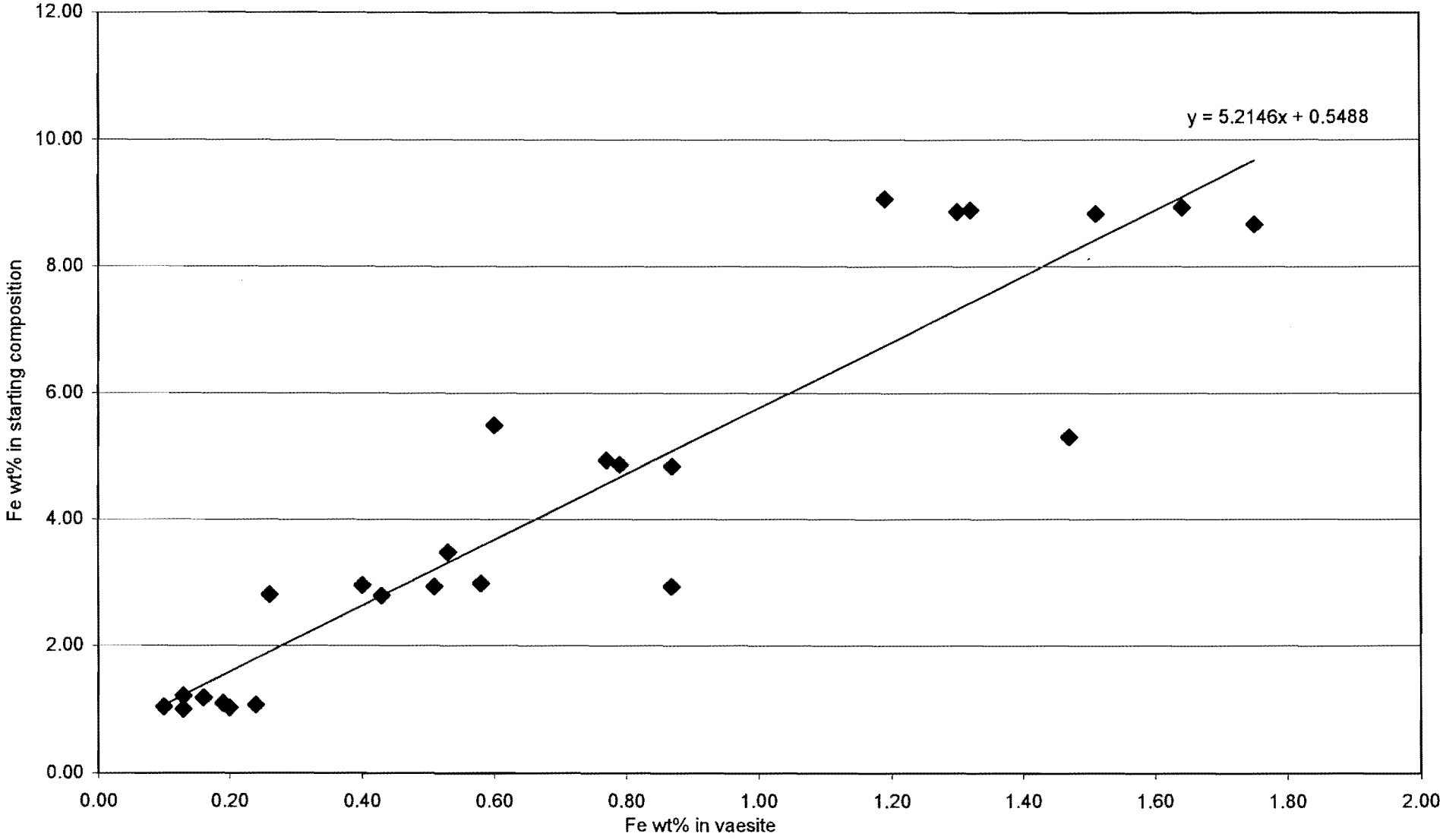

Figure 7.16: The Fe in vaesite against the Fe in the starting composition. The linear regression line and equation are indicated on graph.

Solidus tie-lines indicate the phase relations between solid phases on complete c[illegible] the phase rule, P + F = C + 1 (Ehlers, 1972), with F (degrees of freedom) = 0 for the maximum amount of phases, and C (number of components) = 4, it is derived that P (number of phases) can be up to 5. However, at any composition, a maximum of three phases were observed. Although the gas phase can not be seen, it is always present and must always be included. Therefore the maximum number of solid phases coexisting under equilibrium conditions can only be four. Due to the compositional variation of the alloy phase, the degrees of freedom (F) can be 1 in the lower part of the diagrams, which will explain why only three solid phases were observed.

Each of the triangles that defines which three phases coexist, contains an eutectic point. Three eutectic points are present: E1 in the (alloy-digenite-heazlewoodite)-field, E2 in the (β-phase+millerite+heazlewoodite)-field and E3 in the (β-phase+millerite+vaesite)-field (only in the 1 wt% Fe diagram). The eutectic point in the (digenite+β-phase+heazlewoodite)-field is undetermined by this study.

From any starting composition in the (digenite+heazlewoodite+alloy)-field, crystallization will follow a vector (away from the crystallizing phase) crossing the temperature contours until the cotectic is reached. From there, crystallization will proceed along the cotectic towards the eutectic point E1. Within a phase field, only one phase will crystallize from the melt. On the cotectic two phases will crystallize simultaneously form the melt and at the eutectic point three solid phases will coexist. The three phases would be alloy, digenite and heazlewoodite.

In the case where an alloy will crystallize first from the melt, the composition of the first crystallized alloy will change as the melt evolves, provided the alloy remains in equilibrium with the melt. On final solidification, and under equilibrium conditions, all the alloy grains will have the same composition. This is rarely, if ever, the case in slow cooled mattes under plant conditions.

From any starting composition in the (β-phase+millerite+heazlewoodite)-field, crystallization will proceed away from the crystallizing phase (crossing the temperature contours) to the cotectic and then towards the eutectic point E2, where β-phase, millerite and heazlewoodite crystallize together.

In a similar fashion, crystallization in the (β-phase+millerite+vaesite)-field, will evolve towards the eutectic point E3 where all three phases will crystallize together.

A significant comparison with the schematic phase diagrams of Craig & Kullerud (1969) and Ebel & Naldrett (1997) could not be drawn due to the lack of relevant quantitative data in the Fe deficient part of the quaternary.

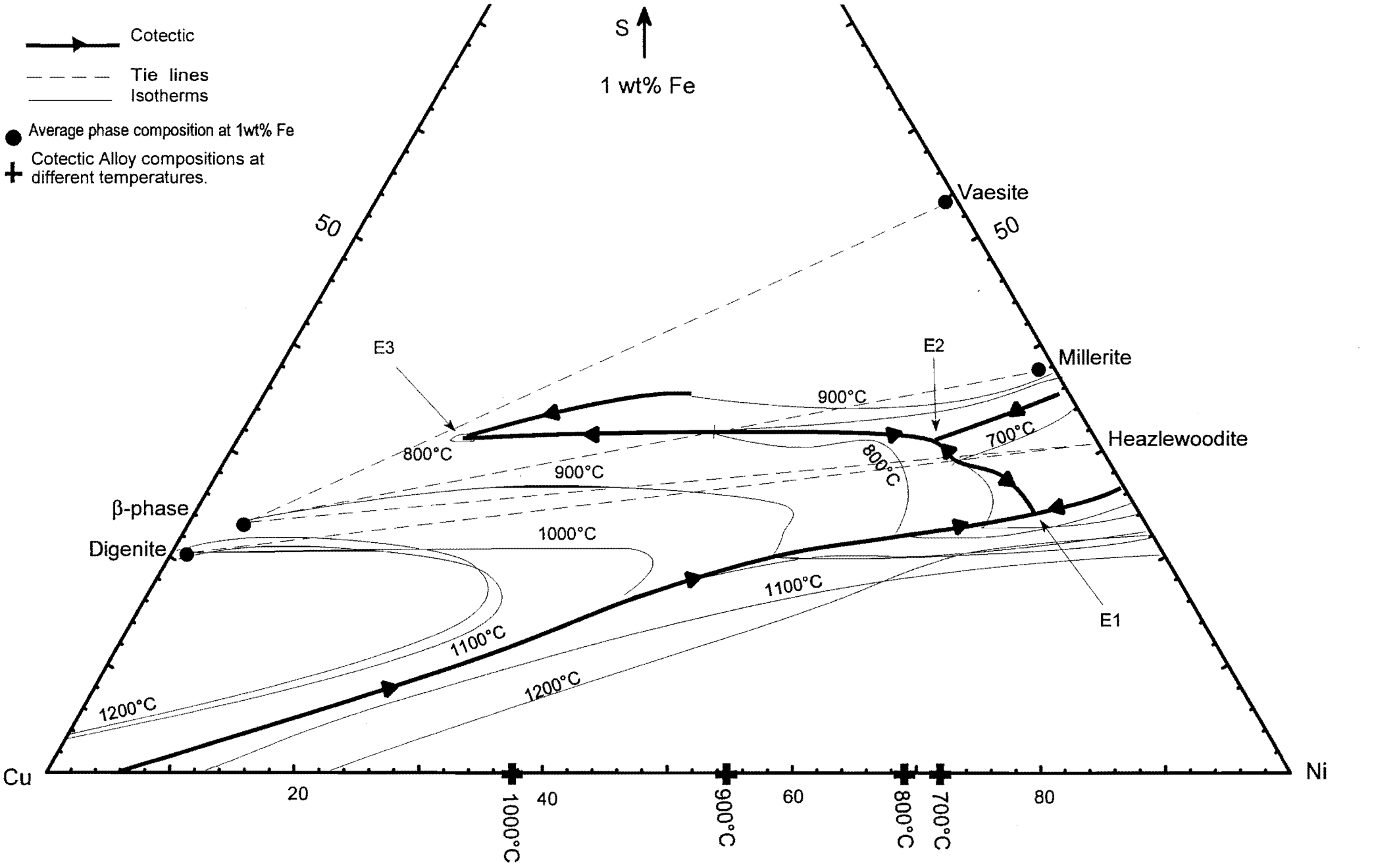

Figure 7.17: The liquidus isotherms and cooling path from 1200°C to 700°C at 1 wt% Fe in the starting composition. The composition of haezlewoodite is schematic.

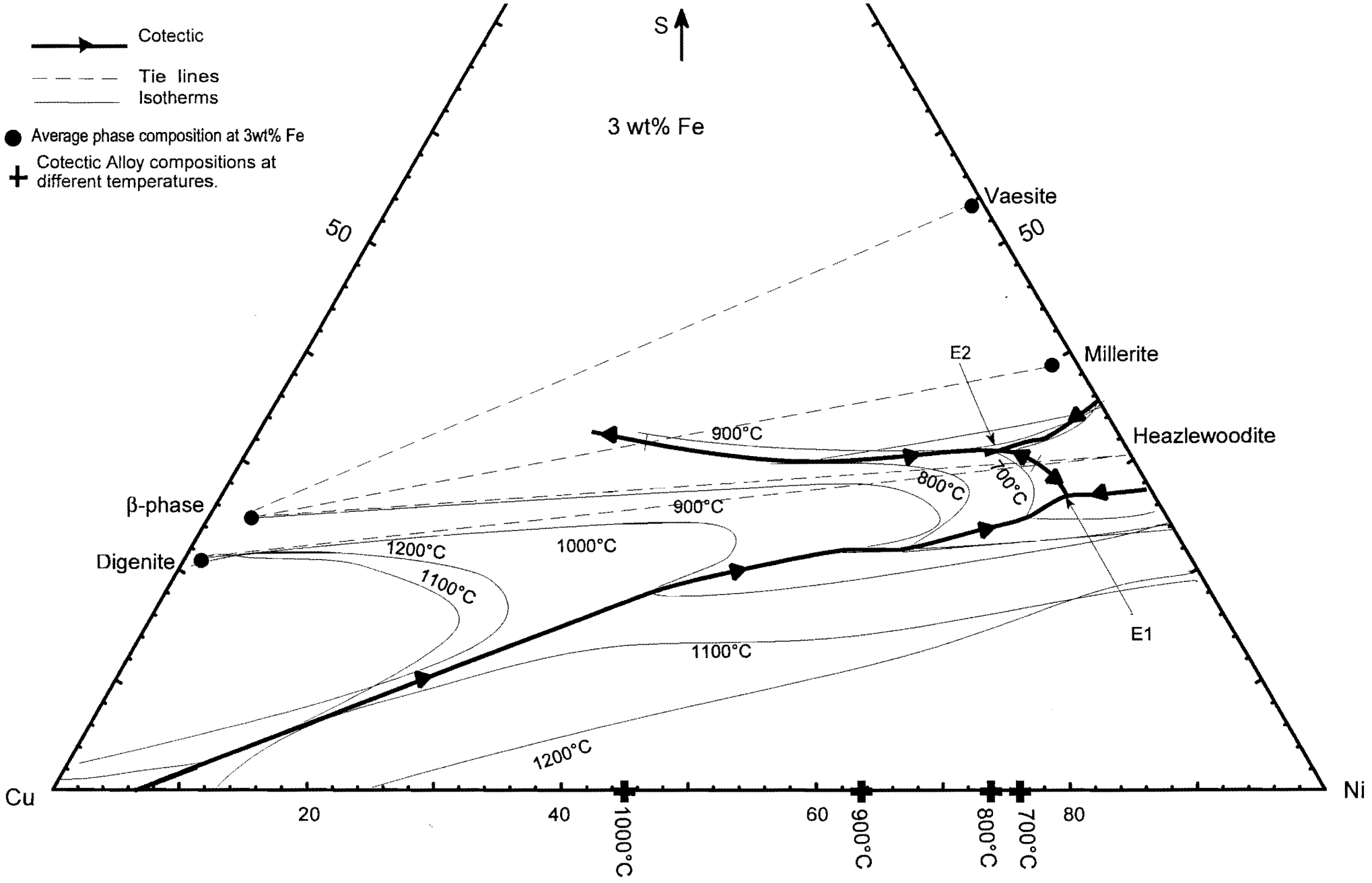

Figure 7.18: The liquidus isotherms and cooling path from 1200°C to 700°C at 3 wt% Fe in the starting composition. The composition of haezlewoodite is schematic.

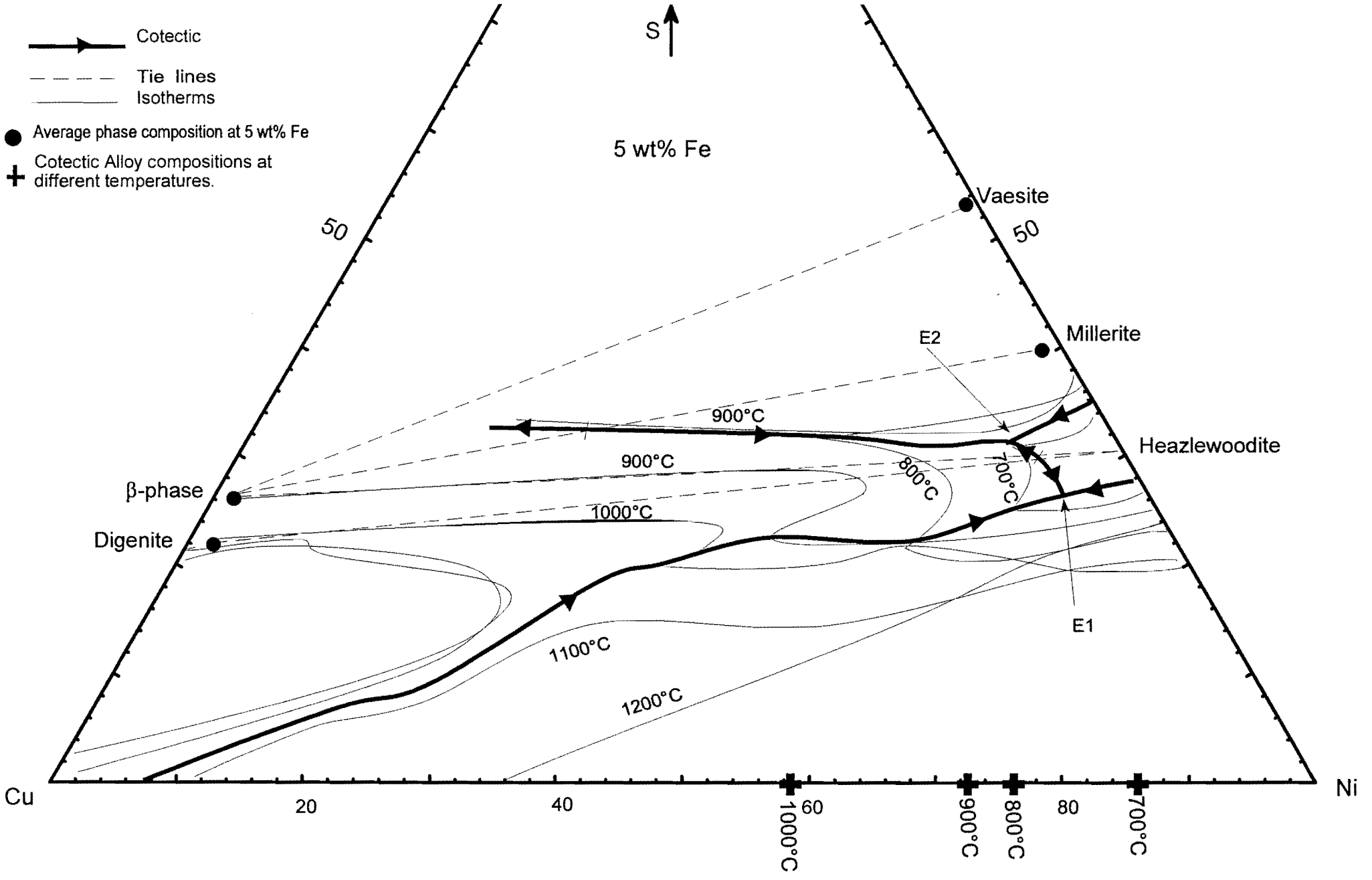

Figure 7.19: The liquidus isotherms and cooling path from 1200°C to 700°C at 5 wt% Fe in the starting composition. The composition of haezlewoodite is schematic

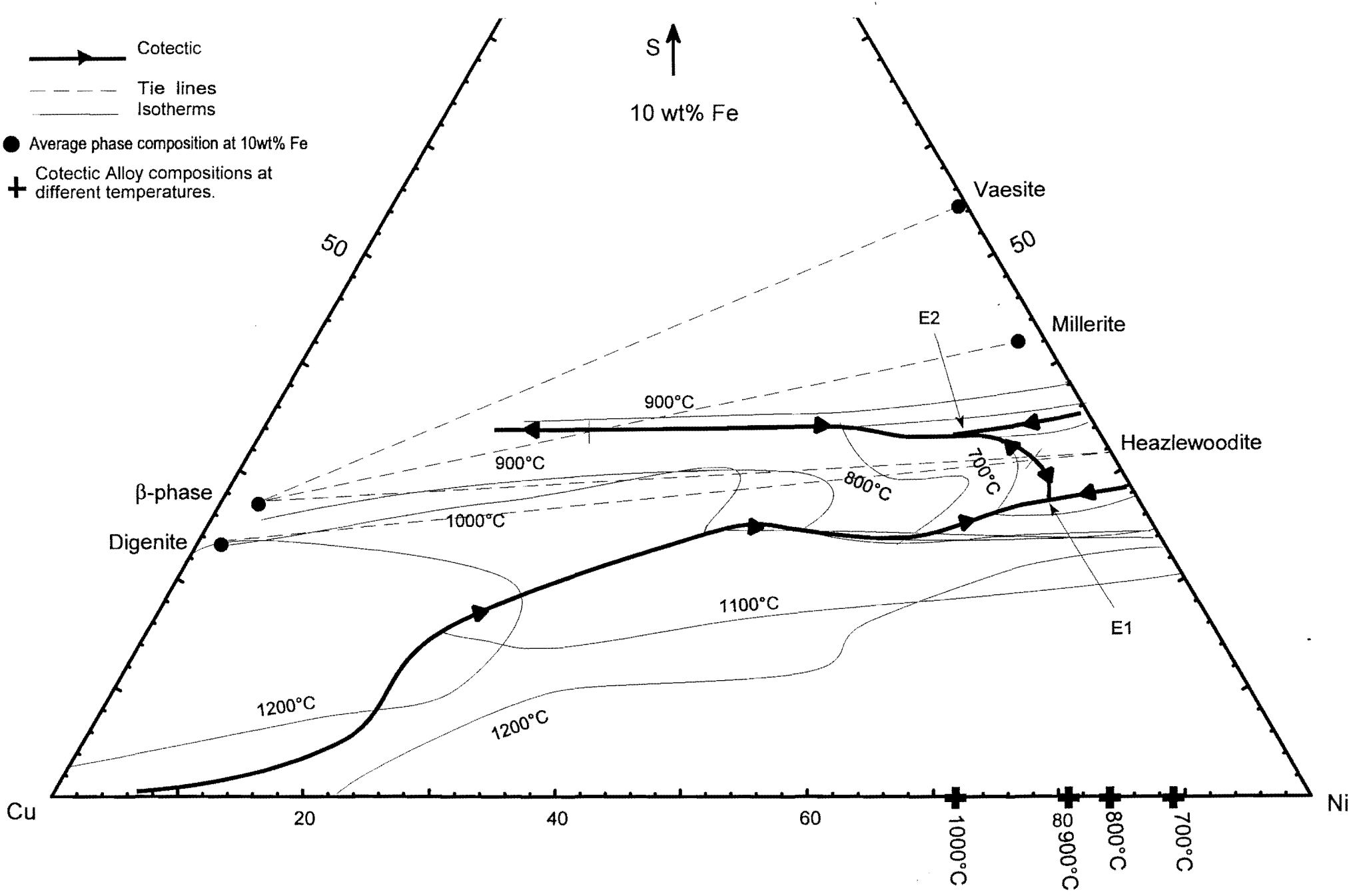

Figure 7.20: The liquidus isotherms and cooling path from 1200°C to 700°C at 10 wt% Fe in the starting position. The composition of haezlewoodite is schematic.

8. IMPLICATIONS

The successful process of slow cooling of converter matte in the beneficiation of platinum group metals requires a detailed understanding of the effect of compositional variation (mainly of the sulphur contents), because the temperature in conjunction with the bulk composition of the converted matte determine the path of crystallization. Under ideal conditions, the converter matte starts slow cooling at a temperature of 1200° - 1100°C with a composition of less than 3 wt% Fe and less than 20 wt% sulphur (Hiemstra, 1988). The average ore from the Bushveld Complex has higher Ni contents than Cu contents, which will result in the converter matte having a Cu/Ni ratio between 0.8 and 0.4 (Bruwer, 1996; Hiemstra, 1988). For economic reasons, the proportion of alloy crystallizing from the matte should not exceed 15 –20 % of the total (Sproule et al., 1960; Schouwstra et al., 1998).

Cooling from these conditions will ensure that a Cu-Ni-Fe alloy will crystallize first, collecting most of the PGMs, followed by the formation of sulphides. If the crystallization of alloy from the melt is preceded by crystallization of a sulphide, or during simultaneous crystallization of alloy and sulphide, the sulphide will compete for collection of the PGMs.

8.1 Cooling Paths for Mattes with Different Starting Compositions

Sproule et al. (1960) determined that the average eutectic alloy on complete crystallization has a composition of $Cu_{20}Ni_{80}$. The composition of the initial alloys differ, but if equilibrium conditions prevail (unlikely in a slow cooled converter matte), the composition of the first formed alloys will change until all alloys in the crystallized matte have a composition of $Cu_{20}Ni_{80}$. The Fe content of the bulk will influence the exact composition of this eutectic alloy. Because there is not a perfect linear relationship between the amount of Fe in the bulk and the amount of Fe in the alloys, the eutectic alloy composition at complete crystallization can not be easily predicted. For low Fe contents it has a composition close to that in the Fe-free system, but at higher Fe contents the composition deviates substantially from that given by Sproule et al. (1960). For the different starting Fe contents in the bulk, the composition of the cotectic alloy is indicated on the stability phase diagrams (Figures 8.1 to 8.4). Eutectic alloy compositions at solidification are completely inferred following the trend of the cotectic alloy at different temperatures.

Because the proportion of alloy in the ingot is ideally 15 – 20% of the mass, it is important to determine the influence of Fe on the amount of alloy that will crystallize. However, alloys crystallizing in the initial stages of slow cooling will have a larger grain size than the alloy forming at the eutectic point (E1) (Schouwstra et al., 1998). Fine intergrowths with sulphides at the eutectic will cause problems in the liberation of the alloy from the sulphide bulk. Therefore, the amount of alloy that form large, non-intergrown grains, which can easily be liberated during crushing, is essential. After crushing the crystallized matte, the magnetic alloy fraction is separated from the less magnetic sulphide fraction. A successful process will ensure that most of the PGE's are removed together with the alloy fraction.

This investigation looks at the influence of Fe on the slow cooling sequence of the matte. For a comparative discussion with the Fe-free system, the same starting compositions (representing that of an average converter matte) are chosen, varying only the Fe content. The crystallization paths are the same for all four diagrams, therefore, they will be discussed simultaneously.

Depending on the starting composition, three fundamentally different crystallization paths are possible, which are called A, B and C: If the starting composition falls into the (alloy)-stability field, crystallization path A will be followed on cooling of the matte. If the starting composition falls into the (digenite or β-phase)-stability field, two possible paths of crystallization can take place depending on the sulphur content. Which path (B or C) is followed, depends on the sulphur content. The critical sulphur content can be derived by a line connecting digenite and the eutectic point E1. At lower sulphur contents (than this line), path B will be followed and at higher sulphur contents path C will be followed. For starting compositions falling directly on the critical sulphur content line, the matte will crystallize digenite and at the eutectic temperature also alloy and heazlewoodite.

Best results are to be achieved if the Cu/Ni-ration is between 0.8 and 0.6 and the sulphur content between 18 and 22 wt%. Indicated on each diagram is an area that represents the typical range of converter matte compositions.

8.2 Path A

For a starting composition of X (Cu/Ni ~ 0.6 and S ~ 20 wt%), alloy will start to crystallize from the matte. Crystallization will proceed along the tie-line (X-A) until the cotectic line at composition A is reached. From A to the eutectic point E1, alloy and digenite will crystallize together. The composition of the alloy will change on cooling along the Cu-Ni join. On reaching the eutectic point E1, heazlewoodite will start to crystallize together with the alloy and digenite, until complete solidification.

8.3 Path B

For a starting composition of Y (Cu/Ni ~ 0.6 and S < critical sulphur content), digenite will start to crystallize first from the matte. Crystallization will proceed along a line directly away from digenite to point B on the cotectic line. At point B, digenite and alloy will crystallize together and follow the cotectic to the eutectic point E1. The composition of the alloy will change on cooling. At E1, heazlewoodite will also start to crystallize together with digenite and alloy until complete solidification.

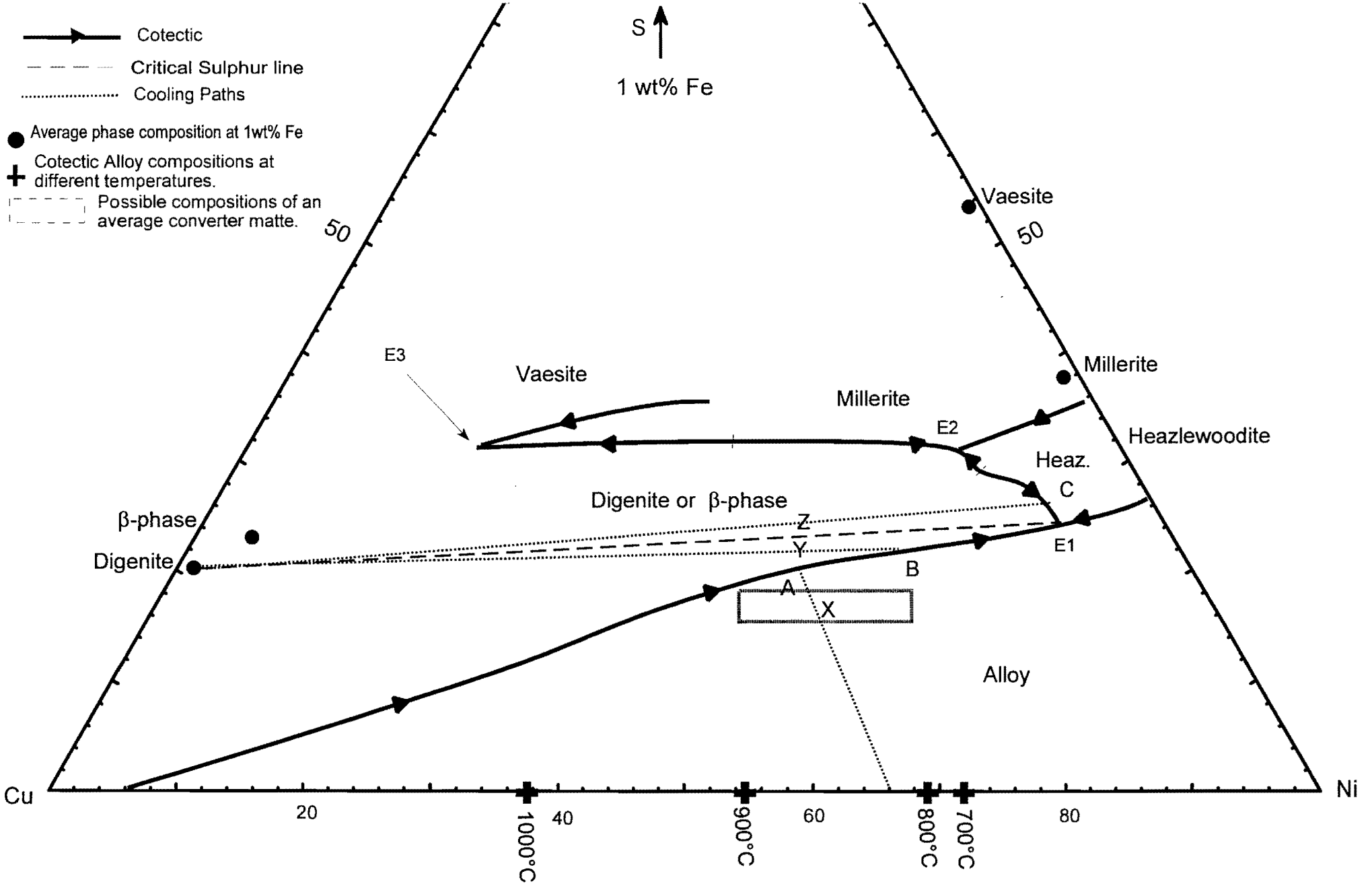

Figure 8.1: Stability phase fields and the cooling path for 1 wt% Fe in the bulk. Starting compositions for paths A, B and C are shown as X, Y and Z respectively. The composition of the cotectic alloy at the different temperatures is indicated on the Cu-Ni join.

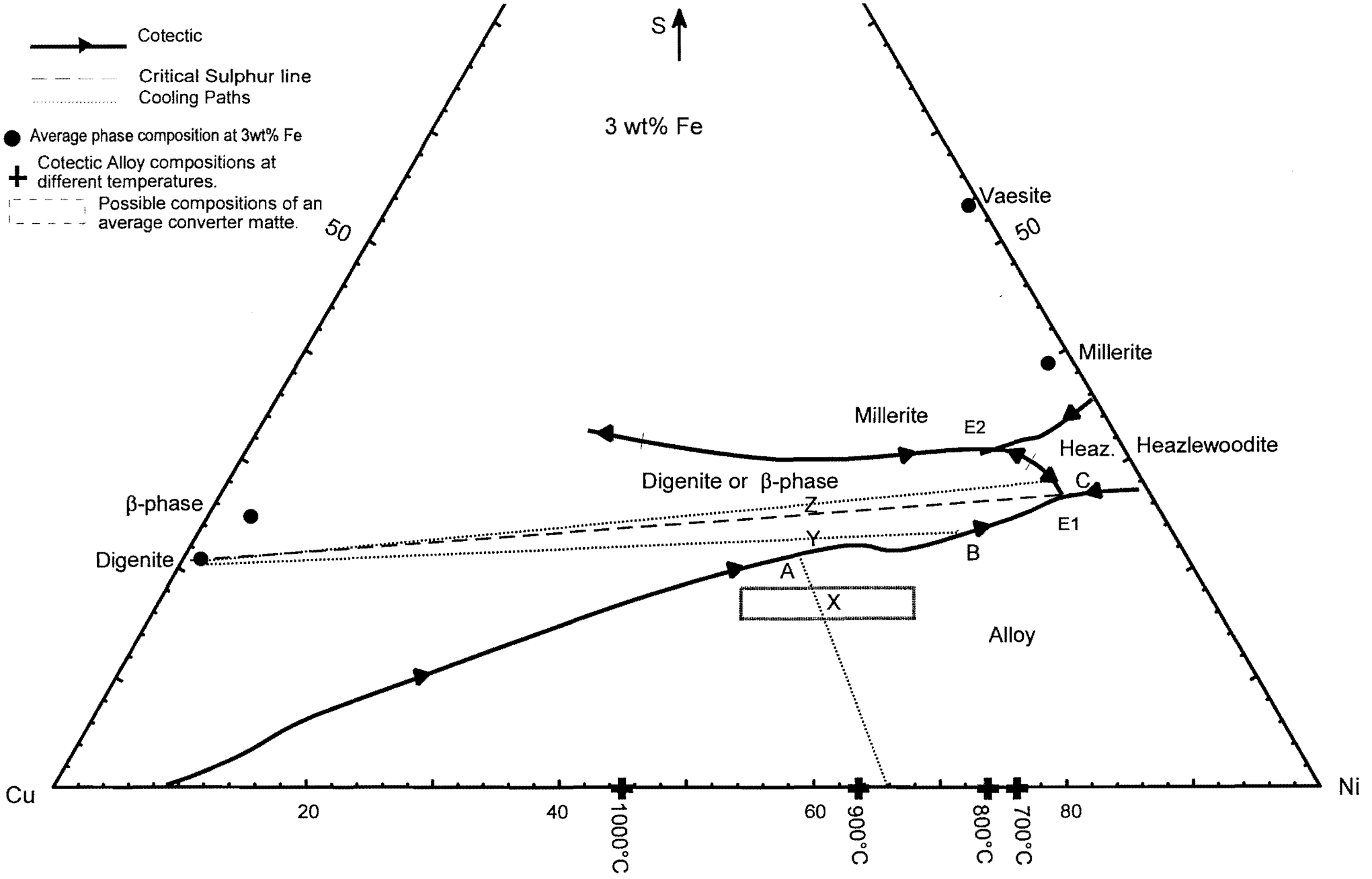

Figure 8.2: Stability phase fields and the cooling path for 3 wt% Fe in the bulk. Starting compositions for paths A, B and C are shown as X, Y and Z respectively. The composition of the cotectic alloy at the different temperatures is indicated on the Cu-Ni join.

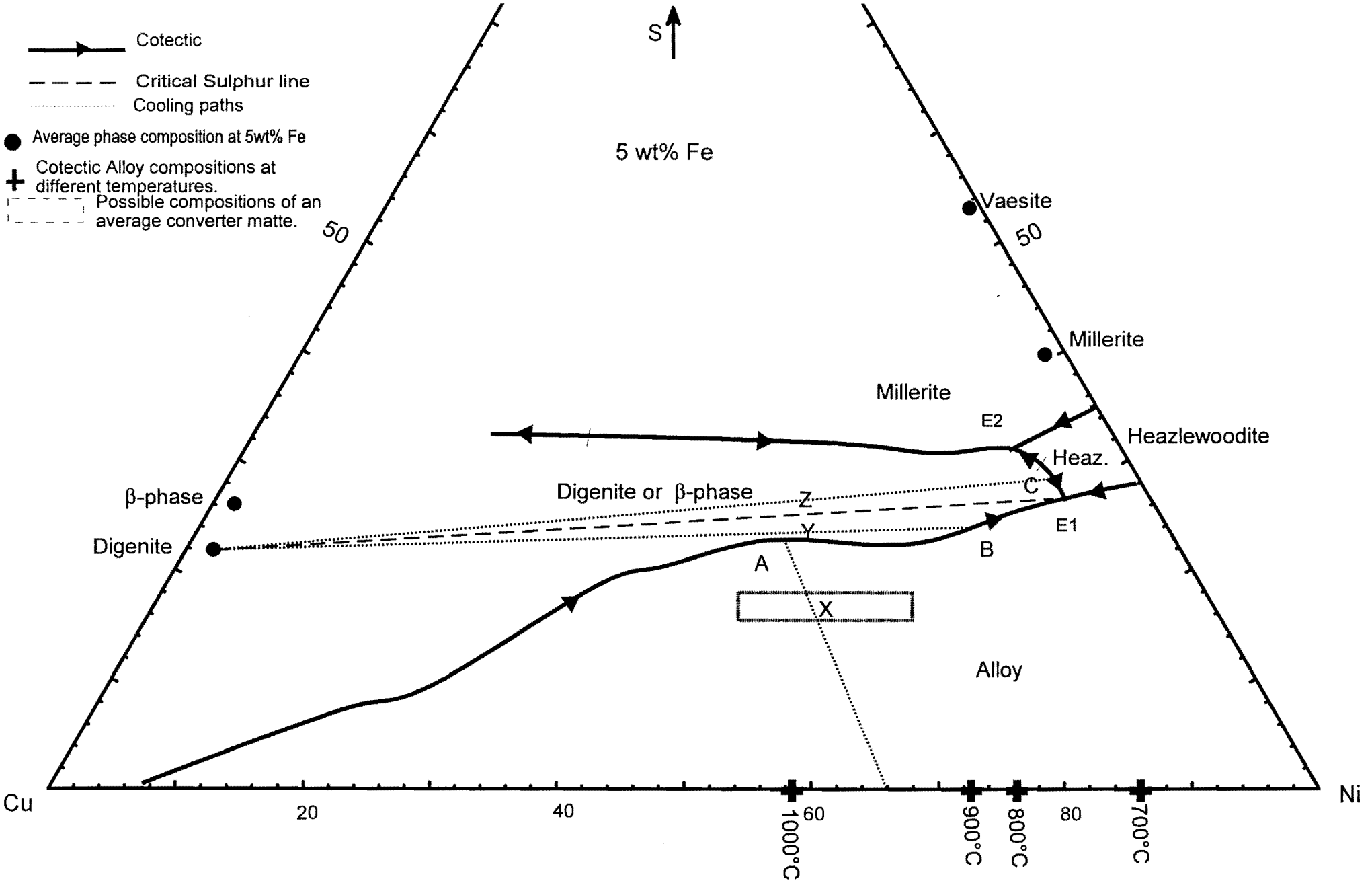

Figure 8.3: Stability phase fields and the cooling path for 5 wt% Fe in the bulk. Starting compositions for paths A, B and C are shown as X, Y and Z respectively. The composition of the cotectic alloy at the different temperatures is indicated on the Cu-Ni join.

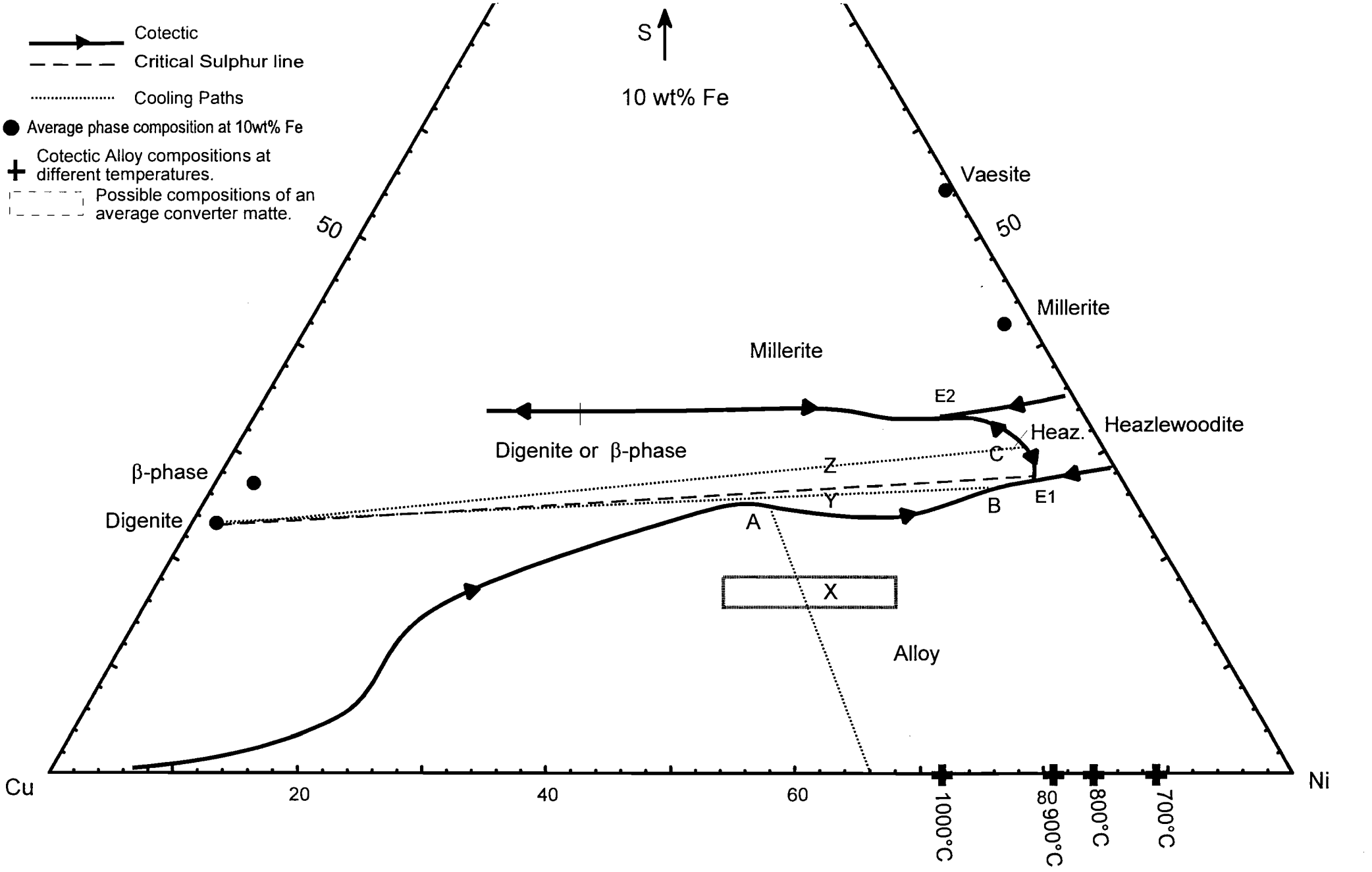

Figure 8.4: Stability phase fields and the cooling path for 10 wt% Fe in the bulk. Starting compositions for paths A, B and C are shown as X, Y and Z respectively. The composition of the cotectic alloy at the different temperatures is indicated on the Cu-Ni join.

8.4 Path C

For a starting composition of Z (Cu/Ni ~ 0.6 and S > critical sulphur content), digenite will be the first phase to crystallize from the matte. Crystallization will proceed along a line directly away from digenite to point C on the cotectic line. At this point, digenite and heazlewoodite will crystallize simultaneously and crystallization will proceed along the cotectic line to the eutectic point E1. At E1, alloy will crystallize together with digenite and heazlewoodite until complete solidification.

8.5 Effect of Fe on Path A

At a fixed Cu/Ni ratio and sulphur content, Fe will influence the amount of alloy crystallizing from the melt. The higher the Fe content in the bulk, the more alloy will form before digenite will start to crystallize. By applying the lever rule (at a starting composition of X and a fixed Cu/Ni of 0.51), the proportion of alloy crystallizing before reaching the cotectic, can be determined. The results (Figure 8.5) show a definite increase in the proportion of alloy crystallizing, as the bulk Fe content increases. It must be kept in mind that additional alloy will crystallize together with digenite as the melt cools down towards the eutectic point. At the eutectic point, alloy will continue to crystallize together with digenite and heazlewoodite, until complete solidification. Because the later crystallized alloy has to compete with simultaneous crystallizing sulphides (e.g. digenite and heazlewoodite), their texture and size will differ from that of the first alloy (Schouwstra et al., 1998).

At a sulphur content of 22 wt%, a small decrease in the Cu/Ni from 0.8 of the bulk at lower than 3 wt% Fe, will move the starting composition into the (digenite or β-phase) stability field. This shift will cause digenite to crystallize first from the melt followed by alloy at the cotectic line. At higher Fe contents, this increase in Cu has to be much larger to cause the same effect. For example, from point X the Cu/Ni must increase by ~0.4 at 1 wt % Fe in the bulk, by ~0.6 at 3 wt% Fe, by ~0.8 at 5 wt% Fe, and by ~1.3 at 10 wt% Fe, to ensure that digenite crystallizes first from the matte.

8.6 Effect of Fe on Paths B and C

From Figure 8.6 it appears as if the position of the critical sulphur content line rises with an increase in the Fe content of the bulk. This is, however, only a result of projection onto the floor of the diagram. For a Cu/Ni ratio of 0.6 the critical sulphur values vary between 24 and 25 wt% for all the different Fe contents. The variation in the position of the critical sulphur line can be explained by a shift in the position of the digenite composition field and the composition of the cotectic melt with an increase in Fe. Although not observed in this study, it stands to reason that the position of the heazlewoodite composition will also change with an increase in Fe, and therefore the phase stability line between digenite and heazlewoodite will also rise to supposedly high sulphur levels.

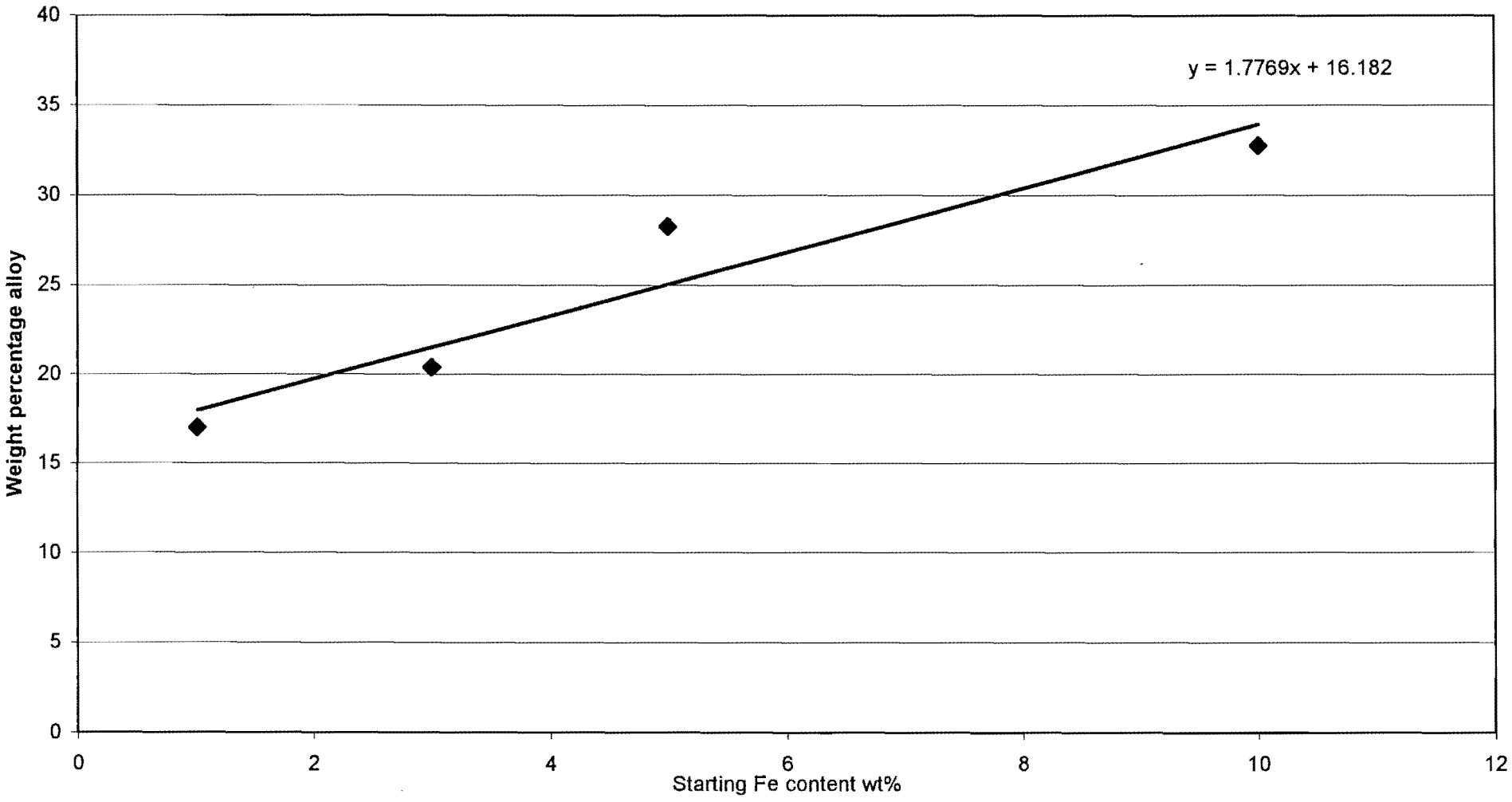

Figure 8.5:The percentage alloy crystallizing singularly form the melt at a starting composition of 20 wt% sulphur and a Cu/Ni of 0.6.

8.7 Summary

With an increase in the bulk Fe content the possibility for an average converter matte to fall into the alloy stability field improves. At Fe contents higher than 5 wt%, a small increase in Cu of the starting composition will not influence the crystallization sequence. It can be expected that the higher the amount of Fe in the bulk composition, the higher the proportion of coarse grained alloy in the total ingot (even though equilibrium conditions do not exist). However, the total amount of alloy will also increase and will influence the amount of material to be treated in the extraction of the noble elements.

An increase in Fe content will not significantly influence the crystallization path at higher levels of sulphur. The critical sulphur content (that determine the initial crystallization of either digenite / β-phase or heazlewoodite) stays virtually the same at any Fe content. This is however, subject to the exact position of the eutectic points (that were not determined by this study).

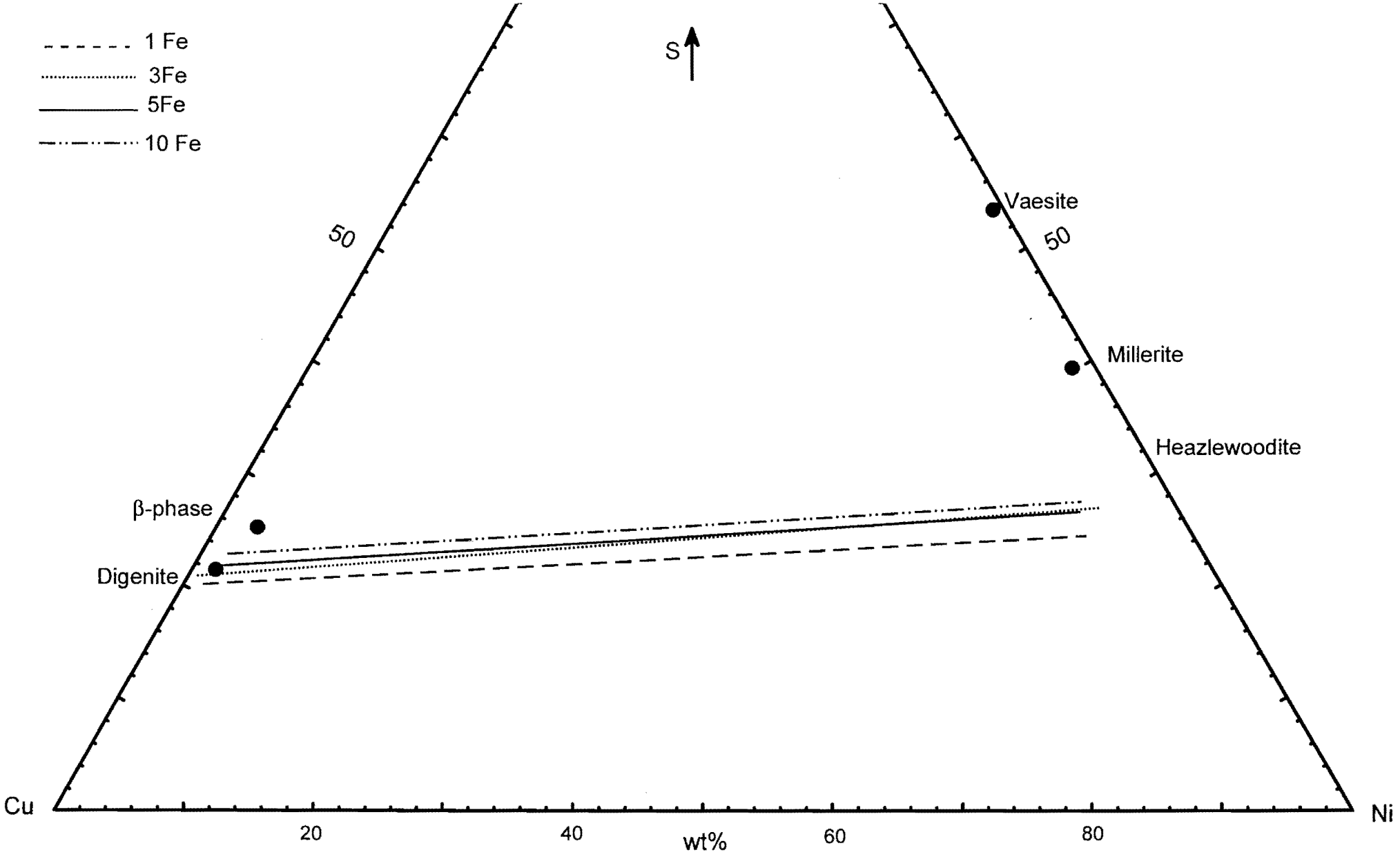

Figure 8.6: The position of the critical sulphur lines in the Cu-Ni-S ternary at variable Fe contents. Allso indicated are the average sulphide compositions.

9. CONCLUSIONS

The aim of the study is to investigate the influence of low concentrations of Fe on the Cu-Ni-S system with relevance to an average Cu-Ni-converter matte. Of particular interest are: (1) the compositions of the alloy and digenite co-existing with melt (generally referred to as the cotectic alloy, cotectic digenite and cotectic melt) at different temperatures; (2) the Fe content of sulphide and alloy phases with an addition of Fe to the starting composition, and (3) the partitioning of Fe between co-existing solid phases.

Alloy is the first phase to crystallize in an average converter matte (provided the composition is favorable) and also the primary collector of PGE's in the matte. In this investigation it was confirmed that at a fixed bulk Fe content, a decrease in temperature causes a decrease in the Cu/Ni of the cotectic alloy. Additionally, it has also been established that at a fixed temperature, an increase in the Fe content of the bulk will cause a decrease in the Cu/Ni of the cotectic alloy. Therefore, if all other parameters are kept stable, it can reasonably be accepted that an increase in the bulk Fe content will produce an increasingly Ni-rich alloy.

The composition of the cotectic melt is essential in determining the cooling path towards the eutectic point where alloy, digenite and heazlewoodite coexist. The cotectic melt in the assemblage (alloy+digenite+melt) shows an increase in Ni, Fe and sulphur content, with an increasing Fe content in the bulk. This causes the cotectic to shift towards higher sulphur contents, which results in a larger stability field for alloy. The implications are twofold: Firstly higher Fe contents increase the amount of alloy that will crystallize from the melt, and secondly it would require a larger variation in starting composition (particular the Cu/Ni) to alter the path of crystallization of a matte.

Examining the second aspect revealed that all of the stable phases are strongly influenced by the amount of Fe present in the bulk composition: The more Fe available, the more Fe will be incorporated in the crystal structures of phases. The relationship is, however, not linear and generally the more Fe available in the bulk the wider the range of Fe contents in the phase.

Lastly, in assemblages containing alloy, the alloy phase has consistently the highest partitioning coefficient for Fe. In other assemblages, Fe does not show any preference for a particular phase, regardless of the sequence of crystallization or temperature of equilibration.

REFERENCES

Alsen (1923) Vorlaufige Mitteilung uber eine Untersuchung der Kristallstrukturen von FeS und NiS. Geologiska Foreningens i Stockholm Forhandlingar. **45,** 606-609.

Alsen (1925) Rontgenographische Untersuchung der Kristallenstrukturen von Magnetkies, Breithaupit, Pentlandit, Millerit, und verwandten Verbindungen. Geologiska Foreningens i Stockholm Forhandlingar **47,** 19-72.

Arnold, R.G. (1956) The pyrrhotite - pyrite relationship. Carnegie Inst. of Washington / Year Book. Carnegie Inst. Washington. 177-178.

Arnold, R.G. and Kullerud, G. (1956) The NiS-NiS_2 join. Year Book / Carnegie Institution of Washington. Washington. 178-179.

Ballhaus, C., Tredoux, M. and Späth, A. (2001) Phase relations in the Fe-Ni-Cu-PGE-S system at magmatic temperature and application to massive sulphide ores of the Sudbury Igneous Complex. Journal of Petrology, **42**, 1911- 1926.

Barton, P.B.J. (1973) Solid solutions in the system Cu-Fe-S. Part I. The Cu-S and CuFe-S joins. Ecomomic Geology **68,** 455-465.

Bruwer, J.S. (1996) Experimental investigation of the phase relations in the system Cu-Ni-S in the temperature range 1200°C to 700°C. University of Pretoria; unpublished thesis, p 157.

Bruwer, J.S. and Merkle, R.K.W. (1998) Experimental investigation of the liquidus isotherms in the system Cu-Ni-S from 1200°C to 700°C. In Proceedings of the 5th International Congress on Applied Mineralogy in the Mineral Industry (ICAM '96), Warsaw, Poland, Edited by A. Niedbalska, A. Szymanski and A. Wiewióra. Subdan Druk s.c. Warsaw, Poland, 130-135.

Cabri, L.J. (1973) New data on phase relations in the Cu-Fe-S system. Economic Geology **68,** 443-454.

Cawthorn, R.G. (1999) The platinum and palladium resources of the Bushveld Complex. South African Journal of Science, **95**, 481-489.

Chakrabarti, D.J. and Laughlin, D.E. (1983) Cu-S. Bulletin of Alloy Phase Diagrams **4,** 953-957.

Chang, Y.A., Neumann, J.P., and Choudary, U.V. (1979) Phase diagrams and thermodynamic properties of ternary copper-sulphur-metal system. INCRA Monograph VII. **7**. The International Copper Research Association, Inc. New York.

Clark, L.A. and Kullerud, G. (1963) The sulfur-rich portion of the Fe-Ni-S system. Economic Geology **58,** 853-885.

Conover, W.J. (1980) Practical Nonparametric Statistics 2ed. John Wiley & Sons, New York.

Cooper, W.C. (1984) Recent developments in the extractive metallurgy of copper, nickel and cobalt and their industrial applications. Canadian Metallurgical Quarterly, **23**, 365-375.

Craig, J.R. & Kullerud, G. (1969) Phase relations in the Cu-Fe-Ni-S system and their application to magmatic ore deposits: Symposium on Magmatic Ore Deposits, Economic Geology, Monograph **4**, 344-358.

Crocket, J.H., Fleet, M.E. and Stone, W.E. (1997) Implication of composition for experimental partitioning of platinum-group elements and gold between sulfide liquid and basalt melt: The significance of nickel content. Geochimica et Cosmochimica Acta, **61**, 4139-4149.

De Jong, W.F. and Willems, H.W.F. (1927) Existenz und Struktur der Disulfide NiS_2 und CoS_2. Zeitschrift für Anorganische und Allgemeine Chemie **160,** 185-189.

Distler, V.V., Malevskiy, A.Y. and Laputina, I.P. (1977) Distribution of platinoids between pyrrhotite and pentlandite in crystallisation of a sulphide melt. Geochemistry International **14**, 30-40.

Durazzo, A and Taylor, L.A. (1982) Experimental exsolution textures in the system bornite – chalcopyrite: genetic implications concerning natural ores. Mineralium Deposita, **17**, 79-97.

Ebel, D.S. and Naldrett, A.J. (1996a) Fractional crystallization of sulfide ore liquids at high temperature. Economic Geology, **91**, 607 – 621.

Ebel, D.S. and Naldrett, A.J. (1997) Crystallization of sulfide liquids and the interpretation of ore composition. Canadian Journal of Earth Science, **34**, 352 – 365.

Ehlers, E.G. (1972) The Interpretation of Geological Phase Diagrams. W.H. Freeman and Company, San Francisco.

Eugster and Kullerud, G. (1956) NiS. Year Book / Carnegie Institution of Washington. Carnegie Institution of Washington, Washington. 179-180.

F*A*C*T (Facility for the Analysis of Chemical Thermodynamics) (1995) A.D. Pelton, C.W. Bale, and W.T. Thomson, Ecole Polytechnique, Montreal, version 2.1.

Fleet, M.E. and Pan, Y. (1994) Fractional crystallization of anhydrous sulfide liquid in the system Fe-Ni-Cu-S, with application to magmatic sulfide deposits. Geochimica et Cosmochimica Acta **58,** 3369-3377.

Fleet, M.E. and Stone, W.C. (1991) Partitioning of platinum-goup elements in the Fe-Ni-S system and their fractionation in nature. Geochimica et Cosmochimica Acta **55**, 245-253.

Fleet, M.E., Crocket, J.H., Liu, M. and Stone, W.E. (1999) Laboratory partitioning of platinum-group elements (PGE) and gold with application to magmatic sulfide-PGE deposits. Lithos, **47**, 127-142.

Goble, R.J. (1980) Copper sulphides from Alberta Yarrowite Cu_9S_8 and spionkopite $Cu_{39}S_{28}$. Canadian Mineralogist **18**, 511-518.

Hawley, J.E., Colgrove, G.L., and Zurbrigg, H.F. (1943) The Fe-Ni-S system. Economic Geology **38,** 335-388.

Hiemstra, S.A. (1988) Concentration and processing of Bushveld ores. In Developments in the exploration and production of platinum. Short Course, Imperial College, London. 24-25 November 1988, 1-18.

Ixer, R.A., Vaughan, D.J., Pattrick, R.A.D. and Alabaster, T. (1986) Mineralogical studies and their bearing on the genesis of masive sulphide deposits from the Semail Ophiolite Complex, Oman. In: Gallagher,M.J., Ixer, R.A., Neary, C.R. and Prichard, H.M. (editors) Metallogeny of Basic and Ultrabasic Rocks. The Institution of Mining and Metallurgy, London, 33-48.

Jones, R.T. (1999) Platinum smelting in South Africa. South African Journal of Science, **95**, 525-534.

Kaiser, H. and Specker, H. (1956) Bewertung und Vergleich von Analysenverfahren. Zeitschrift für Analytische Chemie **149**, 46-66.

Kellogg, H.H. (1967) Thermochemical properties of the system Cu-S at elevated temperature. Canadian Metallurgical Quarterly **8,** 3-23.

Klein, C. and Hurlbut, C.S. (Jr.) (1999) Manual of Mineralogy (after J.D. Dana). 21 Edition, John Wiley & Sons, Inc., New York.

Kongoly, F., Dessureault, Y. and Pelton, A.D. (1998) Thermodynamic modeling of liquid Fe-Ni-Cu-Co-S mattes. Metallurgical and Materials Transactions B, **29B**, 591 – 601.

Kullerud, G. (1956) Subsolidus phase relations in the Fe-Ni-S system. Year book / Carnegie Institution of Washington. Washington. 175-177.

Kullerud, G. (1965) Covellite stability relations in the Cu-S system. Freberger Forschungshefte **C186,** 145-160.

Kullerud, G. and Yoder, H.S. (1959) Pyrite stability relations in the Fe-S system. Economic Geology **54,** 533-572.

Kullerud, G. and Yund, R.A. (1962) The Ni-S system and related minerals. Journal of Petrology **3,** 126-175.

Kullerud, G., Yund, R.A., and Moh, G.H. (1969) Phase relations in the Cu-Fe-S, Cu-Ni-S, and Fe-Ni-S systems.Wilson, H.D.B. (editor) Economic Geology Monograph. Magmatic Ore Deposits. **4.** 343 p

Lundqvist, P. (1947) X-ray studies on the binary system Ni-S. Arkiv för Kemi, Mineralogi och Geologi **24A,** 12

Meddis, R. (1975) Statistical handbook for non-statisticians. McGraw-Hill Book Company (UK) Limited, England.

Merwin, H.E. and Lombard, R.H. (1937) The system, Cu-Fe-S. Economic Geology **32,** 203-283.

Moh, G.H. (1964) Blaubleibender covellite. Carnegie Inst. Washington Year Book. 63th ed. Carnegie Institute, Washington, 208-209.

Moh, G.H. and Kullerud, G. (1963) The Cu-Ni-S system. Carnegie Inst. Washington. 189-192.

Morimoto, N. (1970) Crystal-chemical studies of the Cu-Fe-S system. In: Tatsumi, T. (editor) Volcanism and Ore Genesis. University of Tokyo Press, Tokyo, 323-338.

Mostert, J.C. and Roberts, P.N. (1973) Electric smelting at Rustenburg Platinum Mines Limited of nickel – copper concentrates containing platinum-group metals. Journal of the South African Institute of Mining and Metallurgy, 290-299.

Naldrett, A.J., Craig, J.R., and Kullerud, G. (1967) The central portion of the Fe-Ni-S system and its bearing on pentlandite exsolution in iron-nickel sulfide ores. Economic Geology **62,** 826-847.

Neave, H.R. (1966) A Developments of Tukey's Quick Test of Location. Journal of the Amenrican Statistical Association, **61**, 949-964.

Neave, H.R. (1979) Quick and Simple Test Based on Extreme Observations. Journal of Quality Technology, **11**, 66-79.

Nelson, L.S. (1975) A Quick and Powerful Two-Sample Test. Journal of Quality Technology, **7**, 150-152.

Nylstrom, J.O. and Wickman, F.E. (1991) The Ordovician Chondrite from Brunflo, Central Sweden. 2. Secondary Minerals. Lithos, **27**, 167-185.

Palache, C., Berman, H., and Frondel, C. (1944) Dana's system of mineralogy. 7th ed. John Wiley, & Sons, Inc. New York,

Peach, C.L. and Mathez, E.A. (1996) Constraints on the formation of platinum-group element deposits in igneous rocks. Economic Geology, **91**, 439-450.

Roseboom, E.H. (1966) An investigation of the system Cu-S and some natural copper sulfides between 25° and 700°C. Economic Geology **61,** 641-671.

Roseboom, E.H. and Kullerud, G. (1958) The solidus in the system Cu-Fe-S between 400° and 800°C. Carnegie Inst. Washington. 222-227.

Rosenqvist, T. (1954) A thermodynamic study of the iron, cobalt, and nickel sulphides. Journal of the Iron Steel Inst. **176,** 37-57.

Schouwstra, R.P., Rixom, P.M. & Roberts, J.R.D. (1998) The effect of cooling rates on converter matte alloy microstructures: a laboratory study. In 8th International Platinum Symposium, Abstracts 8th International Platinum Symposium, Abstracts, Geological Society of South Africa and The South African Institute of Mining and Metallurgy, Johannesburg, Symposium Series **S18**, 363-366.

Sillitoe, R.H. and Clark, A.H. (1969) Copper and copper-iron sulphides as the initial products of supergene oxidation, Copiapo mining district, northern Chile. American Mineralogist, **54**, 1684-1710.

Simon, J.L. (1997) Resampling: The "New Statistics". 2nd edition. Resampling Stats Inc. Arlington, VA, 436p.

Sinyakova, E.F., Kosyakov, V.I. and Shestakov, V.A. (1999) Investigation of the Surface of the Liquidus of the Fe-Ni-S System at Xs < 0.51. Metallurgical and Materials Transactions B, **30B**, 715 – 722.

Sproule, K., Harcourt, G.A. and Renzoni, L.S. (1960) Treatment of Nickel-copper matte. Journal of Metals, 214-219

Tarr, W.A. (1935) The linnaeite group of cobalt-nickel-iron-copper sulfides. American Mineralogist **20,** 69-80.

Tukey, J.W. (1959) A Quick, Compact, Two-Sample Test to Duckworth's Specifications. Technometrics, **1**, 31-48.

Viljoen, M.J. and Schurmann, L.W. (1988) Platinum-Group Metals in The Mineral Resources of South Africa (M.G.C. Wilson and C.R. Anhaeusser, eds.): Handbook, Council for Geoscience, **16**, 532-568.

Westfall, P. and Young, S. (1992) Resampling-Based Multiple Testing. Wiley, 340p.

Yund, R.A. and Kullerud, G. (1966) Thermal stability of assemblages in the Cu-Fe-S system. Journal of Petrology **7**, 454-488.

APPENDICES

APPENDIX A

Example of the Resampling Statistics procedure of 20 Analyses of Cu from experiment 10m4:
(Comments are in Italics)

construct a bootstrap confidence interval for the mean
maxsize default 15000
clear list
numbers (42.64 27.33 44.51 73.80 70.85 76.41 64.76 61.50 58.24 66.73 35.62 12.69 21.33 41.17
36.11 23.62 10.71 17.15 27.44 20.13) 10m4
find the mean of the 10m4 data and call it Mean10m4
mean 10m4 Mean10m4
repeat 15000 times
repeat 15000
take a sample of 20 with replacement from the 10m4 data and call it d
sample 20 10m4 d
find the mean of the resample and call it mean$
mean d mean$
keep score of the trial result and put it in dd
score mean$ dd
end
calculate the 15.85 and 84.15 % and put them into error
percentile dd (5 95) error
print the actual mean and the error
print Mean10m4 error
display as a histogram the variation of the mean in the resampled populations
histogram dd
MEAN10M4 = 41.637

ERROR = 33.893 49.521

Vector no. 1: DD

Bin Center	Freq	Pct	Cum Pct
25	15	0.1	0.1
30	372	2.5	2.6
35	2524	16.8	19.4
40	5747	38.3	57.7
45	4688	31.3	89.0
50	1476	9.8	98.8
55	168	1.1	99.9
60	10	0.1	100.0

Note: Each bin covers all values within 2.5 of its center.

Successful execution. (21.1 seconds)

APPENDIX B

Starting compositions for all the experiments.

1200°C				
Exp no.	Cu	Ni	Fe	S
12l1	74.01	20.07	1.03	4.89
12l2	49.40	44.60	1.07	4.93
12l3	30.06	63.84	1.13	4.97
12l4	9.94	83.88	1.20	4.99
12l5	59.69	29.38	1.07	9.86
12l6	30.04	58.93	1.15	9.88
12m1	72.72	19.49	2.90	4.90
12m2	47.91	44.22	2.92	4.95
12m3	29.40	62.82	2.99	4.80
12m4	9.81	82.35	3.00	4.84
12m5	58.43	28.87	2.76	9.94
12m6	29.21	58.39	2.72	9.68
12n1	71.09	19.44	4.80	4.67
12n2	47.59	42.83	4.69	4.89
12n3	28.49	61.82	4.84	4.84
12n4	9.62	80.70	4.77	4.91
12n5	57.26	28.41	4.71	9.62
12o1	67.69	18.45	9.29	4.58
12o2	45.28	41.05	9.10	4.57
12o3	27.30	59.05	9.10	4.55
12o4	9.05	77.18	9.12	4.64
12o5	54.43	27.25	9.16	9.16
12o6	27.33	54.55	8.94	9.18

1100°C				
Exp no.	Cu	Ni	Fe	S
11a1	61.14	34.45	1.10	3.31
11a2	79.24	9.90	1.00	9.86
11a3	69.12	15.04	0.90	14.94
11a4	58.07	25.52	1.07	15.33
11a5	73.76	20.54	1.01	4.69
11b1	64.94	28.70	1.18	5.18
11b2	49.47	44.06	1.46	5.01
11b3	29.29	59.20	1.17	10.34
11b4	9.92	78.75	1.27	10.06
11b5	59.70	29.26	1.17	9.87
11c1	86.79	5.20	2.84	5.17
11c2	76.55	10.32	2.94	10.19
11c3	66.12	16.42	2.91	14.55
11c4	58.67	24.31	3.04	13.98
11c5	72.41	19.54	3.15	4.89
11d1	62.80	29.02	3.17	5.01
11d2	47.72	44.57	2.82	4.89
11d3	28.95	58.16	3.02	9.87
11d4	10.32	77.60	2.76	9.33
11d5	58.47	28.45	2.82	10.27
11e1	48.35	41.93	4.98	4.75
11e2	56.98	28.54	4.86	9.62
11e3	66.62	14.77	4.66	13.95
11e4	57.67	23.81	4.82	13.70
11e5	71.04	19.50	4.66	4.80
11f1	61.45	28.88	4.72	4.96
11f2	28.76	56.94	4.80	9.50
11f3	8.54	77.08	4.87	9.51
11g1	81.90	4.31	9.18	4.61
11g2	71.96	9.27	9.34	9.44
11g3	64.08	13.60	9.07	13.24
11g4	59.20	26.87	9.17	4.75
11g5	67.59	18.77	9.17	4.47
11h1	54.36	23.02	8.96	13.66
11h2	45.02	41.24	9.20	4.55
11h3	27.61	54.27	9.11	9.01
11h4	10.60	71.32	9.09	8.99
11h5	54.35	27.31	9.10	9.24

1000°C				
No.	Cu	Ni	Fe	S
10a	28.74	56.72	5.21	9.32
10b	56.80	28.04	5.77	9.39
10e1	9.14	76.04	5.04	9.78
10e2	75.93	9.37	5.44	9.27
10e3	18.85	66.70	5.57	8.88
10f1	34.14	54.12	3.08	8.65
10f4	54.90	27.50	3.80	13.80
10g1	47.96	29.45	3.01	19.59
10g2	9.46	77.08	3.32	10.14
10g3	19.66	67.42	3.30	9.63
10g4	72.27	8.74	10.06	8.94
10h3	55.22	26.17	10.19	8.42
10h4	17.84	63.79	9.57	8.79
10i1	9.47	71.65	10.10	8.78
10i4	29.63	59.33	1.03	10.01
10i5	10.18	78.74	1.29	9.78
10j1	68.61	16	0.87	14.52
10j3	62.78	31.05	0.88	5.29
10j4	77.36	9.57	3.14	9.93
10k1	67.26	13.96	4.53	14.26
10k2	62.90	29.30	3.23	4.57
10k4	62.65	12.92	12.26	12.17
10k5	47.88	29.16	10.81	12.14
10l3	19.65	69.17	1.06	10.11
10l4	9.88	79.27	1.03	9.81
10l5	69.05	5.25	0.94	24.76
10m3	39.40	44.68	1.16	14.76
10m4	59.04	20.25	1.12	19.59
10m5	29.13	58.05	2.99	9.83
10n2	63.39	28.95	2.90	4.76
10n3	67.89	14.76	3.04	14.30
10n4	67.53	5.12	2.94	24.41
10n5	9.30	68.12	2.68	19.91
10o2	39.01	43.70	2.86	14.42
10o3	58.22	19.19	2.86	19.73
10o4	57.58	28.14	4.71	9.56
10p2	51.39	29.32	4.88	14.41
10p4	9.37	66.62	4.82	19.20
10q2	63.24	4.91	9.19	22.66
10q4	9.43	63.50	8.93	18.13
10q5	36.35	41.18	8.94	13.54
9m3	58.39	4.31	9.16	28.14
9n3	64.22	4.96	1.13	29.68
9n5	9.71	77.71	2.80	9.78
9o2	18.68	67.02	4.79	9.51
9o3	47.99	28.42	4.64	18.95
9o4	36.50	45.12	9.36	9.02
9o5	18.22	63.52	8.99	9.26
9o6	9.34	72.05	9.13	9.47

900°C				
Exp. No.	Cu	Ni	Fe	S
9a3	45.23	35.56	10.00	9.21
9b1	39.81	49.44	0.98	9.77
9b2	21.15	67.30	0.95	10.59
9b4	58.87	17.95	1.15	22.03
9c1	49.25	44.89	0.93	4.93
9c2	67.77	16.26	1.06	14.91
9c3	67.70	14.78	2.94	14.58
9c4	47.32	44.69	2.96	5.03
9c5	48.44	41.44	5.26	4.86
9d1	41.70	38.36	5.12	14.82
9d2	66.16	14.67	5.07	14.11
9d3	45.13	40.52	10.04	4.31
9d4	40.14	36.64	10.41	12.81
9d5	62.40	13.90	10.48	13.22
9e1	68.11	21.07	1.24	9.57
9e2	35.47	47.99	1.24	15.30
9e3	53.78	19.67	1.17	25.38
9e4	5.02	58.60	1.12	35.27
9f1	67.62	19.76	3.10	9.51
9f2	33.32	48.44	3.26	14.98
9f3	5.87	57.15	3.26	33.71
9f4	67.02	18.77	4.96	9.25
9g1	63.44	17.96	9.15	9.45
9g2	50.89	18.34	9.67	21.11
9g3	4.91	52.65	11.35	31.09
9g4	9.77	43.88	10.29	36.06
9h1	44.51	39.23	1.04	15.23
9h2	9.97	49.97	1.00	39.06
9h3	49.37	25.25	0.99	24.39
9h4	45.41	19.26	1.18	34.15
9h5	23.73	39.80	1.08	35.38
9i1	0.00	54.54	1.08	44.39
9i2	43.56	39.55	2.88	14.01
9i3	54.07	19.09	2.95	23.88
9i4	10.35	48.67	2.79	38.18
9i5	48.25	24.18	3.00	24.58
9j1	44.63	19.20	2.87	33.30
9j3	0.00	52.61	2.99	44.40
9j5	34.56	46.16	4.82	14.46
9k1	52.63	18.33	4.79	24.24
9k2	4.71	57.60	4.77	32.92
9k4	48.17	24.23	4.85	22.75
9k5	42.56	19.50	4.55	33.40
9l1	23.49	37.93	4.90	33.68
9l2	0.00	52.33	4.84	42.83
9l3	32.13	44.75	9.51	13.61
9l4	44.94	23.07	9.09	22.90
9l5	40.98	18.74	9.04	31.24
9m1	22.23	35.93	9.49	32.35
9m2	0.00	49.15	8.94	41.91

800°C				
Exp. No.	Cu	Ni	Fe	S
8a1	9.45	58.44	3.60	28.50
8a2	3.89	82.30	3.49	10.32
8a3	14.45	71.79	3.78	9.98
8a4	23.75	63.11	3.07	10.07
8a5	18.34	49.85	3.04	28.77
8b1	75.90	9.97	4.66	9.48
8b2	15.41	69.48	5.05	10.07
8b3	51.33	20.21	4.87	23.59
8b4	47.92	25.11	5.16	21.80
8b5	60.14	10.14	5.47	24.24
8c2	9.94	56.48	5.33	28.25
8c3	66.02	19.47	5.13	9.38
8c4	22.23	58.81	9.76	9.20
8c5	5.92	74.94	9.86	9.27
8d1	49.24	18.02	10.08	22.67
8d2	57.59	9.75	10.10	22.56
8d3	9.12	53.66	10.32	26.90
8d4	18.43	44.82	9.93	26.82
8e1	79.32	9.83	1.05	9.80
8e2	40.14	48.38	1.10	10.38
8e3	25.42	63.27	1.29	10.01
8e4	14.55	74.00	1.03	10.41
8f1	77.58	9.80	2.98	9.64
8f2	48.15	23.74	3.02	25.10
8f3	61.78	10.23	2.94	25.05
8f4	66.93	19.64	3.78	9.64
8f5	38.76	53.04	3.61	4.59
8g1	27.60	54.25	3.28	14.86
8g2	66.67	15.09	3.14	15.09
8g3	38.28	51.65	5.22	4.85
8g4	23.99	61.41	5.01	9.59
8g5	6.27	79.54	4.83	9.37
8h1	28.39	51.49	5.22	14.91
8h3	17.67	48.31	5.10	28.92
8i2	13.06	67.47	10.52	8.94
8i3	44.86	22.95	9.83	22.36
8i4	49.24	18.02	10.08	22.67
8j1	5.07	83.90	1.29	9.74
8j2	49.04	24.81	1.04	25.11
8j3	54.25	20.05	1.06	24.63
8j4	64.11	10.24	1.12	24.53
8j5	44.79	38.98	1.28	14.95
8k1	9.89	58.74	1.12	30.25
8k2	23.34	45.75	1.05	29.87
8k3	69.16	19.99	1.00	9.86
8k4	29.34	39.54	1.21	29.91
8k5	49.31	20.41	1.06	29.23
8k6	0.00	54.34	1.03	44.63
8l1	30.88	27.82	1.19	40.11
8l2	28.40	39.14	2.74	29.73
8l3	18.87	39.31	2.91	38.91

700°C				
Exp. No.	Cu	Ni	Fe	S
7a1	29.82	48.82	1.16	20.2
7a2	5.54	68.63	1	24.83
7a3	78.61	9.38	0.09	11.11
7a4				
7b2				
7b3				
7c1				
7c2				
7c3	10.07	64	1.31	24.62
7c4				
7d5				
7e1	28.67	57.21	9.17	4.96
7e2	18.52	59.09	8.84	13.55
7e3	54.07	23.28	9.42	13.24
7e4	27.21	32.47	9.09	31.23
7e5	10.03	49.79	8.83	31.35
7f1	0.00	51.04	8.87	40.09
7f2	4.28	42.13	8.83	44.76
7f3	29.18	62.30	3.54	4.98
7f4	19.62	62.65	3.14	14.60
7f5	57.73	24.81	3.11	14.36
7g1	29.39	34.45	2.81	33.36
7g2	0.00	53.28	3.47	43.25
7g3	3.88	44.93	2.94	48.24
7g4	19.45	64.42	1.25	14.89
7g5	8.96	55.78	1.05	34.20
7h1	28.91	35.77	1.21	34.10
7h2	58.32	25.50	1.04	15.13
7h3	0.00	54.52	1.10	44.38
7h4	5.51	44.92	1.04	48.53
7h5	28.69	61.56	4.79	4.96
7i1	19.86	60.85	4.73	14.57
7i2	54.12	26.73	4.10	15.05
7i3	26.81	34.59	5.49	33.12
7j2	0.00	51.74	5.31	42.95
7j3	4.50	42.81	4.93	47.75

8l4	0.00	53.65	2.96	43.39
8l5	29.61	28.54	2.94	38.92
8m2	19.12	38.54	4.87	37.46
8m3	28.57	38.04	4.89	28.50
8m4	48.14	19.04	4.74	28.07
8m5	26.88	36.79	9.11	27.22
8n1	45.07	18.95	8.80	27.18
8n2	19.02	35.97	9.07	35.94
8n3	0.00	50.22	8.67	41.11
8n5	27.26	27.92	8.89	35.93

APPENDIX C

Average and 95% confidence interval (ci) Data of Electron Microprobe Analyses for all the experiments. (*Melt = Recalculated melt analyses)

(Digenite°, β-phase°, Millerite° = Sulphide phases with exsolutions)

1200°C										
Exp. no.	Phase	Cu	*ci*	Ni	*ci*	Fe	*ci*	S	*ci*	No. of analyses
1 wt%										
12l1	Melt	74.44	*1.53*	18.66	*1.65*	0.65	*0.04*	6.26	*2.29*	50
12l2	*Melt	48.74	*1.03*	41.76	*1.49*	1.09	*0.13*	8.41	*1.82*	50
12l3	Alloy	27.17	*0.19*	71.54	*0.20*	1.29	*0.01*	0.00	*0.00*	20
	*Melt	32.64	*1.78*	53.05	*2.86*	0.68	*0.10*	13.64	*1.86*	50
12l4	Alloy	9.16	*0.10*	89.29	*0.11*	1.55	*0.02*	0.00	*0.00*	20
	*Melt	15.42	*2.76*	64.85	*3.50*	0.52	*0.10*	19.21	*1.41*	50
12l5	*Melt	55.76	*2.18*	29.48	*1.89*	0.89	*0.06*	13.87	*1.42*	50
12l6	*Melt	31.48	*2.28*	53.04	*3.16*	1.29	*0.19*	14.20	*1.57*	50
3 wt%										
12m1	*Melt	71.19	*0.31*	19.34	*1.01*	2.01	*0.05*	7.47	*0.96*	50
12m2	*Melt	47.63	*0.99*	43.98	*1.54*	2.48	*0.18*	5.90	*1.06*	50
12m3	Alloy	26.09	*0.30*	70.55	*0.34*	3.37	*0.06*	0.00	*0.00*	10
	*Melt	29.69	*1.47*	58.53	*2.02*	1.37	*0.16*	10.41	*1.71*	50
12m4	Alloy	8.84	*0.05*	87.54	*0.06*	3.62	*0.02*	0.00	*0.00*	10
	*Melt	10.83	*0.44*	71.93	*1.06*	1.09	*0.12*	16.16	*1.41*	48
12m5	*Melt 1	64.55	*1.60*	13.33	*1.42*	1.34	*0.05*	20.78	*0.26*	40
	*Melt 2	61.14	*0.86*	25.51	*1.46*	2.06	*0.09*	11.29	*0.77*	50
12m6	*Melt	28.08	*2.01*	57.01	*2.52*	2.12	*0.20*	12.80	*1.39*	50
5 wt%										
12n1	Melt	72.00	*1.27*	17.41	*5.89*	3.84	*0.61*	6.76	*6.09*	50
12n2	Alloy	40.39	*0.18*	52.88	*0.16*	6.73	*0.04*	0.00	*0.00*	10
	Melt	48.78	*4.10*	42.31	*6.75*	4.01	*1.10*	4.91	*5.14*	50
12n4	Alloy	8.89	*0.05*	85.34	*0.07*	5.78	*0.03*	0.00	*0.00*	10
	*Melt	10.36	*0.71*	67.86	*0.98*	1.42	*0.20*	20.37	*1.33*	50
12n5	Melt	26.55	*7.59*	56.44	*9.93*	3.84	*2.20*	13.17	*8.08*	50
10 wt%										
12o1	*Melt	68.63	*0.85*	18.31	*1.16*	8.34	*0.37*	4.72	*1.15*	50
12o2	Alloy	36.67	*0.43*	50.21	*0.39*	13.12	*0.22*	0.00	*0.00*	20
	*Melt	50.65	*1.15*	33.93	*2.01*	6.82	*0.47*	8.61	*1.33*	50
12o3	Alloy	23.97	*0.11*	64.71	*0.18*	11.32	*0.11*	0.00	*0.00*	20
	*Melt	32.12	*1.44*	51.30	*2.23*	6.32	*0.62*	10.27	*1.75*	50
12o4	Alloy	8.01	*0.17*	81.05	*0.21*	10.94	*0.09*	0.00	*0.00*	20
	*Melt	12.31	*1.01*	63.63	*1.27*	4.03	*0.28*	20.04	*0.93*	50
12o5	*Melt 1	57.79	*1.11*	25.17	*1.88*	8.33	*0.37*	8.71	*1.00*	50
	*Melt 2	65.27	*1.12*	6.77	*0.94*	6.46	*0.16*	21.50	*0.43*	50
12o6	Alloy	20.08	*0.13*	65.78	*0.12*	14.14	*0.08*	0.00	*0.00*	20
	*Melt	28.32	*2.09*	51.38	*2.46*	7.30	*0.71*	13.01	*1.79*	50

1100°C										
Exp. no.	Phase	Cu	*ci*	Ni	*ci*	Fe	*ci*	S	*ci*	No. of anal.
1 wt%										
11b1	*Melt	64.72	*1.03*	27.93	*1.11*	0.35	*0.02*	7.00	*1.18*	75
11b2	Alloy	51.33	*0.75*	47.69	*0.75*	0.98	*0.01*	0.00	*0.00*	20
	*Melt	48.41	*1.64*	39.54	*1.64*	0.47	*0.03*	11.58	*1.19*	75
11b3	Alloy	28.52	*0.30*	69.61	*0.30*	1.88	*0.02*	0.00	*0.00*	20
	*Melt	28.68	*1.35*	54.86	*1.50*	0.52	*0.06*	15.95	*1.21*	75
11b4	Alloy	8.55	*0.12*	88.69	*0.15*	2.76	*0.04*	0.00	*0.00*	20
	*Melt	9.85	*0.29*	70.53	*1.03*	0.68	*0.09*	18.94	*1.27*	75
11b5	*Melt	60.13	*0.99*	27.63	*1.50*	0.40	*0.04*	11.84	*0.96*	75
3 wt%										
11c1	Digenite°	71.40	*0.76*	0.54	*0.86*	5.80	*0.28*	22.26	*0.47*	40
	*Melt	90.60	*0.66*	5.57	*0.21*	1.70	*0.09*	2.13	*0.64*	75
11c2	Digenite°	71.53	*1.95*	4.22	*3.21*	3.86	*0.39*	20.39	*1.94*	30
	*Melt	80.15	*0.28*	13.44	*0.55*	2.12	*0.03*	4.29	*0.75*	75
11c4	*Melt 1	59.53	*1.42*	22.07	*1.85*	2.40	*0.15*	16.01	*0.92*	75
	*Melt 2	63.01	*0.82*	13.60	*0.78*	2.28	*0.08*	21.11	*0.42*	75
11c5	*Melt	73.06	*0.21*	17.62	*0.99*	2.94	*0.05*	6.38	*0.90*	75
11d1	Alloy	61.70	*1.13*	33.76	*0.76*	4.54	*0.41*	0.00	*0.00*	19
	*Melt	64.89	*0.65*	23.40	*1.57*	2.46	*0.19*	9.26	*1.07*	75
11d2	Alloy	46.60	*0.38*	49.45	*0.35*	3.95	*0.07*	0.00	*0.00*	20
	*Melt	46.69	*1.19*	38.35	*0.93*	1.52	*0.12*	13.44	*1.33*	75
11d3	Alloy	24.95	*0.28*	69.13	*0.34*	5.91	*0.10*	0.00	*0.00*	20
	*Melt	30.27	*1.06*	53.71	*1.44*	2.20	*0.22*	13.82	*1.34*	75
11d4	Alloy	8.35	*0.13*	86.50	*0.17*	5.14	*0.06*	0.00	*0.00*	20
	*Melt	10.35	*0.21*	70.75	*0.97*	1.49	*0.18*	17.41	*1.22*	75
11d5	*Melt	60.23	*1.00*	24.98	*1.87*	2.50	*0.13*	12.30	*1.20*	75
Exp. no.	Phase	Cu	*ci*	Ni	*ci*	Fe	*ci*	S	*ci*	No. of anal.
5 wt%										
11e1	Alloy	47.08	*1.03*	46.65	*0.79*	6.27	*0.26*	0.00	*0.00*	19
	*Melt	48.11	*1.13*	34.71	*0.74*	2.52	*0.22*	14.66	*1.93*	60
11e2	*Melt	58.92	*1.00*	25.68	*1.67*	4.29	*0.18*	11.12	*0.85*	75
11e3	*Melt 1	66.97	*0.74*	7.60	*0.71*	4.37	*0.08*	21.06	*0.21*	75
	*Melt 2	66.77	*0.62*	20.69	*1.56*	3.66	*0.12*	8.89	*1.04*	75
11e4	*Melt 1	65.09	*0.88*	11.13	*0.82*	3.98	*0.10*	19.81	*0.37*	75
	*Melt 2	56.94	*1.26*	25.78	*1.81*	4.00	*0.22*	13.28	*1.13*	75
11e5	Alloy	68.03	*0.55*	25.86	*0.36*	6.11	*0.20*	0.00	*0.00*	20
	*Melt	71.97	*0.49*	18.42	*1.67*	4.03	*0.27*	5.58	*1.63*	75
11f1	Alloy	58.38	*0.80*	35.19	*0.60*	6.44	*0.22*	0.00	*0.00*	20
	*Melt	64.20	*0.84*	24.61	*1.76*	3.70	*0.15*	7.49	*1.03*	50
11f2	Alloy	23.67	*0.17*	68.80	*0.13*	7.53	*0.10*	0.00	*0.00*	20
	*Melt	30.51	*1.78*	52.02	*1.64*	3.00	*0.27*	14.47	*1.20*	50
11f3	Alloy	6.91	*0.12*	85.79	*0.08*	7.30	*0.08*	0.00	*0.00*	19
	*Melt	10.06	*0.44*	68.36	*1.35*	2.23	*0.45*	19.35	*1.62*	50

10 wt%										
11g2	Alloy	77.88	*0.14*	14.10	*0.13*	8.03	*0.04*	0.00	*0.00*	20
	Digenite°	65.96	*1.32*	1.75	*1.20*	9.90	*0.56*	22.40	*1.33*	75
11g3	Alloy	62.33	*0.25*	26.99	*0.22*	10.68	*0.14*	0.00	*0.00*	20
	Digenite°	67.01	*2.88*	4.20	*3.46*	7.48	*0.88*	21.31	*1.49*	75
11g4	Alloy	58.44	*0.26*	31.75	*0.23*	9.80	*0.09*	0.00	*0.00*	20
	Digenite°	66.46	*3.61*	4.96	*3.04*	5.87	*0.46*	22.71	*0.81*	40
11g5	Alloy	68.58	*0.16*	22.20	*0.16*	9.22	*0.06*	0.00	*0.00*	20
	Digenite°	69.92	*0.80*	0.57	*0.51*	6.70	*0.33*	22.81	*0.25*	60
11h1	Alloy	44.65	*0.31*	41.62	*0.38*	13.73	*0.34*	0.00	*0.00*	20
	*Melt	54.29	*1.40*	25.07	*2.06*	8.07	*0.45*	12.57	*1.16*	75
11h2	Alloy	42.83	*0.55*	46.02	*0.45*	11.14	*0.16*	0.00	*0.00*	20
	*Melt	50.04	*0.92*	31.59	*1.39*	5.73	*0.25*	12.65	*0.90*	75
11h3	Alloy	22.11	*0.20*	64.43	*0.24*	13.46	*0.16*	0.00	*0.00*	20
	*Melt	32.83	*0.70*	45.85	*0.99*	6.19	*0.37*	15.21	*0.97*	75
11h4	Alloy	8.20	*0.14*	79.22	*0.18*	12.58	*0.15*	0.00	*0.00*	20
	*Melt	12.25	*0.72*	64.70	*1.25*	6.17	*0.50*	16.87	*1.40*	75
11h5	Alloy	48.31	*0.43*	39.50	*0.37*	12.19	*0.23*	0.00	*0.00*	20
	Digenite°	67.00	*3.09*	7.21	*2.25*	5.31	*0.28*	20.48	*1.32*	50
	*Melt	57.33	*1.62*	21.73	*2.36*	7.15	*0.43*	13.79	*1.24*	75

1000°C										
Exp. no.	**Phase**	**Cu**	***ci***	**Ni**	***ci***	**Fe**	***ci***	**S**	***ci***	**No. of anal.**
1 wt% Fe										
10i4	Alloy	28.43	*1.59*	69.39	*1.56*	2.18	*0.06*	0.00	*0.00*	32
	*Melt	29.12	*1.93*	50.36	*2.17*	0.36	*0.10*	20.15	*1.61*	20
10i5	*Melt	7.33	*0.80*	70.35	*1.35*	0.25	*0.11*	22.06	*2.46*	20
10j1	Alloy	62.70	*0.93*	36.11	*0.71*	1.18	*0.44*	0.00	*0.00*	45
	Digenite°	74.71	*2.88*	3.66	*2.59*	0.96	*0.11*	20.67	*0.33*	20
	*Melt	44.48	*6.21*	38.52	*6.34*	1.04	*0.16*	15.95	*1.57*	40
10j3	Alloy	60.61	*0.75*	37.95	*0.70*	1.44	*0.22*	0.00	*0.00*	48
	Digenite°	77.45	*2.42*	1.63	*2.22*	0.81	*0.13*	20.11	*0.26*	29
10l3	Alloy	20.39	*0.61*	78.24	*0.60*	1.36	*0.01*	0.00	*0.00*	20
	*Melt	19.41	*1.78*	60.52	*2.02*	0.29	*0.04*	19.79	*1.29*	44
10l4	Alloy	9.85	*0.19*	88.67	*0.20*	1.48	*0.01*	0.00	*0.00*	20
	*Melt	7.54	*0.56*	71.67	*0.68*	0.28	*0.05*	20.50	*1.17*	42
10l5	*Melt	69.85	*0.83*	4.88	*0.60*	0.85	*0.01*	24.42	*0.24*	20
10m3	*Melt	36.44	*4.71*	43.58	*4.20*	0.51	*0.07*	19.47	*1.19*	50
10m4	Digenite°	77.21	*1.87*	2.84	*1.75*	0.40	*0.05*	19.55	*0.28*	75
	*Melt	39.36	*3.12*	42.10	*3.79*	0.64	*0.04*	17.90	*0.71*	20

Exp. no.	Phase	Cu	*ci*	Ni	*ci*	Fe	*ci*	S	*ci*	No. of anal.
3 wt% Fe										
10f1	Alloy	34.66	*0.88*	60.95	*0.88*	4.39	*0.14*	0.00	*0.00*	23
10f4	Alloy	52.71	*0.38*	43.04	*0.39*	4.25	*0.06*	0.00	*0.00*	20
10g1	Digenite°	75.44	*1.55*	1.67	*1.25*	2.22	*0.44*	20.66	*0.46*	111
	*Melt	36.14	*4.16*	40.49	*3.68*	3.42	*0.66*	19.95	*2.10*	20
10g2	Alloy	8.39	*0.10*	86.33	*0.12*	5.28	*0.04*	0.00	*0.00*	10
	Melt	10.66	*1.29*	67.20	*5.06*	1.05	*0.99*	21.09	*5.94*	20
10g3	Alloy	17.90	*0.90*	76.81	*0.86*	5.29	*0.06*	0.00	*0.00*	16
	Melt	19.03	*5.32*	60.05	*5.97*	1.45	*0.41*	19.49	*2.84*	20
10j4	Alloy	75.05	*0.91*	21.99	*0.72*	2.96	*0.26*	0.00	*0.00*	77
	Digenite°	74.19	*1.41*	1.48	*1.49*	3.51	*0.21*	20.82	*0.34*	30
10m5	Alloy	29.89	*0.36*	65.79	*0.37*	4.31	*0.04*	0.00	*0.00*	21
	*Melt	31.50	*2.45*	48.89	*2.37*	1.25	*0.18*	18.35	*1.55*	50
10n2	Alloy	62.28	*0.42*	35.56	*0.42*	2.15	*0.02*	0.00	*0.00*	20
	Digenite°	76.84	*1.36*	2.02	*1.21*	1.07	*0.04*	20.07	*0.24*	30
10n3	Alloy	56.40	*0.55*	40.23	*0.56*	3.37	*0.05*	0.00	*0.00*	20
	Digenite°	76.04	*1.34*	2.26	*1.13*	1.50	*0.10*	20.20	*0.25*	30
10n4	*Melt	68.25	*0.48*	5.19	*0.37*	3.02	*0.02*	23.54	*0.13*	75
10n5	*Melt	9.21	*0.29*	66.85	*0.38*	2.16	*0.07*	21.79	*0.31*	93
10o2	*Melt	39.88	*1.72*	41.50	*1.46*	2.02	*0.16*	16.60	*1.09*	75
10o3	Digenite°	74.03	*2.09*	3.28	*1.94*	1.69	*0.06*	21.00	*0.25*	75
	*Melt	33.39	*3.41*	42.83	*3.42*	2.29	*0.07*	21.49	*0.33*	30
5 wt% Fe										
10a	Alloy	28.40	*0.41*	63.71	*0.50*	7.88	*0.29*	0.00	*0.00*	31
	*Melt	28.34	*2.22*	49.76	*2.48*	2.80	*0.72*	19.10	*2.99*	20
10b	Alloy	52.40	*0.32*	41.08	*0.32*	6.52	*0.13*	0.00	*0.00*	22
	Digenite°	65.94	*2.52*	9.50	*2.54*	2.93	*0.42*	21.71	*1.18*	28
10e1	Alloy	8.10	*0.14*	83.97	*0.13*	7.93	*0.07*	0.00	*0.00*	30
	Melt	10.47	*2.84*	68.03	*5.98*	2.31	*1.96*	19.19	*7.97*	20
10e2	Alloy	80.07	*0.92*	16.53	*0.89*	3.40	*0.13*	0.00	*0.00*	63
	Digenite°	73.70	*2.21*	0.31	*0.70*	4.88	*0.41*	21.10	*1.61*	125
10e3	Alloy	16.53	*0.14*	75.36	*0.17*	8.12	*0.06*	0.00	*0.00*	20
	*Melt	19.95	*4.80*	56.26	*4.57*	1.62	*0.30*	22.17	*1.50*	20
10k1	Alloy	52.90	*0.59*	42.49	*0.45*	4.61	*0.40*	0.00	*0.00*	135
	Digenite°	73.96	*2.71*	2.88	*2.34*	2.24	*0.15*	20.92	*0.69*	33
10k2	Alloy	57.28	*1.30*	37.87	*1.09*	4.83	*0.75*	0.00	*0.00*	90
	Digenite°	75.17	*1.87*	1.24	*1.66*	2.99	*0.20*	20.60	*0.49*	32
10o4	Alloy	44.06	*0.45*	50.46	*0.43*	5.48	*0.05*	0.00	*0.00*	20
	Digenite°	74.89	*2.28*	2.26	*2.02*	1.83	*0.29*	21.01	*0.22*	30
10p2	Alloy	38.55	*1.12*	54.24	*1.03*	7.22	*0.12*	0.00	*0.00*	20
	Digenite°	73.59	*2.07*	2.72	*1.85*	2.25	*0.20*	21.44	*0.28*	30
	*Melt	40.25	*1.88*	37.06	*1.75*	3.51	*0.14*	19.18	*0.45*	60
10p4	Melt	7.79	*1.69*	65.91	*2.59*	3.73	*0.85*	22.57	*2.73*	74

Exp. no.	Phase	Cu	*ci*	Ni	*ci*	Fe	*ci*	S	*ci*	No. of anal.
10 wt% Fe										
10g4	Alloy	76.16	*2.48*	14.78	*1.05*	9.06	*1.46*	0.00	*0.00*	188
	Digenite	67.12	*0.50*	0.19	*0.07*	8.70	*0.28*	23.99	*0.30*	20
10h3	Alloy	46.65	*0.25*	40.92	*0.25*	12.06	*0.16*	0.00	*0.00*	25
	Digenite°	67.51	*2.49*	5.06	*2.31*	5.34	*0.33*	22.09	*0.29*	18
10h4	Alloy	13.37	*0.47*	72.74	*0.53*	13.74	*0.18*	0.00	*0.00*	20
	*Melt	22.68	*2.82*	49.88	*2.68*	3.99	*0.19*	23.45	*0.47*	24
10i1	Alloy	5.29	*0.53*	80.64	*0.77*	14.07	*0.38*	0.00	*0.00*	24
10k4	Alloy	55.86	*2.98*	34.73	*2.22*	9.42	*1.40*	0.00	*0.00*	64
	Digenite°	72.42	*1.34*	0.95	*1.07*	5.28	*0.16*	21.35	*0.43*	20
10k5	Alloy	24.82	*1.35*	59.65	*0.89*	15.53	*0.54*	0.00	*0.00*	209
	Digenite°	70.15	*3.66*	2.12	*3.03*	6.18	*0.58*	21.55	*0.54*	24
	*Melt	33.97	*4.14*	35.48	*4.13*	7.07	*0.57*	23.49	*1.22*	20
10q2	Digenite°	64.95	*2.91*	2.90	*1.75*	9.03	*0.85*	23.12	*0.42*	51
10q4	*Melt	10.00	*1.03*	59.76	*1.66*	8.70	*0.60*	21.55	*1.73*	50
10q5	Alloy	23.26	*0.25*	62.01	*0.43*	14.73	*0.20*	0.00	*0.00*	20
	*Melt	33.18	*1.63*	36.57	*1.40*	6.78	*0.40*	23.46	*1.10*	50

900°C										
Exp. no.	**Phase**	**Cu**	***ci***	**Ni**	***ci***	**Fe**	***ci***	**S**	***ci***	**No. of anal.**
1 wt% Fe										
9b1	Alloy	45.70	*0.54*	52.46	*0.51*	1.85	*0.03*	0.00	*0.00*	20
	Digenite°	76.93	*1.74*	2.29	*1.62*	0.45	*0.12*	20.33	*0.35*	15
	Melt	33.65	*1.31*	46.96	*1.33*	0.82	*0.05*	18.56	*0.37*	8
9b2	Alloy	19.72	*0.56*	79.58	*0.65*	0.70	*0.41*	0.00	*0.00*	40
	Melt	13.67	*3.78*	66.92	*4.14*	0.36	*0.02*	19.06	*0.89*	10
9b4	Digenite°	78.82	*0.93*	0.29	*0.49*	0.65	*0.58*	20.26	*0.65*	119
	*Melt	27.65	*5.8*	46.88	*6.2*	1.10	*0.12*	24.37	*0.54*	15
9c1	Alloy	45.91	*0.82*	52.83	*0.81*	1.26	*0.03*	0.00	*0.00*	75
	Digenite°	77.26	*1.57*	1.73	*1.42*	0.44	*0.06*	20.57	*0.26*	40
9c2	Alloy	43.87	*0.45*	53.49	*0.44*	2.64	*0.04*	0.00	*0.00*	48
	Digenite	77.84	*1.12*	1.11	*1.06*	0.85	*0.06*	20.20	*0.24*	22
9e1	Alloy	61.96	*0.39*	36.48	*0.38*	1.57	*0.03*	0.00	*0.00*	77
	Digenite	78.49	*0.39*	0.53	*0.29*	0.87	*0.13*	20.11	*0.32*	34
9e2	Alloy	44.75	*0.17*	53.31	*0.16*	1.94	*0.01*	0.00	*0.00*	20
	Digenite°	77.74	*1.70*	2.10	*1.57*	0.59	*0.04*	19.56	*0.22*	65
	*Melt	30.35	*7.50*	49.46	*6.73*	0.78	*0.18*	19.41	*2.02*	20
9e3	β-phase°	67.61	*5.28*	7.91	*4.23*	1.35	*0.06*	23.13	*1.13*	20
	*Melt	49.28	*6.65*	23.46	*5.22*	0.98	*0.06*	26.27	*1.22*	20
9e4	Millerite	3.91	*0.32*	59.32	*0.52*	0.97	*0.02*	35.81	*0.34*	50
	*Melt	13.25	*1.14*	51.19	*0.85*	0.85	*0.02*	34.71	*0.30*	121
9h1	Alloy	43.00	*0.81*	54.79	*0.72*	2.21	*0.09*	0.00	*0.00*	20
	Digenite°	77.80	*0.86*	1.40	*0.67*	0.43	*0.07*	20.38	*0.38*	34
	*Melt	32.51	*7.83*	48.11	*7.35*	0.91	*0.17*	18.47	*1.74*	20
9h2	Millerite	2.80	*0.79*	59.50	*0.79*	1.04	*0.02*	36.65	*0.68*	20
	Vaesite	1.27	*0.14*	46.17	*0.71*	0.13	*0.01*	52.43	*0.74*	20
	Melt	30.05	*2.78*	34.07	*2.45*	0.90	*0.05*	34.98	*1.37*	36
9h3	β-phase°	71.39	*2.81*	6.11	*2.42*	0.78	*0.06*	21.73	*0.58*	25
	*Melt	38.55	*3.60*	34.89	*3.01*	0.62	*0.03*	25.94	*0.50*	48
9h4	*Melt	45.52	*2.15*	20.94	*1.28*	1.28	*0.05*	32.26	*1.18*	32
9h5	*Melt	23.64	*2.96*	40.43	*2.44*	1.18	*0.02*	34.75	*0.62*	33
9i1	Millerite	0.11	*0.02*	59.91	*0.26*	1.49	*0.02*	38.49	*0.26*	87
	Vaesite	0.09	*0.02*	46.49	*0.32*	0.24	*0.07*	53.17	*0.31*	77
9n3	β-phase°	66.79	*3.57*	6.14	*2.18*	1.13	*0.11*	25.94	*1.49*	20

Exp. no.	Phase	Cu	*ci*	Ni	*ci*	Fe	*ci*	S	*ci*	No. of anal.
3 wt% Fe										
9c3	Alloy	50.71	*0.32*	43.91	*0.31*	5.38	*0.07*	0.00	*0.00*	47
	Digenite	76.12	*0.54*	0.67	*0.56*	2.13	*0.15*	21.07	*0.17*	17
9c4	Alloy	38.67	*0.43*	57.48	*0.43*	3.85	*0.04*	0.00	*0.00*	48
	Digenite°	77.74	*1.97*	1.19	*1.56*	0.93	*0.06*	20.14	*0.53*	36
9f1	Alloy	62.97	*1.57*	33.29	*1.24*	3.73	*0.34*	0.00	*0.00*	38
	Digenite	78.02	*0.74*	0.30	*0.20*	1.81	*0.45*	19.88	*0.35*	40
9f2	Alloy	34.26	*0.55*	59.51	*0.57*	6.23	*0.06*	0.00	*0.00*	46
	Digenite°	78.41	*1.28*	0.69	*1.10*	1.37	*0.27*	19.53	*0.26*	37
	*Melt	25.24	*2.62*	50.57	*2.55*	2.27	*0.17*	21.92	*0.77*	106
9f3	Millerite	2.91	*0.97*	57.80	*0.99*	3.68	*0.04*	35.61	*0.33*	17
	*Melt	14.31	*2.54*	52.46	*2.23*	2.71	*0.09*	30.51	*0.41*	30
9i2	Digenite°	77.27	*1.26*	1.43	*1.15*	1.05	*0.08*	20.25	*0.22*	55
	*Melt	20.81	*3.68*	55.14	*3.30*	1.27	*0.07*	22.78	*0.29*	49
9i3	β-phase°	69.31	*2.99*	5.80	*2.71*	2.81	*0.09*	22.07	*0.42*	96
	Melt	21.31	*1.91*	49.96	*1.85*	1.68	*0.06*	27.05	*0.35*	37
9i4	Millerite	3.12	*0.27*	55.37	*0.31*	3.32	*0.04*	38.19	*0.27*	82
	Vaesite	1.42	*0.02*	44.45	*0.43*	0.43	*0.01*	53.69	*0.43*	96
	Melt	36.61	*10.41*	29.10	*9.37*	2.75	*0.11*	31.54	*1.71*	45
9i5	β-phase°	68.50	*4.16*	6.19	*3.77*	3.17	*0.10*	22.14	*0.52*	47
	*Melt	25.50	*2.94*	45.83	*2.78*	2.40	*0.04*	26.28	*0.30*	83
9j1	Melt	43.04	*12.60*	20.10	*7.40*	2.72	*0.67*	34.13	*6.07*	50
9j2	Melt	21.39	*12.13*	40.80	*10.02*	2.91	*0.12*	34.90	*2.31*	50
9j3	Millerite	0.10	*0.02*	56.31	*0.54*	4.22	*0.07*	39.37	*0.48*	105
	Vaesite	0.08	*0.02*	45.93	*0.36*	0.58	*0.16*	53.41	*0.43*	91
9j4	*Melt	63.56	*0.71*	6.33	*0.46*	2.69	*0.05*	27.42	*0.33*	50
9n5	Alloy	9.41	*0.06*	85.82	*0.08*	4.77	*0.03*	0.00	*0.00*	10
	Melt	8.71	*1.44*	68.10	*1.26*	0.62	*0.11*	22.57	*1.59*	20
5 wt% Fe										
9c5	Alloy	42.20	*1.13*	52.04	*0.92*	5.76	*0.24*	0.00	*0.00*	54
	Digenite	76.19	*0.99*	1.23	*1.09*	1.95	*0.12*	20.63	*0.50*	25
9d1	Melt	29.86	*1.11*	45.16	*0.89*	3.63	*0.14*	21.35	*0.61*	184
9d2	Alloy	55.12	*1.82*	37.13	*1.67*	7.75	*0.20*	0.00	*0.00*	86
	Digenite	74.72	*0.60*	0.48	*0.25*	2.98	*0.39*	21.81	*0.26*	35
9f4	Alloy	63.74	*0.47*	30.42	*0.41*	5.84	*0.10*	0.00	*0.00*	33
	Digenite	75.66	*0.68*	0.22	*0.25*	3.16	*0.39*	20.96	*0.37*	69
9j5	Alloy	25.50	*0.20*	64.99	*0.27*	9.51	*0.13*	0.00	*0.00*	88
	Digenite°	75.03	*1.18*	2.07	*1.18*	1.66	*0.10*	21.24	*0.28*	63
	*Melt	32.03	*7.44*	44.99	*6.47*	3.07	*0.62*	19.92	*2.00*	20
9k1	Digenite°	65.43	*0.94*	7.03	*0.75*	4.75	*0.07*	22.79	*0.54*	37
	*Melt	35.74	*2.96*	34.40	*2.76*	3.96	*0.09*	25.89	*0.32*	40
9k2	Millerite	0.80	*0.04*	56.23	*0.72*	6.34	*0.07*	36.63	*0.71*	20
	*Melt	9.46	*0.78*	57.00	*0.74*	3.75	*0.03*	29.78	*0.22*	40
9k4	Digenite°	70.00	*2.47*	4.06	*2.21*	4.49	*0.26*	21.46	*0.44*	20
	*Melt	21.28	*2.12*	48.78	*1.88*	5.36	*0.19*	24.58	*0.15*	48
9k5	*Melt	44.51	*1.51*	19.40	*0.84*	2.11	*0.06*	33.97	*0.77*	32
9l1	Millerite	2.52	*0.55*	54.47	*0.59*	5.74	*0.08*	37.26	*0.63*	20
	*Melt	39.56	*2.41*	25.04	*2.13*	4.59	*0.06*	30.81	*0.61*	40
9l2	Millerite	0.07	*0.01*	57.07	*0.59*	6.03	*0.07*	36.83	*0.65*	20
	Vaesite	0.04	*0.01*	46.99	*0.64*	0.87	*0.12*	52.10	*0.62*	20
9o2	Alloy	18.33	*0.44*	74.35	*0.37*	7.32	*0.15*	0.00	*0.00*	20
	*Melt	21.25	*2.02*	56.28	*1.80*	1.97	*0.18*	20.50	*0.88*	75
9o3	Alloy	23.62	*0.23*	64.83	*0.22*	11.55	*0.07*	0.00	*0.00*	20
	Digenite°	72.8	*1.71*	2.28	*1.59*	3.09	*0.07*	21.83	*0.22*	70
	*Melt	30.72	*3.20*	44.08	*3.14*	4.72	*0.29*	20.47	*0.82*	75

Exp. no.	Phase	Cu	*ci*	Ni	*ci*	Fe	*ci*	S	*ci*	No. of anal.
10 wt% Fe										
9a3	Alloy	21.17	*2.00*	51.15	*1.15*	27.69	*0.76*	0.00	*0.00*	15
	Digenite	73.46	*0.75*	0.00	*0.00*	5.20	*0.51*	21.34	*0.50*	273
9d3	Alloy	37.61	*1.38*	46.01	*1.30*	16.38	*0.30*	0.00	*0.00*	22
	Digenite	72.66	*0.67*	0.30	*0.19*	4.40	*0.41*	22.64	*0.27*	67
9d4	Alloy	15.32	*0.22*	67.73	*0.30*	16.95	*0.14*	0.00	*0.00*	18
	Digenite°	69.95	*1.79*	2.69	*1.41*	5.18	*0.26*	22.19	*0.26*	38
9d5	Alloy	42.07	*4.47*	37.45	*2.63*	20.48	*1.93*	0.00	*0.00*	50
	Digenite	70.10	*0.76*	0.42	*0.47*	6.16	*0.49*	23.32	*0.37*	61
9g1	Alloy	61.53	*0.55*	28.23	*0.36*	10.23	*0.23*	0.00	*0.00*	11
	Digenite	72.17	*0.97*	0.63	*0.89*	5.53	*0.28*	21.67	*0.29*	40
9g2	β-phase°	65.08	*2.97*	3.63	*1.86*	7.46	*0.84*	23.83	*0.35*	34
	*Melt	23.53	*3.82*	39.45	*3.41*	11.24	*0.37*	25.78	*0.38*	35
9g3	Melt	4.71	*1.97*	52.82	*2.31*	12.04	*1.10*	30.43	*0.41*	47
9g4	Millerite	2.97	*0.07*	47.15	*0.40*	11.40	*0.20*	38.49	*0.38*	55
	*Melt	29.42	*4.20*	30.03	*3.49*	8.39	*0.13*	32.15	*0.95*	20
9l3	Alloy	16.92	*0.80*	67.21	*0.66*	15.87	*0.22*	0.00	*0.00*	25
	Digenite°	70.54	*1.33*	2.34	*1.17*	4.39	*0.14*	22.73	*0.18*	29
	*Melt	26.45	*3.94*	44.29	*3.74*	6.13	*0.23*	23.12	*0.61*	28
9l4	β-phase°	65.16	*3.56*	3.98	*2.35*	7.68	*0.86*	23.18	*0.42*	40
	*Melt	24.11	*3.65*	42.05	*3.23*	10.38	*0.27*	23.46	*0.32*	40
9l5	Melt	41.44	*0.31*	18.58	*0.23*	8.51	*0.11*	31.47	*0.23*	50
9m1	Millerite	3.65	*1.10*	49.95	*0.92*	10.80	*0.18*	35.60	*0.33*	50
	*Melt	26.23	*1.38*	35.20	*1.29*	7.88	*0.11*	30.70	*0.18*	29
9m2	Millerite	0.14	*0.02*	49.63	*0.27*	11.56	*0.18*	38.67	*0.26*	98
	Vaesite	0.10	*0.02*	44.91	*0.24*	1.64	*0.04*	53.35	*0.24*	100
9m3	*Melt	58.08	*1.07*	3.98	*0.71*	9.47	*0.14*	28.47	*0.45*	92
9o4	Alloy	20.97	*0.78*	66.22	*0.52*	12.82	*0.39*	0.00	*0.00*	20
	Digenite°	72.42	*1.35*	2.1	*1.22*	3.51	*0.17*	21.98	*0.28*	40
9o5	Alloy	15.30	*0.31*	72.07	*0.50*	12.63	*0.24*	0.00	*0.00*	20
	*Melt	20.65	*1.65*	53.31	*1.57*	4.46	*0.33*	21.59	*0.86*	74
9o6	*Melt	10.99	*0.65*	61.98	*0.92*	4.24	*0.32*	22.78	*0.90*	75

800°C										
Exp. no.	Phase	Cu	*ci*	Ni	*ci*	Fe	*ci*	S	*ci*	No. of anal.
1 wt%										
8e1	Alloy	81.49	*0.21*	17.97	*0.21*	0.54	*0.02*	0.00	*0.00*	20
	Digenite	78.00	*0.45*	0.41	*0.84*	1.35	*0.08*	20.25	*0.67*	40
8e2	*Melt	24.57	*2.41*	54.91	*2.09*	0.47	*0.05*	20.04	*0.72*	75
8e3	Alloy	30.39	*0.33*	67.64	*0.36*	1.97	*0.04*	0.00	*0.00*	20
	*Melt	21.79	*1.55*	56.75	*1.52*	0.40	*0.06*	21.06	*0.90*	75
8e4	Alloy	15.76	*0.41*	82.26	*0.41*	1.98	*0.04*	0.00	*0.00*	20
	*Melt	12.93	*0.59*	64.95	*0.59*	0.22	*0.01*	21.91	*0.22*	75
8j1	Alloy	5.19	*0.07*	92.55	*0.08*	2.26	*0.03*	0.00	*0.00*	20
	Melt	4.26	*0.80*	71.94	*1.39*	0.19	*0.08*	23.60	*1.87*	73
8j2	β-phase°	72.04	*2.12*	5.46	*1.76*	1.11	*0.04*	21.39	*0.45*	75
	*Melt	17.60	*0.60*	51.04	*0.28*	0.57	*0.01*	30.79	*0.11*	70
8j3	β-phase°	70.72	*3.17*	6.35	*2.54*	1.08	*0.04*	21.84	*0.70*	75
	*Melt	19.82	*0.15*	49.18	*1.00*	0.48	*0.02*	30.52	*0.21*	75
8j4	β-phase°	69.83	*1.49*	5.62	*1.26*	1.07	*0.01*	23.48	*0.38*	75
8j5	Digenite°	77.97	*2.28*	1.61	*2.11*	0.34	*0.05*	20.08	*0.25*	50
	*Melt	20.53	*2.73*	57.28	*2.43*	0.52	*0.04*	21.66	*0.51*	75
8k1	*Melt	9.30	*0.96*	57.99	*0.90*	1.27	*0.04*	31.44	*0.36*	33
8k2	*Melt	24.48	*0.83*	44.56	*0.75*	1.10	*0.03*	29.87	*0.15*	90
8k3	Alloy	60.93	*0.46*	37.97	*0.46*	1.09	*0.02*	0.00	*0.00*	20
	Digenite	77.90	*0.88*	0.42	*0.57*	0.69	*0.29*	20.99	*0.60*	14
8k4	*Melt	33.75	*2.12*	36.24	*1.86*	1.08	*0.04*	28.94	*0.35*	59
8k5	*Melt	48.96	*1.03*	19.57	*1.07*	1.20	*0.02*	30.28	*0.46*	70
8k6	Vaesite	0.04	*0.01*	46.74	*0.49*	0.20	*0.01*	53.02	*0.49*	18
	Millerite	0.06	*0.01*	60.10	*0.69*	1.71	*0.05*	38.13	*0.71*	20
8l1	β-phase°	70.45	*1.82*	3.37	*1.46*	2.40	*0.10*	23.79	*0.47*	50
	Vaesite	1.78	*0.38*	44.72	*0.48*	0.16	*0.02*	53.34	*0.41*	20

Exp. no.	Phase	Cu	*ci*	Ni	*ci*	Fe	*ci*	S	*ci*	No. of anal.
3 wt%										
8a1	Melt	9.00	*3.75*	58.98	*3.49*	3.27	*0.18*	28.74	*0.57*	64
8a2	Alloy	3.77	*0.11*	90.57	*0.08*	5.66	*0.11*	0.00	*0.00*	89
	Melt	4.13	*0.43*	72.87	*1.07*	0.63	*0.11*	22.36	*1.40*	25
8a3	Alloy	13.35	*0.41*	80.69	*0.38*	5.97	*0.08*	0.00	*0.00*	72
	Melt	15.72	*3.89*	62.11	*3.84*	0.99	*0.18*	21.19	*1.74*	16
8a4	Alloy	25.06	*0.34*	70.28	*0.32*	4.65	*0.11*	0.00	*0.00*	47
	*Melt	23.58	*2.84*	54.96	*2.61*	1.09	*0.14*	20.38	*1.04*	18
8a5	*Melt	16.98	*2.77*	50.93	*2.52*	3.02	*0.08*	29.07	*0.48*	30
8f1	Alloy	81.42	*0.16*	16.76	*0.17*	1.82	*0.04*	0.00	*0.00*	20
	Digenite	75.38	*0.57*	0.42	*0.26*	3.18	*0.42*	21.03	*0.26*	20
8f2	*Melt	26.61	*2.13*	42.45	*1.83*	2.06	*0.07*	28.88	*0.31*	75
8f3	Millerite	1.56	*0.87*	59.19	*0.69*	1.70	*0.02*	37.54	*0.26*	40
	β-phase°	70.77	*1.31*	2.52	*0.98*	3.14	*0.06*	23.58	*0.40*	60
8f4	Alloy	60.03	*0.47*	35.44	*0.36*	4.53	*0.16*	0.00	*0.00*	18
	Digenite	77.91	*0.46*	0.16	*0.06*	1.57	*0.30*	20.36	*0.27*	17
8f5	Alloy	27.75	*0.23*	67.73	*0.22*	4.51	*0.08*	0.00	*0.00*	20
	Digenite°	76.44	*0.99*	1.48	*0.87*	0.80	*0.10*	21.27	*0.21*	60
8g1	Digenite°	76.76	*0.78*	4.53	*0.76*	0.98	*0.07*	20.73	*0.19*	38
	*Melt	21.46	*2.36*	55.50	*1.98*	1.69	*0.14*	21.35	*0.69*	75
8g2	Alloy	41.85	*0.26*	51.64	*0.23*	6.51	*0.10*	0.00	*0.00*	20
	Digenite	77.91	*0.36*	0.59	*0.13*	1.18	*0.24*	20.32	*0.23*	19

8l2	β-phase°	67.20	*1.74*	5.68	*1.47*	3.93	*0.07*	23.19	*0.41*	72
	Millerite°	5.15	*0.31*	56.55	*0.39*	2.64	*0.04*	35.67	*0.36*	20
	*Melt	27.72	*2.13*	41.13	*1.86*	2.00	*0.06*	29.15	*0.33*	75
8l3	β-phase°	69.51	*1.36*	1.15	*1.21*	5.40	*0.13*	23.94	*0.33*	40
	Millerite°	3.40	*0.37*	55.24	*0.38*	3.32	*0.04*	38.04	*0.27*	40
8l4	Millerite	0.04	*0.01*	58.14	*0.20*	3.59	*0.04*	38.24	*0.18*	20
	Vaesite	0.02	*0.02*	46.38	*0.28*	0.40	*0.02*	53.21	*0.28*	30
8l5	β-phase°	66.94	*2.13*	2.70	*1.66*	5.58	*0.12*	24.78	*0.54*	50
	Vaesite	3.06	*2.23*	43.58	*1.80*	0.87	*0.40*	52.49	*0.82*	20
Exp. no.	**Phase**	**Cu**	***ci***	**Ni**	***ci***	**Fe**	***ci***	**S**	***ci***	**No. of anal.**
5 wt%										
8b1	Alloy	80.15	*0.34*	16.65	*0.27*	3.20	*0.11*	0.00	*0.00*	34
	Digenite	72.30	*0.65*	0.03	*0.04*	5.03	*0.37*	22.65	*0.33*	40
8b2	Alloy	15.38	*0.13*	77.23	*0.24*	7.39	*0.14*	0.00	*0.00*	7
	Melt	16.10	*0.65*	61.93	*0.98*	1.65	*0.22*	20.32	*1.03*	27
8b3	Digenite°	72.81	*1.34*	1.31	*1.18*	4.30	*0.29*	21.57	*0.31*	46
	*Melt	19.79	*5.65*	49.41	*4.78*	6.06	*0.17*	24.75	*0.56*	20
8b4	β-phase°	70.79	*1.38*	2.12	*1.06*	4.56	*0.28*	22.53	*0.23*	36
	*Melt									32
8b5	β-phase°	68.74	*2.16*	2.76	*1.80*	5.03	*0.14*	23.47	*0.51*	15
	*Melt	19.34	*2.88*	44.39	*2.78*	2.76	*0.54*	33.51	*1.53*	12
8c2	*Melt	9.32	*1.95*	57.21	*1.64*	5.58	*0.04*	27.89	*0.28*	20
8c3	Alloy	63.79	*4.48*	31.20	*3.30*	5.00	*1.19*	0.00	*0.00*	40
	Digenite°	74.90	*1.13*	0.37	*0.87*	3.38	*0.52*	21.36	*0.40*	47
8g3	Alloy	27.86	*0.42*	65.67	*0.33*	6.48	*0.12*	0.00	*0.00*	20
	Digenite	78.67	*0.58*	0.56	*0.38*	0.70	*0.26*	20.06	*0.25*	20
8g4	Alloy	21.90	*0.18*	70.28	*0.22*	7.82	*0.17*	0.00	*0.00*	20
	Digenite°	75.67	*1.27*	1.96	*1.20*	1.45	*0.04*	20.92	*0.18*	60
	*Melt	21.35	*2.64*	54.45	*2.42*	2.01	*0.13*	22.20	*0.58*	75
8g5	Alloy	6.33	*0.10*	87.50	*0.24*	6.17	*0.16*	0.00	*0.00*	20
	Melt	7.04	*0.95*	69.99	*0.79*	0.88	*0.10*	22.42	*0.75*	100
8h1	*Melt	20.59	*3.74*	55.00	*3.53*	3.57	*0.40*	20.84	*1.19*	100
8h3	*Melt	17.19	*6.23*	47.44	*4.84*	5.49	*0.12*	29.88	*0.84*	20
8m2	β-phase°	65.86	*0.77*	0.65	*0.52*	8.26	*0.20*	25.23	*0.32*	20
	Millerite°	3.48	*0.71*	52.48	*0.56*	6.27	*0.09*	37.77	*0.30*	49
	Vaesite	1.62	*0.10*	43.62	*0.70*	0.79	*0.04*	53.97	*0.75*	40
8m3	β-phase°	67.39	*2.40*	1.21	*1.28*	7.73	*0.82*	23.68	*0.41*	55
	Melt									91
8m4	β-phase°	67.44	*2.59*	2.41	*2.12*	5.59	*0.14*	24.56	*0.61*	69
	Millerite°	2.91	*0.40*	56.04	*0.33*	3.37	*0.05*	37.68	*0.30*	50
10 wt%										
8c4	Alloy	13.85	*0.19*	72.58	*0.24*	13.57	*0.15*	0.00	*0.00*	50
	Digenite°	75.16	*1.75*	0.60	*1.05*	3.01	*0.51*	21.27	*0.74*	20
	*Melt	20.90	*1.72*	53.40	*1.38*	4.52	*0.11*	21.18	*0.44*	12
8c5	Alloy	5.01	*0.13*	81.35	*0.28*	13.64	*0.20*	0.00	*0.00*	116
	Melt	8.43	*0.34*	65.64	*0.56*	3.56	*0.13*	22.38	*0.31*	9
8d1	β-phase°	64.32	*5.36*	3.81	*2.38*	7.83	*1.97*	24.04	*1.04*	11
	*Melt	13.19	*2.27*	51.23	*1.55*	12.33	*0.18*	23.24	*1.08*	20
8d2	*Melt	9.71	*1.21*	53.14	*1.82*	11.87	*0.37*	25.29	*0.42*	50
8d3	Melt	8.56	*0.59*	53.52	*1.02*	10.27	*0.46*	27.65	*0.38*	9
8d4	*Melt	16.04	*1.88*	46.68	*1.97*	9.51	*0.08*	27.78	*0.11*	15
8i2	Alloy	11.06	*0.15*	74.43	*0.21*	14.51	*0.13*	0.00	*0.00*	20
	*Melt	17.92	*1.55*	54.88	*1.21*	5.30	*0.23*	21.90	*0.65*	75

8i3	β-phase°	66.44	*3.71*	2.42	*2.02*	8.19	*1.19*	22.95	*0.61*	42
	Melt	11.85	*5.94*	51.10	*3.85*	12.49	*0.78*	24.56	*2.72*	80
8i4	*Melt	16.90	*2.18*	45.66	*1.82*	12.73	*0.28*	24.71	*0.89*	100
8m5	β-phase°	64.46	*1.51*	2.31	*1.26*	7.83	*0.17*	25.40	*0.42*	57
	Millerite°	3.23	0.44	*53.44*	*0.37*	5.69	0.09	*37.63*	*0.33*	60
8n1	β-phase°									
	*Melt	18.37	*5.64*	44.63	*4.73*	6.22	*0.20*	30.78	*0.62*	20
8n2	β-phase°	60.16	*1.60*	2.41	*1.42*	10.56	*0.17*	26.88	*0.35*	20
	Millerite	3.26	*1.15*	48.75	*0.92*	9.70	*0.12*	38.29	*0.34*	20
	Vaesite	1.51	*0.03*	43.72	*0.21*	1.19	*0.04*	53.58	*0.20*	24
8n3	Millerite	0.06	*0.02*	50.40	*0.13*	10.74	*0.07*	38.80	*0.12*	20
	Vaesite	0.06	*0.01*	44.71	*0.69*	1.75	*0.65*	53.48	*0.10*	20
8n5	β-phase°	59.33	*1.41*	2.27	*1.27*	11.22	*0.19*	27.18	*0.34*	20
	Millerite	2.87	*0.79*	47.98	*0.63*	10.93	*0.15*	38.21	*0.25*	20
	Vaesite	1.60	*0.06*	43.64	*0.26*	1.32	*0.06*	53.45	*0.19*	20

700°C										
Exp. no.	**Phase**	**Cu**	***ci***	**Ni**	***ci***	**Fe**	***ci***	**S**	***ci***	**No. of anal.**
1 wt%										
7a1	Digenite°	79.20	*0.55*	0.09	*0.11*	0.60	*0.17*	20.11	*0.45*	96
	*Melt									
7a2	Melt	7.92	*2.63*	69.34	*2.93*	0.22	*0.17*	22.52	*1.87*	86
7a3	Alloy	78.76	*4.69*	20.65	*4.56*	0.59	*0.20*	0.00	*0.00*	29
	Digenite	79.87	*0.74*	0.10	*0.11*	0.82	*0.24*	19.22	*0.54*	21
7a4	Millerite	2.45	*1.35*	61.45	*1.30*	0.36	*0.03*	35.73	*0.20*	9
	β-phase°	75.19	*2.47*	1.77	*1.82*	0.95	*0.15*	22.09	*0.78*	136
7c3	*Melt	12.99	*0.70*	63.11	*0.74*	1.63	*0.10*	22.28	*0.51*	150
7g4	Alloy	24.84	*0.34*	72.01	*0.31*	3.15	*0.04*	0.00	*0.00*	27
	Digenite	79.05	*0.27*	0.26	*0.18*	0.35	*0.08*	20.34	*0.20*	30
	Melt									
7g5	β-phase°	72.80	*1.92*	2.62	*1.41*	1.74	*0.05*	22.84	*0.53*	30
	Millerite	0.88	*0.19*	61.71	*0.51*	0.84	*0.02*	36.57	*0.37*	20
7h1	β-phase°	74.11	*1.75*	1.85	*1.25*	1.83	*0.04*	22.20	*0.65*	40
	Vaesite	0.85	*0.19*	45.82	*0.46*	0.13	*0.02*	53.19	*0.33*	29
	Millerite	1.10	*0.42*	60.20	*0.54*	0.82	*0.03*	37.88	*0.54*	29
7h2	Alloy	27.29	*0.53*	71.04	*0.52*	1.67	*0.02*	0.00	*0.00*	18
	Digenite	78.49	*1.04*	0.66	*0.90*	0.10	*0.02*	20.75	*0.51*	30
	Melt	12.87	*7.37*	63.70	*7.47*	0.22	*0.05*	23.21	*1.34*	50
7h3	Vaesite	0.02	*0.02*	46.70	*0.23*	0.19	*0.12*	53.09	*0.16*	29
	Millerite	0.05	*0.02*	60.75	*0.28*	1.30	*0.02*	37.91	*0.28*	30
7h4	β-phase	76.51	*0.42*	0.13	*0.07*	0.24	*0.02*	23.11	*0.42*	40
	Millerite	0.47	*0.16*	59.17	*0.27*	1.73	*0.03*	38.63	*0.29*	30
	Vaesite	2.19	*1.59*	43.45	*2.06*	0.10	*0.04*	54.25	*0.55*	30

Exp. no.	Phase	Cu	*ci*	Ni	*ci*	Fe	*ci*	S	*ci*	No. of anal.
3 wt%										
7b2	Alloy	58.52	*4.22*	37.03	*3.38*	4.44	*0.94*	0.00	*0.00*	49
	Digenite	76.32	*1.12*	0.36	*0.95*	1.64	*0.23*	21.68	*0.32*	57
7c4	Alloy	22.23	*0.43*	74.74	*0.42*	3.02	*0.08*	0.00	*0.00*	97
	Digenite	79.43	*0.51*	0.18	*0.22*	0.40	*0.10*	19.99	*0.46*	55
7f3	Alloy	24.08	*0.29*	72.09	*0.30*	3.83	*0.03*	0.00	*0.00*	25
	Digenite	79.41	*0.43*	0.19	*0.22*	0.48	*0.23*	19.92	*0.20*	40
	*Melt									16
7f4	*Melt	10.40	*2.52*	63.65	*2.07*	1.51	*0.09*	24.45	*0.47*	45
7f5	Alloy									25
	Digenite	78.10	*0.52*	0.65	*0.23*	1.00	*0.26*	20.25	*0.30*	30
7g1	β-phase°	70.46	*0.89*	1.38	*0.68*	4.63	*0.08*	23.53	*0.28*	30
	Vaesite	1.06	*0.08*	46.20	*0.19*	0.26	*0.02*	52.48	*0.16*	30
	Millerite	1.61	*0.69*	57.75	*0.62*	2.23	*0.05*	38.40	*0.64*	30
7g2	Vaesite	0.06	*0.02*	46.11	*0.39*	0.53	*0.17*	53.30	*0.33*	30
	Millerite	0.08	*0.02*	58.72	*0.29*	3.64	*0.06*	37.57	*0.28*	30
7g3	β-phase									
	Vaesite	1.22	*1.24*	45.67	*1.17*	0.51	*0.13*	52.61	*0.25*	30
	Millerite									
5 wt%										
7c1	Alloy	14.29	*0.65*	78.19	*0.55*	7.52	*0.17*	0.00	*0.00*	20
	Digenite	77.60	*1.15*	0.38	*0.84*	0.95	*0.20*	21.07	*0.69*	191
7h5	Alloy									
	Digenite	77.49	*0.80*	0.31	*0.53*	0.81	*0.23*	21.39	*0.47*	39
	*Melt	11.47	*3.02*	60.37	*2.80*	3.26	*1.04*	24.90	*0.50*	30
7i1	Alloy	12.53	*0.45*	77.60	*0.45*	9.86	*0.09*	0.00	*0.00*	20
	Digenite	77.39	*1.15*	0.41	*0.93*	1.53	*0.19*	20.67	*0.47*	18
	*Melt	11.30	*1.76*	62.58	*1.39*	1.93	*0.10*	24.19	*0.33*	39
7i2	Alloy	12.87	*0.78*	77.09	*0.58*	10.04	*0.28*	0.00	*0.00*	16
	Digenite°	75.08	*1.36*	1.25	*1.20*	2.20	*0.10*	21.48	*0.43*	30
7i3	β-phase°	66.42	*0.65*	0.80	*0.37*	7.99	*0.22*	24.78	*0.43*	55
	Vaesite	1.37	*0.42*	45.58	*0.38*	0.60	*0.08*	52.46	*0.41*	9
	Millerite	1.43	*0.45*	55.48	*0.48*	4.65	*0.09*	38.44	*0.57*	24
7j2	Vaesite	0.12	*0.06*	45.79	*1.19*	1.47	*1.02*	52.63	*0.27*	20
	Millerite	0.09	*0.01*	55.90	*0.32*	6.33	*0.09*	37.67	*0.36*	20
7j3	β-phase	68.21	*0.63*	0.26	*0.25*	4.71	*0.15*	26.82	*0.53*	23
	Millerite	0.97	*0.27*	54.20	*0.36*	7.04	*0.14*	37.80	*0.40*	20
	Vaesite	0.74	*0.13*	45.75	*0.30*	0.77	*0.04*	52.74	*0.28*	20

Exp. no.	Phase	Cu	*ci*	Ni	*ci*	Fe	*ci*	S	*ci*	No. of anal.
10 wt%										
7b3	Alloy	17.98	*0.32*	70.01	*0.27*	12.01	*0.16*	0.00	*0.00*	49
	Digenite	75.97	*1.73*	0.78	*1.83*	2.03	*0.25*	21.22	*0.53*	111
7c2	Alloy	13.86	*0.29*	77.61	*0.25*	8.53	*0.16*	0.00	*0.00*	27
	Digenite	77.98	*1.15*	0.38	*1.05*	1.11	*0.24*	20.52	*0.33*	86
7d5	Melt	8.65	*3.19*	56.37	*3.27*	10.46	*1.16*	24.51	*1.52*	75
7e1	Alloy	14.80	*0.84*	72.85	*0.74*	12.35	*0.82*	0.00	*0.00*	29
	Digenite°	76.46	*1.41*	0.68	*0.56*	2.24	*0.58*	20.62	*0.58*	35
7e2	Alloy	9.39	*0.28*	75.76	*0.37*	14.85	*0.17*	0.00	*0.00*	30
	Digenite°	72.13	*1.60*	0.82	*1.36*	3.60	*0.10*	23.46	*0.30*	19
7e3	Alloy	66.73	*3.44*	29.29	*2.57*	3.98	*0.89*	0.00	*0.00*	19
	Digenite	74.48	*0.55*	0.32	*0.23*	3.71	*0.37*	21.49	*0.25*	15
7e4	β-phase	63.69	*2.16*	2.66	*1.59*	8.98	*0.28*	24.67	*1.10*	21
	Millerite	1.71	*0.22*	52.93	*0.52*	9.27	*0.13*	36.09	*0.57*	12
7e5	β-phase	66.54	*0.62*	1.03	*0.15*	8.13	*0.53*	24.30	*0.35*	10
	Millerite°	1.63	*0.45*	53.08	*0.87*	10.40	*0.51*	34.90	*0.81*	17
7f1	Vaesite	0.08	*0.01*	44.76	*0.23*	1.30	*0.08*	53.87	*0.20*	30
	Millerite	0.09	*0.02*	51.75	*0.38*	9.79	*0.08*	38.36	*0.34*	40
7f2	Vaesite	0.75	*0.12*	43.99	*0.36*	1.51	*0.26*	53.75	*0.32*	40
	Millerite	1.73	*0.61*	47.00	*0.64*	12.37	*0.14*	38.90	*0.37*	38

APPENDIX D

Experiment labels according to starting Fe content:

The phase relations and experiment labels at 1200°C.

Starting Fe content	2-Melt field	Alloy + Melt	Melt
1 wt% Fe	12l5	12l2 12l3 12l4 12l6	12l1
3 wt% Fe	12m5	12m2 12m3 12m4	12m1 12m6
5 wt% Fe	12n1	12n2 12n4 12n5	
10 wt% Fe	12o5	12o2 12o3 12o4 12o6	12o1

The phase relations and experiment labels at 1100°C.

Starting Fe content	2-Melt field	Alloy + Melt	Alloy + Digenite + Melt	Alloy + Digenite
1 wt% Fe	11b5	11b1 11b2 11b3 11b4		
3 wt% Fe	11c1 11c2 11c4	11c5 11d1 11d2 11d3 11d4		
5 wt% Fe	11e3 11e4	11e1 11e5 11f1 11f2 11f3		
10 wt% Fe		11h1 11h2 11h3 11h4	11h5	11g2 11g3 11g4 11g5

The phase relations and experiment labels at 1000°C.

Starting Fe content	Alloy + Digenite	Alloy + Digenite + Melt	Alloy + Melt	Digenite + Melt	Melt
1 wt% Fe		10j1 10j3	10i4 10l3 10l4	10i2,3 10m4	10i5 10l5 10m3
3 wt% Fe	10j4 10n2 10n3	10f4	10f1 10g2 10g3 10m5 10o2	10g1 10o3	10n4 10n5
5 wt% Fe	10b 10e2 10k1 10k2 10o4	10p2	10a 10e1 10e3	10p1 10p3	10p4
10 wt% Fe	10g4 10h3 10k4	10h1 10k5 10q5	10h4 10i1 10q4		**Digenite:** 10q2

The phase relations and experiment labels at 900°C.

Starting Fe content	Alloy + Digenite	Alloy + Digenite + Melt	Alloy + Melt	β-phase + Melt	Digenite + Melt	Millerite + Melt	Millerite + Vaesite + Melt	Millerite + Vaesite	Melt
1 wt% Fe	9e1	9b1 9c1 9c2 9e2 9h1	9b2	9h3 9e3	9b4	9e4 9h5	9h2	9i1	9h4 9n3
3 wt% Fe	9f1 9c3	9c4 9f2 9i2 9n4 9n6	9n5	9i3 9i5		9f3	9j2 9i4	9j3	9j1 9j4
5 wt% Fe	9c5 9d2 9f4	9d1 9j5 9o1 9o3	9o2	9k1	9k4	9k2	9k3 9l1	9l2	9k5
10 wt% Fe	9g1 9d5 9d3 9a3	9l3 9d4 9o4	9o5 9o6	9l4 9g2		9g4 9m1		9m2	9g3 9l5 9m3

The phase relations and experiment labels at 800°C.

Starting Fe content	Alloy + Digenite	Alloy + Digenite + Melt	Alloy + Melt	β + Melt	Millerite + Melt	Millerite + Vaesite	Millerite + β + Melt	Millerite + Vaesite + β	Millerite + β	Vaesite + β	Melt
1 wt% Fe	8e1 8k3	8e2 8e3 8j5	8e4 8j1	8j2 8j3 8j4	8k4	8k6				8l1	8k1 8k2 8k5
3 wt% Fe	8f1 8f4 8f5 8g2	8g1	8a2 8a3 8a4	8f2		8l4	8l2	8l3 8l5	8f3		8a1 8a5
5 wt% Fe	8b1 8c1 8c3 8g3	8g4 8h1	8b2 8g5	8b3 8b4 8b5 8m3				8m2	8m4		8c2 8h3
10 wt% Fe		8c4	8i2 8c5	8d1 8d2 8d4 8i3 8i4 8n1		8n3		8n2 8n5	8m5		8d3

The phase relations and experiment labels at 700°C.

Starting Fe content	Alloy + Digenite	Alloy + Digenite + Melt	Alloy + Melt	β + Melt	Millerite + Vaesite + β	Millerite + β	Millerite + Vaesite	Melt
1 wt% Fe	7a3	7a1 7h2 7g4			7h1 7h4	7g5	7h3	7a2 7c3 7d1
3 wt% Fe	7b2	7c4 7f3 7f4 7f5			7g1 7g3		7g2	
5 wt% Fe		7i1 7i2 7h5	7d2		7i3 7j3		7j2	
10 wt% Fe	7b3 7c2 7e1 7e3	7e2 7d4	7d3		7f2	7e4 7e5	7f1	7d5

APPENDIX E

X-ray diffraction patterns of the β – phase and associated Ni-sulphides.

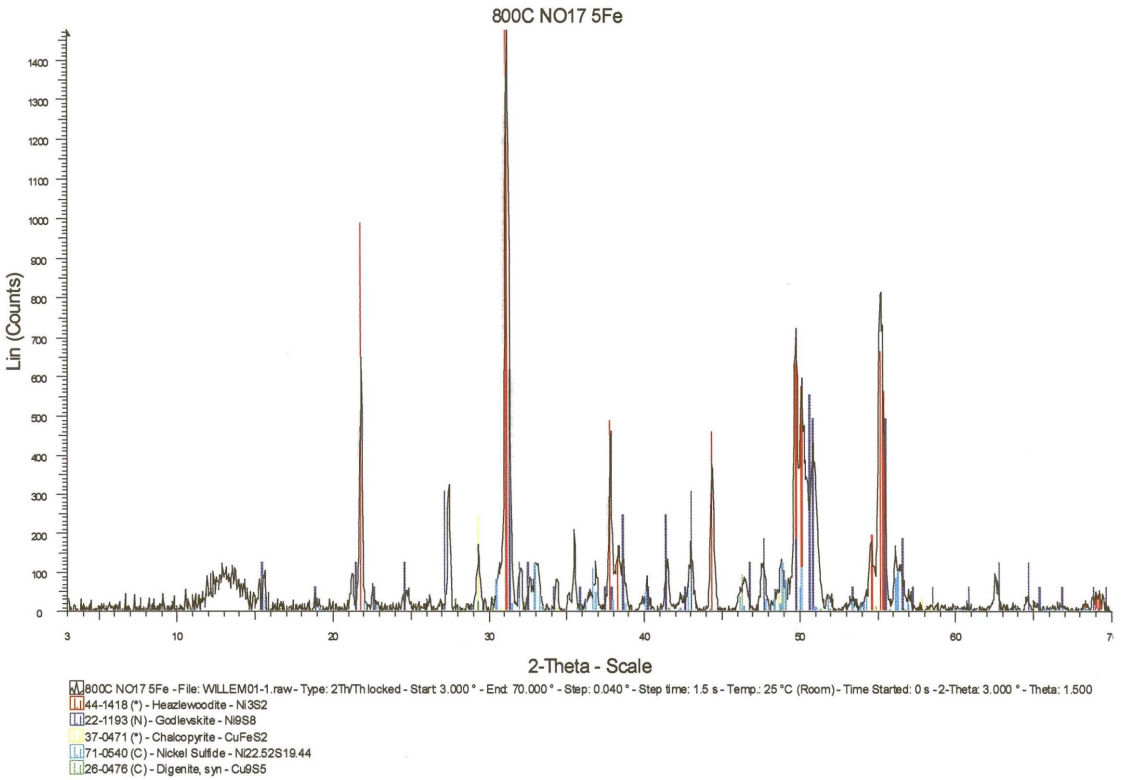

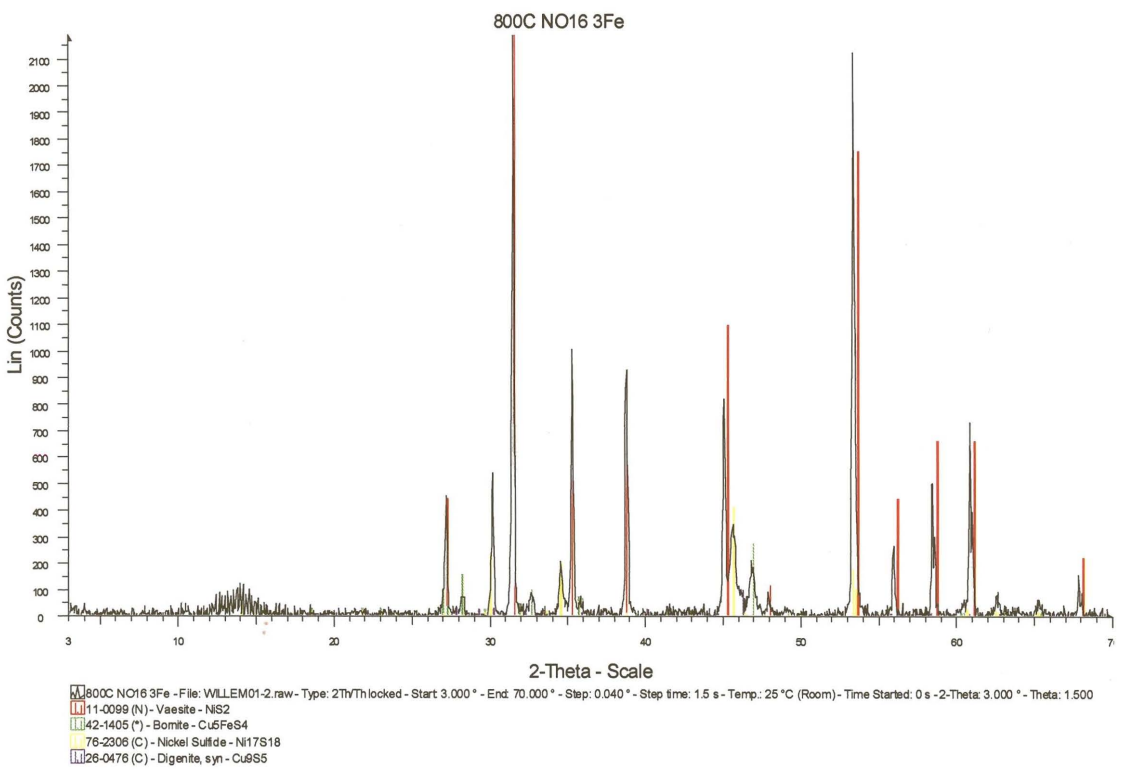

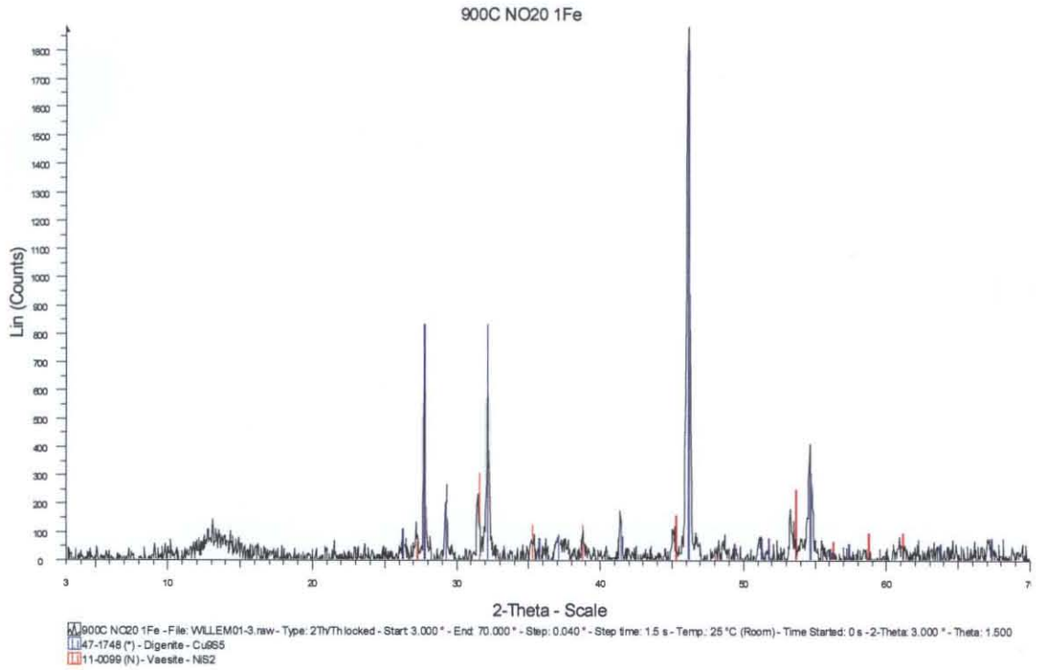
900C NO20 1Fe
Lin (Counts)
2-Theta - Scale
900C NO20 1Fe - File: WILLEM01-3.raw - Type: 2ThTh locked - Start: 3.000 ° - End: 70.000 ° - Step: 0.040 ° - Step time: 1.5 s - Temp.: 25 °C (Room) - Time Started: 0 s - 2-Theta: 3.000 ° - Theta: 1.500
47-1748 (*) - Digenite - Cu9S5
11-0099 (N) - Vaesite - NiS2

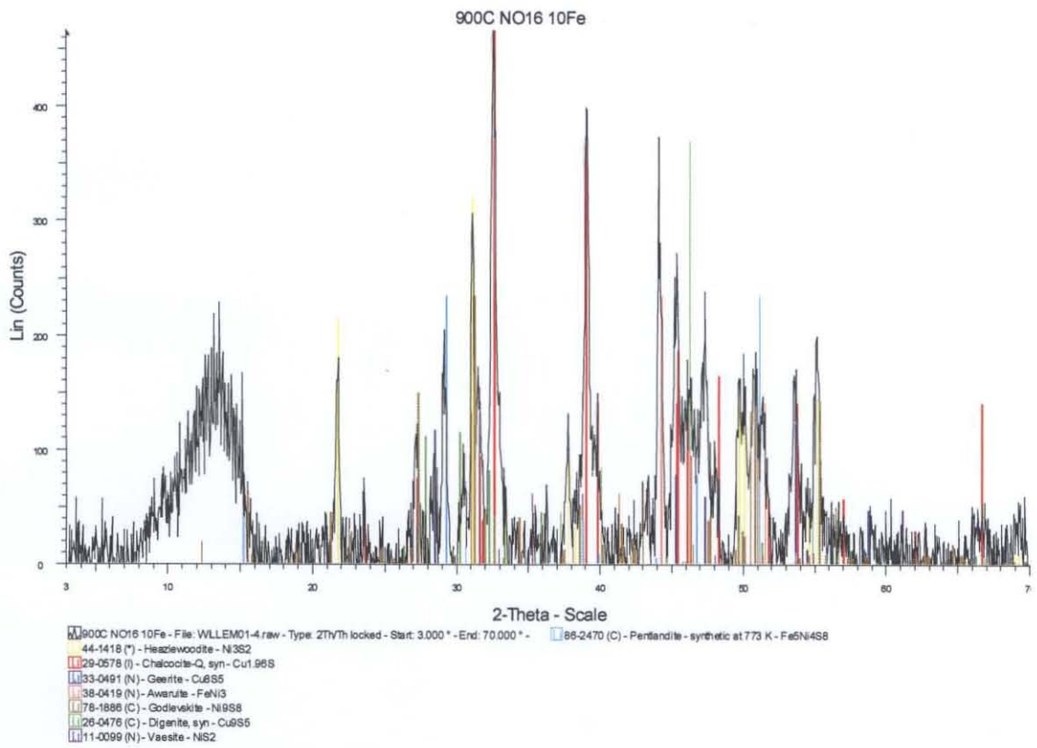
900C NO16 10Fe
Lin (Counts)
2-Theta - Scale
900C NO16 10Fe - File: WILLEM01-4.raw - Type: 2ThTh locked - Start: 3.000 ° - End: 70.000 ° -
86-2470 (C) - Pentlandite - synthetic at 773 K - Fe5Ni4S8
44-1418 (*) - Heazlewoodite - Ni3S2
29-0578 (I) - Chalcocite-Q, syn - Cu1.96S
33-0491 (N) - Geerite - Cu8S5
38-0419 (N) - Awaruite - FeNi3
78-1886 (C) - Godlevskite - Ni9S8
26-0476 (C) - Digenite, syn - Cu9S5
11-0099 (N) - Vaesite - NiS2